NASA Contractor Report 3966

Jet Shielding of Jet Noise

John C. Simonich, Roy K. Amiet,
and Robert H. Schlinker

NASA

NASA Contractor Report 3966

Jet Shielding of Jet Noise

John C. Simonich, Roy K. Amiet,
and Robert H. Schlinker
United Technologies Research Center
East Hartford, Connecticut

NASA

National Aeronautics
and Space Administration

**Scientific and Technical
Information Branch**

1986

Jet Shielding of Jet Noise

TABLE OF CONTENTS

TABLE OF CONTENTS (Cont'd)

FIGURES

SUMMARY

An experimental and theoretical study was conducted to develop a validated first principle analysis for predicting the jet noise reduction achieved by shielding one jet exhaust flow with a second, closely spaced, identical jet flow. A generalized dual jet noise analytical model was formulated in which the acoustic radiation from a source jet propagates through the velocity and temperature discontinuity of the adjacent shielding jet. Input variables to the prediction procedure include jet Mach number, spacing, temperature, diameter, and source frequency. Refraction, diffraction, and reflection effects, which control the dual jet directivity pattern, are incorporated in the theory. The analysis calculates the difference in sound pressure level between the dual jet configuration and the radiation field based on superimposing two independent jet noise directivity patterns.

Assessment of the theory involved conducting dual jet noise and single jet noise experiments to establish the difference in directivity pattern due to jet shielding. The experiments were conducted with two 4.45 cm diameter parallel jets installed on the centerline of the United Technologies open jet Acoustic Research Tunnel. Microphones located in a fixed polar array measured the radiated noise as the source jet slowly rotated about the shielding jet, thereby, providing a complete directivity pattern measurement on a hemispherical surface surrounding the dual jet system. Converging and converging/diverging nozzle sets were used to provide subsonic and supersonic shock-free flows. Finally, detailed Mach number and temperature surveys were conducted to determine which jet spacing conditions altered the individual acoustic source regions due to aerodynamic interference of the jet flows.

Jet shielding was found experimentally to reduce noise levels in the common plane of the dual jet system relative to the noise generated by two independent jets. The shielded region extends to observer angles on either side of the dual jet common plane. Outside of this region an increase of noise occurs due to the redirection of sound rays from the shielded region in addition to acoustic reflections between the adjacent flow fields. A balance exists between the noise reduction and noise increase existing over a hypothetical sphere surrounding the dual jet system. This balance confirms that acoustic energy is conserved by the acoustic wavefront-flow field interaction phenomena which control the dual jet directivity pattern. It also demonstrates that a beneficial noise reduction at one observer angle is negated by a noise penalty at other observer angles.

Jet shielding effectiveness increases with increasing Helmholtz number. Shielding is most effective for Strouhal numbers above the jet noise spectrum peak. Increasing subsonic Mach number enhances shielding and shifts the onset of shielding to Strouhal numbers below the spectrum peak. Further increases

to supersonic Mach number provide little improvement in shielding. For non-interfering dual jet flows, jet spacing has little affect on noise radiation in the common plane of the jet system. However, for small jet spacing resulting in the aerodynamic merger of the jet flows, sound pressure levels increase due to changes in the acoustic source region downstream of the jet merger. Changes of jet temperature were found to have a minimal effect on the dual jet directivity pattern. The maximum attainable noise reduction for two adjacent non-interfering jets with identical operating conditions is 3 dB. This limit is based on complete masking of one jet when the observer is in the common plane of the dual jet system.

Measured dual jet shielding effects were successfully modelled by the first principles theoretical model. Jet noise reduction in the common plane of the dual jet system was well predicted while directivity patterns outside the common plane were also calculated. Predicted dependence on Mach number, jet spacing, temperature, and source frequency were verified experimentally. The analysis, therefore, successfully models changes in the acoustic directivity pattern generated by two adjacent, random-noise, distributed-source jets.

2

INTRODUCTION

Although current jet aircraft are considerably quieter than their predecessors, the environmental impact of aircraft noise near airports continues to be a problem. Many novel techniques have been proposed to reduce the various components of aircraft noise. A recently proposed technique for reducing turbo-fan jet exhaust noise is to use one jet, of a closely spaced dual jet arrangement, to shield the sound produced by the second jet exhaust. Noise reductions of from 3 to 6 dB appear to be possible with this arrangement based on previous experimental and theoretical studies.

The dual jet shielding concept is illustrated in Figure 1. The sound radiated from the source jet is modified by interacting with the fluid discontinuity of the adjacent shielding jet through which the sound is transmitted. The shielding jet serves to refract, reflect, diffract, scatter, and attenuate the source jet noise radiation. These effects can alter the acoustic source directivity pattern with the final perceived directivity no longer being the superposition of the two independent jet noise radiation fields. The lack of a firm understanding of the potential noise reduction at a fixed radiation angle due to these propagation effects created a clear need for a fundamental study of the jet-by-jet shielding effect.

An understanding of the jet shielding phenomenon is also critical to the use of aircraft noise contours for evaluating and controlling airport noise levels. Presently, noise predictions superimpose the sound field of each engine to obtain the total turbo-fan engine noise level at the sideline observer station shown in Figure 2. However, several factors involving both propagation path modifications and noise redirection influence the sound pressure level sensed by the observer. One of the postulated mechanisms is the jet shielding phenomenon. Thus, failure to adequately account for the potential noise reduction due to jet shielding on current side-by-side engine geometries could result in erroneous noise contour predictions. The jet shielding mechanism addressed here is therefore considered to be potentially important for aircraft noise control.

An investigation of the potential noise reduction from dual jet shielding also contributes to the understanding and improvement of the jet noise suppression available from multitube nozzles. In this case, the dual jet geometry provides a fundamental approach for isolating the noise reduction achieved by two adjacent multitube nozzles. Once the noise reduction mechanism is quantified, the most promising multinozzle geometry and operating conditions can be optimally combined into a new suppressor design.

The present study was also stimulated by the need to optimize engine locations on future aircraft for the purpose of reducing jet exhaust noise. Based on the success of the shielding concept, optimal mounting geometries

could be selected to provide the greatest noise reduction below the flight path. In addition, current supersonic cruise vehicle technology evaluation studies with over/under the wing engine configurations would benefit from an understanding of the shielding phenomenon.

In summary, a need existed for the development of an experimentally validated jet shielding analyses in which the jet velocity, temperature, diameter, and spacing were input parameters. The present study was directed towards these needs.

The authors wish to acknowledge helpful discussions with J. C. Yu (NASA) and R. W. Paterson (UTRC) relative to interpretation and assessment of the experimental and analytical results.

4

LIST OF SYMBOLS AND NOMENCLATURE

a Radius of shielding jet

A_m, B_m Amplitudes of waves reflected from and transmitted through shear layer

c_o, c_1 Sound speeds outside and inside shielding jet

D Jet diameter

f Frequency, Hz

F_m Fourier transform of solution; see Eq. (21)

$H_m^{(2)}$ Hankel function of the second kind of order m

J_m Bessel function of first kind of order m

k_o Wavenumber (ω/c_o) outside shielding jet, see Eq. (7)

k_1 Wavenumber (ω/c_1) inside shielding jet, see Eq. (7)

k_z Wavenumber along z direction

$\bar{k}_z$ Stationary phase point; see Eq. (26)

K_o, K_1 Wavenumbers defined in Eq. (7)

$\bar{K}_o$, $\bar{K}_1$ Wavenumbes $\bar{K}_o$ and $\bar{K}_1$ evaluated at stationary phase point

kD Helmholtz number

L Jet core length, jet merging length

M Local Mach number, also jet exit Mach number

M_c Eddy convection Mach Number

p Acoustic perturbation pressure

P_a Ambient pressure

$\overline{P_D^2}$ Total power spectral density with shielding operative.

P_s Mean static pressure

$\overline{P_T^2}$ Total power spectral density for two independent jets

r Distance of far-field observer from origin; see Fig. 5
Also, radial displacement in aerodynamic measurements

R_o, R Distances of source and observer from jet axis, respectively; See Fig. 5

S Lateral jet separation distance

St Strouhal Number $= fD/V_j$

SPL Sound Pressue Level

T Parameter defined by Eq. (19)

T_a Ambient temperature

T_o Total temperature

T_s Static temperature

U Local streamwise jet velocity component

V_o, V_i Fluid velocity outside and inside shielding jet respectively for observer moving with trace speed

V_j Jet exit velocity

V_z Trace velocity of wave along shear layer

x, y, z Cartesian coordinate system defined in Fig. 5

X Axial displacement

x_o Source location on x axis

α Amplitude factor defined in Eq. (9), also weighting factor in expression for OASPL in Eq. (B-1)

β Jet expansion ratio $= \sqrt{M^2-1}$

δ Dirac delta function

ϵ_m 1 if $m = 0$; 2 if $m \neq 0$

6

θ Theoretical azimuthal angle of far-field observer; $\theta = 0°$ for observer in same plane as source and axis of shielding jet (See Fig. 5)

θ Experimental azimuthal angle of far field observer; $\theta = 90°$ for observer in same plane as source and axis of shielding jet (See Fig. 7)

ρ_o, ρ_1 Densities outside and inside shielding jet respectively

ϕ Velocity potential function

ψ Theoretical polar angle of far field observer, measured from a line through the source and parallel to jet axis (See Fig. 5)

ψ Experimental polar angle measured from shielding jet axis to observer or microphone (See Fig. 7)

ω Circular frequency, radians

PREVIOUS INVESTIGATIONS

Previous studies demonstrated that an adjacent jet can provide an acoustic shield to suppress the noise from a source jet. The following discussion presents the relevant experimental and analytical state-of-the-art which formed the basis for development of the current program.

Experimental Studies

Early work on noise reduction of jet engines involved designing noise suppression nozzles. A multitube nozzle arrangement was used to break one large jet into multiple small jets. The observed noise reduction of this arrangement was initially thought to be due to such effects as rapid mixing, reduced shear, shifts of peak noise to higher frequencies and shock interactions. Progressively, researchers postulated that jet shielding might be partially responsible for noise reduction in this multi-element nozzle arrangement.

In an effort to define the noise reduction, the simplest combination was selected, namely two parallel jets. The earliest example is the study by Greatrex and Brown in 1958 (ref. 1). Although their data show approximately a 3 to 4 dB difference in noise between ΔSPL ($\theta = 90°$) and ΔSPL ($\theta = 180°$) the authors indicate an uncertainty in the reliability of the measurements. The noise reduction benefit appeared to decrease with increasing spacing as S/D increased from 1.2 to 1.4.

A study of the effects of jet shielding on two jets of unequal size was carried out by Morris, Richarz and Ribner in 1973 (ref. 2). A small secondary jet was mounted at an angle to the main jet so as to eliminate any aerodynamic interference and hence avoid degradation of the main jet performance. The objective was to alter the directivity pattern of the main jet by refracting, reflecting, and diffracting the sound field using the secondary jet. They found a maximum reduction of 5 dB. The attenuation increased for both increasing secondary jet velocities and temperatures.

A study of the shielding effect of multi-tube nozzles was done by Gray, Gutierrez and Walker in 1973 (ref. 3). They measured the noise produced from 37 tube nozzles and single tube nozzles using both 1/4 scale and full scale configurations. At low velocities, no shielding was detected. However, at transonic velocities and above, a nearly complete shielding was observed.

As part of a larger study on jet noise reduction from shrouded multi-nozzles, Goethert and Borchers (ref. 4) reported on twin jet experiments

conducted in 1974. For spacing to diameter ratios between 1.2 to 2.0, they found that the total sound power was approximately 1 dB lower than the noise produced by two independent jets. At larger spacings, however, only a .1 to .2 dB reduction was noted.

A study of acoustic shielding in annular jets was performed by Ahuja and Dosanjh in 1977 (ref. 6). They examined the effect of shielding a noisy, circular inner jet with an annular outer jet. With the outer jet at the same temperature as the inner jet, little shielding benefit was observed. However, by heating the outer jet a 10 dB reduction could be obtained. A true reduction in acoustic power levels was observed, as opposed to a redistribution of acoustic energy by refraction. The shielding effect was seen at all angles, but was stronger at higher frequencies.

A study of the acoustic shielding from twin, round heated jets was presented in 1977 by Bhat (ref. 7). In his test, the effects of spacing, dissimilar velocity, dissimilar jet size, and longitudinal stagger on acoustic shielding were examined. Sound pressure measurements were made about an arc only in the common plane of the dual jet system. For equal size jets with no longitudinal stagger, up to a 5 dB difference between the twin jets and a single jet incremented by 3 dB was noted at 40° from the jet axis. At 90° from the jet axis, no effect was observed. Although the range of lateral jet spacing tested was small (from S/D = 1.12 to 2.0) an increase in shielding effect was observed at the closest spacing. The importance of acoustic source changes due to aerodynamic interactions at these close spacings was not evaluated. An increase in shielding effect was also noted for an increase in streamwise stagger.

An acoustic study of heated twin jets was performed by Kantola in 1977 (refs. 7, 8). Sound pressure measurements were made in an arc around the jet nozzle exit at only 3 polar angles, 0°, 45°, and 90° from the dual jet plane. Lateral jet spacing, velocity and temperature were varied. Kantola found that as the spacing increased from S/D = 1.33 to 3.0, the measured overall power level (OAPWL) decreased in the plane of the jets. No additional effect was noted for larger spacings. In the loud plane, 90° from the plane of the jets, OAPWL varied from less than the single jet noise level incremented by 3 dB level to greater than the single jet level incremented by 3 dB. Kantola interpreted this to indicate mixing suppression and additional noise generation respectively. At frequencies below about 2 kHz, little difference was noted between the load and the quiet measurements planes. At higher frequencies, however, over 8 dB of difference was noted for a microphone at 30° from the jet axis. Even for the 90° off axis microphone, up to 2 dB difference was seen. The frequency at the onset of shielding was seen to decrease as the spacing increased. Kantola attributed this to an internozzle layer of cold fluid which exists between the jets and extends further downstream as the spacing increases. As the layer extends further downstream,

the lower frequency jet noise sources are shielded. It was also noted that the shielding. It was also noted that the shielding effect increased with jet velocity up to sonic conditions.

Several other model scale and full scale experimental studies have been conducted to confirm the shielding phenomena although the geometries involved did not correspond to the engineering problem addressed here. Two specific investigations are important to the present investigation.

First, Shivashankara and Bhat (ref. 10) conducted a study of the noise reduction by two parallel jets with significantly unequal flows. It was observed that the sound of the high velocity (loud) jet could be shielded by the low velocity (quiet) jet by as much as 7.5 dB OASPL. No benefit was perceived at azimuthal angles greater than 75° from the plane of the jets. Since these effects occurred at small jet spacings (lateral spacing to diameter ratio of 1.5 to 1.6) it was necessary to evaluate the acoustic source changes due to aerodynamic interaction of the jet flows. By comparing velocity profiles obtained with single jet versus the dual jet configuration at a streamwise station of $X/D = 5$, it was reported that no significant mean flow interaction occurred. However, the present authors believe that more sensitive criteria are needed to determine jet interference effects. In addition acoustic source regions upstream of $X/D = 5$ contribute primarily to the high frequency content of the jet noise spectrum. In contrast, the spectrum peak is controlled by acoustic source regions downstream of $X/D = 5$ where the present authors feel aerodynamic interactions can occur.

While the general results of reference 10 suggest that dissimilar jets should also be investigated, current and future aircraft engine operations continue to be based on similar flows with equal thrust from each engine. Thus, the present study concentrated on the dual jet shielding by similar flows. However, the dissimilar jet concept represents a further improvement in jet shielding noise reduction technology.

A second important experimental study was conducted by Yu and Fratello (ref. 11) to isolate the acoustic effect of the jet-by-jet shielding phenomenon from potential source changes due to the dual jet flow field interaction. This was accomplished by using a point source of sound in conjunction with the shielding jet. Different discrete tones and also 1/3 octave band random noise were emitted from a small acoustic source. Room temperature air and helium were used as the working fluids for the jet. The helium was used to simulate heating at a high temperature ratio. Since there was only one jet, no aerodynamic interaction was present, and the effect of acoustic shielding alone could be studied. Yu and Fratello found that the peak value of shielding, as measured by the differential power level between acoustic source only and both acoustic source and jet, increased with frequency, jet velocity, jet heating, and longitudinal source position. No trends were identified for the effect of

lateral spacing on acoustic shielding Helmholtz number greater than 2. Quali-
tative comparisons with Kantola (ref. 8) and Bhat (ref. 7) confirmed the
trends reported in previous dual jet studies in addition to the present
study.

The following general observations were presented in various combinations
in the above described investigations: 1) as much as a 5 dB decrease in noise
is possible at a given operating condition; 2) the shielding effect generally
decreases as the lateral spacing between the twin jets increases; 3) little
shielding benefit is provided at low jet velocities and the effect increases
with velocity; 4) no shielding benefit is present at low frequencies; 5) a
larger shielding effect occurs when the jets are heated.

Constraints of Previous Experimental Studies

Although general conclusions obtained from earlier studies demonstrated
the feasibility of the shielding concept, there were limitations in the scope
and details of the experimental assessment. For example, measurements were
often confined to one or two azimuthal angles, θ (see Fig. 2), near the common
plane of the dual jet system where the noise reduction was most effective.
Consequently, noise penalties due to redirection of sound into other azimuthal
planes was not determined. In addition, it is possible that for the close jet
spacings used in many of the studies the acoustic source field was modified by
premature merging of the jets. In this case, the two jets no longer func-
tioned as independent source regions at large downstream distances where the
low frequency jet noise sources are located. Finally, previous experiments
were often restricted to cold flows while in other cases only a single jet
velocity was tested.

A final constraint of previous studies was the use of convergent nozzles
employed in subsonic experiments to extend the velocity dependence measure-
ments into the supersonic operating regime. The generation of shock noise and
screech by the convergent nozzles introduces new noise mechanisms which
presumably alter the relative acoustic source distribution on the jet axis.
Furthermore, the rapid expansion of the jet plumes due to the shock structure
at the jet exit planes possibly results in premature merging of the jets and
consequent alteration of the jet noise source region. These acoustic source
changes complicate the interpretation of the acoustic shielding effect as the
jet velocity becomes supersonic.

Theoretical Studies

The jet shielding analytical model is based on calculating the sound
transmission across a shear layer. Early studies of the phenomenon utilized

simplified geometries in their analytical models to facilitate assessment of the concept. For example, the studies by Cowan and Crouch (ref. 12) and Kantola (ref. 9) employ the theoretical model of Yeh (ref. 13) for sound transmission through two parallel shear layers. The work of Yeh is a minor extension of the work of Miles (ref. 14) and Ribner (ref. 15) since it uses two shear layers in place of the single shear layer model in references 14 and 15. The model developed by Yeh is highly simplified and restricted when applied to the present problem since it treats both shear layers as plane and parallel. It also considers only rays contained in the plane which is normal to the shear layers and aligned with the jet velocity vector. Another limitation is that the transmitted ray propagates in the same direction as the original ray, eliminating any focusing effects which might occur in the cylindrical jet geometry addressed in the present study. Finally, the plane shear layer model of Yeh assumes that the wavelength of the incident ray is much smaller than the jet diameter.

The analysis of Parthasarathy, Cuffel and Massier (ref. 16) uses the plane shear layer analysis of Ribner which they apply at the crossing point of each shear layer. In this analysis, multiple reflections inside the shielding jet are assumed not to occur; that is, once a ray is reflected, it is assumed to propagate outwards and the acoustic energy is lost. This model is accurate only if the reflection coefficient is small. For example, if the furthest shear layer (of the shielding jet) from the noise source reflected 90 percent of the energy incident on it, 90 percent of this reflected energy or 81 percent of the original incident energy would again be reflected in the direction of the sideline observer. Neglecting these multiple reflections could easily lead to an overestimate of the jet noise shielding effect.

One of the first calculations specifically directed toward the jet shielding geometry was developed by Gerhold (refs. 17, 18). The boundary conditions of the continuity of pressure and displacement are identical to those used in earlier shear layer refraction studies. (A detailed review of the impact of the earlier shear layer refraction studies is given in the section titled "Theoretical Development of the Jet Shielding Analysis"). The source field modeled by Gerhold was expressed in terms of plane waves incident on a cylindrical shear layer. Qualitative confirmation of the analysis was presented in the study of Yu and Fratello (ref. 11) which duplicated the point source/single shielding jet geometry of the theoretical model.

PRESENT INVESTIGATION

Objective

The primary objective of the present program was to conduct an experimental study of the effect of flow from a jet on the radiated sound field of a neighboring jet with the same operating condition. Although previous investigators have conducted similar studies, the present experiment represents a definitive program in which the following comprehensive set of parameters were varied: a) jet Mach number, b) jet temperature, and c) jet spacing. The program was structured to vary only one parameter at a time thereby isolating the effect of the selected variable. By using small microphone intervals the experiment also provided the improved directivity information needed to identify possible redirection of sound. Also by using a shock-free converging-diverging nozzle system for the supersonic tests, potential source changes existing in previous converging nozzle experiments were avoided. Finally, detailed Mach number and temperature surveys were conducted to determine if the small jet spacings created jet flow interaction. This permitted the identification of changes in the radiated sound field due to alterations in the downstream acoustic source region.

A secondary effort was directed towards development of an analytical model to predict the shielding dependence on the experimental parameters. The theory models the shielding of discrete tones from a point source of sound by a nonspreading cylindrical jet with a uniform velocity profile. Although the present analysis is similar to the formulation by Gerhold, this separate theoretical effort was implemented to provide an independent check on the existing method for prediction of jet noise shielding. In addition, the availability of the analysis facilitated the present closely coupled theoretical and experimental program. This was critical to determining the conditions for which the discrete source/single jet combination adequately models the dual jet random noise distributed source configuration.

Experimental Approach

The dual jet and anechoic chamber experimental arrangement used in the present study is shown in Figures 3 and 4. Each of the 4.45 cm nozzles in the side-by-side jet configuration was supplied from a common plenum with heated high pressure air. Microphones located in a fixed polar array were used to measure the radiated noise as the source jet slowly rotated, thereby providing a fine azimuthal directivity measurement as θ varied from $0°$ to $180°$. Both converging (for subsonic flows) and converging/diverging (for supersonic shock free flows) nozzle sets were used. Flow visualization by the Schlieren technique in addition to a unique static pressure probe were used to set the shock-free supersonic operating conditions of the converging/diverging

15

nozzles. Finally, extensive aerodynamic measurements were conducted to identify the jet spacings conditions for which aerodynamic merging and interference altered the acoustic shielding measurements.

Analytical Approach

A theory was developed to predict changes in the jet noise directivity patterns due to the presence of an adjacent shielding jet. The analysis models the dual jet configuration in terms of a discrete tone radiation from a point source of sound interacting with the cylindrical zero thickness shear layer of a single shielding jet. The global effects of reflection, refraction and diffraction of sound rays by velocity and temperature discontinuities of the shielding jet are implicitly included in the analytical model. Multiple reflections and acoustic focusing are also incorporated in the model. The analysis applies for all ratios of acoustic wavelength to jet diameter and permits nonplanar wavefronts incidence at the shielding jet.

THEORETICAL DEVELOPMENT OF THE JET SHIELDING ANALYSIS

The Shielding Mechanism and Selection of the Analytical Approach

The transmission of sound through an adjacent jet is controlled by the flow and temperature discontinuity. Under certain conditions, these discontinuities partially or totally reflect sound since the shielding jet has a different impedance compared to the surrounding ambient air. In other cases, the sound wave penetrates the shielding fluid but is refracted by the flow field resulting in a change of the noise directivity pattern. Finally, the sound can be diffracted by the discontinuity at the jet interface or scattered by the turbulent flow regime of the shielding jet. The difference between the sound pressure level measured by an observer in the presence and in the absence of the fluid shield defines the noise reduction due to the phenomena of reflection, refraction, diffraction and scattering.

The present analysis models the combined effects of the reflection, refraction, and diffraction mechanisms but does not treat the scattering mechanism. While the individual mechanisms incorporated in the analysis are easily described, the general theory implicitly predicts the global effects. Contributions from the individual mechanisms are, therefore, not separable due to the complex interaction of the resulting waves arriving at the far field observer location. For example, phasing between refracted and diffracted waves must be known if these mechanisms are to be isolated. In this case phasing between wavefronts can result in an increase or decrease of the sound pressure level relative to the non-shielded environment.

The theory models the dual jet geometry as a single point source emitting a discrete tone which propagates through the adjacent shielding jet. Selection of the point source approach is based on the results of jet noise acoustic source distribution measurements which show that specific source frequencies are confined to a local axial region of the source jet. Selection of the discrete tone model was based on the need to model the random jet source in a tractable format. Also the analysis assumes a nonspreading shielding jet with a uniform velocity profile. The effects of finite shear layer thickness or potential aerodynamic merging which exist in realistic dual jet configurationa are not included. Finally, scattering of sound by the turbulent jet flow is not included because of the complexity of modeling this mechanism for the radially distributed axially varying turbulent shear flow. Considering the above analytical simplifications, the objective of the current study was to determine if the resulting model predicts the experimental results of the dual jet configuration.

Review of Previous Analyses and Experimental Confirmation

The analytical treatment of the jet shielding problem is based on calculating the sound transmission across a shear layer. Although many of the previous analyses in this field did not treat the specific jet shielding geometry, they are discussed here since they formed the theoretical basis for the present analysis.

The first correct analysis of sound transmission across a shear layer was formulated by Miles (ref. 14) and independently by Ribner (ref. 15). Both investigators considered the case of a plane wave incident on a two-dimensional zero thickness shear layer. At the shear layer the incident wave gives rise to a transmitted and a reflected wave. The amplitudes of these waves are determined by matching pressure and fluid displacement across the shear layer. These boundary conditions at the shear layer interface correctly model the acoustic transmission process. Earlier studies had matched normal velocity across the shear layer. This was an incorrect boundary condition because of the difference in mean velocity across the shear layer.

Gottlieb (ref. 19) considered the case of a point sound source near a plane shear layer. This replaced the assumption of an incident plane wave and allowed the calculation of the directivity pattern of point sources in the presence of a shear layer. His formulation differs from the present jet shielding analysis and the analysis of Gerhold only in the geometry of the shear layer.

Graham and Graham (ref. 20) extended the analytical capability to shear layers of finite thickness. However, for finite shear layers, pressure and fluid displacement cannot be matched across the interface. Instead the finite thickness shear layer problem requires the numerical integration of an ordinary differential equation across the shear layer to determine the reflected and transmitted wave amplitudes.

Howe (ref. 21) considered the time dependent problem of an impulse produced by a point source impinging on a plane zero-thickness shear layer. This approach allows the study of shear layer instabilities induced by the incident wave. In all the other studies, including the present one, the instabilities are suppressed by assuming a steady state.

Shear layer refraction phenomena have also been included in jet noise analyses which model the effect of flow on the assumed quadrapole sources. In this case, the Lighthill approach, which distributes quadrupoles in a free-stream, is modified by imbedding the quadrupoles in the jet shear flow and calculating the resulting radiation. This approach, used for example by Tester and Burrin (ref. 22) for jet noise calculations, is similar in many respects to the problem treated here. The primary difference is that reference 22 assumes the shear layer has a finite thickness whereas the

present model assumes a zero thickness. Also, reference 22 imbeds the source in the refracting shear layer whereas the source is external to the shear layer in the present model.

Several other studies relevant to the prediction of jet noise have been formulated using approaches similar to reference 22. These include the work of Mani (refs. 23, 24) and Goldstein (ref. 25). As in reference 22, these studies placed the sound source inside the jet whereas in the present problem the sound source is located outside the shielding jet.

A different approach was developed by Amiet (refs. 26, 27) and Jacques (ref. 28). These investigators assumed that the acoustic wavelength of the incident wave is small compared to the jet diameter permitting the application of geometrical acoustics techniques to calculate an angle and an amplitude correction. This method is useful for subtracting out the effects of shear layer refraction when the source type is not known. The correction in angle and amplitude is not dependent on source type, making the technique useful for analyzing noise data obtained in an open jet acoustic wind tunnel. However, the method ignores multiple reflections such as might occur inside a jet, and also assumes the acoutic wavelength is much smaller than the jet diameter. Whereas this method has the advantage of being independent of source type, the high frequency limitation precludes its use for the present calculation.

Methods for correcting acoustic data obtained in open jet wind tunnels have also been developed by Candel (ref. 29) and Tester and Morfey (ref. 30). Candel employed a ray tracing technique to obtain the angle and amplitude correction. Thus, realistic jet velocity profiles with finite thickness and axial velocity variations could be investigated. The use of ray tracing in this case, however, limits the analysis to high frequency. Tester and Morfey devised a simpler model by locating a source on the jet centerline and surrounding it with a finite thickness shear layer. While radial velocity variations were represented in this way, axial variations were not included. The resulting model was then used to calculate low frequency and high frequency shear layer transmission effects. The results at high frequency compare closely with those of Amiet (ref. 27) and Jacques (ref. 28) for the zero thickness shear layer case at moderate Mach numbers of the order of 0.5 or less. This indicates that for many problems the shear layer thickness may not be an important parameter, at least for angles outside the zone of silence.

One of the first analyses specifically directed toward the jet shielding problem was that of Gerhold (refs. 17, 18). In his analysis the jet is modeled as a plug flow with a zero thickness shear layer. The boundary conditions of continuity of pressure and displacement at the shear layer are identical to those used in earlier studies which assumed a zero thickness shear layer. The source field modeled by Gerhold is expressed in terms of cylindrical harmonic incident on the cylindrical shear layer. Thus, the difference between his work and earlier studies is in the circular shear layer geometry.

The geometry difference between the formulation of Gerhold and the earlier studies can be demonstrated by a comparison with the analysis of Gottlieb (ref. 19) which uses a plane zero thickness shear layer. The latter analysis expresses the source field in terms of plane waves incident on a zero thickness plane shear layer. Similarly expressing the incident sound field in terms of plane waves in the analysis of Gerhold would result in difficulties in applying the boundary conditions at the shear layer interface. Instead Gerhold expresses the incident sound field in terms of cylindrical harmonics which conform to the cylindrical boundary of the shear layer. Similar methods were employed by Tester and Burrin (ref. 22) for a finite thickness cylindrical shear layer, and by Mani (ref. 23) for a cylindrical zero thickness shear layer.

Verification of the above described fundamental shear layer transmission theories and boundary conditions applicable to the present problem have been provided by several investigators. A preliminary experiment by Amiet (ref. 26) showed agreement between theory and experiment for the angle correction. More detailed testing by Schlinker and Amiet (refs. 31, 32) provided further confirmation of both angle and amplitude corrections. Experimental studies with a sound source inside a jet were also performed by Candel, et. al. (ref. 33) and Ahuja et. al. (refs. 34, 35). The latter experiments provided similar confirmation of the fundamental theory used in the analysis of sound propagation through a shear layer.

Analysis

Formulation of the Approach - The analytical model permits a pure tone point source and an observer to be located at arbitrary points outside the shielding jet flow field (see Fig. 5). The cylindrical shear layer of the shielding jet has zero thickness; i.e., plug flow of diameter, 2a, and velocity V. The Z axis is aligned with the jet axis and the X axis passes through the source. The azimuthal angle, θ, is defined to be the angle between the X-Z plane and the plane containing the jet axis and the observer. (Note that in the experiment, the point where $\theta = 0°$ is rotated by 90° compared to that point in the theory). The polar angle ψ is the angle between a line parallel to the jet axis and the line joining the source and observer. The jet interior has density ρ_1 and sound speed c_1, while the values in the exterior region are ρ_0 and c_0. The sound source is at a distance $R_0 = x_0 > a$ from the axis and the observer is at a distance $R > a$ from the axis. The z component of the distance between the source and observer is z_0.

Summary of the Approach - The analytical approach used in the present report and in the studies of Gerhold (refs. 17, 18) employs a standard formulation used by previous authors (e.g., Mani (ref. 23) in the study of shear layer refraction. The method begins with the wave equation for the

velocity potential inside and outside the shielding jet. Since the jet flow field conditions in the z direction are constant the wave equation can be easily Fourier transformed. This simplifies the analysis by eliminating the z variable until the inverse transform is performed. Assuming a sinusoidal dependence for the acoustic source and identifying a separation of variables results in a Helmholtz equation in terms of the variables R, θ and ω. The source field in these variables is given by Equation 8, below. This source field impinges on the shear layer leading to transmitted and reflected waves given by Equations 10 and 11. The unknown amplitudes of the transmitted and reflected waves are determined by matching pressure and fluid displacement at the jet boundary. A Fourier inversion is then performed on k_z to obtain the final acoustic pressure result.

To avoid performing the inversion numerically, the observer is assumed to be located in the far field allowing the integral to be approximated analytically. This approximation is based on the method of stationary phase which is commonly used to make such far-field approximations. The details of the analysis are given below.

General Expression for the Far Field Sound – The wave equation for the velocity potential ϕ outside and inside the jet flow field is

a) Outside
$$\nabla^2 \phi + k_o^2 \phi = \frac{q_o}{\rho_o} \delta(x - x_o) \delta(y) \delta(z) \qquad (1)$$

b) Inside
$$\nabla^2 \phi - 2i\omega \frac{M}{c_1} \phi_z - M^2 \phi_{zz} + \frac{\omega^2}{c_1^2} \phi = 0 \qquad (2)$$

The velocity potential is related to the pressure field by the linearized momentum equation

$$p = -\rho_o \frac{D\phi}{Dt} \qquad (3)$$

where $k_o = \omega/c_o$ and a time dependence $\exp(i\omega t)$ has been assumed in the above three equations. (Gerhold uses $\exp(-i\omega t)$ so that many of his results are complex conjugates of the results found here.)

If the velocity potentials in Equations 1 and 2 are decomposed into their spatial Fourier components

$$\phi = \int_{-\infty}^{\infty} \tilde{\phi}(k_z) e^{ik_z z} dk_z \qquad (4)$$

these equations then become

a) Outside $\qquad (\nabla_2^2 + K_0^2)\, \tilde{\phi} = \dfrac{q_0}{2\pi \rho_0}\, \delta(x-x_0)\, \delta(y) \qquad (5)$

b) Inside $\qquad (\nabla_2^2 + K_1^2)\, \tilde{\phi} = 0 \qquad (6)$

where

$$\nabla_2^2 \equiv \frac{\partial^2}{\partial x^2} + \frac{\partial^2}{\partial y^2}$$

$$k_1 \equiv \left(\frac{\omega}{c_1} + M k_z\right)$$

$$K_0 \equiv \sqrt{k_0^2 - k_z^2} \qquad (7)$$

$$K_1 \equiv \sqrt{k_1^2 - k_z^2}$$

It should be noted that k_z in Equation 7 employs a plus sign in the definition of k_1 whereas Gerhold uses a minus sign. This difference in the definition of the Fourier transform results in $\bar{k}_z$ in Equation 26 being negative while Gerhold defines it to be positive.

The solution of these equations can be written as a combination of incident, transmitted and reflected waves. The source given in Equation 1 produces an incident wave which can be represented as

$$\tilde{\phi}_{in} = a \sum_{m=0}^{\infty} \epsilon_m \cos m\theta \begin{cases} J_m(K_0 R)\, H_m^{(2)}(K_0 R_0) & R < R_0 \\ H_m^{(2)}(K_0 R)\, J_m(K_0 R_0) & R > R_0 \end{cases} \qquad (8)$$

where

$$\begin{aligned} \epsilon_m &= 1 \quad m = 0 \\ &= 2 \quad m \neq 0 \end{aligned} \qquad a \equiv \frac{iq_0}{8\pi\rho_0} \qquad R_0 = x_0 \qquad (9)$$

Here R_0 is the distance of the source from the jet axis and R the distance of the observer from the jet axis; i.e., the field point. (See Equation 7.3.18 of reference 36). The reflected and transmitted waves can now be written as

$$\tilde{\phi}_R = \sum_{m=0}^{\infty} A_m H_m^{(2)} (K_0 R) \cos m \theta \qquad (10)$$

$$\tilde{\phi}_T = \sum_{m=0}^{\infty} B_m J_m (K_1 R) \cos m \theta \qquad (11)$$

Boundary Conditions - The constants A_m and B_m in Equation 10 and 11 are determined by matching boundary conditions at the jet interface R = a. First, the pressure must be continuous at R = a. From Equations 3 and 4, pressure is related to $\tilde{\phi}$ by

$$p = -i \rho_1 c_1 k_1 \tilde{\phi} \qquad R < a$$

$$= -i \rho_0 c_0 k_0 \tilde{\phi} \qquad R > a \qquad (12)$$

From Equations 9-11,

$$\rho_0 c_0 k_0 \left\{ \sum_{m=0}^{\infty} \left[\alpha \, \epsilon_m \cos m \theta \, J_m (K_0 a) \, H_m^{(2)} (K_0 R_0) + A_m H_m^{(2)} (K_0 a) \cos m \theta \right] \right\}$$

$$= \rho_1 c_1 k_1 \sum_{m=0}^{\infty} B_m J_m (K_1 a) \cos m \theta \qquad (13)$$

Because θ is a variable, this equation must match on a term by term basis, or

$$\alpha \, \epsilon_m \, J_m (K_0 a) \, H_m^{(2)} (K_0 R_0) + A_m H_m^{(2)} (K_0 a) = \frac{c_1 k_1 \rho_1}{c_0 k_0 \rho_0} B_m J_m (K_1 a) \qquad (14)$$

Also, there must be continuity of shear layer displacement at R = a. Note that this condition is not the same as continuity of radial velocity, an error that appeared in analyses prior to the works of Miles (ref. 14) and Ribner (ref. 15) (The continuity of displacement and velocity are not the same because there is a zero order velocity jump across the shear layer). Satisfying continuity of displacement for the interface requires determining the

speed at which the disturbance travels along the jet shear layer. The Fourier component, exp $(i \omega t + i k_z z)$, of the potential function is a wave which travels with velocity given by

$$V_z = - \omega / k_z \qquad (15)$$

In a coordinate system moving with the wave this wave component remains steady in time. In this coordinate system the fluid velocity inside the jet is

$$V_i = V + \omega / k_z \qquad (16)$$

while the fluid velocity outside the jet is

$$V_0 = \omega / k_z \qquad (17)$$

Continuity of shear layer displacement is insured by equating the slopes of the flow vectors across the shear layer, i.e., the perturbation radial velocities divided by V_i or V_0 respectively. Thus, from Equations 9-11.

$$a \; \epsilon_m \; J_m' \; (K_0 \; a \;) \; H_m^{(2)} (K_0 R_0) + A_m \; H_m^{(2)'} \; (K_0 a) = B_m T \; \frac{\rho_1 \; c_1 \; k_1}{\rho_0 \; c_0 \; k_0} \; J_m' \; (K_1 a) \qquad (18)$$

where

$$T \equiv \frac{k_0^2 \rho_0 \; c_0^2 \; K_1}{k_1^2 \rho_1 \; c_1^2 \; K_0} \qquad (19)$$

Equations 14 and 18 are two equations for the two unknowns A_m and B_m. Elimination of B_m gives

$$A_m = \frac{a \; \epsilon_m \; H_m^{(2)} (K_0 R_0) \left[- T J_m' \; (K_1 a) \; J_m (K_0 a) + J_m' \; (K_0 a) \; J_m (K_1 a) \right]}{- H_m^{(2)'} (K_0 a) \; J_m (K_1 a) + H_m^{(2)} (K_0 a) \; J_m' \; (K_1 a) \; T} \qquad (20)$$

24

where the primes denote differentiation of the Bessel functions with respect to the argument.

The potential field for $R > R_0$ is the sum of ϕ_{in} and ϕ_R which, after inverting the Fourier transform, gives

$$\phi = a \sum_{m=0}^{\infty} \epsilon_m \cos m \, \theta \int_{-\infty}^{\infty} H_m^{(2)}(K_0 R) \, F_m(K_0, K_1) \, e^{ik_z z} \, dk_z \qquad (21)$$

where

$$F_m(K_0, K_1) \equiv J_m(K_0 R_0) + \frac{H_m^{(2)}(K_0 R_0) \left[J_m(K_1 a) \, J_m'(K_0 a) - T J_m(K_0 a) \, J_m'(K_1 a) \right]}{T H_m^2(K_0 a) \, J_m'(K_1 a) - J_m(K_1 a) \, H_m^{2\prime}(K_0 a)}$$

$$(22)$$

This is the complex conjugate of the result derived by Gerhold.

The Stationary Phase Method – The summation and integration in Equation 21 can be performed numerically. However, since the far-field solution will be of the greatest interest, the method of stationary phase can be used to analytically perform the integration for $\omega R/c_0 \gg 1$. For the case of large R,

$$H_m^{(2)}(K_0 R) \rightarrow \sqrt{\frac{2}{\pi K_0 R}} \, e^{-i\left(K_0 R - \frac{\pi}{2} m - \frac{\pi}{4}\right)} \qquad (23)$$

The method of stationary phase applies to the integrals with a rapidly varying phase; this gives a cancelling effect except at the point of stationary phase where the phase varies the slowest. Introducing Equation 23 into Equation 21 gives a phase

$$\psi = -K_0 R + k_z z \qquad (24)$$

The point of stationary phase is now determined by setting the derivative of the phase equal to zero. Thus,

$$\frac{d\psi}{dk_z} = 0 = \frac{\overline{k}_z R}{K_o} + z \qquad (25)$$

giving

$$\overline{k}_z = k_z \bigg|_{\frac{d\psi}{dk_z} = 0} = -\frac{z k_o}{r} \qquad (26)$$

$$\overline{K}_o \equiv K_o \bigg|_{\overline{k}_z} = R k_o / r \qquad (27)$$

$$\overline{K}_1 = K_1 \bigg|_{\overline{k}_z} \qquad (28)$$

Also,

$$\frac{d^2 \psi}{dk_z^2} \bigg|_{\overline{k}_z} = \frac{r^3}{k_o R^2} \qquad (29)$$

Note that $\overline{k}_z$ in Equation 26 is negative whereas Gerhold defines it to be positive. The difference lies in the definition of the Fourier transform. In Equation 7 k_z appears with a plus sign in the definition of k, whereas Gerhold employs a minus sign.

The method of stationary phase indicates that all quantities, except for the phase factor, can be evaluated at the point of stationary phase $\overline{k}_z$ and taken outside the integral. The phase is evaluated in a Taylor series so that the integration can be performed analytically. Thus, the integral in Equation 21 becomes

$$I_m = F_m (\overline{K}_o, \overline{K}_1) \sqrt{\frac{2}{\pi \overline{K}_o R}} \; e^{i(m + 1/2) \pi/2 - i k_o r} \int_{-\infty}^{\infty} e^{i \frac{r^3 k_z^2}{2 k_o R}} dk_z \qquad (30)$$

Using the relation from page 395 of reference 37, the integral remaining in Equation 30 is

$$I' = 2 \int_0^\infty \cos\left(\frac{r^3 k_z^2}{2 k_0 R}\right) dk_z = \sqrt{\pi k_0 R^2 / r^3} \qquad (31)$$

The final result for the velocity potential is then

$$\phi = a \frac{\sqrt{2}}{r} e^{i(\pi/4 - k_0 r)} \sum_{m=0}^\infty \epsilon_m F_m(\overline{K}_0, \overline{K}_1) i^m \cos m\theta \qquad (32)$$

Introducing this result in Equation 3 then gives the following expression for the pressure

$$P = -i\rho_0 \omega \phi \qquad (33)$$

There remains an infinite summation to be performed in Equation 33. This in general must be performed numerically. However, the summation over the first term in F_m can be carried out to give the result for a free field source for an observer in the far field; i.e.,

$$\sum_{m=0}^\infty \epsilon_m J_m(\overline{K}_0 R_0) i^m \cos m\theta = e^{i k_0 R_0 \cos \theta / r} \qquad (34)$$

This result follows from Equation 8.511.1 of reference 37 after making the substitution $t = ie^{i\theta}$.

Application of Theory

Procedure - The solution for the far-field acoustic pressure, created by the point source/single jet combination illustrated in Figure 5 is given by Equation 33. Here the velocity potential is obtained from Equation 32 with the particular values of K_0 and K_1 given by Equations 27 and 28. As noted earlier, the first term in the expression for the parameter, F_m, in Equation 32, can be evaluated directly using the closed form expression given in

Equation 34. This closed form approach avoids long computation times, especially if $\overline{K}_0 R_0$ is large, since numerical solutions for this term generally give significantly slower convergence compared to the remaining term in the expression for F_m.

To quantify the change in the source noise level at the observer station when the shielding jet is present, the far field pressure, given by Equation 33, is normalized by the incident pressure. The incident pressure is determined from the far field equation (Eq. 33) except that the incident velocity potential ϕ_{in} (Eq. 8) is employed. Thus, the ratio of free-field-to-shielded acoustic pressures, is given by the ratio of $\phi/\tilde{\phi}_{in}$. In terms of the decibels, the change in pressure is defined by $\Delta SPL = 10 \log_{10} (\phi/\tilde{\phi}_{in})^2$.

Comparison with Previous Investigations and Numerical Test Cases - The analytical results presented here agree with the corresponding results of Gerhold. As a check on the numerical predictions generated by the Gerhold analyses, an independent computer code was developed during the present study to calculate the sound pressure level changes associated with jet sheilding. The program predicts the parameter ΔSPL for specific values of R_0, R, ϕ, ψ, a and ω.

Input conditions employed in the comparison of the two computer codes corresponded to the values reported by Gerhold in reference 18. Calculated values obtained from the UTRC code were compared with values generated independently at NASA Langley where the computer model of the Gerhold analysis was available. Comparison of the separate predictions confirmed that the computer codes provided the identical numerical values, to within four decimal places, for the acoustic pressure ratio determined from $\phi/\tilde{\phi}_{in}$.

Based on the above described evaluation of the generalized sheidling analyses and the associated computer code the theory was applied during the present closely coupled theoretical and experimental program. The objective was to determine the conditions for which the discrete source/single jet combination adequately models the dual jet random noise distributed source configuration. Without the on-site jet shielding prediction capability developed in the present study, such direct assessments would not be possible. This is evident in the section titled "Experimental Assessment of Dual Jet Shielding" where the critical selection of the single jet/point source geometry for simulation of the dual jet experiment is discussed.

As a further check on the numerical solution, an energy balance calculation was performed for the geometry shown in Figure 5. Analytically, there is no mechanism for the interchange of energy between the mean flow and the acoustic field. For the experiment it is possible for the shielding jet to modify the acoustic impedance seen by the source if the source is less than an acoustic wavelength from the jet. However, for the analytical model, the

28

far-field assumption should ensure that the acoustic impedance is the same with and without the shielding jet. Thus, the energy radiated to the far field should be invariant with the addition of the shielding jet.

The energy calculation was obtained by numerically integrating the far-field intensity over a spherical surface surrounding the point source/shielding jet configuration shown in Figure 5. Within the numerical accuracy of the calculation the acoustic energy radiation was found to be the same with and without the shielding jet.

DESCRIPTION OF EXPERIMENT

Acoustic Research Tunnel

The experiment was conducted in the UTRC Acoustic Research Tunnel which is described in detail in reference 38. Figure 6 shows the open circuit open jet design of the acoustic tunnel and the air supply system used for model jet noise simulation studies. High pressure air, up to 27.5 bar (400 psi) at 4.5 kg/sec (10 lbm/sec), is supplied to a propane combustor which provides heated high speed air up to 538°C (1000°F). A muffler downstream of the combustor attenuates the combustion noise and valve noise before the air supply line enters the side of the acoustic tunnel inlet section. Beyond this point the air supply line is routed along the tunnel centerline terminating at the model nozzles which, in the present experiment, extended approximately 1.5 m into the anechoic chamber. The open jet test section surrounding the nozzles typically provides forward flight simulation although the present test was conducted under static operating conditions.

The test section is surrounded by a sealed anechoic chamber 4.9 m high, 5.5 m long (in the jet centerline direction), and 6.7 m wide. The chamber walls are lined with 0.5 m high fiberglass wedges which provide an anechoic acoustic environment above 175 Hz. Downstream of the test section, the air-flow enters a diffuser through a circular collector with acoustic treatment on its flow impingement surface. The diffuser is designed to operate unstalled and hence is not a major source of background noise. To avoid tunnel fan noise from propagating upstream into the anechoic chamber, a Z-shaped muffling section with two right angle bends and parallel treated baffles is located between the diffuser and the fan. The flow is exhausted to the atmosphere by a 1100 kW centrifugal fan.

Experimental Arrangement

Figure 7 shows the anechoic chamber experimental arrangement. A fixed array of 9 microphones on a 3.05 m (10 ft) radius arc was centered on the shielding jet exit plane. The microphones were located in a horizontal plane at 10° increments between 20° and 100° from the shielding jet centerline. Acoustic shielding effects were investigated by rotating the source jet on a fixed radius arc about the shielding jet. This technique of rotating one jet while fixing the microphone location was equivalent to the observer in Figure 2 being situated at different azimuthal angles relative to the air-craft. The multiple engine configuration in Figure 2 was, however, replaced by the present dual jet configuration. This simplified geometry isolated the side-by-side acoustic and aerodynamic interactions in addition to providing a fundamental experiment capable of assessing the present theory.

Approximately a 200° source jet rotation range was obtained using the technique shown schematically in Figure 8. Here high pressure air from the upstream propane burner was supplied to a common plenum (located in the tunnel inlet) for the purpose of delivering equal pressure and temperature flows to each nozzle. The source jet was constrained to move in a circular arc by a bearing situated at a fixed radius in the rotating disk. A variable speed electric motor with a chain and sprocket arrangement was used to rotate the disk. The air supply line for the fixed shielding jet penetrated a hole in the rotating disk. A flexible stainless steel tube connected the rotating source jet and the fixed upstream plenum. Since the plenum and rotating disk obstructed the open jet test section the model nozzles could not be tested with forward flight simulation.

Two matched sets of nozzles with an exit diameter of 4.45 cm (1.75 in.) were used in the experiment, a converging pair and a converging/diverging (C/D) pair. The converging nozzles were employed for subsonic tests (M = 0.6, 0.94 and the C/D nozzle set was used for supersonic tests. The interior geometry of each C/D nozzle duplicated the contour used earlier by Laufer, Schlinker, and Kaplan (ref. 39) to study single flow shock free supersonic jet noise at M = 1.5. Although the nozzle profile in reference 39 was designed using an inviscid code shadowgraph measurements demonstrated the shock free operating point to be M = 1.47. Similar measurements, using Schlieren methods in addition to static pressure probe measurements, were performed in the present study to identify the shock free operation point. The improved sensitivity of the static pressure measurement, however, resulted in a slightly different operating point relative to reference 39 with M = 1.46.

Jet spacing (S), relative to nozzle diameter (D), was varied by changing the initial radial displacement between the source jet and the shielding jet. This was accomplished by connecting to the source jet a supply pipe with an offset centerline.

To minimize the generation of upstream turbulence (which can alter the jet noise spectrum) large diameter (15 cm) supply lines were used between the plenum and the rotating disk. A liner was also installed on the interior wall of the flexible tube used on the source jet supply line. This provided a smooth wall for the purpose of minimizing the generation of turbulence. The maximum flow angle change in the offset section used to change jet spacing was limited to 15 degrees. This minimized the generation of secondary flows in the turning sections which could be another source of flow disturbance. In addition a 1.2 m length of the 10 cm diameter pipe was used downstream of the offset pipe on the source jet supply line (also on the shielding supply line) to permit the turbulence to decay before entering the source jet nozzle. Finally, a pipe-to-nozzle-area contraction-ratio of approximately 5 was employed to further reduce the initial turbulence level at exit plane of each jet. This ratio was limited by the upstream 10 cm diameter supply pipe and the smallest jet spacing ratio.

The complicated equipment associated with rotating the source jet blocked the acoustic tunnel open jet flow surrounding the test nozzles. Consequently, forward flight effects were not tested and the study was limited to static jet noise directivity patterns. However, to avoid developing locally hot regions in the anechoic chamber when conducting the high temperature jet noise studies under these static conditions, the tunnel fan system was operated at approximately 3 m/sec. Ambient air in the anechoic chamber entrained in this process was replaced by air flow through large holes in the rotating disk (34 percent open area). Also, an access door to the chamber was partially opened to entrain cooler outdoor air.

The above described rotating jet configuration was essential to defining the azimuthal directivity patterns for which limited documentation was obtained in previous experiments. Also, the decision to rotate the jet in place of rotating the microphones on an arc in the azimuthal direction was based on the requirement to minimize ambient air temperature gradients, in the anechoic chamber. Rotation of the microphone array to an azimuthal location above the nozzle would have placed the microphones near the ceiling of the chamber where the hot air from the heated jets could migrate. The temperature limit for microphone operation in addition to the potential thermal gradients through which the jet noise would propagate precluded using the rotating microphone approach. Instead, the nozzles were rotated while the microphones were located in a horizontal plane 1.6 m above the floor of the anechoic chamber.

Instrumentation

Acoustic Measurements – Measurements of the far field jet noise were made with 0.635 cm diameter microphones at normal incidence. Signals from the microphone preamplifiers were high-pass filtered (at 200 Hz), amplified and finally recorded on magnetic tape, using a 15 track, FM tape recorder system. Acoustic data was reduced to 1/3 octave band levels on an analyzer with 0.1 dB resolution. The analyzer generated absolute sound pressure levels for the 31 bands between 50 Hz and 50 kHz. A narrow band spectrum analyzer was also used, mainly for diagnostic purposes.

Frequency response of the above described data acquisition system was calibrated prior to performing the test program. Microphone cartridge calibrations conducted according to National Bureau of Standards procedures indicated a maximum variation of ±1 dB over the 200 Hz to 50 kHz range of the present study. The frequency response of the microphone preamplifer-to-tape recorder section of the data acquisition system was also calibrated. In this case, a white noise signal was injected into the preamplifier and recorded on analog tape. Playback of the signal from each recording channel was compared on a spectrum analyzer with the initial white noise input signal. The

frequency response was observed to be flat within ±1 dB for all microphones from 200 Hz to 50 kHz.

Frequency response variations of the above described data system suggest potential uncertainties in the experimental results since changes in the radiated source jet directivity due to shielding were of comparable magnitude. However, the shielding phenomenon is defined by the difference between the dual jet and a corresponding single jet sound pressure level measurement. Since the same microphones and instrumentation channels were used for each data set, the previously described variations in response with frequency do not impact the results of the present study. In essence, the shielding phenomenon addressed here is not a function of absolute sound pressure level, but instead is represented by a relative level change.

Velocity and Pressure Measurements - Mean Mach number profiles of the developing region of the subsonic merging jets were obtained with pitot probes. A 1.58 mm (1/16 in) tip diameter tube and support was used to survey the total pressure field in radial and axial directions.

To determine the shock free operating point for the supersonic nozzle set, measurements of both total and static pressure were obtained on the centerline of each jet. A square edged, round pitot tube measured the total pressure. The probe generated a detached normal shock which was accounted for in the data reduction. Total pressure measurements were corrected by the Rayleigh equation to give local Mach number. A separate probe, similar to one used by Pinckney (ref. 40), measured the static pressure in the supersonic region of the jet flow. The same probe configuration was employed by Seiner in an earlier supersonic jet noise study (ref. 41). A 5.08 cm (2 inch) span-wise separation of the total and static pressure probes eliminated probe interference during flow traverses.

The pressure sensing probes were mounted on a double wedge wing support (diamond shaped cross-section) with a wedge half angle of 7°. A small wedge angle was selected to ensure an attached shock wave on the support strut. A detached shock wave could interfere with the pressure field sensed at the pressure sensing probe location 3.8 cm (1.5 inches) forward of the support.

Both the subsonic and supersonic probes were traversed across the twin jet flow field using a 3 axis traverse system. Stepping motors moved the probes in two orthogonal directions within a plane normal to the jet axis. Traverse increments of 0.0127 mm (0.0005 in) were used. Axial traverses were obtained with a DC motor and a controller providing a resolution of approximately 2.5 mm (0.1 in). The traverse system, shown in Figure 9, was moved continuously. Voltages from the pressure and temperature sensing transducers, in addition to the encoder positions, were stored on the computer data acquisition system (discussed in detail in the subsection titled Computer Data Acquisition and Data Reduction System).

In addition to the downstream jet profile measurements, static and total pressure measurements were obtained at a reference station in the 10 cm pipe upstream of each nozzle. These upstream pressures were used to set the jet Mach number during the acoustic study when the flow traversing system was removed from the anechoic chamber. In the case of subsonic flows, the upstream pressures were calibrated relative to the desired nozzle exit conditions determined during the jet flow surveys. For the supersonic converging/diverging nozzles, a three step process was used to identify the upstream pressure required for shock free operation. Details are presented in the subsection titled Shock Free Operating Conditions.

During the above calibration process, a small difference was observed between the dual jet nozzle exit Mach numbers. This was attributed to the different flow losses in the piping sections linking the upstream plenum and each nozzle. Jet operating conditions were, therefore, based on the upstream pressure in the source jet air supply line. Differences between the source and shielding jet exit Mach numbers were not considered to have an impact on the present jet shielding acoustic study as discussed in the section titled Aerodynamic Measurements.

Temperature Measurements – Total temperature profiles of the heated merged jet flow field were obtained with a specially designed double shielded thermocouple probe. Design criteria, based on the earlier work of Moffat (ref. 42), limited errors from velocity, radiation, and conduction to less than 5°C over the entire range of Mach numbers and temperatures tested. An outer shield with a 6.35 mm (0.25 inch) diameter provided a smaller sensing area and less flow blockage than commercially available units. An independent check on the probe calibration was obtained by comparing measurements taken with a larger commercially available 9.53 mm (3/8 inch) diameter triple shielded thermocouple probe. Temperature readings from the two units were within 5°C of each other. During the temperature flow surveys the UTRC designed unit was mounted on the traverse unit along with the total pressure probe and separated by a distance of 3.8 cm (1.5 inches).

Jet total temperature operating conditions were set using temperature readouts from thermocouples mounted upstream of each nozzle. The sensors were located at the same reference station where total and static pressure measurements were obtained when setting the jet flow Mach number. Similar to the calibration of the upstream pressure sensors, the upstream thermocouples were calibrated relative to the specially designed UTRC probe situated at the jet exit.

Flow Visualization – Figure 10 shows the Schlieren system used to determine the shock free operating condition for the M = 1.5 converging diverging supersonic nozzles. This technique was also helpful when documenting the onset of jet merging as the dual jet spacing was decreased.

The Schlieren system used 25.4 cm (10 in) diameter mirrors which were fixed at the nozzle exit. A video camera permitted viewing the resulting optical image from the control room. Photographic records were obtained using a 35 mm single lens reflex camera with a strobe light (nano-second pulse duration) to capture the jet structure. A sample photo obtained for an off design pressure setting on the supersonic converging diverging nozzle system is shown in Figure 11.

Source Jet Rotation Position and Rotation Rate - A digital encoder was employed to sense the rotating source jet position. By using a 12 to 1 gearing ratio between the encoder and the chain driven rotation system, a 0.1° angular resolution was provided. Rotation rate was adjusted to produce a 90° azimuthal change in approximately 8 minutes. This slow rotation, which created an 8 minute tape record for the microphone signals, was experimentally determined to provide a pseudo steady state during the 1 second data processing time used for the repetitive spectrum analyses (described further in following subsection).

Computer Data Acquisition and Data Reduction System - Acquisition and processing of the large acoustic data base obtained in the present study was performed by a computer controlled system. A schematic of the automated system is shown in Figure 12.

Data acquisition proceeded in the following sequence. After the desired Mach number and total temperature were established, the jet rotation and computerized data acquisition system were activated. The computer controlled the tape recorder, which recorded the signals from the 9 far field microphones, the time code generator, and the upstream reference station pressure and temperature sensors. (Temperature and pressure data was later used to correct the acoustic sound pressure levels for small changes in jet velocity as the source jet rotated). In addition the angular position encoder output was stored on the computer hard disk along with the time code. Both signals were sampled once per second during the jet rotation.

Data reduction involved playback from the tape recorder to the 1/3 octave band spectrum analyzer. The desired data record was located by searching the analog tape for the associated time code signal. Processing by the spectrum analyzer was computer activated 15 seconds after identifying the start of the record. A time delay was introduced to permit setting (remotely by the computer) the maximum input amplifier sensitivity on the analyzer without overloading the circuitry. A 1 second repetitive averaging time was selected on the analyzer with the computer sampling the output from the 31 frequency bands (stored in a digital buffer) every 2 seconds, or, approximately every 0.5° of source jet rotation. The sampled spectrum was stored on the computer mass storage disk. During playback, the pressure and temperature data from the tape record was also digitized every 2 seconds, converted to engineering units, and stored on disk.

Since the acoustic signals and jet rotation position were initially stored on separate systems (FM tape for acoustic signals, disk storage for jet position) it was necessary to merge these records to create sound pressure level versus azimuthal position information. This was achieved by using the time code generator signal. During playback of acoustic data each digitally sampled record from the 1/3 active band analyzer was linked with the appropriate time code which was simultaneously sampled at the tape recorder output by the computer. A similar set of jet position versus time code files was also available on the computer disk storage system. Merging of these files provided the required sound pressure level versus azimuthal angle information. The same technique was used to determine the jet operating pressure (used to calculate Mach number) and total temperature at each azimuthal station. This permitted correcting the dual jet noise for small changes in the upstream operating pressure.

Test Program

Selection of Acoustic Test Conditions – To provide a broad data base for current and future turbo-fan engine aircraft, a wide range of test conditions was selected. To assess the affect of Mach number on the jet noise shielding mechanism, both subsonic (M = 0.6 and 0.94) and supersonic (M = 1.46) jet exit Mach numbers were used. The subsonic operating conditions are typical of current commercial aircraft jet engines. The supersonic test condition simulated the pressure ratio of previously proposed engines for supersonic cruise vehicles.

To assess the effect of thermal discontinuties, the above defined Mach numbers were investigated over a range of total temperatures. One series of tests was conducted without heat addition to the flows such that the jet exit static temperature was approximately equal to the ambient air temperature (nominally 25°C). This operating condition minimizes the temperature effect, thereby isolating the Mach number discontinuity dependence. Three additional temperatures of nominally 316°C (600°F), 427°C (800°F), and 538°C (1000°F) were selected to simulate current engine operating conditions. These temperatures span the range from the fully mixed temperature downstream of a high-bypass ratio turbofan to typical turbojet operating conditions.

Engine spacing effect on current full scale aircraft was investigated using three lateral separation distances, S/D = 3.1 (nominal), 5.5, and 8.1. The smallest distance simulates present Boeing 727 (S/D ≈ 2.5) aircraft and earlier Boeing 707 (S/D ≈ 4) aircraft. The largest spacing corresponds to the distance between the opposing inboard engines on under-the-wing mounted airframe designs. For example, for the Boeing 737 S/D ≈ 7 while S/D ≈ 8 on the Boeing 747. The intermediate value of S/D = 5.5 was selected to establish the trend with increasing separation.

The source jet azimuthal rotation range initially extended from $\theta = 0$ to $200°$. (See Fig. 7). To shorten the 16 minute tape record created by the slow rotation rate through this large azimuthal range, θ was confined to rotate from $80°$ to $200°$. This was possible since both jets in the dual jet system operated at the same Mach number and total temperature. Under this condition, the radiated acoustic directivity pattern was symmetric about $\theta = 90°$ permitting a significant reduction in the rotation range. Verification of the symmetry properties is given in the Section titled Experimental Assessment of Dual Jet Shielding.

It is important to recognize that the laboratory coordinate system is rotated $90°$ compared to the coordinate system used in the theoretical development section. For the laboratory coordinate system, $\theta = 90°$ occurs when the $\psi = 90°$ microphone, the shielding jet, and the source jet are in line. In the theoretical coordinate system, this condition corresponds to $\theta = 0°$. These differences in θ are evident when comparing Figures 5 and 7.

For the supersonic test points, azimuthal measurements were limited to two fixed angles given by $\theta = 90°$ and $180°$ in the laboratory coordinate system. This limitation occurred because of the difficulty of controlling the supersonic jet operating pressure. Tight tolerances for shock free operation could not be satisfied during the approximately 8 minutes required for the azimuthal rotation. Instead acoustic data was obtained at the two fixed angles which, after comparison of the sound pressure levels, were expected to show the largest effect of jet shielding.

The above described difficulty in controlling the total pressure did not represent a problem for the subsonic test cases. For subsonic test conditions, small variations in the upstream plenum chamber pressure were corrected using jet noise scaling laws (see section titled Data Acquisition and Data Reduction and Appendix B). Most corrections were smaller than 0.3 dB with the maximum correction during the test program being 0.75 dB.

Aerodynamic Study - The extensive range of separation distances defined above delineates the effect of engine separation on the magnitude of jet noise shielding for current airframe configurations. The smallest separation distance also permits evaluating the acoustic effects created by aerodynamic interference or merging. In this case, noise reduction or additional noise generation can occur due to alteration of the acoustic source regions. The potential acoustic impact of the aerodynamic merging at small S/D necessitated conducting detailed aerodynamic measurements to document the merging process of the dual jet configuration.

Aerodynamic measurements were conducted for S/D = 2.7, 3.1, 3.8, 5.5, and 7.9. In comparison to the acoustic measurements, acquisition of aerodynamic data was possible at smaller spacings due to a mechanical equipment simplification. For the acoustic study with rotation of the source jet around the shielding jet, a spacing plate was required to maintain the jets at a fixed

separation distance. This plate was not required for the aerodyamic phase of the experiment where the nozzles were stationary.

Aerodynamic measurements involved mean total pressure and mean total temperature surveys. With the dual jet system oriented in a fixed vertical plane (see Fig. 7) probe traverses were conducted along horizontal lines surveys at different heights, relative to each jet centerline. This approach provided sufficient data to generate a contour plot of total pressure and total temperature in the plane normal to the jet axis. Measurements were repeated at selected downstream stations to trace the development of the jet flow field.

In addition to the planar surveys at selected axial stations, continuous axial traverses were conducted to identify the location at which the independent jets merged aerodynamically. This was achieved by traversing in the axial direction on a line midway between the two jet centerlines.

Acoustic and Aerodynamic Qualification Tests

Background Noise - Several preliminary acoustic measurements were conducted to establish the quality and limitations of the acoustic data. To demonstrate that the jet noise phenomena investigated in the present study were not masked by facility noise, background noise levels were compared to the jet noise levels at selected operating points.

Background noise tests were performed by removing both jet nozzles from their upstream 10 cm diameter air supply lines. Mass flow rate and total temperature in the air supply lines duplicated the operating conditions with the nozzles attached. The resulting jet velocity and, hence, the jet noise were significantly reduced at the exit of the 10 cm diameter pipe, thereby, providing a calibration of the noise generated in the upstream piping. Both cold and hot tests, with combustion noise present, were performed. The mass flow was measured using ASME procedures for standard sharp edged orifice plates installed upstream of the combustor.

Background noise measurements, obtained with flow in both air supply lines, were compared to the noise from a single jet in the dual jet shielding configuration. The single jet comparison, instead of a dual jet comparison, was selected since it represented the maximum background noise source for which an adequate signal-to-noise ratio was critical. In the limit, total masking of the source jet by the shielding jet would result in only the shielding jet radiation arriving at the far field microphone location.

Comparisons between background noise levels and noise from a single jet are shown in Figure 13. To assess the effect of flow rate on the upstream piping and combustor noise, the lowest ($M = 0.6$) and highest ($M = 1.46$) exit

Mach numbers are presented. In both cases, the highest jet exit temperature (700 K) is shown since this condition was expected to generate the maximum noise in the upstream propane heater.

The comparison for the subsonic test case in Figure 13a shows a minimum of 6 dB signal-to-noise ratio at all polar radiation angles when the acoustic source frequency is approximately 400 Hz. At frequencies above 1 kHz, where the jet shielding phenomenon dominated, large signal to noise ratios occurred with values ranging from 15 dB to 40 dB. Similar results were observed for the supersonic test conditions shown in Figure 13b. These examples illustrate that over the spectrum range where the jet shielding mechanism was operative, an adequate signal-to-noise ratio existed permitting conclusions to be drawn directly from the data.

Comparison of Jet Noise Spectra with Previous Investigations - To further establish that the present facility provides clean jet noise data, single jet noise measurements were compared with previously published data. For this purpose, 1/3 octave band sound pressure levels from the shielding jet were compared with measurements reported by Plumblee et al (ref. 43). The results for three polar angles are shown in Figure 14 for a common M = 0.6 operating condition. The data are presented in terms of Strouhal number since the jet exit diameters differed. Absolute sound pressure levels are referenced to the present jet exit diameter by using the standard area scaling relationship. Finally, a 0.3 m difference in the microphone array radius was compensated for by using the inverse square law decay relationship to convert the data in reference 43 to the equivalent radius used in the present study.

A comparison of the spectra in Figure 14 indicates the spectrum shapes are similar demonstrating that the present jet noise study is typical of other jet noise experiments. The absolute sound pressure levels are, however, different between the two experiments. While the source of the difference was not clear, conclusions of the present study were not impacted. This is because the jet noise shielding phenomenon is independent of the specific spectrum shape or amplitude and instead represents a relative level change due to propagation through the adjacent jet.

An evaluation of the spectra shown in Figure 14 also indicates an anomoly at high frequency in the present experiment. Absolute sound pressure levels in the 31.5 kHz and 40 kHz bands fall outside the general spectrum shape suggested by the dashed line. Since this exception occurred in a frequency range with a large signal-to-facility-background-noise ratio, the source of this deviation was considered to be the jet itself. While the precise origin of this noise was not identified, it did not impact the present study since data at frequencies above 20 kHz was not used to develop conclusions. Humidity effects at these high frequencies were significant relative to the procedure used for experimentally isolating the jet shielding effect (see

Appendix B). Consequently, data above 20 kHz could not be used for quantitative interpretations of the jet shielding phenomenon.

Shock Free Operating Conditions - The supersonic shock-free jet operating pressure was determined by minimizing the strength of the potential core shock cells. A three step process was used to identify the correct operating pressure. First, Schlierern visualization was used to define the pressure range where the strong shock cells associated with over-expanded or under-expanded flow disappeared. Second, static pressure surveys along the jet centerline were used to further isolate the shock free operating point. In this case the upstream total pressure was adjusted to minimize the small static pressure changes associated with weak shocks and expansion fans which occur at slightly off-design operating conditions. Finally acoustic measurements were conducted at $\psi = 90°$ to the jet to check for shock associated noise.

Relative to the acoustic measurements narrowband spectra were used to confirm the absence of shock associated discrete tones. Figure 15 shows a typical spectrum for the shielding jet nozzle operating at $M = 1.46$ with $T_o = 300°K$. The measurement was obtained at a polar angle of $\psi = 90°$ where screech is easily detected in comparison to angles close to the jet axis. No evidence of screech was observed in this spectrum or any of the supersonic spectra examined.

One third octave band measurements were also used to search for increased broadband noise due to accelerated mixing of the jet flows by the shock cells. Although the 1/3 octave band levels indicated a minimum noise level as a function of upstream nozzle pressure, the acoustic sensitivity to operating pressure adjustments was weak compared to changes in the jet centerline static pressure. Consequently, the final criterion used to select the upstream shock free operating pressure was based on minimizing the jet centerline static pressure variations (an example is provided in the section titled Aerodynamic Measurements).

AERODYNAMIC MEASUREMENTS

Objective and Approach

The objective of the aerodynamic measurements was to define the axial location at which the dual jet merging occurred. A knowledge of this merging distance was required to assist interpretation of acoustic results. Close to the nozzles, the jets were expected to develop independently. Further downstream merging was expected with the location of merging depending on jet spacing, and possibly Mach number or temperature.

A secondary objective of the aerodynamic measurements was to establish that the jet flow fields exiting from the model nozzles initially developed as standard turbulent jets. In most previous acoustic studies of jet shielding, such flow documentation was not provided. The present qualification tests were particularly important for the supersonic test conditions where a shock free flow was required from the converging-diverging nozzles.

Mach Number Distributions

Radial Profiles - Jet Mach number radial surveys at sequential downstream axial locations are shown in Figure 16 for a typical test condition. This figure corresponds to a cold (T_o = 300 K), M = 0.6 jet operating condition with the two jets at close spacing (S/D = 2.7). Plotted in Figure 16 is jet Mach number, calculated from total pressure measurements, as a function of normalized radial position (r/D) for various axial locations ranging from the nozzle exit (X = 0) to forty-one diameters downstream. From the figure, merging of Mach number profiles in the gap between the jet centerlines is observed to occur at a position between 4.6 and 9.1 diameters downstream of the exit plane. A more precise definition of the merging location is given subsequently.

Measurements at the same M = 0.6 nozzle exit Mach number but with elevated temperature (T_o = 811 K) show similar trends in Mach number profile development. These results are given in Figure 17. In this case, the jet spacing was smaller (S/D = 2.3) due to differential thermal expansion in the two pipes supplying the nozzles. This difference in spacing is believed responsible for the fuller mid-gap profiles obtained in the hot test at X/D = 9.1. Further downstream (X/D = 18.3), where initial spacing effects would be expected to have less influence, the cold and hot profiles are similar. Results suggest that stagnation temperature changes at constant Mach number conditions do not affect jet merging length.

Figures 18 and 19 show that isothermal and hot jet Mach number distributions at a supersonic exit condition (M = 1.46) were similar, as observed in

subsonic tests. Differences between profiles in Figures 18 and 19 tend to be within several percent of exit Mach number except for station X/D = 18.3 where a ten percent difference occurs. The reason for the change in profile shape at this station is not known. The location of jet merging is observed to occur between 4.6 and 9.1 diameters downstream of the exit as in the previously discussed subsonic 0.6 Mach number case.

Potential Core Length - In addition to the radial profile measurements, jet centerline surveys were performed to document the aerodynamic behavior of the jets. A typical centerline Mach number distribution is given in Figure 20a, with an enlargement of the potential core region provided in Figure 20b. For this subsonic test case, the potential core length, where the flow is basically inviscid, is observed to extend to approximately five nozzle diameters. Figure 21 shows this length increased monotonically with increasing Mach number as would be expected. As in the case of the radial profiles, the data show that a change in jet temperature ratio from unity to 2.7 had no measurable effect.

Jet Merging Length - The distance from the nozzle exit plane at which jet interaction occurs, termed the jet merging length, can be defined based on Mach number or temperature measurements. Since the thermal spreading rate of jets exceeds the momentum spreading rate, this length varies with the definition employed. Here, merging length will be taken as the distance from the nozzle exit plane to the axial station at which a measureable Mach number is obtained. For this measurement, a traverse is performed along a line parallel to and midway between the two jet centerlines. Typical traverse results are shown in Figure 22 for unheated, 0.6 Mach number jet with various initial jet spacings. As shown in the figure, an abrupt increase in Mach number from zero occurs at various distances depending on jet spacing, thereby allowing merging length to be determined accurately. Based on the summary plot in Figure 23, the merging length for isothermal jets was found to be relatively independent of jet exit Mach number and to increase linearly with jet spacing. Heated jet measurements were not obtained although results presented above suggest that temperature effects would be small. Based on the data of Figure 23, the merging length can be taken as approximately three times the lateral jet spacing.

The above described use of Mach number profiles to determine the jet merging length may appear inappropriate when compared to using absolute velocity profiles. Admittedly, the hot jet will have a higher local velocity than the cold jet at corresponding radial locations for the same Mach number. However, the procedure for determining merging location is not based on absolute velocity but on the asymptotic extrapolation of the data points presented in the profiles of Figure 22. The axial intersection of the extrapolated points is expected to be the same whether Mach number or velocity

profiles are employed. Mach number profiles, which require only total
pressure surveys, were selected to simplify the experimental determination of
the merging location. In comparison, velocity profiles require both total
pressure and total temperature surveys to deduce local velocities.

Total Temperature Distributions

Jet total temperature distributions were measured to establish that nor-
mal heated jet conditions had been achieved. Radial and jet centerline dis-
tributions were measured for an exit stagnation temperature conditon of 811°K
at exit Mach numbers of 0.6, 0.94 and 1.5. Typical radial profiles are given
in Figure 24 for a M_e = 0.6 condition. Based on temperature, jet merging is
observed to occur between the nozzle exit and axial station X/D = 4.6. Com-
parison of these profiles with the results of Figure 23 indicates that the
merging length based on thermal spreading is shorter than that derived from
the Mach number distributions, as would be expected.

Supersonic Flow

Static Pressure and Mach Number Distributions - For supersonic exit con-
ditions, jet centerline static pressures were measured since they provide a
more precise means of establishing shock-free operation than Schlieren flow
visualization. Figure 25 shows the axial static pressure distribution on the
jet centerline for a cold, M = 1.46 operating condition, the Mach number which
minimized the axial pressure fluctuations of the M = 1.5 shock free nozzle
design. The shock cell pressure fluctuations observed at this operating point
were very small (on the order of 8 percent of reference static pressure) and
of the same magnitude as those measured by Seiner and Norum (ref. 41) in
similar "shock-free" experiments. Spacing between shock cells varied from
about 1.4 diameters near the jet exit plane to 0.9 diameters at X/D = 10.

Variations of Mach number on the jet centerline are shown in Figure 26
for the shock free operating point. Parts b and c of this figure represent
enlargements of Part a. Mach number oscillates in the potential core region,
similar to the static pressure variations, due to the weak shock cell struc-
ture.

Flow Visualization - Figure 27 shows a series of 7 Schlieren photographs
obtained at T_o = 300 K and S/D = 2.7 for the converging diverging nozzle set
at different operating conditions. The first photograph shows the dual jet
system with an underexpanded operating condition. The subsequent photographs
show the effect of increasing the upsteam stagnation pressure until the flow
becomes overexpanded. The data is presented as a function of $\beta = (M^2-1)^{1/2}$.

Near the optimal shock free operating point, $\beta = 1.06$, the flow exits the nozzle with a very small jet divergence angle. As the pressure is lowered the divergence increases and diamond shaped shock cells appear in the jet. Even at the smallest jet spacing there appears to be no shock wave interaction between the two jets.

DATA ACQUISITION AND DATA REDUCTION PROCEDURE

The experimental technique for investigating the jet shielding phenomenon involved continuous rotation of the source jet about the shielding jet. This approach documented the directivity pattern changes close to the plane of the two jets, corresponding to the sideline observer in Figure 2. In addition, this method defined the changes at angles corresponding to the observer directly below the aircraft flight path in Figure 2. To quantify the experimental results, the present chapter begins with a summary of the general features of the jet shielding noise reduction mechanism. Based on this discussion a quantitative definition of the shielding phenomenon is formulated. This is followed by a description of the data acquisition and data reduction procedures which were used to assign numerical values to the shielding mechanism.

General Features of Noise Reduction Due to Jet Shielding

The jet shielding phenemonon is represented in a simplified form in Figure 28. The jet closest to the observer is referred to as the shielding jet since it potentially masks the second jet which is referred to as the source jet. To understand the resulting changes in the far field directivity pattern, each jet is considered to be an isolated independent acoustic source operating in the presence of an adjacent flow field. The following discussion, which begins with the source jet, uses the schematic in Figure 28 to illustrate the acoustic wave interactions between two adjacent jets.

Radiation from the source jet impinges on the shielding jet as it propagates towards the observer at a specific sideline angle (Fig. 28a). During the acoustic wavefront interaction with the shielding jet several mechanisms can conceptually result in a noise reduction. First, refraction, reflection, and turbulence scattering of sound to other sideline angles can decrease the noise level sensed at the fixed observer station. It should be noted, however, that since acoustic energy is conserved during these different interaction processes, noise levels must increase at other observer orientations. Benefits achieved at the fixed sideline observer station in Figure 2 may, therefore, create acoustic penalties at other radiation angles. This observation represents the basis for the extensive azimuthal and polar acoustic survey in the present experiment.

The second mechanism which potentially reduces source jet noise involves phasing of the acoustic waves after interaction with the shielding jet. In this case diffracted and/or scattered waves can combine with each other and with the transmitted (refracted) waves to cancel acoustic pressure waves at

the observer station thereby, reducing the noise levels. However, this same phasing mechanism can also increase noise due to wavefront reinforcement.

In summary, the source jet noise changes observed in the common plane of the two jets in Figure 2 are considered to be controlled by redirection of the source jet radiation to other observer angles and phasing of transmitted and diffracted waves. In the limit of total redirection of all acoustic radiation, the source jet would be completely masked and only the shielding jet noise would be sensed by the observer.

With the discussion of the source jet completed, the shielding jet can now be considered (Fig. 28b). Here the radiation pattern is controlled by a) acoustic waves propagating directly from the shielding jet to the observer and b) waves initially radiated towards the source jet. In the latter case, the waves incident on the source jet are reflected and propagate towards the shielding jet where they again encounter the same transmission phenomena described above. Similar to the source jet case, a noise reduction can occur involving a) redirection of the reflected waves, and b) phasing between the direct acoustic radiation (from the shielding jet) and the reflected waves (after diffraction, turbulence scattering and transmission through the shielding jet).

In the limit of total reflection of the shielding jet noise by the source jet and no redirection of this reflected sound, the observer hears a second source with the same strength as the shielding jet. This represents a 3 dB increase in noise relative to the two independent jets in the dual jet system (or a 6 dB difference relative to a single jet). In contrast if the reflection coefficient is zero or all reflected energy is redirected by the shielding jet to other sideline angles the observer senses only direct radiation from the shielding jet.

It should be noted that larger noise reductions or noise increases are possible if the two jets contain coherent noise source regions. In this case, phasing between the source regions results in cancellation or reinforcement of acoustic wavefronts, thereby, accentuating the effects of shielding. However, coherence between the jets requires the jet flows to be acoustically coupled, a condition which is not expected for the random noise distributed source regions of the present dual jet geometry. Acoustic coupling, is possible with a supersonic dual jet flow with screech present. Since this operating condition is outside the scope of the present study, noise reductions or increases due to phasing between coherent source regions of the two adjacent jets is not considered to be an operative physical phenomenon.

Quantitative Definition of Shielding Effect

A quantitative definition of the jet shielding phenomenon can now be formulated based on the fundamental noise reduction mechanisms described in the previous subsection. The formulation employs the under-the-wing engine configuration shown in Figure 2 although the results apply in general to side-by-side engine geometries.

In the absence of shielding, the observer senses acoustic radiation from each jet exhaust flow. Considering the individual jet flows to be incoherent sources (no acoustic/flow coupling), the measured total power spectral density, $\overline{p_T^2}$, considering adjacent engines is given by $\overline{p_T^2} = \overline{p_1^2} + \overline{p_2^2}$. Here p_1^2 and p_2^2 are the individual acoustic power spectral density contributions which are a function of f, R, θ and ψ.

Simplifications, such as assuming a geometric far field condition for the observer, would replace the different engine-to-observer distances, R_1 and R_2 in the expression for $\overline{p_T^2}$, with a common distance. However, such differences in distance are retained for the purpose of generality since aircraft may be in close proximity to sideline observers during ground operations where the assumption of $R_1 \neq R_2$ does not apply. Also, by retaining the specific distance dependence, the equation for $\overline{p_T^2}$ duplicates the present experimental test geometry. Experimentally, geometric far field conditions could not be achieved for the largest dual jet spacing corresponding to S/D = 8.1 or S = 36 cm. (A further discussion is given in the next subsection.)

With shielding operative, $\overline{p_T^2}$ is replaced by $\overline{p_D^2}$. The resulting change in noise relative to two independent jets is then defined by the expression

$$\Delta SPL = 10\log_{10} \frac{\overline{p_D^2}}{\overline{p_1^2} + \overline{p_2^2}} \tag{35}$$

The parameter ΔSPL can also be defined relative to a single jet. In this case the denominator in Equation 35 is replaced by the mean-squared sound pressure level from a single jet. Ideally, for large jet-to-observer distances $\overline{p_1^2} = \overline{p_2^2}$ so that only a single measurement is needed for the denominator. However, due to the differences in jet-to-observer (microphone) distances in the present study, $\overline{p_1^2} \neq \overline{p_2^2}$. In this case the single jet

reference level must be represented as the average of the dual independent jets, i.e., $1/2 \left(\overline{p_1^2} + \overline{p_2^2} \right)$. Relative to the single jet, Equation 35 becomes

$$\Delta SPL = 10 \log_{10} \frac{\overline{p_D^2}}{\frac{1}{2} \left(\overline{p_1^2} + \overline{p_2^2} \right)} \tag{36}$$

This single jet reference level was selected in the present study since it represents the minimum noise level possible when one jet in the incoherent dual jet system is totally shielded (assuming phasing is not operative). In this case, $\overline{p_D^2} = \overline{p_1^2}$ and $\Delta SPL = 0$ so that relative to a single jet, the dual jet generates the same noise level. On the other hand, with shielding inoperative, $\Delta SPL = 3$. The 3 dB change in sound pressure level now indicates that the dual jet system is perceived as two independent jets in comparison to the single jet.

Acoustic Data Acquisition and Data Reduction Procedure

Single Jet Reference Level - To determine the shielding parameter ΔSPL from the experimental data, each test condition was investigated with a) the dual jet configuration and b) a single jet operating at the same flow condition. The latter measurement was used to synthesize the dual independent jet configuration needed in the denomenator of Equation 36 (see Appendix C for details). Due to the axial symmetry of the single-jet directivity pattern, the acoustic survey was reduced to one data record. In this case the shielding jet was used in conjunction with the fixed microphone array. During this measurement the source jet air supply line was terminated with a cap confining the flow to the shielding jet. To avoid converting the test arrangement from single to dual jet configurations at each test condition, all single jet measurements were conducted after completion of the dual jet study.

It should be noted that early efforts to change the operating configuration using a butterfly valve installed in the source jet air supply line downstream of the common plenum were not successful. Noise generated by the valve in addition to a small pressure loss across the valve resulted in background noise and a significantly dissimilar jet operating condition. The use of two separate air supply systems was also initially considered during the facility hardware design phase but the potential dissimilar operating conditions resulted in selection of the common plenum shown in Figure 8.

Corrections to Acoustic Data - A jet noise velocity scaling law was also applied to the data to correct for small variations in jet exit pressure and temperature as the jet rotated. These minute changes occurred as the control valve supplying the common plenum responded to the gradual decrease in the upstream facility pressure during the approximately 8 minute data acquisition phase. Details of the correction procedure are discussed in Appendix B. Such corrections were not necessary for the supersonic data since the test time was short (continuous source jet rotation was not applied). Also the operating pressures were held to a tolerance of ±0.15 psi to avoid screech tones.

Although relative humidity was monitored in the anechoic chamber during each test condition, corrections for humidity effects were not applied to the acoustic data. This decision was based on the detailed discussion presented in Appendix B.

EXPERIMENTAL ASSESSMENT OF DUAL JET SHIELDING

Objective

The objective of this phase of the study is to experimentally assess the acoustic shielding of jet exhaust noise by an adjacent jet flow field. The shielding mechanism is investigated using a dual jet system with variable spacing between the parallel jet flows. Tests performed over a range of jet Mach number, jet temperature, and jet spacing determine the shielding sensitivity to isolated changes of each parameter.

Several evaluation procedures are employed in the assessment of the experimental data. First, changes in the dual jet noise spectrum shape, plotted as a function of Strouhal number, are examined at selected radiation angles as the test conditions vary. This approach provides a simple evaluation of the shielding effectiveness relative to the jet noise spectrum. In addition, changes in azimuthal or polar directivity shape are examined at fixed Helmholtz numbers. (The Helmholtz number, kD, is defined as the product of wavenumber and frequency). The objective in this case is to assess the jet noise reduction (due to shielding) and jet noise increase (due to reflections) over the azimuthal range $0° \leqslant \theta \leqslant 180°$. Finally, the complex interdependence of jet noise source frequency and radiation angle is evaluated in a series of sound pressure level contours plotted as a function of Strouhal number versus azimuthal angle for various polar angles. These results provide guidelines for application of the shielding concept as a jet noise reduction technique.

In each of the above evaluations, the effect of shielding is defined as the difference between the sound pressure levels generated by the dual jet configuration and a single jet operating at the same flow condition. The single jet is selected as a reference since it represents the minimum noise level when one jet in the dual jet system is totally shielded (See section titled Data Acquisition and Data Reduction Procedure for a discussion of the shielding mechanism and the minimum noise level).

The experimental results described in the present section also form the basis for the critical evaluation of the jet noise shielding theory. However, prior to comparing experimental and predicted shielding effects, the point source/single jet combination which best models the dual jet geometry must be selected. Based on this selection, theoretical predictions are presented for comparison with the dual jet random noise distributed source field.

It should be noted that evaluation of the shielding effect as a function of Strouhal number and Helmholtz number represents evaluating the phenomenon from two different, but important, viewpoints. The first approach identifies the frequency domain of the jet noise generation for which shielding provides

a noise reduction. The second viewpoint addresses only the dependence of the propagation phenomenon on the acoustic source frequency and the shielding jet characteristics. This latter approach is necessary for theory-experiment comparisons and represents an assessment of the propagation phenomenon.

Spectrum Dependence on Isolated Parameters

The Shielding Effect - To show the general effects of introducing an adjacent shielding jet on the source jet radiation, results are presented for 1/3 octave band spectra for four cases. Two of the conditions correspond to the dual jet at an observer azimuthal angle of $\theta = 90°$ and $180°$. For comparison purposes the two remaining conditions correspond to single jet measurements synthesized according to the denominator of Equation 36, at the same azimuthal angles. Here the $\theta = 90°$ case represents the dual jet orientation associated with maximum possible noise reduction since the noise from the source jet is masked by the shielding jet. On the other hand, the $\theta = 180°$ dual jet measurement conceptually represents the orientation for maximum noise radiation since the observer senses sound from both jets. (Note that with identical flows from each nozzle in the dual jet system, the acoustic radiation pattern is expected to be symmetric about $\theta = 90°$. Thus, either $\theta = 0°$ or $180°$ can be used in this evaluation.)

The noise radiation dependence on these different dual-jet orientations can now be illustrated using the spectra in Figure 29a. The test conditions associated with each spectrum in this figure correspond to $M = 0.6$, $T_0 = 300°K$, $S/D = 8.1$ and $\psi = 40°$. Sound pressure is presented in terms of 1/3 octave band levels. Indicated values are obtained by averaging the azimuthal directivity data (to be described shortly) within a $\pm 5°$ region centered at $\theta = 90°$ or $180°$. Frequency dependence is given in terms of Strouhal number to permit comparison with other jet operating conditions.

The effectiveness of the shielding mechanisms in the common plane containing the two jets is determined from the parameter, $\Delta SPL(\theta = 90°)$, which represents the difference between the dual jet $\theta = 90°$ measurement and the single jet measurement in Figure 29a. The calculated values in Figure 29d show that near the spectrum peak, ΔSPL is approximately 2.5 dB. Jet shielding appears, therefore, to be small. In contrast, at high Stouhal number, $\Delta SPL(\theta = 90°) \approx 1.5$ dB indicating the shielding mechanism is operative.

These results describe the effectiveness of masking one jet when the observer is in the common plane of the dual jet system. However, an observer at an orientation normal to this common plane ($\theta = 180°$) senses the degree to which the dual jet system operates as two independent source jets. This feature is determined from the parameter, $\Delta SPL (\theta = 180°)$. Based on Figure 29d, this parameter is approximately 4 dB throughout the acoustic spectrum. Since two non-interacting jets would give $\Delta SPL = 3$ dB, it appears that excess noise is radiated at $\theta = 180°$.

One potential source of the excess jet noise at θ = 180° is the aerodynamic interaction of the two jets. In concept, such an interaction could alter the acoustic source distribution by creating a merged jet flow field. But, aerodynamic measurements for this test condition demonstrated (Fig. 23) that the dual jet merger is delayed until x/D = 23. Source alteration would, therefore, be controlled by acoustic source regions beyond this axial station. Based on directional microphone measurements (ref. 44) acoustic sources at x/D ≥ 23 contribute primarily to the spectrum range St ≤ 0.1. Since the 4 dB spectrum difference in Figure 29d occurs over the range 0.1 ≤ St ≤ 10 aerodynamic merging is not expected to be the origin of the observed excess noise. (For smaller jet spacing, source alteration was postulated to be an effective noise mechanism as described in the subsection titled Lateral Spacing Effects).

In the absence of source alterations, a possible explanation for the excess noise at θ = 180° is the reflection and turbulence scattering of sound from one jet by the flow field of the adjacent jet. Support for this postulated mechanism is provided by detailed azimuthal surveys which indicate a consistent trend of excess noise when the far field microphone array is approximately normal to the plane of the dual jet system (θ = 0° or 180°). Furthermore, excess noise has been observed in previous experimental studies as will be described shortly. Finally, the present analytical model for the dual jet shielding mechanism predicts ΔSPL noise levels exceeding 3 dB at large azimuthal angles as described in theory-experiment comparisons in the following subsections.

Mach Number Dependence – The sequence of differential spectra shown in Figure 29d, 29e, and 29f can now be used to establish the effect of Mach number on the dual jet shielding process. Similar to the approach developed in the previous subsection, conclusions are drawn from comparison of single jet and dual jet spectra at θ = 90° and 180°. In each case the polar angle corresponds to ψ = 40°. Data is presented only for the largest jet spacing test condition (S/D = 8.1) to isolate the Mach number effect.

Measurements described here are also limited to unheated jet flows with the total temperature (T_0 = 300°K) approximately equal to the ambient air temperature, T_a. By confining the present evaluation to unheated jets, changes due to temperature gradients across the heated jet shear layer are minimized, thereby isolating the Mach number discontinuity dependence. This approach was considered reasonable since the ratio of jet static temperature-to-ambient temperature, T_s/T_a, assumed values of 0.94, 0.85 and 0.7 for the three Mach numbers M = 0.6, 0.94, and 1.46. Based on the present analytical model, the shielding mechanism would not be sensitive to these temperature discontinuities at the jet shear layer interface.

The effect of Mach number on jet shielding can now be determined by comparing ΔSPL(θ = 90°) for the sequence of spectra shown in Figure 29. The

first of the required figures (Fig. 29d) was evaluated in detail in the previous subsection. Using this result as a reference the trend in Figure 29 indicates that shielding in the plane of the jet becomes more effective as Mach number increases. For example near the spectrum peak, ΔSPL decreases from approximately 2.5 dB to 1.25 dB as Mach number changes from M = 0.6 to 0.94. However, with an additional increase in Mach number to M = 1.46 the shielding effect remains constant. Similar trends occur at Strouhal numbers below the spectrum peak, with the largest changes again occurring between M = 0.6 and 0.94. In general, the onset of shielding shifts to lower Strouhal numbers as Mach number increases.

While shielding effectiveness increases with Mach number near the spectrum peak (and at lower Strouhal numbers), changes at high Strouhal number are weaker. A comparison of the sound pressure level difference at St = 2 indicates an improvement in shielding effectiveness of, at most, 0.25 dB between M = 0.6 and 1.46. This change in ΔSPL is small because the magnitude of the noise reduction approaches the maximum expected value (ΔSPL = 0 dB in the absence of phasing) at M = 1.46 since ΔSPL is approximately 1.25 dB.

The degree to which the dual jet system is perceived as two independent source jets at θ = 180° as Mach number increases can also be determined from Figure 29. Here ΔSPL(θ = 180°) maintains a consistent value of approximately 4 dB as Mach number is varied. Since ΔSPL exceeds the 3 dB value associated with two independent jets, this dual jet radiation corresponds to excess noise. Similar to previous discussions, the origin of this excess noise is postulated to be the reflection and scattering of sound from one jet by the adjacent jet. This mechanism is shown to be Mach number independent based on Figure 29.

Temperature Dependence - Evaluation of the heated dual jet data following completion of the test program indicated an anomolous acoustic attenuation in the experimental measurements. Sound pressure level differences between the dual jet and the single jet resulted in negative values for ΔSPL in the common plane of the dual jet system. This efect is best explained with the azimuthal directivity data discussed in a following subsection. Interpretations regarding the influence of temperature on jet shielding can, however, still be postulated from the measured data and these observations are presented as part of the azimuthal directivity discussion.

Lateral Spacing Dependence - The influence of jet spacing is shown by the series of spectra in Figure 30 as S/D varies from 8.1 to 3.1. Here Mach number and jet temperature are held fixed at M = 0.94 and T_0 = 300°K, while the polar radiation angle corresponds to ψ = 40°. Note that the minimum S/D value in this sequence is slightly larger than the spacing conditions tested during the aerodynamic study where values of S/D = 2.7 and 2.3 were employed. The difference is due to the addition of a clamping mechanism during the acoustic

study to retain the source jet at a constant radius as it rotated. Such hardware was not required for the stationary aerodynamic measurements permitting a closer jet spacing.

Relative to the $\theta = 90°$ measurement plane, shielding is insensitive to spacing changes at all Strouhal numbers as S/D decreases from 8.1 to 5.5. For example, at Strouhal numbers above the spectrum peak, ΔSPL ($\theta = 90°$) is consistently 1.25 to 1.5 dB. In contrast, at low Strouhal numbers, shielding is weaker with ΔSPL = 2 or 3 dB. Near the spectrum peak, shielding remains constant with ΔSPL = 2.5 dB approximately.

The spectrum at $\theta = 90°$ for the closest spacing, S/D = 3.1, is similar to the S/D = 8.1 test condition at high Strouhal number. The only exception is the Strouhal range below St = 0.4. In this region, higher absolute sound pressure levels occur with ΔSPL even exceeding 3 dB. This indicates an increase in noise in the common plane of the dual jets for small spacing. It is postulated that for the close spacing condition, changes in acoustic source distributions are responsible for the noise increase. This is based on directional microphone measurements which show the acoustic source region responsible for the spectrum range below St = 0.4 is located downstream of X/D = 8. Based on Figure 23, jet flow merging begins at X/D = 7. Consequently, source alterations are considered to be the origin of the increased noise at low Strouhal number and small S/D.

Phasing was also considered to be a possible explanation for the noise increase in the common plane at St < 0.4. However, in the St range, differences in propagation paths between diffracted and transmitted wavefronts were small in comparison to the acoustic wavelength. Consequently, phasing was postulated to be weak in this instance. However, other examples of noise dependence on phasing between the source jet and shielding jet were observed and will be described later.

For the $\theta = 180°$ orientation, the sequence of spectra in Figure 30 show a small decrease in excess noise as spacing changes from S/D = 8.1 to 5.5. This trend, however, is reversed by a 2 dB increase in ΔSPL near the spectrum peak as spacing changes to S/D = 3.1 indicating significant excess noise. In general the value of ΔSPL exhibits excess noise at $\theta = 180°$ irrespective of the spacing.

Summary and Evaluation of Shielding Effect on Jet Noise Spectrum – For non-interfering dual jet flow conditions, shielding is operative in the common plane of the dual jet system with the largest effect occurring for increasing subsonic Mach numbers. Simultaneously, increasing Mach number shifts the onset of shielding to lower Strouhal numbers.

Specifically, for low Mach numbers (M = 0.6) shielding provides a 1.5 dB noise reduction but only at Strouhal numbers above the jet noise spectrum peak. As Mach number increases to M = 0.94, the onset of shielding occurs at lower frequencies so that approximately a 2 dB noise reduction exists at the jet noise spectrum peak. However, a further increase to M = 1.46 has little effect on the jet noise reduction with at most a 0.5 dB improvement in shielding effectiveness below the spectrum peak.

Jet spacing has little effect on jet noise shielding in the common plane of the dual jet system as S/D decreases. The only exception occurs at the closest spacing of S/D = 3.1 and Strouhal numbers below the jet noise spectrum peak (St < 0.4). In this case, acoustic source alteration due to aerodynamic merging of the dual jet flow field increases the noise radiation by approximately 1 dB.

Observers situated at 90° to the common plane of the dual jet system, experience excess noise relative to the noise radiated by two independent jets at the same orientation. The excess noise level is approximately 1 to 1.5 dB above the noise level of the independent jets and is essentially invariant with Mach number. The excess noise is also independent of spacing for S/D values of 8.1 and 5.5 but for the closest spacing a significant increase occurs near the spectrum peak. The origin of this additional noise is postulated to be the reflection and scattering of sound from one jet by the adjacent jet for large spacing and source alteration at the closest spacing.

Azimuthal and Polar Directivity

Objective and Approach - The previous discussion of the shielding mechanism employed spectra measured at two polar angles, θ = 90° and 180°, while ψ was fixed at 40°. Although important conclusions regarding the shielding effectiveness were developed, the dual jet sound pressure level dependence on azimuthal and polar angle was not defined in detail. The objective of the following subsection is to establish the directivity dependence on each of the parameters evaluated experimentally during the present study. In addition, theoretical predictions based on different analytical combinations of the point source/single jet geometry used to represent the dual jet will be compared with measurements.

General Features of Azimuthal Directivity - Prior to evaluating the directivity dependence on each parameter, general features of the radiation pattern for the dual jet system will be established. Figure 31 shows the sound pressure level measured at ψ = 20° for the M = 0.6, T = 300°K, S/D = 8.1 test condition. The resulting data curve corresponds to the 200° rotation range of the dual jet system shown in Figure 7. The measurement, presented for the 1/3 octave band centered at 4 kHz (Helmholtz number, kD = 3.22) is normalized by the synthesized single jet amplitude at θ = 90°.

Based on Figure 31, the directivity pattern is symmetric about θ = 90°. This result is expected since each jet in the dual jet system operates at the same test condition. Figure 31 also shows that the local maxima can occur within the 0° ≤ θ ≤ 180° azimuthal range. In particular, the maxima at 30° and 145° were not expected from previous studies which were predominantly confined to measurements at θ = 90° and 180° (or 0°). This is because the earlier studies assumed the directivity pattern varied monotonically from a minimum at θ = 90° to a maximum at θ = 0° or 180° (the maximum was based on the viewpoint that θ = 0° or 180° corresponded to the orientation for which the dual jet system radiated as two independent jets). Consequently, measurements were limited to a few azimuthal angles and the directivity details associated with the dual jet radiation field were not evident.

The local maxima in Figure 31 demonstrates that the dual jet system interacts acoustically at angles outside the shielding regime. Thus, in addition to shielding at θ = 90°, excess noise occurs at other angles. The origin of the excess noise will be shown shortly, using the analysis, to be due to acoustic reflections from the adjacent jet (scattering by turbulence is also a valid mechanism although the analysis does not model this phenomenon).

The effect of reflections is illustrated using geometric acoustics in the sketch of Figure 32. Here, equal angles of incidence and reflection result in the observer sensing reflected radiation in addition to direct radiation from the source jet when θ = 135°. Similarly, reflections of the shielding jet radiation by the source jet (not shown) may result in additional noise perceived at the observer station. (However, as will be indicated shortly, this latter interaction is a small contribution to the measured noise due to the 1/3 octave band analysis procedure). The total sound field, therefore, contains excess noise when compared with the direct radiation from the two acoustically noninteracting jets. These acoustic interaction features will be discussed farther in the following subsections.

It should be noted that the symmetry of the excess noise peaks in Figure 31 confirms the anechoic characteristics of the facility. A non-anechoic environment would create a non-symmetric directivity pattern as the source jet is rotated. Thus, the local maxima are not created by reflections within the anechoic chamber.

Verification that the measured peaks at θ = 30° and 145° are a direct consequence of the shielding jet is given by the azimuthal directivity plots in Figure 33a. Here the azimuthal range is limited to 80° ≤ θ ≤ 190° since the radiation patterns have been shown to be symmetric about θ = 90°. Measured absolute sound pressure levels are presented for the same test condition shown in Figure 31. Two data sets are indicated corresponding to a) the dual jet system, and b) the isolated source jet with the shielding jet capped. The constant sound pressure level associated with the isolated source jet

directivity pattern confirms that the local maxima for the dual jet system are created by the presence of the shielding jet. Additional directivity patterns are given in Figure 33b for the source jet alone at frequencies spanning the acoustic spectrum range. These curves demonstrate that the source jet rotation is not the origin of the local maxima.

The constant source jet directivity patterns in Figure 33b also confirm the simple point source assumption used in the distance correction applied to the term in the denominator of Equation 36. Specifically, the correction accounted for the source jet-to-microphone distance changes which occurred as the source jet rotated during the dual jet study. The correction procedure modelled the two jets as point sources centered at the nozzle exit plane. To check this point source approach, measured sound pressure levels for the single jet at each azimuthal angle in Figure 33 were converted to a common source distance corresponding to the 3m radius used for the microphone array. This simple conversion employed the same inverse square law decay relationship used in calculating the synthesized single jet reference levels (See Appendix C). If this approach appropriately modeled the distributed source region of the actual jets, then a constant sound pressure level would be expected during the single jet azimuthal rotation (an amplitude change of 0.9 dB would occur without this correction for the S/D spacing condition shown in Figure 33). The constant amplitudes in Figure 33 demonstrate that the point source representation adequately compensates for any distance changes occurring in the experimental data.

Figure 33b also shows that, within the accuracy of the measurements, each microphone continues to sense the same polar directivity pattern as the source jet rotates. This is critical since jet noise directivity patterns are known to change rapidly near the jet axis. In the present experiment, the fixed microphone array centered on the shielding jet could sense different source jet polar radiation information as θ varies. The impact on the combined dual jet radiation could lead to erroneous directivity information as illustrated schematically by the different acoustic rays, ψ_1 and ψ_2, in Figure 34. But, the constant sound pressure levels for the single jet in Figure 33b establishes that directivity pattern changes have a nominal impact.

Selection of Analytical Model Simulating Dual Jet Geometry - To permit assessment of the theoretical predictions relative to the shielding effects described in the previous subsection, the appropriate analytical model which best represents the dual jet geometry must first be selected. The issues controlling the selection process are illustrated in Figure 35 where the dual jet configuration in Part (a) is modeled as a sum of the separate point source/single jet geometries shown in Part (b). In the case of the observer-shielding jet-point source configuration the point source rotates about the shielding jet. On the other hand, for the observer-point source-reflecting jet geometry, the reflecting jet rotates about the point source. Assuming the

acoustic point sources representing each jet are incoherent, superposition of the analytical predictions for the separate geometries in Part (b) might be expected to provide the best simulation of the dual jet problem. It should be noted that the shielding jet and reflecting jet are not noise sources in the separate analytical models.

Test Case – Predictions using this superposition model are presented in Figure 36 for a selected test case. Here, the input parameters correspond to the experimental test condition presented in Figure 33a. Calculated sound pressure levels are normalized relative to the direct radiation from each acoustic point source. This normalization, which gives ΔSPL, is identical to the single jet reference level used for the experimental data. The only exception is that the theory is a geometric far field model which is insensitive to the different source-to-observer distances in Figure 35b. Consequently $\overline{p_1^2} = \overline{p_2^2}$ in Equation 36. In contrast, these differences in distance influenced the experimental data and resulted in normalizing the measured dual jet data by the synthesized average single jet data which is a function of θ. Once the normalization is completed distance effects are removed from the measured data permitting direct comparison with the separately normalized prediction.

Locating the shielding jet between the point source and the far-field observer, as illustrated in Figure 35b, results in predicted ΔSPL levels given by Curve 1 in Figure 36a. Here negative sound pressure levels occur near $\theta = 90°$ indicating that shielding is operative. However, near $\theta = 130°$ noise levels increase due to reflection of sound in the direction of the observer as illustrated earlier in Figure 32. In this case, the phasing between direct and reflected point source jet radiation creates reinforcement of the acoustic wavefront. This increases the sound pressure level relative to the direct radiation from the source alone.

A further increase of azimuthal angle again results in negative ΔSPL values near $\theta = 140°$. Negative values are now considered to be due to cancellation between the direct and reflected wavefronts. Without phasing to create a cancellation of acoustic pressure wavefronts such a minimum cannot occur.

Reversing the above desired jet and acoustic source positions gives Curve 2. Positive ΔSPL values now occur at $\theta = 90°$ due to the in-phase superposition of the direct and reflected radiation. In contrast, negative values exist at other angles due to cancellation of the wavefronts.

The total predicted field sensed at the observer station is given by Curve 3 in Figure 36a which is obtained by mean-square superposition of Curves 1 and 2. Assessment of the resulting superposition analytical model is based

on comparison with the experimental data also shown in the same figure.
Measured results show reasonable agreement with theory near the common plane
of the dual jet system. Also, the experimentally observed increase in ΔSPL
which begins near θ = 110° and the excess noise peak near θ = 130° are calcu-
lated. Finally, the oscillatory features at larger azimuthal angles are
predicted. However, it should be recognized that the random distributed
source characteristics of the actual dual jet geometry smooth out the oscilla-
tory features in comparison to the analytically predicted details.

Frequency or Helmholtz Number Sensitivity - While the good compari-
sons in Figure 36a suggest closure of the theory-experiment assessment, the
issue of Helmholtz number (or frequency) sensitivity remains to be addressed.
This is important since phasing between direct and reflected acoustic wave-
fronts has been incorporated in the analytical model. Figure 37a evaluates
the predicted sensitivity by presenting ΔSPL curves for frequencies within the
1/3 octave band centered at f = 4 kHz or kD = 3.22. The large variation in
ΔSPL values within the 1/3 octave band shows that the analytical model is
highly sensitive to Helmholtz number. In particular, the good agreement
between theory and experiment in Figure 36a must, for the moment, be regarded
as coincidental.

Gerhold (Ref. 18) did not report the above described Helmholtz sensi-
tivity. Consequently, conclusions regarding the absolute magnitude of his
predicted directivity patterns must be carefully evaluated. While his calcu-
lated results are numerically correct, Figure 37 indicates that small changes
in Helmholtz number give dramatically different results.

The origin of the frequency dependent variations near θ = 90° was traced
to the observer point-source reflecting-jet geometry shown in Figure 35b.
This is demonstrated in Figure 38a where predictions, for the individual point
source/single jet geometries represented by Curves 1 and 2 in Figure 36a, are
presented over a frequency range which spans the 1/3 octave band centered at 4
kHz. The calculations in Figure 38a are confined to θ = 90°, ψ = 40° as the
frequency is varied. The observer-jet-source curve (No. 1), which represents
the shielding effect, varies monotonically. In contrast Curve 2 displays the
oscillatory features observed in Figure 37. These different far field radia-
tion characteristics continue to exist at all frequencies as indicated by
Figures 38b and 38c. (Figure 38c shows only Curve 1). An important observa-
tion from Figure 38c is that noise reduction due to shielding is non-existent
at low frequencies.

Predictions Based on 1/3 Octave Bands - The above described oscilla-
tory nature of the calculated ΔSPL level complicates the comparison of
theoretical calculations with experimental data. A possible solution to this
problem is to integrate the predicted spectrum to give 1/3 octave band predic-
tions similar to the measured data. The integrated result is then normalized

by the bandwidth which is shown in Figure 38a for the 4 kHz test case. Based on this approach, the discrete tone calculation in Figure 36a is replaced by the 1/3 octave band prediction in Figure 36b. A comparison of Curve 2 in each calculation shows large differences. (On the other hand there are only small differences for Curve 3 with the exception of the $\theta = 90°$ prediction and the minima at large azimuthal angles).

The apparent small change in Curve 3 between Figures 36a and 36b is coincidental. As indicated by Figure 38a, the frequency integration range extends over one cycle of the period for Curve 2. The integrated result for $\theta = 90°$ (ΔSPL = 1.7dB) is within 0.4dB of the discrete tone prediction (ΔSPL = 1.3dB) at f = 4 kHz. If the frequency integration range is shifted so as to center it at 4.3 kHz, the same integrated result of ΔSPL = 1.7 dB is obtained since the oscillatory feature of Curve 2 is periodic. But the discrete tone calculation, in this case, gives a different value of ΔSPL = 2.5 dB. Furthermore, increasing or decreasing the filter bandwidth gives a different integrated result.

The above observations provide guidance on the application of the discrete tone acoustic source model for experiments involving a random noise source. If acoustic measurements are obtained with a large bandwidth filter, then application of the discrete tone model will require calculating an integrated spectrum which is then normalized by the measurement bandwidth. For the example given in Figure 38 this represents calculating the shielding effect within the indicated 1/3 octave bands. This appoach is primarily required for the observer-source-jet geometry represented by the cyclic variations in Curve 2 of Figure 38b. In contrast the observer-jet-source geometry can be approximated by the calculated ΔSPL at the 1/3 octave band center frequency.

Final Selection of the Analytical Model - Implementing the 1/3 octave band calculation involves long computing times since the discrete tone calculation must first be performed with small frequency increments over the complete acoustic spectrum. This problem is evident in Figure 38b where numerous cycles of Curve 2 must be calculated before the integrated ΔSPL value can be determined. Due to computing time constraints during the present study, the following simplification was employed to circumvent these difficulties. Based on Figure 38a, the integrated value of ΔSPL associated with the 1/3 octave band calculation is comparable to the average ΔSPL value for one period of the oscillations in Curve 2. Furthermore, the average value is ΔSPL (average) = 0 dB as indicated by the ΔSPL value for Curve 2 at $\theta = 90°$ in Figure 36b. This approximation of ΔSPL (average) = 0 dB over the 1/3 octave band range continues to hold over a large of azimuthal angles as indicated by visually examining the predictions for Curve 2 in Figures 39a-39e and Curve 2 in Figure 36b. The only exceptions occur over a small angle range between $\theta = 160°$ anb 180° as indicated in Figure 36b.

While the above observations are based on predictions for Curve 2 at low frequencies similar results are expected at high frequencies. For example, at 20 kHz (Figure 38b) six cycles of the ΔSPL function occur within the associated 20 kHz 1/3 octave band. In this case ΔSPL (average) normalized by the filter bandwidth will again give, 0 dB.

Application of the above argued approximation ΔSPL = 0 dB for 1/3 octave bands is equivalent to removing the reflecting jet in the lower portion of Figure 35b. The dual jet configuration is then modeled by the observer-shielding jet-point source and observer-point source geometries shown in Figure 35c. Linear summation of sound pressure levels associated with these two geometries results in the predicted frequency dependence given by Curve 4 in Figure 39. Previous oscillatory features associated with Curve 3 are removed by this approach.

Removal of the reflecting jet (Fig. 35c) does not invalidate the physical arguments given earlier in the subsection titled Test Case. The earlier discussion explained the local increase in noise near $\theta = 145°$ is based on phasing between direct and reflected sound (Fig. 32). This mechanism still exists in the final analytical model selected here. Following the ray paths in Figure 32, direct radiation from the source jet and reflected radiation (originating at the source jet) from the shielding jet are modeled by the source-shielding jet-observer model in the upper portion of Figure 35c. Also, the direct radiation from the shielding jet in Figure 32 is modeled by the source-observer combination in the lower portion of Figure 35c. Where the final analytical model differs is that radiation from the shielding jet reflected by the source jet in Figure 32 is not modeled. (Ray paths not shown in Figure 32 for this feature.)

The above arguments contain a recognized limitation for $\theta = 180°$ (or $0°$) in Figure 32. In this case, the source jet and shielding jet are identical relative to the observer. Now radiation from the shielding jet reflected by the source jet located at $\theta = 180°$ is not modeled. This limitation of the current analytical model is exemplified by the lower sound pressure level predictions near $\theta = 180°$. A more accurate model would include this effect. This could be achieved by using the full analytical model in Figure 35b. However, this would require long computing times to calculate the complete discrete tone spectrum needed for the 1/3 octave band response associated with the observer-source-jet geometry. It is recommended that future investigators implement this prediction procedure.

Experimental Assessment of the Final Analytical Model - The predicted azimuthal directivity pattern for the final combination of analytical point source/ single jet geometry is shown in Figures 40-42 for a range of frequencies including the previous f = 4 kHz (kD = 3.22) test case. The

64

selected frequencies span the acoustic spectrum for the jet operating condition shown in Figure 29a with the 4 kHz result defining the directivity shape near the jet noise spectrum peak. Also shown in Figure 40 is the experimentally determined directivity pattern.

The experimental results for the 800 Hz (kD = .644) test case (Fig. 40a) show that shielding is non-existent in the common plane of the dual jet system. This agrees with the conclusions obtained earlier from the acoustic spectrum in Figure 29a. As θ increases from 90° to 180°, excess noise is observed. The increase is, however, monotonic without the previously observed local maxima. Comparison of the above described experimental results with the corresponding predictions (Fig. 40b) shows good agreement near θ = 90°. In addition, the monotonic increase in ΔSPL with increasing θ is predicted.

A comparison of the measured and predicted results at 4 kHz (kD = 3.22) is shown in Figure 41b. The shielding effect at θ = 90° is closely predicted. Also, the experimentally determined increase in ΔSPL near θ = 110° in addition to the oscillatory features at larger azimuthal angles is calculated. For example, the excess noise peak near θ = 130° is closely predicted. However, it must be recognized that the random distributed source characteristics of the actual dual jet geometry smooth out the oscillatory details predicted analytically at large azimuthal angles.

The experimentally determined azimuthal directivity pattern for f = 20 kHz (kD = 16.1) is shown in Figure 42a. Relative to the 4 kHz test condition, a small improvement in shielding effectiveness occurs at θ = 90° for this higher frequency. However, this benefit is countered by the earlier onset of excess noise which now occurs near θ = 110°. As frequency increases, the experimentally determined excess noise peak shifts from θ = 180° at 0.8 kHz to θ = 110° at 20 kHz. In the latter case, the onset of excess noise results in a constant ΔSPL level without the oscillatory features observed at 4 kHz.

The success of the analytical model at 20 kHz is illustrated by the theory-experiment comparison available in Figure 42b. Again shielding is closely predicted in the common plane of the dual jet system. Also, the sudden increase in ΔSPL resulting in excess noise near θ = 110° is predicted. Finally, the experimentally observed constant ΔSPL values for θ > 110° are also predicted. However, as noted earlier for the 4 kHz test condition, the oscillatory details observed in the prediction are absent in the experimental result due to the random distributed source characteristics of the jet noise.

Mach Number Dependence - Having selected the appropriate point source/jet combination for modeling the dual jet system, assessment of the predicted directivity dependence on the various jet operating conditions can now proceed. Mach number sensitivity was assessed by increasing M from 0.6 to

0.94 (Azimuthal data for M = 1.46 was not obtained due to the difficulty of holding a constant shock free operating condition during the long source jet rotation time). Figures 43-46 show the Mach number effect at four jet frequencies spanning the dual jet acoustic spectrum range. Here the 2 kHz condition represents an additional frequency used to monitor changes near the spectrum peak. Results are presented for the same operating conditions shown in Figure 33. A fixed polar directivity angle, ψ = 40°, is employed here to facilitate the discussion. Variations with ψ will be presented in a following subsection.

Experimentally, the effect of increasing Mach numbers from M = 0.6 to 0.94 has only a minor effect on the general shape of the directivity pattern at all frequencies or Helmholtz numbers. However, specific changes in shielding effectiveness do occur at θ = 90°. At low frequencies, shielding improves as indicated by the 1 dB reduction in ΔSPL at 800 Hz. At high frequencies (20 kHz) shielding effectiveness is invariant with ΔSPL $\approx$ 1.25 dB. These results agree with the trends observed earlier in the discussion of the jet noise spectrum dependence (Fig. 29). Near the spectrum peak corresponding to 2 kHz, a larger change in ΔSPL occurs with increasing Mach number at θ = 90°.

For θ = 180°, Figures 43 through 46 indicate consistent excess noise at all frequencies. The specific ΔSPL levels are observed to be independent of Mach number. These general trends are in agreement with the changes observed in the previous subsection titled Spectrum Dependence on Isolated Parameters.

Predicted changes as Mach number increases from M = 0.6 to 0.94 are illustrated by the trends in Part (c) of Figures 43-46. The weak dependence on Mach number at high frequencies is verified experimentally. Larger changes are observed at low frequencies in agreement with experiment.

The good comparison between theory and experiment suggests that the analysis can be used to assess the shielding effect as Mach number increases to M = 1.46. Predictions for this Mach number are also shown in Part c of Figures 43-46. In general, changes in the azimuthal directivity pattern occur only at low frequencies as indicated by comparing the M = 0.6 and 1.46 predictions. High frequencies remain unaltered in agreement with the trend in Figure 29.

The above conclusions regarding Mach number dependence were based on comparisons at constant frequency or Helmholtz number. However, relative to reducing jet noise levels, the assessment can also be conducted at constant Strouhal number. Such a comparison is provided by the prediction in Figure 45d. The Strouhal number selected here (St = .854) is based on the frequency used in the Helmholtz number of Figure 45c and the jet speed corresponding to M = 0.6. For the constant Strouhal number condition shown in Figure 45d, Mach

number changes affect the location of the excess noise peak although changes in shielding effectiveness near $\theta = 90°$ are weak. Based on a comparison of Figures 45c and 45d Mach number has little impact on azimuthal directivity patterns at constant Helmholtz number but for constant Strouhal number the radiation patterns are altered.

It should be noted that assessment of the Mach number dependence at constant Helmholtz number and fixed polar angle is equivalent to evaluating Mach number effects at constant jet noise source frequency. It would appear that this procedure is invalid since Mach number changes are known to alter jet noise source characteristics at a fixed frequency. For this reason, Mach number dependence is typically evaluated at constant Strouhal number instead of constant Helmholtz number or source frequency. However, the present study includes relative sound pressure level changes due to propagation effects rather than just changes in the jet noise source characteristics. But, normalizing the dual jet measurements at each operating condition by the averaged single jet reference measurement at the identical operating condition accounts for changes in the jet noise spectrum. This applies for either Mach number or temperature effects. Consequently, comparisons at constant Helmholtz number are possible. A similar concern arises when Mach number dependence is evaluated at constant polar angle. But the same normalization by the single jet reference measurement eliminates the problem.

Lateral Spacing Dependence - The effect of jet spacing is shown in a series of directivity patterns in Figure 47 as S/D varies from 8.1 to 3.1 for f = 800 Hz (kD = .644). Similar results are shown in Figures 48-49 for higher jet noise source frequencies. In each case, the jet operating condition and microphone measurement angle correspond to the same conditions presented in the Mach number dependence evaluation. Both measured and predicted directivity patterns are shown.

Experimentally, the influence of spacing is weak at f = 800 Hz as S/D decreases from 8.1 to 5.5. A further decrease to S/D = 3.1 results in a increase in ΔSPL due to the changes in jet source distribution described earlier. The primary effect occurs near $\theta = 90°$ with ΔSPL increasing from approximately 2 dB to 3.5 dB indicating a reversal of shielding and an onset of excess noise. At $\theta = 180°$, there is little change in the measured ΔSPL levels as S/D decreases. Predicted directivity shapes generally agree with experiment at S/D = 8.1 and 5.5. But, differences exist for the S/D = 3.1 test condition due to the acoustic source changes.

At the higher frequency of 4 kHz (Fig. 48) spacing changes influence only the shape of the directivity pattern as S/D decreases from 8.1 to 5.5. For example the maximum ΔSPL location shifts to higher azimuthal angles as S/D decreases, but the shielding effect remains constant with ΔSPL($\theta = 90°$) = 1 dB

approximately. These trends are, in general, predicted analytically. However, the theory indicates an improvement in shielding as S/D decreases near $\theta = 90°$ while the experiment indicates a constant value of ΔSPL.

A further decrease of spacing to S/D = 3.1 in Figure 48 results in a change of the directivity pattern and ΔSPL levels. But, the changes are confined to the excess noise region at large azimuthal angles. This suggests that the radiated noise associated with the accelerated jet mixing occurring at smaller S/D, contributes predominantly to the azimuthal directivity pattern beyond $\theta = 130°$. It is possible that the resulting merged flow field has the characteristics of high aspect ratio rectangular jets which are known to have an azimuthally varying directivity pattern.

At 20 kHz, decreasing S/D has a minimal effect on the jet azimuthal directivity pattern as indicated by the sequence of curves in Figure 49. Sound pressure level changes are limited to approximately a 0.5 dB increase in excess noise at large azimuthal angles. Changes in directivity pattern shape are limited to a small shift in the maximum ΔSPL location to higher azimuthal angles as S/D decreases. The general shape in addition to the shift of the maximum ΔSPL location is predicted analytically. However, predicted oscillations in the directivity pattern are not observed experimentally due to a smoothing of the directivity pattern by the random and spatially distributed nature of the acoustic source field. Also the predicted small improvement in ΔSPL near $\theta = 90°$ is not observed experimentally possibly due to the scatter in the data.

Temperature Dependence – The influence of temperature could not be clearly determined due to an anomolous acoustic attenuation in the experimental mesurements. The problem is illustrated in Figure 50 for M = 0.94, S/D = 8.1 and $\psi = 40°$. A comparison of Part (a) and Part (b) indicates ΔSPL assumes negative values as temperature increases from $T_0 = 300$ K to 811 K. This effect was observed consistently at all Mach numbers and all jet spacings.

Phasing between the source jet and source jet radiation reflected from the shielding jet was considered as one source of this effect. While such phasing was identified as responsible for the maxima observed in the azimuthal directively patterns near 130°, phasing was determined to be inoperative for the heated flows. If phasing was responsible for the negative ΔSPL values observed in Figure 50, similar results would be expected for the unheated jet conditions. The only difference between heated and unheated flows would be the acoustic frequency at which this effect occurs. This is because the ray paths and propagation speeds change with temperature. Consequently, 1/2 cycle phase differences between propagating wavefronts would occur at different frequencies for heated and unheated flows. However, the absence of such negative ΔSPL values for unheated jets demonstrates that phasing was not a viable physical mechanism.

While the source of the problem in Figure 50 is presently unknown, the influence of tempreature can still be interpreted experimentally. Conclusions however, are dependent on the observation that differences between the unheated and heated dual jet operating condition in Figure 50 remain approximately constant with jet rotation angle. This suggests that the magnitude of the attenuation is only a function of frequency. Therefore, for a fixed frequency, the influence of temperature on directivity shape can be isolated. Also, since the potential sources of the attenuation in Figure 50 are limited to propagation losses or a drift in the microphone sensitivity, presumably the impact of these effects on the acoustic measurements would be confined to high frequencies. This argument permits extending the evaluation of temperature effects on the dual jet noise directivity shape to include a comparison of ΔSPL levels at low frequencies (f = 800 Hz, 4 kHz).

Based on the above qualifications and limitations, assessment of the temperature dependence can now proceed. For the low frequency 800 Hz case shown in Figures 51a and 51b, the approximately flat azimuthal directivity pattern changes to a radiation pattern with a 3 dB variation between θ = 90° and 180° as temperature increases. However, shielding effectiveness remains constant at θ = 90° indicating that the major change is due to an increase of excess noise near θ = 180°. These general trends are predicted as indicated by the calculated directivity patterns shown in Figure 50C.

For jet source frequencies near the spectrum peak, corresponding to f = 4 kHz (Figs. 52a and 52b), increasing temperature has little effect on shielding at θ = 90°. At larger azimuthal angles, the predominant changes are represented by a shift in the location of the local excess noise maxima to larger θ as temperature increases. Otherwise, the magnitude of the local peaks remains constant. Analytically, these shifts are predicted.

The above experimentally observed shift in local maxima also occur at the highest frequency of 20 kHz described earlier in Figure 50. Analytically, this trend is, again, predicted but the calculated magnitude of the shift is smaller than the measured result. Comparisons of measured ΔSPL values, as in the 800 Hz and 4 kHz cases, is not possible in this case due to the previously described acoustic attenuation effects. Predictions, however indicate ΔSPL levels near θ = 90° are invariant with jet temperature.

Polar Angle Dependence - Previous subsections demonstrated the azimuthal directivity dependence on various jet operating conditions. The following discussion documents the polar directivity features.

Figures 53a-53d present a sequence of azimuthal directivity patterns at polar angles, ψ, varying from 20° to 90°. In general the presence of the shielding jet provides a maximum noise reduction in the common plane of the dual jet system (θ = 90°) when the observer is close to the jet axis system

(small ψ). Simultaneously, the excess noise reaches a maximum at larger azimuthal angles. As ψ increases, the noise reduction benefit, in addition to the excess noise, decreases. Finally for $\psi = 90°$, ΔSPL $\approx$ 3.75 dB for all values of θ. Numerous data sets were examined, and the constant value ΔSPL = 3.75 dB at $\theta = 90°$ was observed regardless of Mach number, spacing or frequency. This ΔSPL is larger than the sum of two independent jets, and is attributed to multiple reflections between the jets.

Figure 53e also provides predicted ΔSPL azimuthal curves for the various polar radiation angles. A comparison of the measured and predicted trends shows good agreement for ψ greater than 20°. In particular, the shift of the local maximum towards $\theta = 90°$ as ψ increases is well predicted. But for $\psi = 20°$, large differences are observed between the measured and predicted ΔSPL levels. These differences, however, occur outside the jet shielding azimuthal angle range and are instead associated with the reflection and scattering effects responsible for excess noise at large θ.

Limitations of the Theory - Several possible reasons can be cited for the differences observed between measured and predicted ΔSPL levels for small polar angles. These will now be discussed in an effort to provide a better understanding of the physical phenomena in addition to identifying improvements needed in the analytical model.

One potential theoretical limitation often cited by researchers deals with the jet flow region which the sound waves intersect at small polar angle ψ. In this case, sound reaching the observer interacts with the fully developed region of the shielding jet. Under this condition the jet shear layer deviates significantly from the plug flow model used in the analysis. Also, for small ψ the observer is stationed within the zone of silence. It is known that for angles within this zone of silence, shear layer thickness effects can be significant. This is because an acoustic wave which has penetrated the shielding jet flow will reach a Mach number where it is reflected from the finite thickness shear layer closest to the source. In addition to being reflected part of the acoustic wavelength is transmitted but with an exponentially decaying amplitude until it reaches the corresponding point on the opposite side of the jet. Here it again begins to interact with the shear layer as an acoustic wave but with diminished amplitude due to the initial reflection and exponential decay. (The degree of exponential decay depends on the details of the jet nozzle.) The final wavefront which emerges from the jet can have a reduced amplitude which is not accounted for in the present analysis.

The above described finite shear layer thickness effects suggest a significant impact on the predicted noise levels for small ψ. But, these arguments apply only for azimuthal angles near $\theta = 90°$ and, thus, do not explain the differences between theory and experiment for θ near 180° in Figure 53.

In fact, near θ = 90° differences between theory and experiment are small. This is because the shear layer thickness effects are masked by direct radiation from the shielding jet which represents the minimum noise level. If, for example, the present experiment were conducted with a single point sound source and a shielding jet, then the finite shear layer would impact the measurements. Under this condition, significant differences between theory and experiment would be observed as described by Yu and Fratello (ref. 11) who evaluated the shielding effect using this approach. However, the general conclusion is that for small ψ and θ near 90° the inability to measure an expected deviation between theory and experiment due to the shear layer thickness is caused by masking of the effect by direct radiation from the shielding jet.

While the zone of silence and finite thickness shear layer fail to account for the theory-experiment differences at large azimuthal angles when the observer is close to the jet axis, reflections between the adjacent jets in the dual jet system are considered potential sources of the documented differences. It is known that multiple reflections occur between the jets for acoustic waves initially propagating in the direction of the zone of silence. These reflections occur at a curved boundary which tends to scatter the radiation outwards from the common plane of the dual jet system. This results in the excess observed at angles on either side of the plane formed by the two jet axes. Based on the ψ = 20° theory-experiment comparison in Figure 53 further improvement is needed in the analytical model to better predict this reflected radiation.

Summary and Evaluation of Dual Jet Directivity Pattern and the Analytical Prediction Method - The experimentally observed dual jet azimuthal directivity pattern indicates that shielding is most effective in the common plane of the dual jet system at frequencies (or Helmholtz numbers) above the spectrum peak. The directivity pattern in this case is defined by a minimum ΔSPL value at θ = 90° followed by an increase near θ = 110° (depending on M, S/D, and source frequency) which results in a local excess noise maximum of ΔSPL = 4 or 5 dB. Beyond this region smaller amplitude local excess noise maxima continue to occur. For frequencies below the jet spectrum peak, the directivity pattern increases monotonically reaching a maximum at θ = 180°.

The existence of the higher frequency excess noise maxima at azimuthal angles outside the common plane of the dual jet system follows from the conservation of acoustic energy criterion. The noise reduction benefit which occurs near θ = 90° requires a noise increase at other radiation angles since the shielding mechanism essentially redirects acoustic wavefronts. Consequently, application of jet shielding as a noise reduction technique must also consider the noise penalties at other azimuthal angles.

Azimuthal directivity pattern shapes are generally insensitive to Mach number changes in the subsonic range between M = 0.6 and 0.94 for all jet

noise source frequencies or Strouhal numbers. However, changes in shielding do occur at θ = 90° with shielding becoming more effective at low frequencies. At high frequencies, shielding is already operative and increasing Mach number has little effect. Near the jet noise spectrum peak, a 1 dB change in ΔSPL is observed.

The primary effect of decreasing jet spacing from S/D = 8.1 to 3.1 is to shift the location of the maximum excess noise peak to larger azimuthal angles. There is little effect on the measured ΔSPL levels with the exception of two changes. First, at low frequencies (below the jet noise spectrum peak) acoustic source changes created by merging of the jet flows increases noise in the common plane of the dual jet system. Second, near the spectrum peak, and at higher frequencies, a small increase in excess noise occurs at large azimuthal angles outside the common plane of the dual jet system.

Based on the limited temperature data, increasing jet temperature has little effect on shielding in the plane of dual jet system. The only exception is an increase in excess noise at large azimuthal angle for low frequencies. Similar to the effect of spacing, temperature changes shift the location of the high frequency excess noise maxima to larger θ.

Relative to polar angle dependence, jet shielding effectiveness in the common plane of the dual jets increases as ψ decreases (observer approaches the jet axis system). Simultaneously, for an observer located at large angles outside the common plane, excess noise reaches a maximum at small ψ. As ψ increases, the noise reduction benefit due to shielding in addition to the excess noise decreases. At ψ = 90°, the measured dual jet ΔSPL curve is invariant with θ. However, measured ΔSPL levels exceed 3 dB indicating the jets do not radiate as two independent sources. In this case it is postulated that jet interaction and consequently acoustic source changes are responsible for these effects. Phasing between direct and reflected radiation, as in Figure 32, was not considered operative in this case since the measured ΔSPL curves are invariant with θ. (However, such phasing is operative at smaller ψ angles as indicated by the variation with θ in Figure 33.)

Prediction of the above described experimental results requires selecting the appropriate analytical combination of discrete tone acoustic point source/single jet geometry which best represents the dual jet random noise and spatially distributed source features. Based on a detailed assessment, the realistic dual jet configuration can be approximated by a combination of observer-shielding jet-acoustic point source and an observer-acoustic point source geometry. Using this analytical model good agreement between measured and predicted jet shielding effects is obtained in the common plane of the dual jet system. In addition, the previously described experimental trends

72

for the jet shielding dependence on Mach number, jet spacing, temperature, and polar directivity are calculated. The present analytical model, therefore, represents an experimentally confirmed dual jet shielding acoustic prediction method. The only exception to the good agreement occurs in the spatial region defined by small polar angles and large azimuthal angles where reflections and scattering of sound results in experimentally measured excess noise which exceeds predictions.

Sound Pressure Level Contours

Shielding Dependence on the Jet Noise Spectrum - In an effort to understand the shielding dependence on the jet noise source characteristics, previous subsections evaluated spectra or directivity information at selected Strouhal number or Helmholtz number. A more general, although qualitative, assessment can be obtained by considering contours of ΔSPL as a function of Strouhal number and azimuthal angle. An example of such a plot is given in Figure 54a for $M = 0.6$, $T_o = 300°K$ and $\psi = 40°$. Areas of the figure where ΔSPL is below 3 dB have been shaded. These regions represent conditions for which some shielding of the source jet occurs.

Mach Number Dependence - Figures 54a and 54c show the effect of Mach number on jet shielding effectiveness and azimuthal angle. As Mach number changes from $M = 0.6$ to 0.94 the 3 dB contour line is observed to extend to lower Strouhal numbers, increasing the jet shielding effectiveness area. Relative to the azimuthal angle dependence, shielding is confined to approximately $±20°$ about $\theta = 90°$ irrespective of Mach number. Also shown in Figure 54b and 54d are the predicted ΔSPL contours. The strong similarity of the 2 dB and 3 dB contour lines when compared to the measurement indicates good agreement between theory and experiment. Included with the predicted contour cases is the $M = 1.46$ condition.

Lateral Spacing Dependent - The influence of lateral spacing changes on measured jet shielding contours is shown in Figure 55 for three ratios of S/D. Little change in contour shape or effectiveness area is observed as S/D decreases from 8.1 to 5.5. However a further change to S/D = 3.1 results in a decrease of shielding effectiveness due to contour line changes at low Strouhal numbers. Simultaneously, there is an increase in excess noise at azimuthal angles beyond $\theta = 130°$ as indicated by the larger effective areas contained by the 4 dB and 5 dB contour lines. The origin of this increase was identified earlier to be due to acoustic source changes created by merging of the dual jet flow. These general trends are in agreement with previous conclusions obtained from assessment of jet noise spectra at selected θ in addition to azimuthal directivity patterns.

Also shown in Figure 55 are the corresponding predicted contours. While the S/D = 8.1 and 5.5 calculations are similar to the experiment, the S/D = 3.1 result differs due to the source changes.

<u>Temperature Dependence</u> - Due to the frequency dependent anomalies identified earlier in the temperature dependence data, experimentally based contour plots cannot be generated. However, predictions are presented in Figure 56 for T_O = 300°K and 811°K. A comparison of the two operating conditions shows only a small increase in shielding effectiveness area with increasing temperature.

<u>Polar Angle Dependence</u> - The effect of polar angle on jet shielding is shown in Figure 57 where contour plots are presented for 6 different polar angles. The shielding effectiveness area is maximized at ψ = 20° with a significant range in both the Strouhal number and azimuthal angle domain. Simultaneously the peak excess noise is a maximum for this polar angle. Shielding effectiveness and excess noise decrease with increasing polar angle until, at ψ = 90°, shielding is absent and excess noise levels are approximately 4 dB. Similar results were observed at other flow conditions. Also shown in Figure 57 are the predicted contours for the corresponding polar angles. The general trend agrees with experiment, confirming the capability of the analytical model to predict the physical phenomenon.

Differential Power Spectrum

Previous sections identified acoustic source changes as a possible mechanism for the increase in the dual jet noise level as jet spacing decreased. The origin of these acoustic changes includes aerodynamic interaction of the dual jet flow fields and acoustic/flow coupling. The latter mechanism is usually observed as a broadband jet noise amplification or attenuation. A quantitative assessment of these mechanisms is obtained from a comparison of the dual jet and the synthesized dual jet power spectrum levels. This change, represented by the differential power spectrum parameter, ΔPWL, was determined by numerically integrating over the experimentally determined measurement surface employed in the present study. A detailed discussion describing the integration over $20° \leq \psi \leq 100°$ and $80 \leq \theta \leq 195°$ is given in Appendix D. The parameter, ΔPWL, is illustrated in Figure 58 for the three jet spacings tested in the present study. Also shown is the original dual jet and the corresponding synthesized <u>dual</u> jet (not the synthesized average single jet) acoustic power spectrum used to calculate ΔPWL.

For the largest S/D value, where aerodynamic interaction was limited to Strouhal numbers below 0.1, ΔPWL is small (0.3 dB to 0.7 dB) near the dominant portion of the jet noise power spectrum. Errors due to experimental inaccuracies and numerical integration in addition to acoustic/flow coupling are potential sources of this difference. Experiments by Yu and Fratello (ref. 11), however, indicated that acoustic coupling could not be detected within a 0.5 dB difference attributed to experimental errors in their study.

In the absence of such coupling the 0.3 to 0.7 dB difference in Figure 58a represents a similar calibration of the experimental error in the present study.

The above assessment concentrated on the differential power for the largest spacing and Strouhal numbers near the jet noise spectrum peak. For the same spacing but Strouhal numbers below 0.1, ΔPWL is observed to systematically increase as St decreases. Since the acoustic source region for this portion of the spectrum is in the dual jet merging region (X/D $\geq$ 23) the observed increase in ΔPWL is considered to be a calibration of the downstream jet merging effect on the radiated power for the largest spacing condition of S/D = 8.1.

As S/D decreases to 5.5, the differential power spectrum remains approximately the same except for a small reduction in ΔPWL at the lower Strouhal numbers. This observation is in agreement with earlier discussions which indicated a minimum effect on ΔSPL level as S/D changed from 8.1 to 5.5. A further decrease of S/D to 3.1 creates an increase in jet noise radiated power particularly at low frequencies where a 1 dB change occurs. While this 1 dB change is perceptable in Figure 58 it is smaller than the 2 dB increase in noise observed at large azimuthal angles in previous contour plots as S/D changes from 8.1 to 3.1. This result indicates that the close spacing condition impacts the directivity shape but has a weaker effect on the total power radiation.

CONCLUSIONS

1. The sound field radiated by an isolated jet is modified when it interacts with the velocity and temperature discontinuity of an adjacent shielding jet. The fluid in the shielding jet refracts, diffracts, and reflects the isolated jet noise field. These effects alter the jet noise directivity pattern with the final radiation field of the dual jet configuration no longer being the superposition of two independent jet noise radiation fields.

2. Sound pressure levels in the plane of the dual jet system are reduced relative to the noise level generated by two independent jets. Effectiveness of this refraction and diffraction controlled shielding phenomenon improves as the polar angle approaches the jet axes. The shielded region extends 20 to 40 degrees in the azimuthal direction on either side of the dual jet common plane depending on the jet operating conditions and the source frequency. Outside of this region, an increase of noise occurs due to the redirection of sound rays from the shielded region.

3. Sound pressure levels in a plane orthogonal to the dual jet common plane are increased relative to two independent jets. This excess noise, which is due to acoustic reflections between the adjacent flow fields, demonstrates that acoustic interactions also exist at observer angles where previous investigations assumed the jet system operated as two independent sources.

4. The dual jet azimuthal directivity pattern is strongly frequency dependent. At Stouhal numbers below the jet noise spectrum peak location, the directivity pattern increases monotonically from a minimum sound pressure level in the common jet plane to a maximum noise level at 90 degrees to the common plane. For the high frequency end of the jet noise spectrum, the azimuthal directivity pattern varies from a minimum noise level, controlled by shielding, to a local maximum situated at aproximately 20 to 40 degrees on either side of the common jet plane. This maximum, which can exceed the noise of two independent jets by 3 dB, is larger than the excess noise condition existing in the plane orthogonal to the dual jet common plane. The origin of this maximum is attributed to phasing between the direct radiation from the source jet and source jet radiation reflected by the shielding jet. As frequency decreases this localized maximum shifts away from the common plane of the dual jet system.

5. A balance exists between the noise reduction and noise increase occurring over a hypothetical sphere surrounding an aerodynamically non-interfering dual jet system. This balance confirms that acoustic energy is conserved by the refraction, diffraction, and reflection processes existing in the presence of the adjacent shielding jet. It also demonstrates that a beneficial noise reduction at one observer angle is negated by a noise penalty at other observer angles.

6. Jet shielding effectiveness increases with increasing Helmholtz number. Relative to the jet noise spectrum shape, shielding is most effective above the peak Strouhal number.

7. Increasing subsonic Mach number enhances the jet noise shielding and shifts the onset of shielding to Strouhal numbers below the spectrum peak. At high subsonic Mach numbers typical of current jet engines, approximately a 2 dB noise reduction occurs at the jet noise spectrum peak. Further increases to supersonic Mach number provide little improvement for jet shielding. Mach number changes have only a minor effect on the shape of the dual jet direc-tivity pattern.

8. For non-interfacing dual jet flows, jet spacing has little effect on the noise radiation in the common plane of the jet system. The primary change is a shift of the high frequency localized excess noise maximum to larger azimuthal angles. For small jet spacing resulting in the aerodynamic merger of the jet flows, sound pressure levels increase relative to two independent jets. Resulting changes in the jet noise spectrum shape are controlled by acoustic source alterations in the region downstream of the jet merger. Since jet merging occurs beyond the end of the potential core where the jet acoustic source region generates primarily low frequency noise, the spectrum changes associated with close spacing are confined to Strouhal numbers below the jet noise peak. Shifting of the localized excess noise maximum to larger azimuthal angles continues to occur for close spacing.

9. Differences between heated and unheated jets are minimal in the common plane of the dual jets where shielding is operative. Similar to the effect of spacing, the primary change due to temperature is a shift to larger azimuthal angles of the localized excess noise maximum.

10. The maximum experimentally observed noise reduction for two adjacent aerodynamically non-interfering jets with the same operating condition is 3 dB. Although phasing could conceptually improve the noise reduction beyond this 3 dB limit, such effects are not experimentally observed with two adjacent jets. The present noise reduction limit is based on complete masking of one jet when the observer is in the common plane of the dual jet system. The resulting radiation perceived by the observer corresponds to direct radiation from the shielding jet alone. Since total masking of the source jet also applies for dissimilar flows, placement of the quieter jet between the observer and the noisy jet may provide significant noise reduction in the shielding region. Further shielding studies with dissimilar jets are, therefore, recommended.

11. Improved shielding (exceeding 3 dB) experiments involving a shielding jet-discrete tone point source combination indicate only the noise reduction of the point source. This measured noise, which depends on phasing between

wavefronts arriving at the observer station, excludes the direct radiation from the shielding jet. In a dual jet geometry, such improvements are masked by the direct radiation from the shielding jet which determines the 3 dB noise reduction limit. Further improvements in noise reduction for two adjacent jets would require coherent acoustic source regions in each jet with appropriate phasing between them.

12. Dual jet noise shielding is modelled by a first principles theory based on a discrete tone point source interacting with a constant diameter cylindrical, uniform flow shielding jet. Measured jet noise reduction in the common plane of the dual jet is well predicted. In addition, directivity patterns outside the common jet plane are predicted. Finally, experimentally observed trends based on Mach number, jet spacing, temperature, and source frequency are calculated. The analysis, therefore, successfully models the acoustic directivity pattern generated by two adjacent, random-noise, distributed-acoustic-source jets.

13. Finite shear layer thickness effects, which are not modelled in the analytical prediction, have little impact on the radiated noise in the common plane of the dual jets. This conclusion is based on the experimentally observed maximum attainable 3 dB noise reduction for the dual jet configuration. In this case, shear layer thickness effects are masked by direct radiation from the shielding jet.

APPENDIX A

REVIEW OF PREVIOUS EXPERIMENTAL RESEARCH

The earliest reference to work on acoustic shielding from circular jets appears is the study by Greatrex and Brown in 1958 (ref. 1). Although their data show approximately a 3 to 4 dB difference in noise between ΔSPL ($\theta = 90°$) and ΔSPL ($\theta = 180°$) the authors indicate an uncertainty in the reliability of the measurements. The noise reduction benefit appeared to decrease with increasing spacing as S/D increased from 1.2 to 1.4.

A study of the effects of jet shielding on two jets of unequal size was carried out by Morris, Richarz and Ribner in 1973 (ref. 2). A small secondary jet was mounted at an angle to the main jet so as to eliminate any aerodynamic interference and hence avoid degradation of the main jet performance. The object was to alter the directivity pattern of the main jet by refracting, reflecting, and diffracting the sound field using the secondary jet. They found a maximum reduction of 5 dB. The attenuation increased for both increasing secondary jet velocities and temperatures.

A study of the shielding effect of multi-tube nozzles was done by Gray, Gutierrez and Walker in 1973 (ref. 3). They measured the noise produced from 37 tube nozzles and single tube nozzles using both 1/4 scale and full scale configurations. At low velocities, no shielding was detected. However, at transonic velocities and above, a nearly complete shielding was observed.

As part of a larger study on jet noise reduction from shrouded multi-nozzles, Goethert and Borchers (ref. 4) reported some twin jet results in 1974. For spacing to diameter ratios between 1.2 to 2.0, they found that the total sound power was approximately 1 dB lower than the noise produced by two independent jets. At larger spacings, however, only a .1 to .2 dB reduction was noted.

A study of acoustic shielding in annular jets was performed by Ahuja and Dosanjh in 1977 (ref. 6). They examined the effect of shielding a noisy, round inner jet with an outer jet. When the outer jet was at the same temperature as the inner jet, little shielding benefit was observed. However, when the outer jet was heated, up to a 10 dB noise reduction was seen. A genuine reduction in acoustic power levels was observed, as opposed to a redistribution of acoustic energy by refraction. The shielding effect was seen at all angles, but was stronger at higher frequencies.

A study of the acoustic shielding from twin, round heated jets was presented in 1977 by Bhat (ref. 7). In his test, the effects of spacing, dissimilar velocity, dissimilar jet size, and longitudinal stagger on acoustic shielding were examined. Sound pressure measurements were made about an arc

only in the common plane of the dual jet system. For equal size jets with no longitudinal stagger, up to a 5 dB difference between the twin jets and a single jet incremented by 3 dB was noted at 40° from the jet axis. At 90° from the jet axis, no effect was observed. Although the range of lateral jet spacing tested was small (from S/D = 1.12 to 2.0) an increase in shielding effect was observed at the closest spacing. The importance of acoustic source changes due to aerodynamic interactions at these close spacings was not evaluated. An increase in shielding effect was also noted for an increase in streamwise stagger.

An acoustic study of heated twin jets was performed by Kantola in 1977 (refs. 8, 9). Sound pressure measurements were made in an arc around the jet nozzle exit at only 3 polar angles, 0°, 45°, and 90° from the dual jet plane. Lateral jet spacing, velocity and temperature were varied. Kantola found that as the spacing increased from S/D = 1.33 to 3.0, the measured overall power level (OAPWL) decreased in the plane of the jets. No additional effect was noted for larger spacings. In the loud plane, 90° from the plane of the jets, OAPWL varied from less than the single jet noise level incremented by 3 dB level to greater than the single jet level incremented by 3 dB. Kantola interpreted this to indicate mixing suppression and additional noise generation respectively. At frequencies below about 2 kHz, little difference was noted between the loud and the quiet measurement planes. At higher frequencies, however, over 8 dB of difference was noted for a microphone at 30° off the jet axis. Even for the 90° off axis microphone, up to 2 dB difference was seen. The frequency at the onset of shielding was seen to decrease as the spacing increased. Kantola attributes this to an internozzle layer of cold fluid which exists between the jets and extends further downstream as the spacing increases. As the layer extends further downstream, the lower frequency jet noise sources are shielded. It was also noted that the shielding effect increased with jet velocity up to sonic conditions.

A study of two round parallel jets with unequal flow was made by Shivashankara and Bhat in 1980 (ref. 10). It was found that the sound of the high velocity (loud) jet could be shielded by the low velocity (quiet) jet by as much as 7.5 dB OASPL. No benefit was perceived at azimuthal angles greater than 75° from the plane of the jets. For a lateral spacing to diameter ratio of 1.5 to 1.6, total pressure and temperature surveys were taken. By comparing velocity profiles obtained with single jet versus the dual jet configuration at a streamwise station of X/D = 5, it was concluded that no significant mean flow interaction occurred. In the polar directivity plane, the frequency at which noise reduction first occurs increases as the observer angle increases.

An experiment on the acoustic shielding provided by a turbulent jet from a point source of sound was conducted by Yu and Fratello in 1981 (ref. 11). A one inch diameter jet was rotated about a fixed acoustic source. Sound pressure measurements were obtained with a fixed microphone array. Four

different discrete tones and also 1/3 octave band random noise were emitted from a small acoustic source. Room temperature air and helium were used as the working fluids for the jet. The helium was used to simulate heating at a high temperature ratio. Since there was only one jet, no aerodynamic interaction was present, and the effect of acoustic shielding alone could be studied. Yu and Fratello found that the peak value of shielding, as measured by the differential power level between acoustic source only and both acoustic source and jet, increased with frequency, jet velocity, jet heating, and longitudinal source position. No trends were identified for the effect of lateral spacing on acoustic shielding at values of Kd greater than 2.

APPENDIX B

CORRECTIONS TO ACOUSTIC DATA

Humidity Changes

Although relative humidity was monitored in the anechoic chamber during
each test condition, corrections for humidity effects were not applied. This
decision was based partially on the limited range of applicability of the cur-
rent prediction procedures. For example, ARP 866A (ref. 45) which is the
aerospace industry standard, is confined to frequencies below 10 kHz and tem-
peratures between -18°C and 38°C (0°F to 100°F). In contrast, third octave
band data were acquired for frequencies up to 50 kHz in the present experi-
ment. Also, during testing at high Mach number and jet temperature condi-
tions, the anechoic chamber temperature occasionally approached 60°C (140°F).
Since ARP 866A predicts approximately a 3 dB change in acoustic sound pressure
level (at 50 kHz and 10% relative humidity) as temperature increases 10°C,
comparison of the heated and unheated (25°C average temperature) jet test
conditons would require large amplitude corrections. These corrections would
exceed the changes due to jet shielding. A final example of the limited range
of the current humidity corrections is evident when considering the frequency
dependence. Attenuation due to humidity is highly nonlinear and increases
with frequency. Efforts to extrapolate the theory to frequencies above the
present 20 kHz limit would, therefore, introduce unknown errors.

Another major reason for not applying humidity correctons was the signif-
icant disagreement between correction procedures reported in the literature.
The approach developed by Bass and Shields (ref. 46) gives differences of 3 dB
(at 10 kHz, 288.7°K, and 70% relative humidity) relative to the corrections
obtained from ARP 866A. As indicated earlier, this difference is comparable
to the magnitude of the jet shielding effect investigated in the present
study.

A final constraint on application of humidity corrections was the non-
uniformity of the anechoic chamber temperature. Gradients existed in the
chamber due to the entrainment of cooler outside air through an access door.
This possibly resulted in recirculation cells inside the chamber complicating
the application of humidity corrections. In this case, a detailed knowledge
of the temperature field, between the dual jet system and the microphone
array, would be needed before applying the correction.

Based on the above described constraints, it was concluded that correct-
ing hot jet data could potentially introduce errors in the acoustic data.
Therefore, only uncorrected heated jet data below 20 kHz was evaluated since
the predicted humidity corrections are small in the region. For the unheated
jet data, 1/3 octave band spectra were therefore, also limited to frequencies

below 20 kHz. Most of the previous experiments neglected atmospheric humidity corrections.

Jet Velocity Changes

Acoustic data obtained during the subsonic dual jet rotation experiments was corrected to a common jet Mach number to account for small pressure and temperature variations in the air supply system. Total pressure and temperature monitored upstream of the nozzle exit planes was recorded as a function of time and jet rotation angle for this purpose. The data was used to convert the sound pressure levels to the reference Mach number and temperature associated with each specific test condition.

The correction was based on a jet scaling law employed by Plumblee, et al. (ref. 43). The noise dependence on jet operating conditions was obtained from the proportionality expression for overall sound pressure level (OASPL).

$$\text{OASPL} \sim 10 \log (V_j^{5.5}\{1 - M_c \cos \theta)^6/[(1 - M_c \cos \theta)^2 + \alpha^2 M_c^2]^{9/2}\} \qquad \text{(B-1)}$$

Here, M_c, the eddy convection Mach number, is assumed to be 0.67 V_j, and the weighting factor, α is taken to be 0.3, although it was applied in the present study for 1/3 octave band levels.

Total pressure changes were accounted for by the velocity dependence in Equation B-1. Similarly, the effect of total temperature changes was determined from the velocity term which is also an implicit function of the temperature dependent speed of sound inside the jet. As a first approximation, the resulting corrections to the acoustic data were applied to the dual jet data assuming two independent source jets with shielding inoperative. In most cases, the magnitude of the correction was a few tenths of a decibel.

APPENDIX C

SYNTHESIZATION OF THE AVERAGE SINGLE JET RADIATION FIELD

The method selected for quantifying the jet shielding effectiveness
involved comparing dual jet noise measurements with a simulated single jet
geometry. The latter configuration was calculated as the average of two,
independent single jets whose sound pressure levels were added. The radiated
noise field in this case was free from the propagation effects present in the
experimental dual jet data, thereby, providing a baseline case without
shielding.

Quantitatively, the shielding effectiveness was defined by Equation 36
where the numerator represents the shielded noise and the denominator repre-
sents the average noise from two independent jets. Ideally, for source-to-
microphone distances which are large relative to jet spacing, distance changes
during rotation of the source jet about the shielding jet would not impact the
numerator of Equation 40. Similarly, the denominator would be independent of
the precise source jet-to-microphone distance and could be replaced by $\overline{p_1^2}$
since $\overline{p_1^2} = \overline{p_2^2}$.

However, in the present study, the 3 m radius of the microphone array was
insufficient to provide a geometric far field measurement location relative to
the 0.36 m maximum jet spacing. For example, for the $\psi = 90°$ microphone
station the ratio of source jet sound pressure levels associated with $\theta = 90°$
and $\theta = 180°$ is given by $(3/3.36)^2$. In terms of decibels, this corresponds to
a 0.9 dB difference in sound pressure level. To assess the shielding
effectiveness as the source jet rotated about the shielding jet, it was
necessary to account for this difference in distance and its corresponding
impact on the measured sound pressure levels. Due to the small magnitude of
the shielding effect observed experimentally during the present study such
changes could not be neglected.

The above described distance effects were accounted for in the
denominator of Equation 36. The approach is illustrated schematically in
Figure C-1. Part (a) of this figure represents the dual jet shielding experi-
ment while Part (b) indicates the procedure involved in converting single jet
mesurements, also obtained as part of the test program, to the synthesized
dual jet configuration. Here, distance corrections, based on the inverse
square law decay model, were applied to the single jet measurements. This
method analytically shifted the single jet measurement location to the appro-
priate shielding jet and source jet locations employed during each dual jet
test geometry. In essence, this procedure ensured the same relative jet loca-
tions and azimuthal orientation in the expressions representing the numerator
and denominator of Equation 36. In this way the impact of distance changes

was minimized in the present experimental assessment of the shielding mechanism.

The above described shift in location was based on a simple point source model with the noise source situated at the jet exit plane. Precise distances were calculated from the nozzle exit plane to the individual microphones. In general, the jet-to-microphone distance was determined from the expression

$$R_2 = \left[(S \cos \theta + R_1 \sin \psi)^2 + (S \sin \theta)^2 + (R_1 \cos \psi)^2\right]^{1/2} \qquad (C-1)$$

The resulting synthesized dual jet sound pressure level, which was also a function of S/D and θ, was then obtained from the equation

$$\overline{P_d^2} = \overline{P_s^2} \left\{[Rm/R_1]^2 + [Rm/R_2]^2\right\} \qquad (C-2)$$

where

$\overline{P_d^2}$ = simulated dual jet pressure squared

$\overline{P_s^2}$ = measured single jet pressure squared (all measurements conducted at S/D = 3.19)

Rm = distance from the microphone to the single jet (3.19 m)

R_1 = distance from the microphone to the shielding jet (3.05 m)

R_2 = distance from the microphone to the source jet

APPENDIX D

DIFFERENTIAL POWER SPECTRUM

The jet shielding concept is based on the idea that sound radiation from an isolated jet is redirected after propagation through an adjacent jet flow field. A fundamental assumption during this process is that acoustic energy is conserved. However, for sufficiently close spacings, the two adjacent jets may interact aerodynamically altering the initial jet noise source characteristics. Under this condition, increased noise levels can be generated by the dual jet system relative to two separate and independent jets.

One method for identifying acoustic source changes involves a comparison of the dual jet and synthesized dual jet power spectra. This comparison, represented quantitatively as a ratio of power spectrum levels (PWL), provides a differential power parameter, ΔPWL, which can be expressed in terms of decibels.

In principle, the individual power spectra needed to calculate ΔPWL would be obtained from acoustic measurements on a hypothetical sphere (or hemisphere if symmetry exists) surrounding the dual jet system. However, microphone locations in the present experiment were confined to approximately a quarter of a hemisphere. The primary limitation was in the polar angle range which was defined by $20° \leq \psi \leq 100°$. Ideally, this measurement range should include angles beyond $\psi = 100°$ since this region contains sufficient acoustic energy to influence the power spectrum calculation. Thus the present power spectrum calculations must be regarded as estimates.

It should be noted that the azimuthal angle range, $80° \leq \theta \leq 200°$, did not present a limitation to the power spectrum calculation. Symmetry of the dual jet directivity pattern about $\theta = 90°$ could be used to define the complete azimuthal directivity pattern for $0° \leq \theta \leq 360°$. In principle, however, differences in ΔPWL can be determined from measurements limited to the range $90° \leq \theta \leq 180°$ based on azimuthal symmetry. This approach was used in the present study, i.e., power spectrum levels are based on numerical integrations over $90° \leq \theta \leq 180°$.

Although the polar and azimuthal angle range did not account for the total acoustic power radiated by the dual jet system, the impact on the differential power, ΔPWL, was a minimum. This is because for the non-interfering jet spacings tested here, the primary redirection of sound by the adjacent jet flow field was confined to the region $20° \leq \psi \leq 90°$. Also, due to symmetry, relative changes observed in the region $90° \leq \theta \leq 180°$ were representative of the changes observed in the remaining three quadrants of the azimuthal direction. Under these conditions, it was sufficient to assess

changes in ΔPWL as a function of spacing over the range $20° \leq \psi \leq 100°$ and $90° \leq \theta \leq 180°$.

Power spectra were calculated for both the experimentally documented dual jet configuration and a synthesized combination of two independent jets. The latter geometry was calculated from a single jet measurement using the synthesization process defined in Appendix C.

REFERENCES

1. Greatrex, F. B. and D. B. Brown: Progress in Jet Engine Noise Reduction. Advances in Aeronautical Sciences, Vol. 1, pp. 364-392, Proceedings of the First International Congress in the Aeronautical Sciences, Madrid, 1958.

2. Morris, P. J., W. Richarz and H. S. Ribner: Reduction of Peak Jet Noise Using Jet Refraction. J. Sound and Vib., Vol. 29, No. 4, pp. 443-455, 1973.

3. Gray, V. H., O. A. Gutierrez and D. Q. Walker: Assessment of Jets as Acoustic Shields by Comparison of Single and Multimode Suppressor Nozzle Data. AIAA Paper 73-1001, 1973.

4. Goethert, B. H. and I. U. Borchers: Noise and Thrust Characteristics of Shrouded Multi-Nozzles of Circular Cross Section. AIAA Paper 74-45, 1974.

5. Borchers, I. U.: An Experimental Study of the Noise Radiation of Interfering Free Jets, AIAA Paper 77-1285, 1977.

6. Ahuja, K. K. and D. S. Dosanjh: Heated Fluid Shroud as an Acoustic Shield for Noise Reduction - An Experimental Study. AIAA Paper 77-1286, 1972.

7. Bhat, W. V: Acoustic Characteristics of Two Parallel Flow Jets. AIAA Paper 77-1290, 1977.

8. Kantola, R. A.: Shielding Aspects of Heated Twin Jet Noize. AIAA Paper 77-1288, 1977.

9. Kantola, R. A.: Acoustic Properties of Heated Twin Jets. J. Sound and Vib., Vol. 79, No. 1, pp. 79-106, 1981.

10. Shivashankara, B. N. and W. V. Bhat: Noise Characteristics of Two-Parallel Jets of Unequal Flow. AIAA Paper 80-1068, 1980.

11. Yu, J. C. and D. J. Fratello: Measurement of Acoustic Shielding by a Turbulent Jet. AIAA Paper 81-2019, 1981.

12. Cowan, S. J. and R. W. Crouch: Transmission of Sound Through a Two Dimensional Shielding Jet. AIAA Paper No. 73-1002, 1973.

13. Yeh, C.: A Further Note on the Reflection and Transmission of Sound Waves by a Moving Fluid Layer. J. Acoustical Soc. Amer., Vol. 43, No. 6, pp. 1454-1455, 1968.

14. Miles, J. W.: On the Reflection of Sound at an Interface of Relative Motion. J. Acoust. Soc. Amer., Vol. 29, 1957, pp. 226-228.

15. Ribner, H. S.: Reflection, Transmission and Amplification of Sound by a Moving Medium. J. Acoust. Soc. Amer., Vol. 29, 1957, pp. 435-441.

16. Parthasarathy, S. P., R. F. Cuffel and P. F. Massier: Twin Jet Shielding. J. Aircraft, Vol. 17, No. 9, pp. 618-626, 1980.

17. Gerhold, C. H.: Two-Dimensional Analytical Model of Twin Jet Shielding. J. Acoust. Soc. of America, Vol. 69, 1981, pp. 904-908.

18. Gerhold, C. H.: Analytical Model of Jet Shielding. AIAA Journal, Vol. 21, 1983, pp. 694-698.

19. Gottlieb. P: Sound Source Near a Velocity Discontinuity. J. Acoust, Soc. Amer., Vol. 32, 1960, pp. 1117-1122.

20. Graham, E. W. and B. B. Graham: Effect of a Shear Layer on Plane Waves of Sound in a Fluid. J. Acoust. Soc. Amer., Vol. 46, 1969, pp. 169-175.

21. Howe, M. S.: Transmission of an Acoustic Pulse through a Plane Vortex Sheet. J. of Fluid Mech., Vol. 43, 1970, pp. 353-367.

22. Tester, B. J. and R. H. Burrin: On Sound Radiation from Source in Parallel Sheared Jet Flows. AIAA Paper #74-57, 1974.

23. Mani, R.: A Moving Source Problem Relevant to Jet Noise. J. Sound and Vibration, Vol. 25, 1972, pp. 337-347.

24. Mani, R: The Influence of Jet Flow on Jet Noise, Part 1, The Noise of Unheated Jets. J. of Fluid Mechanics, Vol. 73, 1976, pp. 753-778.

25. Goldstein, M. E.: The Low Frequency Sound from Multiple Sources in Axisymmetric Shear Flows, with applications to Jet Noise. J. of Fluid Mech., Vol. 70, 1975, pp. 595-604.

26. Amiet, R. K.: Correction of Open Jet Wind Tunnel Measurements for Shear Layer Refraction. Progress in Astronautics and Aeronautics, Ed. Martin Summerfield, 1976, pp. 259-280. Also AIAA Paper 75-532, 1975.

27. Amiet, R. K.: Refraction of Sound by a Shear Layer. J. Sound and Vibration, Vol. 58, 1978, pp. 467-482. Also AIAA Paper #77-59, 1977.

REFERENCES (Cont'd)

28. Jacques, J. R.: Noise from Moving Aircraft: Some Relevant Models. PhD Thesis, Cambridge University, 1975.

29. Candel, S. M.: Application of Geometrical Techniques to Aeroacoustic Problems: AIAA Paper #76-546, 1976.

30. Tester, B. J. and C. L. Morfey: Developments in Jet Noise Modelling-Theoretical Predictions and Comparisons with Measured Data. J. Sound and Vibration, Vol. 46, 1976, pp. 791-103.

31. Schlinker, R. H. and R. K. Amiet: Experimental Assessment of Theory for Refraction of Sound by a Shear Layer. NASA CR-145359, 1978. Also AIAA Paper #79-0628, 1979.

32. Schlinker, R. H. and R. K. Amiet: Refraction and Scattering of Sound by a Shear Layer. NASA CR-3371, 1980.

33. Candel, S. M., A. Guedel and A. Julienne: Radiation, Refraction and Scattering of Acoustic Waves in a Free Shear Flow. AIAA Paper 76-544, 1976.

34. Ahuja, K. K.; Tester, B. J.; Tanna, H. K.; and Searle, N.: Experimental Study of Transmission, Reflection and Scattering of Sound in a Free-Jet Flight Simulation Facility and Comparison With Theory. AIAA Paper 77-1266, 1977.

35. Ahuja, K. K., B. J. Tester and H. K. Tanna: The Free Jet as a Simulator of Forward Velocity Effects on Jet Noise. NASA Contractor Report 3056, 1978.

36. Morse, P. M. and K. U. Ingard: Theoretical Acoustics, McGraw Hill Book Company, New York, 1968.

37. Gradshteyn, I. S. and I. M. Ryzhik: Table of Integrade Series and Products. Academic Press, New York, 1965.

38. Paterson, R. W., P. G. Vogt, and W. M. Foley: Design and Development of the United Aircraft Research Laboratories Acoustic Research Tunnel. J. of Aircraft, Vol. 10, No. 7, pp. 427-433, 1973.

39. Laufer, J., R. H. Schlinker, and R. E. Kaplan: Experiments on Supersonic Jet Noise. AIAA Journal, Vol. 14, No. 4, pp. 489-497, 1976.

REFERENCES (Cont'd)

40. Pinckney, S. Z.: A Short Static-Pressure Probe Design for Supersonic Flow. NASA TN D-7978, July 1975.

41. Seiner, J. M. and T. D. Norum: Experiments of Shock Associated Noise on Supersonic Jets. AIAA Paper 79-1526, 1979.

42. Moffat, R. J.: Gas Temperature Measurement. Temperature - Its Measurement and Control in Science and Industry, Volume 3, Part 2, Reinhold Pub. Corp., c.1962, pp. 553-571.

43. Plumbee, H. E., Jr., et al: A Study of the Effects of Forward Velocity on Turbulent Jet Mixing Noise. NASA CR-2702, July, 1976.

44. Laufer, J., R. E. Kaplan and W. T. Chu: Acoustic Modeling of the Jet Noise Abatement Problem. Interagency Symposium on University Research in Transportation Noise, Stanford University, Stanford, California, March 28-30, 1973, pp. 37-42.

45. Standard Values of Atmospheric Absorption as a Function of Temperature and Humidity. Society of Automotive Engineers ARP 866A, 1975.

46. Shields, F. D. and H. E. Bass: Atmospheric Absorption of High Frequency Noise and Application to Fractional-Octave Bands. NASA CR-2760, June, 1977.
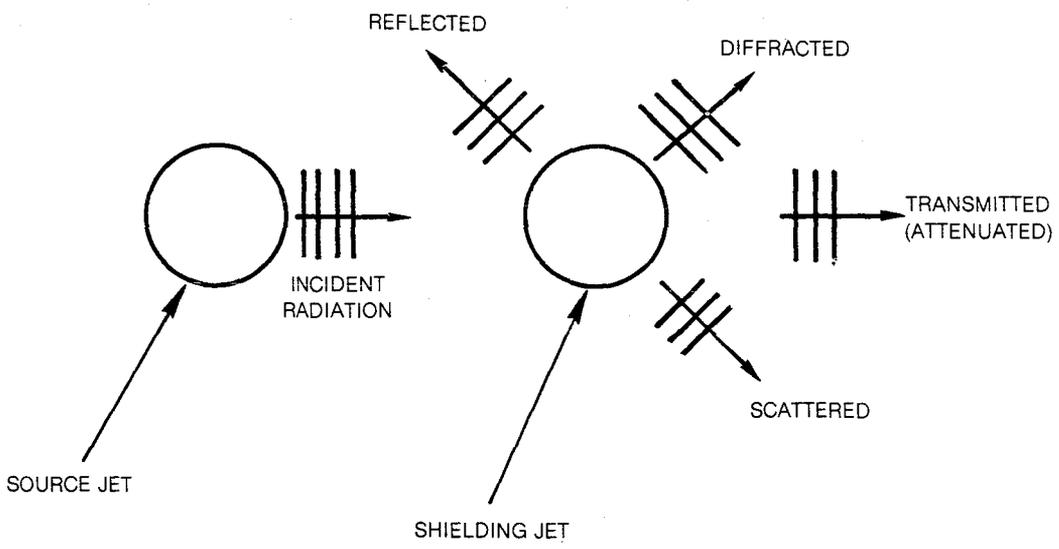
Figure 1 — Jet Shielding Concept

COMBINED ACOUSTIC
RADIATION FROM
MULTIPLE JETS

AIRCRAFT

SIDELINE
OBSERVER

4

3

2

ENGINE NO. 1

θ

x

x ◄——— OBSERVER BELOW FLIGHT PATH
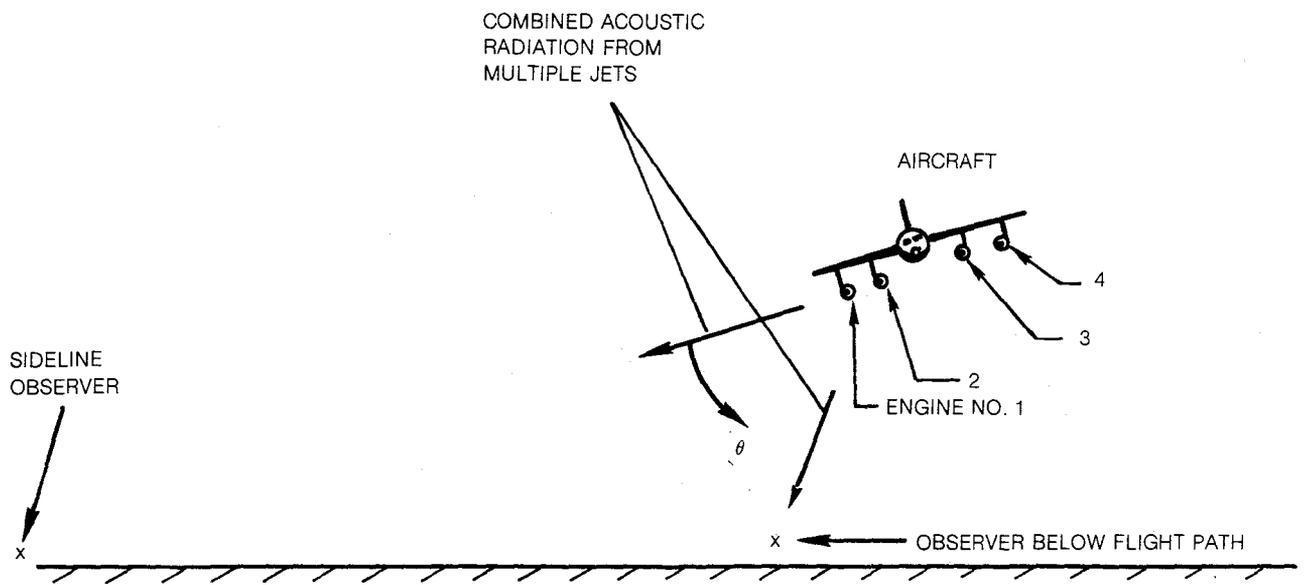
Figure 2 — Aircraft Sideline Noise Dependence on Sound Propagation Through Adjacent Jet Flows
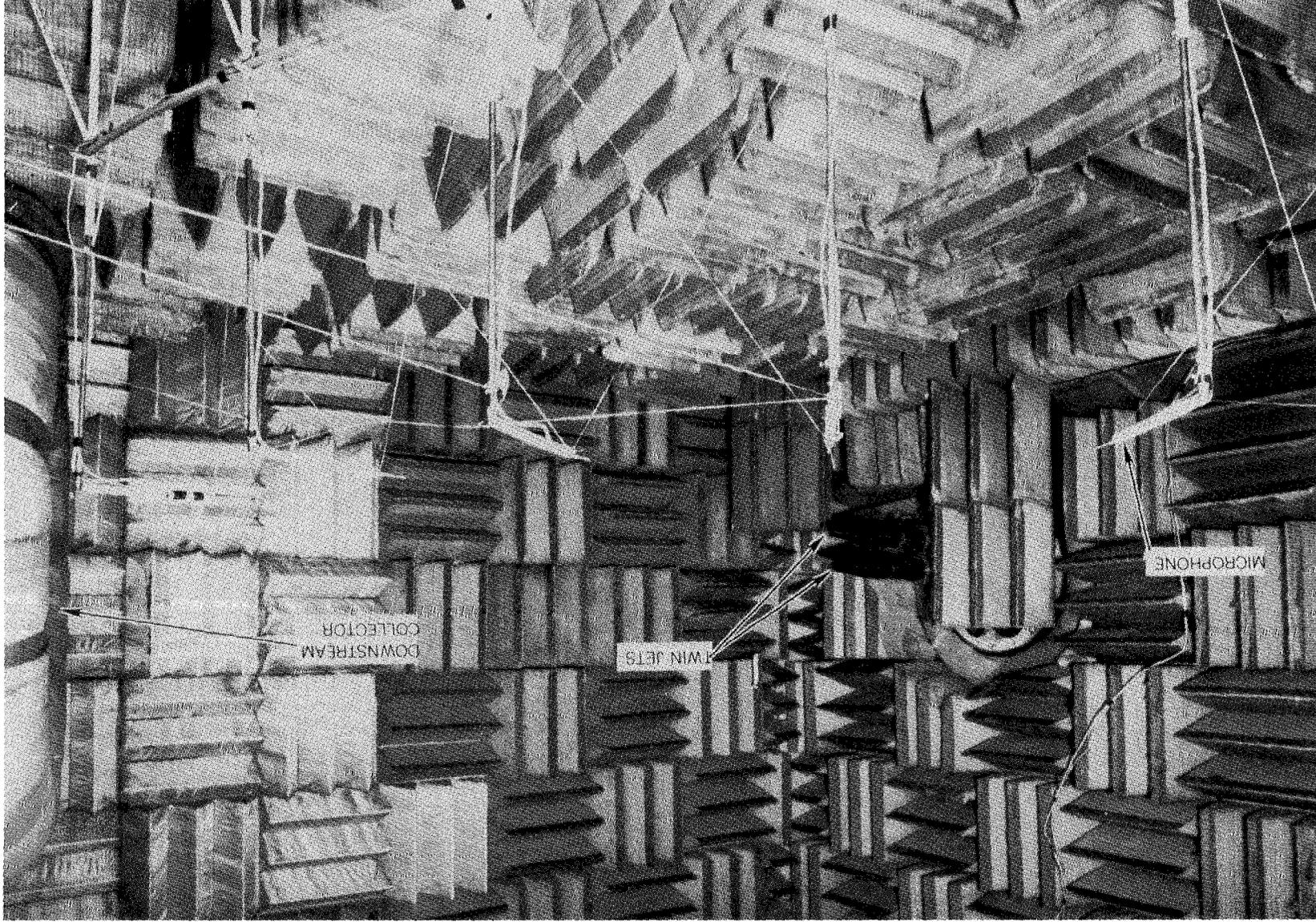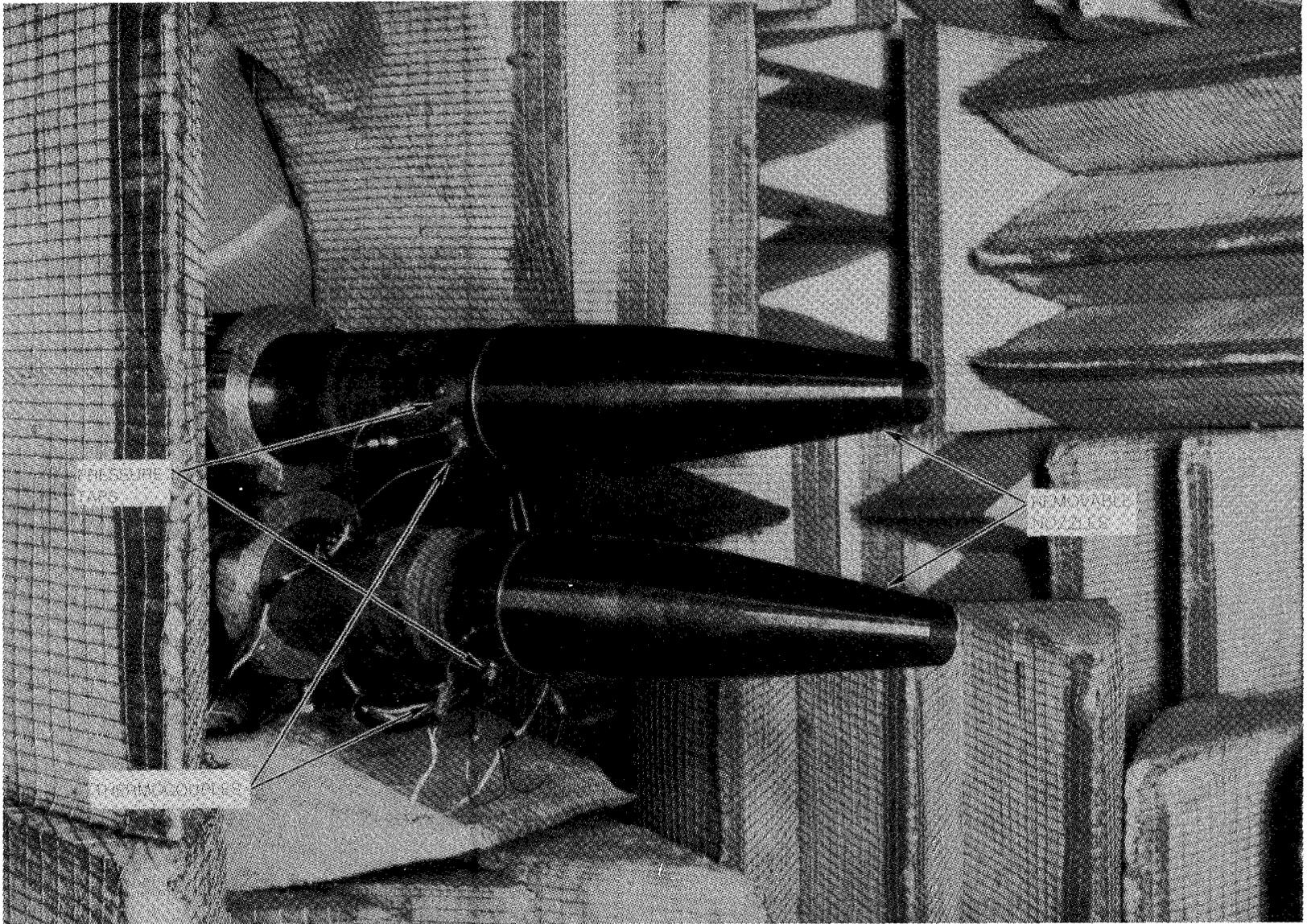
Figure 4 — View of Dual Jet Nozzles
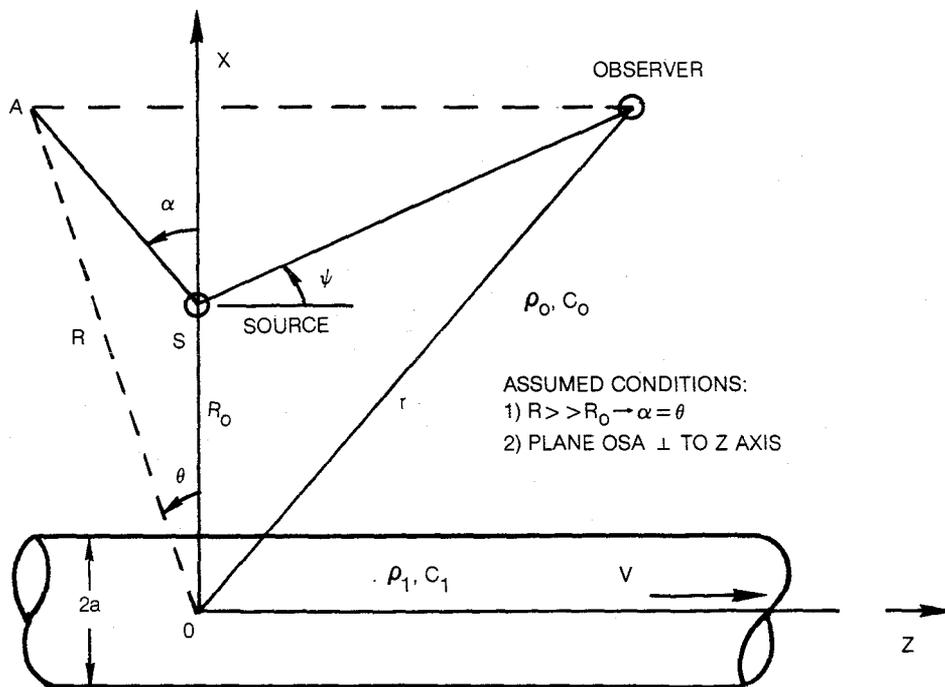
NOTE: THE REFERENCE AXIS FOR THE THEORETICAL AND EXPERIMENTAL (SEE FIG. 7) DEFINITIONS OF θ DIFFER BY 90°.
      SEE TEXT — DESCRIPTION OF EXPERIMENT FOR DISCUSSION.

Figure 5 — Coordinate System with Acoustic Source, Shielding Jet and Observer Locations for Theoretical Analysis

TOP VIEW

- TURBULENCE SCREENS
- LINED ACOUSTIC CORNERS
- ACOUSTIC WEDGES
- CONTRACTION OUTLET
- FREE JET COLLECTOR
- AIR FLOW
- HONEYCOMB
- HEATER AND MUFFLERS
- CONTROL ROOM
- HIGH PRESSURE AIR SUPPLY SYSTEM
- EXHAUST TOWER
- PARALLEL BAFFLES
- 17m

SIDE VIEW

- 46m
- INLET
- ANECHOIC CHAMBER
- DIFFUSER
- MUFFLER
- DRIVER
- CENTRIFUGAL FAN
- DRIVE MOTOR
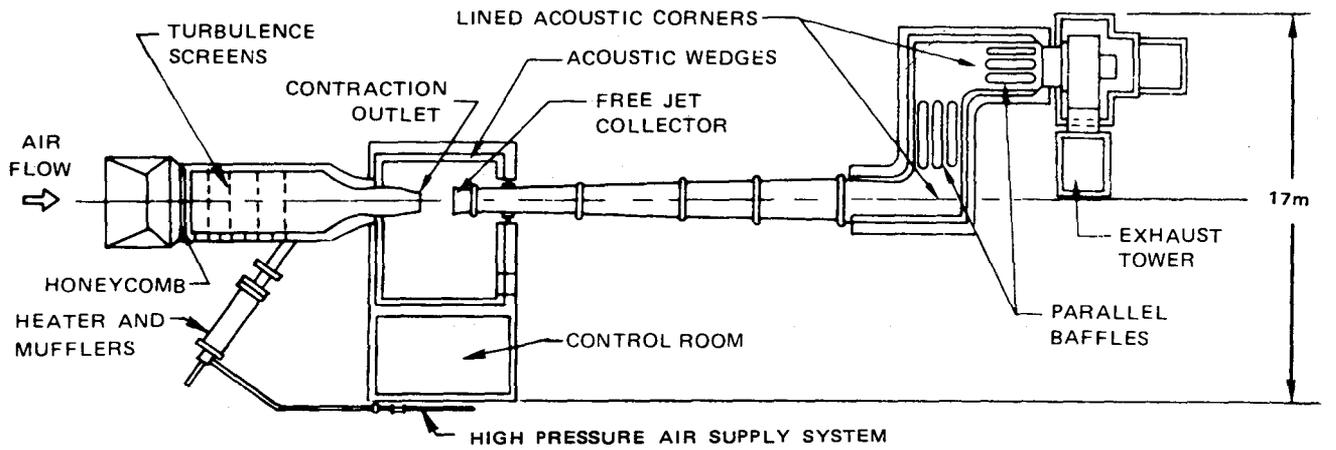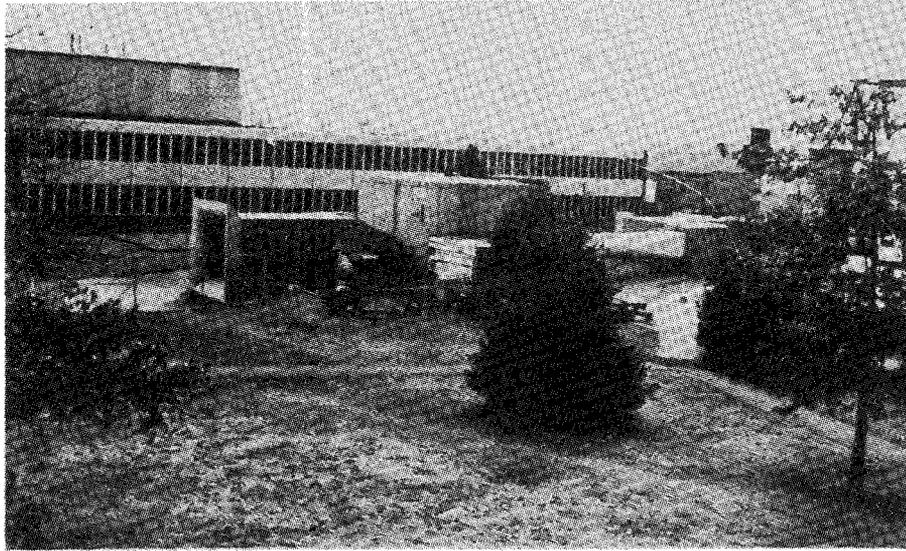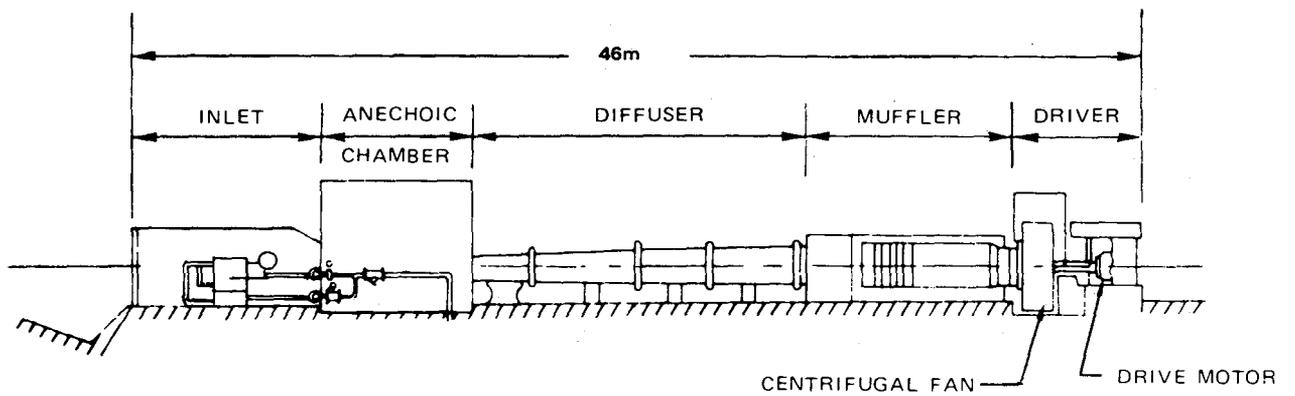
Figure 6 — UTRC Acoustic Research Tunnel

100
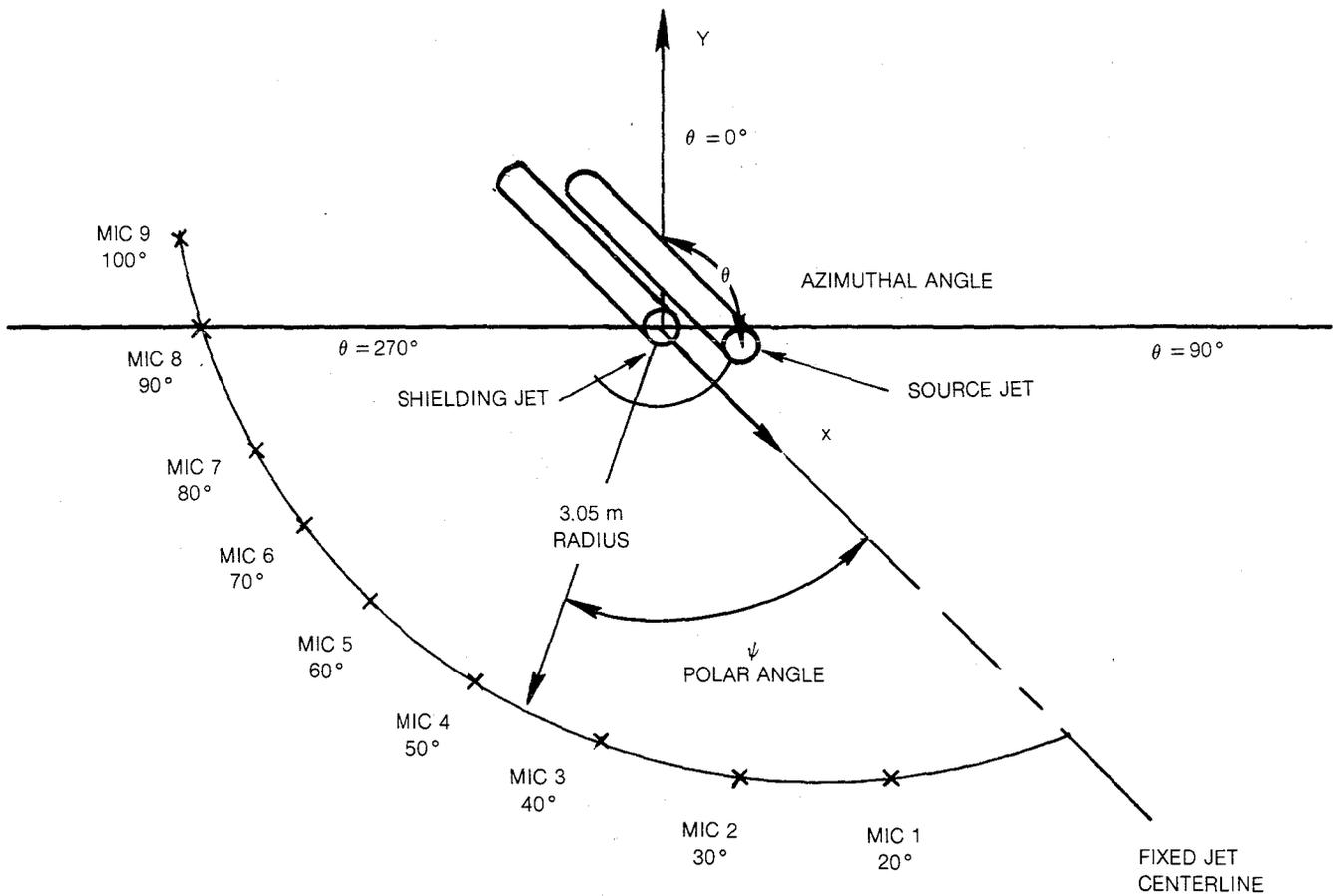
NOTE: THE REFERENCE AXIS FOR THE THEORETICAL (SEE FIG. 5) AND EXPERIMENTAL DEFINITIONS OF θ DIFFER BY 90° SEE TEXT — DESCRIPTION OF EXPERIMENT FOR DISCUSSION.

Figure 7 — Coordinate System with Microphone and Dual Jet Orientation Used in Experimental Program

PLENUM

FLEXIBLE TUBING

HEATED
SUPPLY

ROTATING DISK

SOURCE JET

SHIELDING JET

REMOVABLE, MATCHED
NOZZLE SET

FIXED MICROPHONE

DRIVE
MOTOR
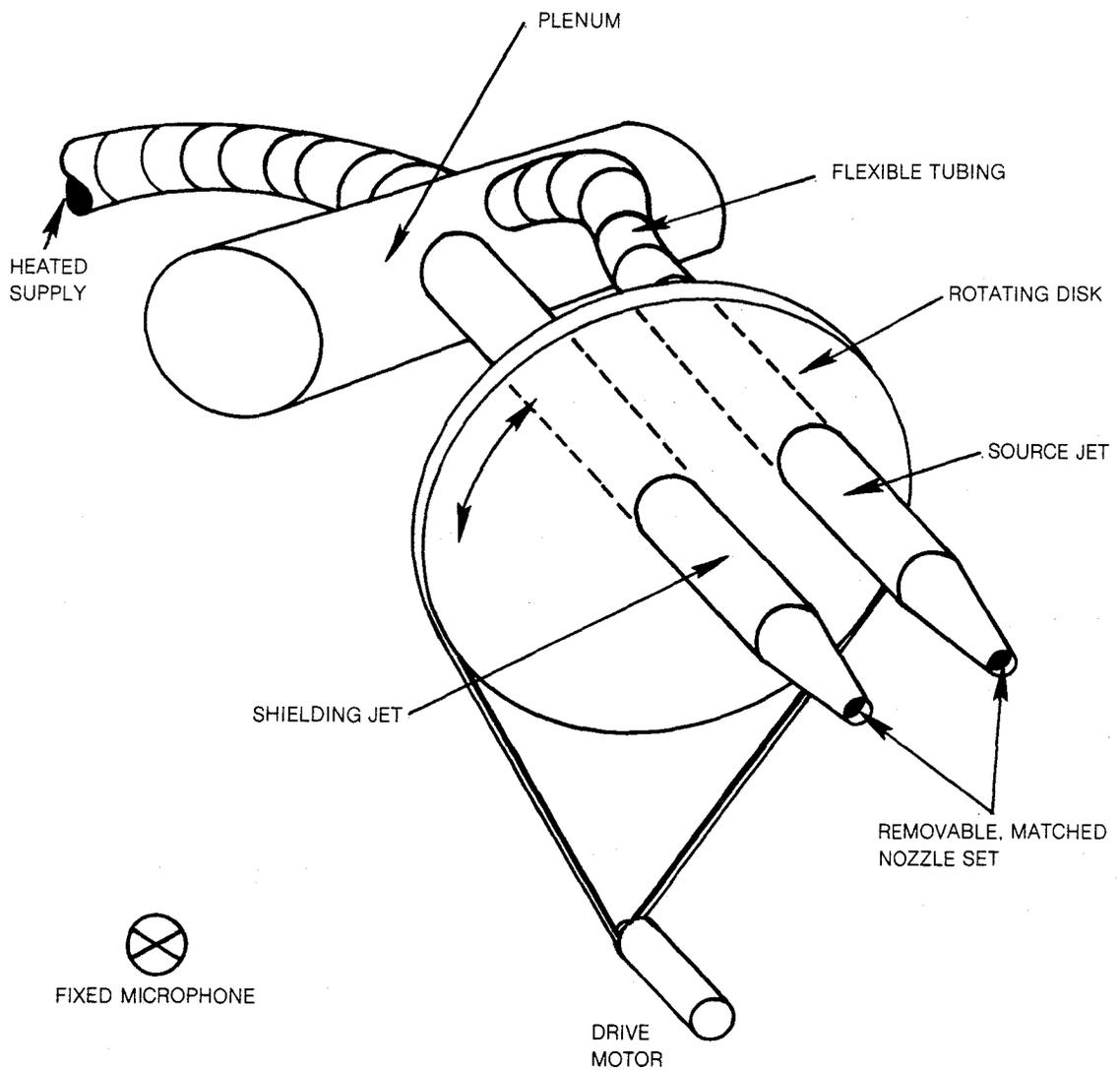
Figure 8 — Schematic Diagram of Source Jet Rotation Mechanism

Figure 9 — Photograph of Traversing System
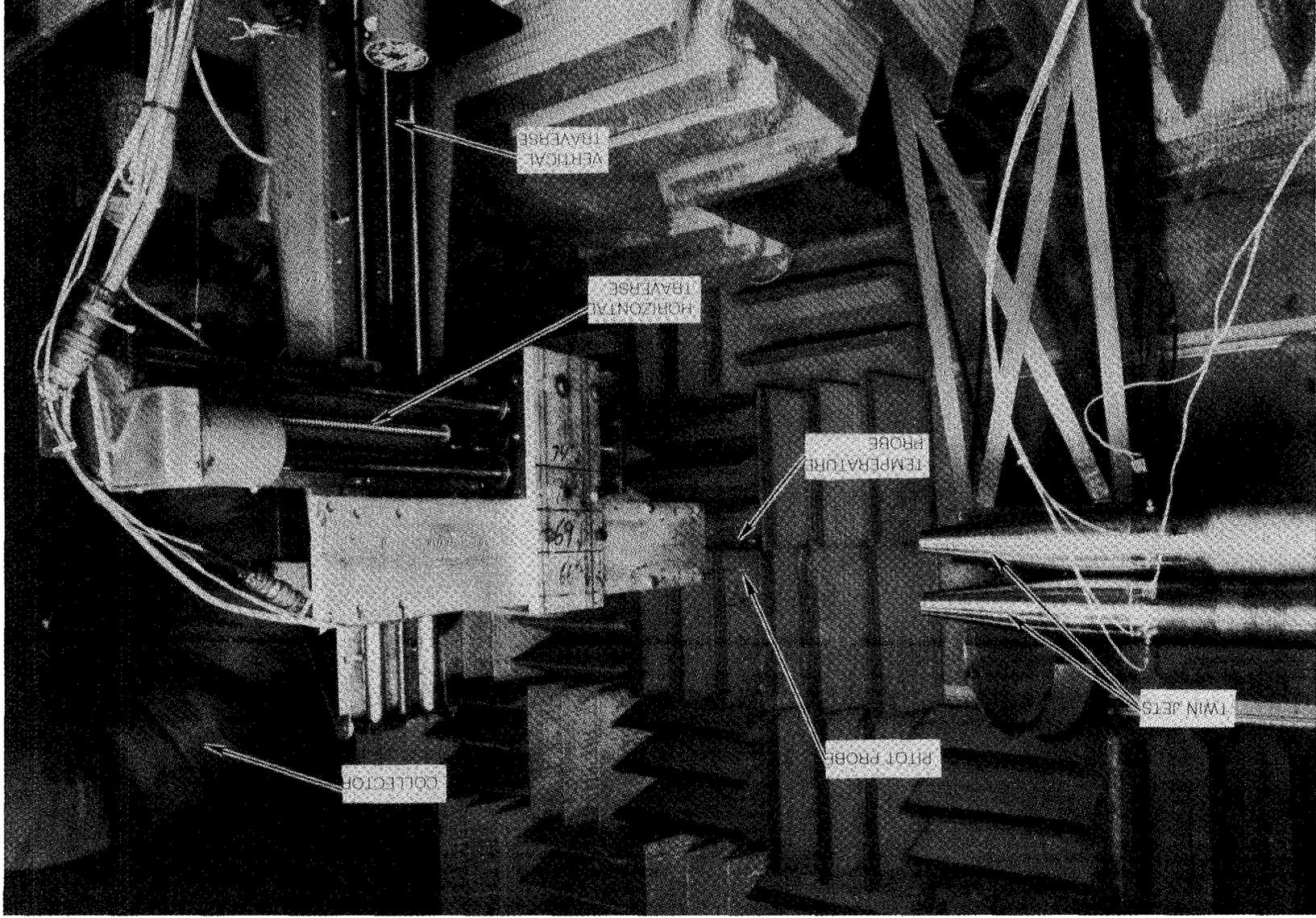
Figure 9 — Photograph of Traversing System
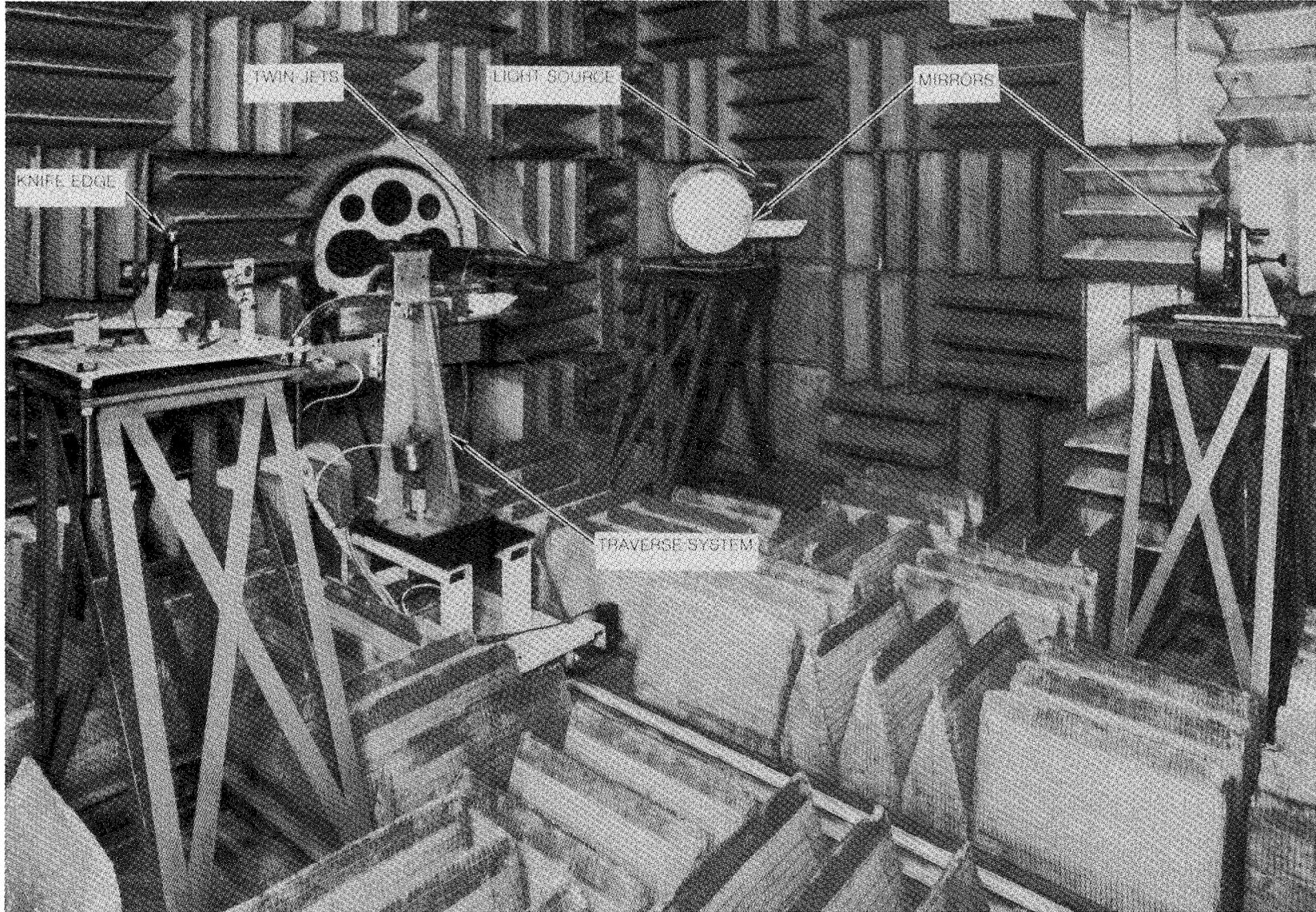
Figure 10 — Photograph Showing Schlieren System
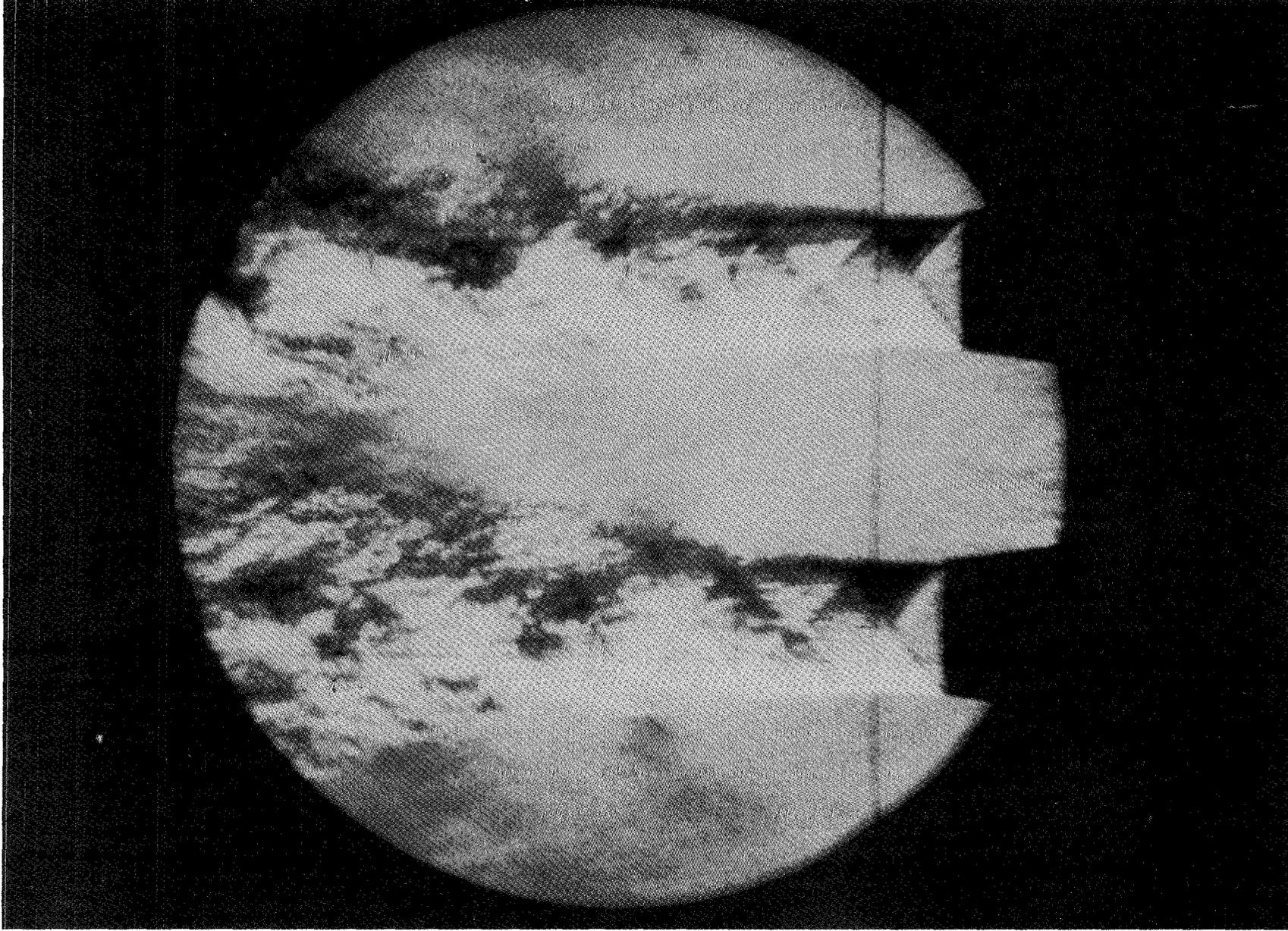
Figure 11 — Schlieren Photograph of Dual Jet System at Off Design Condition
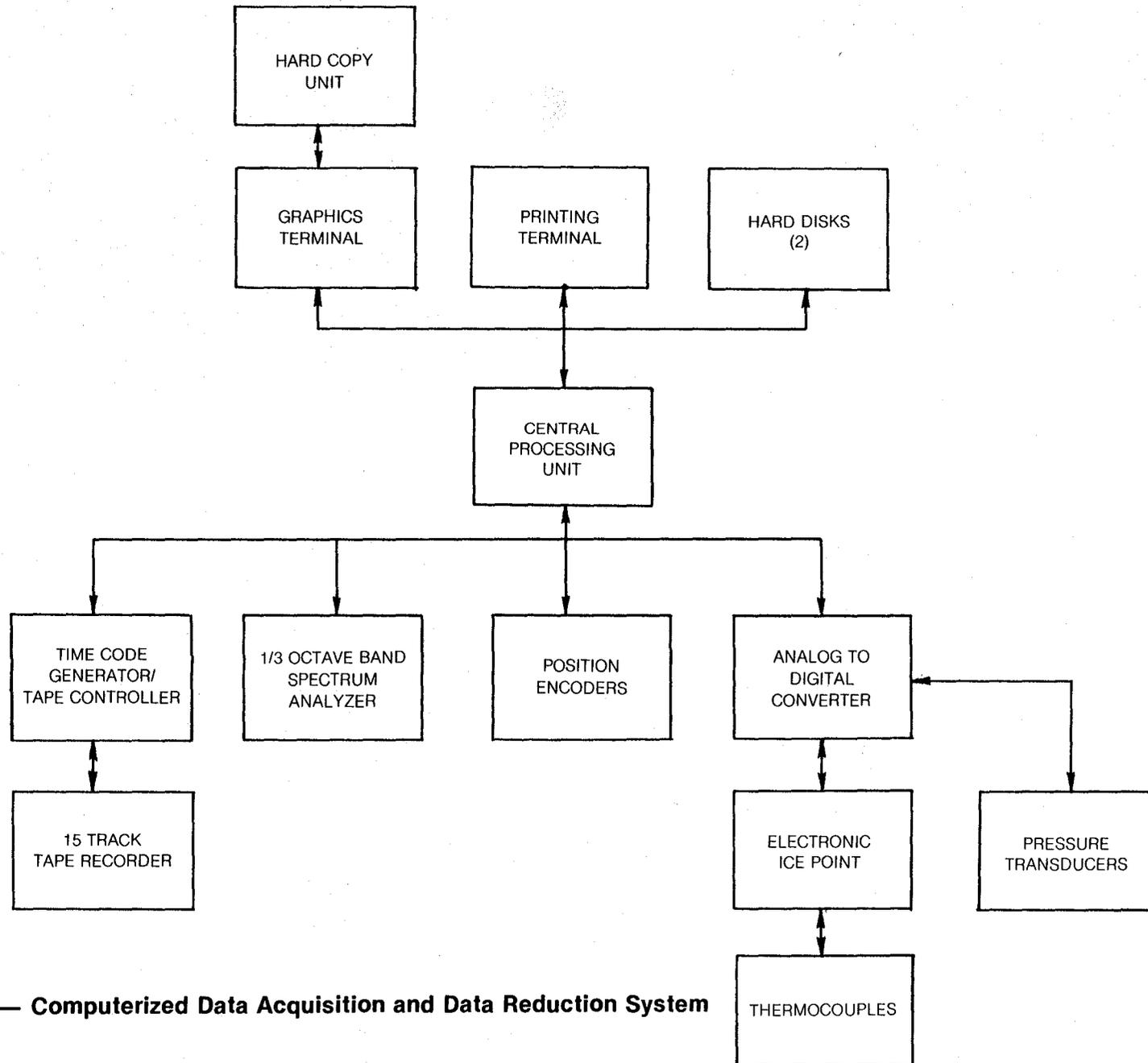
Figure 12 — Computerized Data Acquisition and Data Reduction System
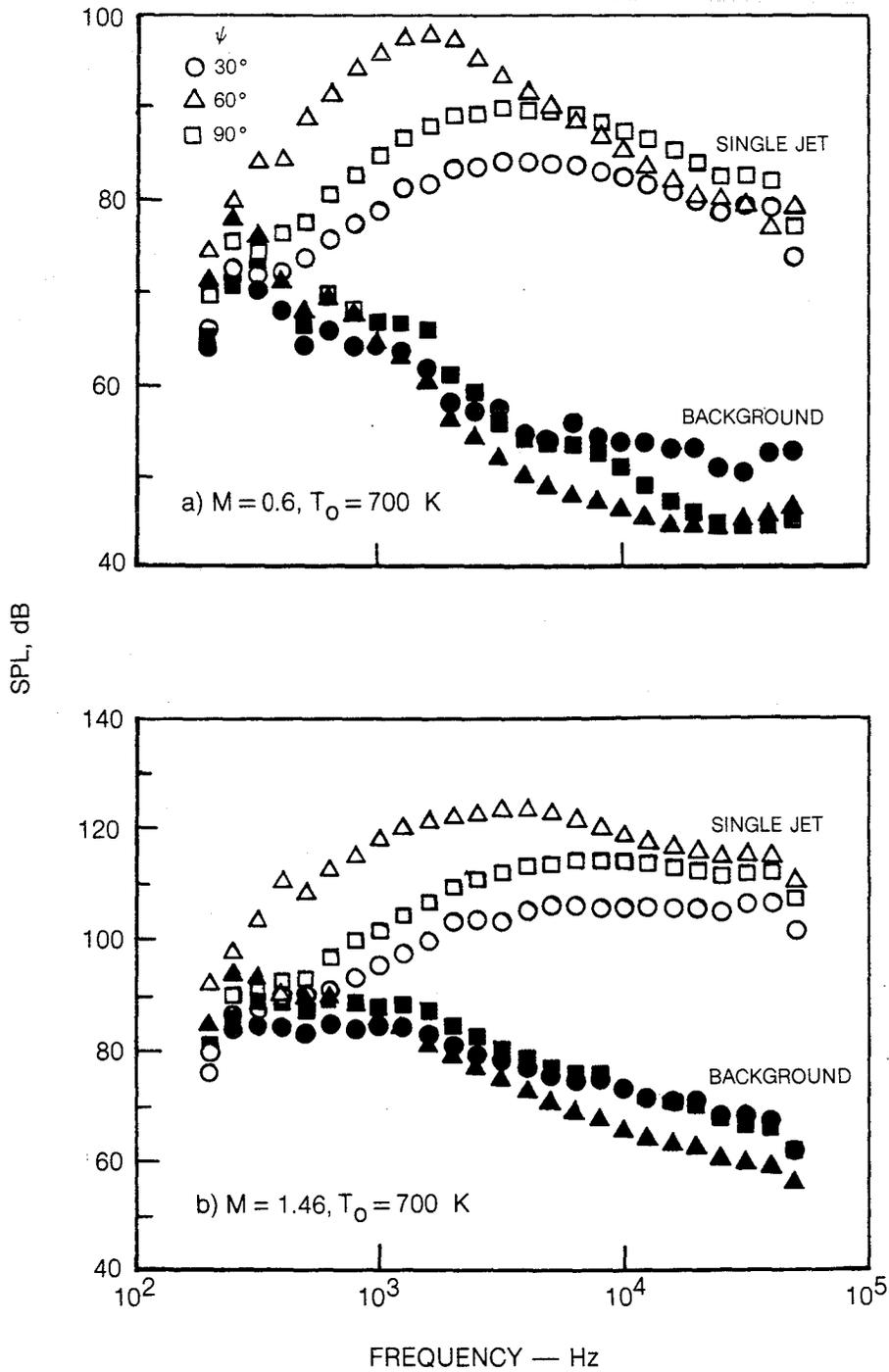
Figure 13 — Single Jet vs Background Noise Levels
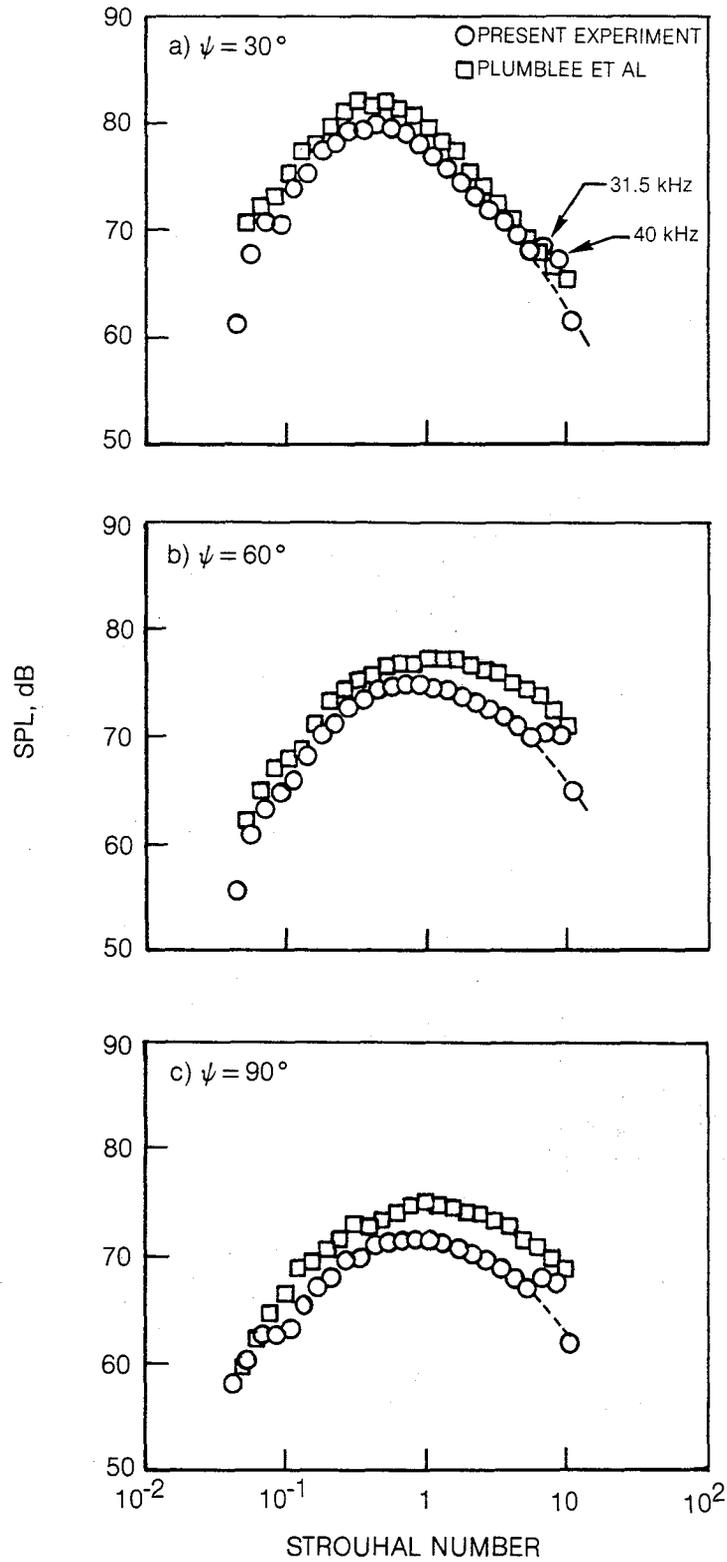
Figure 14 — Comparison Between Current Single Jet Spectrum and Previous Experiment of Plumblee, M = 0.6, T_o = 300K
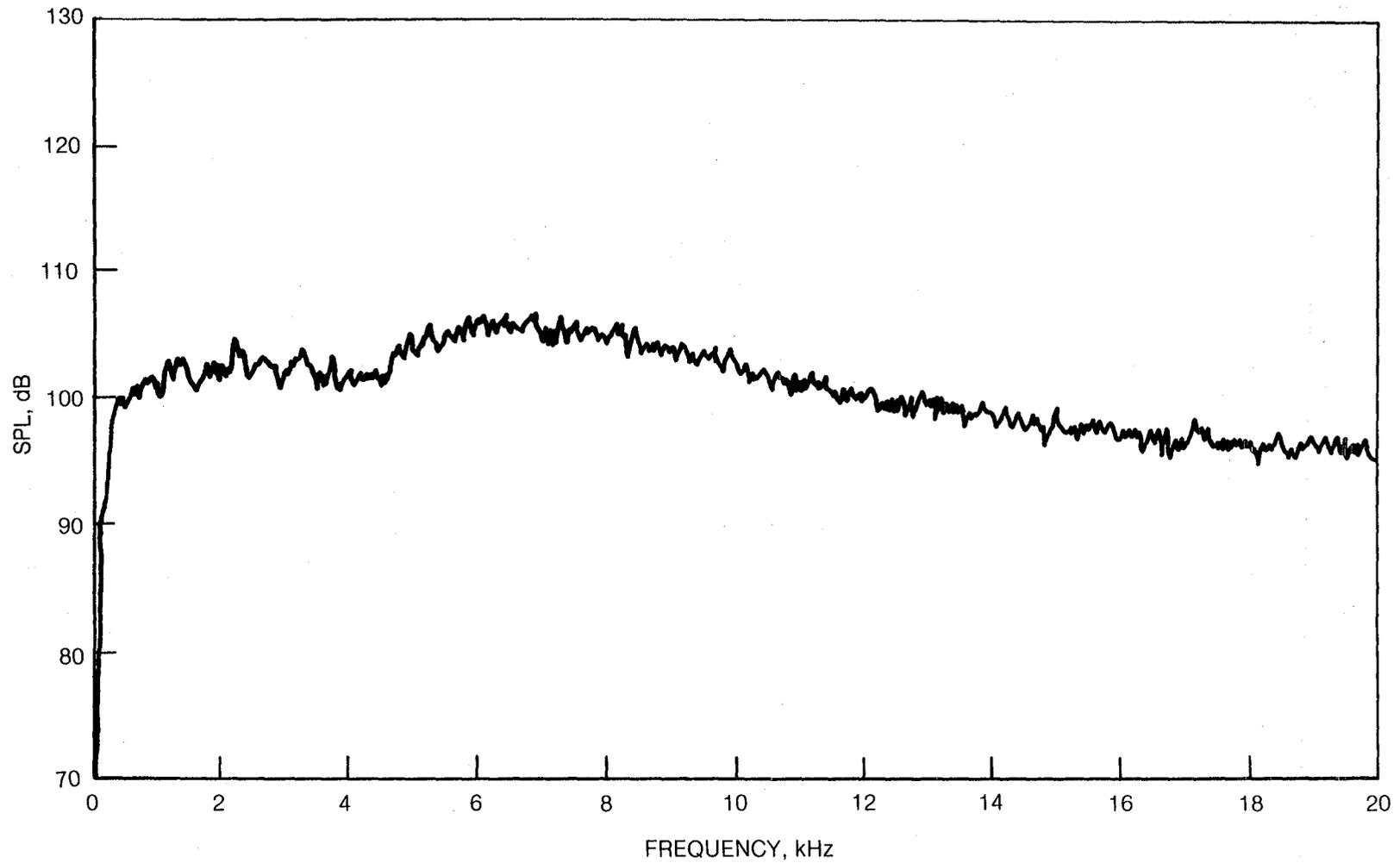
Figure 15 — Narrowband Spectra Showing Shock Free Operation of Single Supersonic Jet
M =1.46, T_o =300 K, ψ =90°
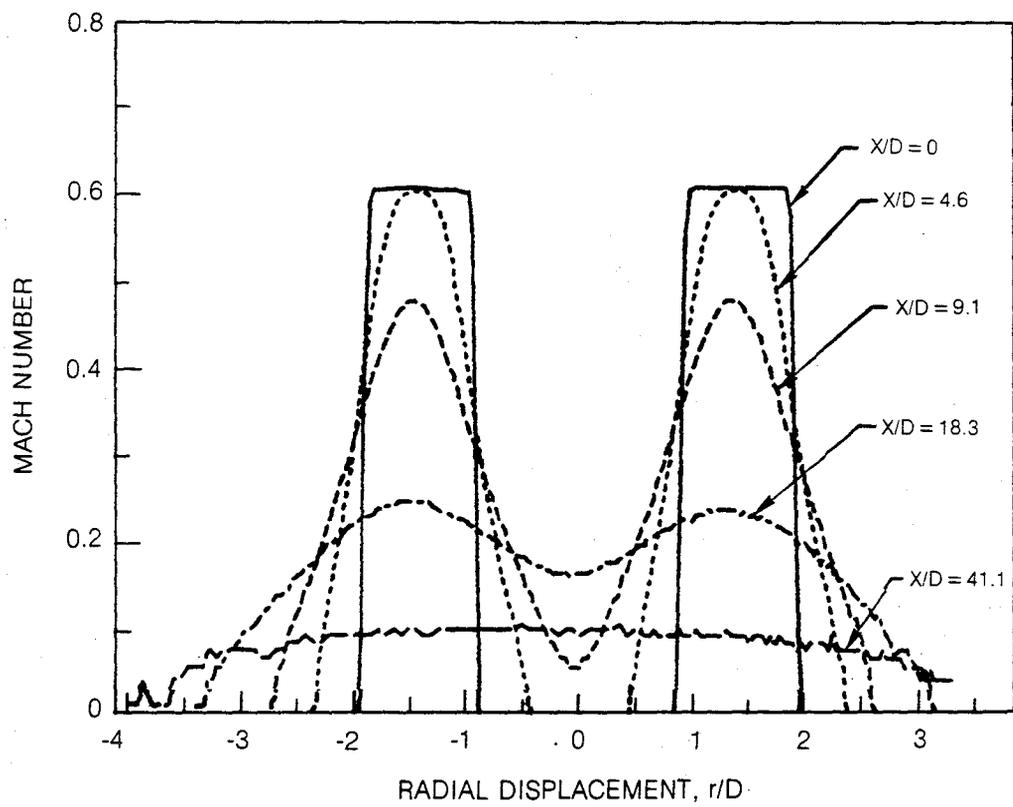
Figure 16 — Dual Jet Radial Mach Number Profile, $T_0 = 300$ K, M = 0.6, S/D = 2.7

110
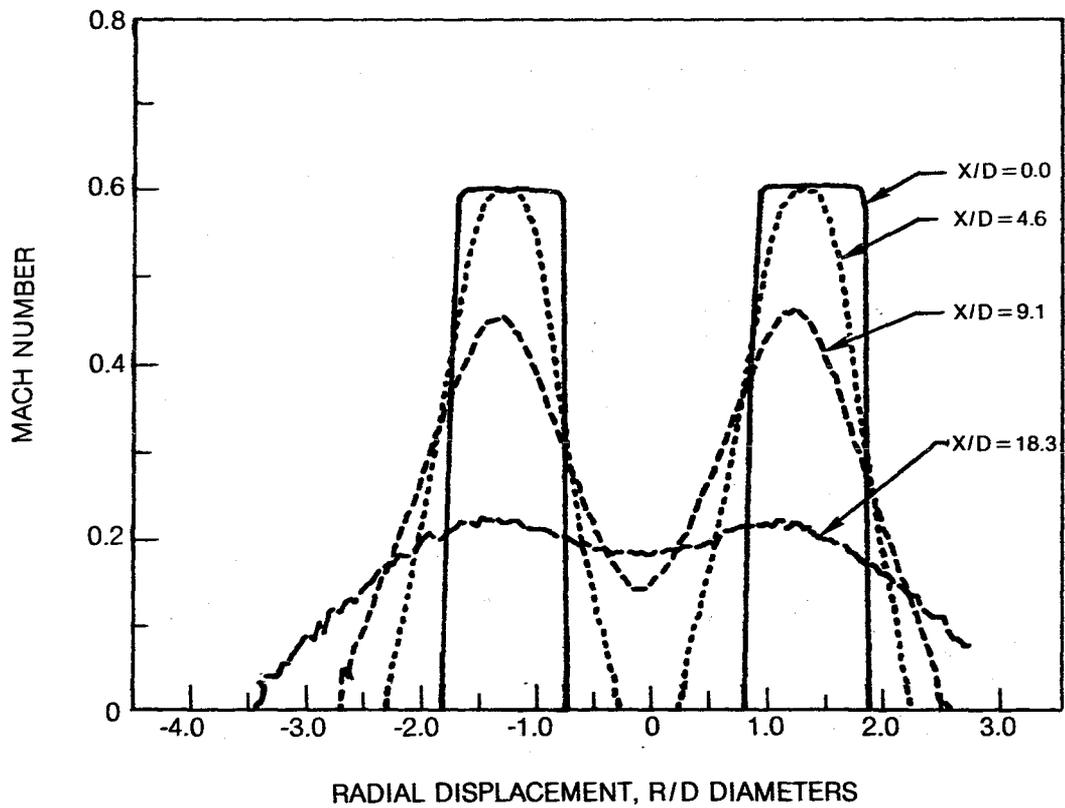
Figure 17 — Dual Jet Radial Mach Number Profile, $T_o = 811$ K, M = 0.6, S/D = 2.3
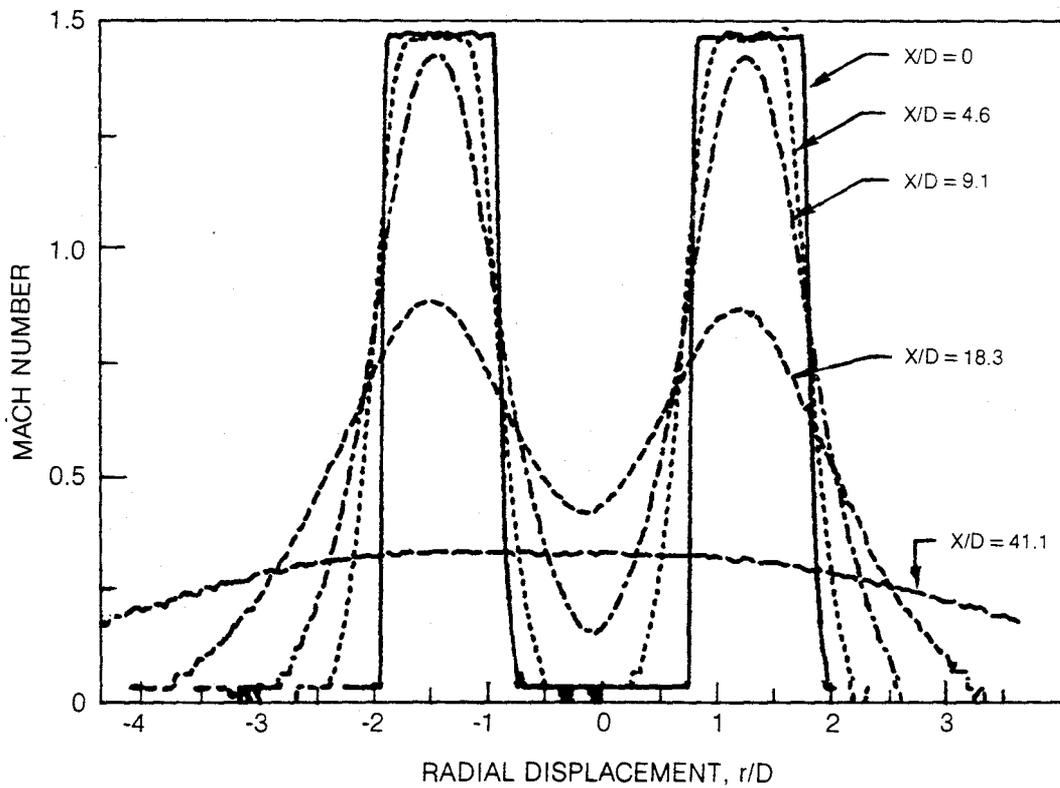
Figure 18 — Dual Jet Radial Mach Number Profile, $T_o = 300$ K, M =1.46, S/D =2.7
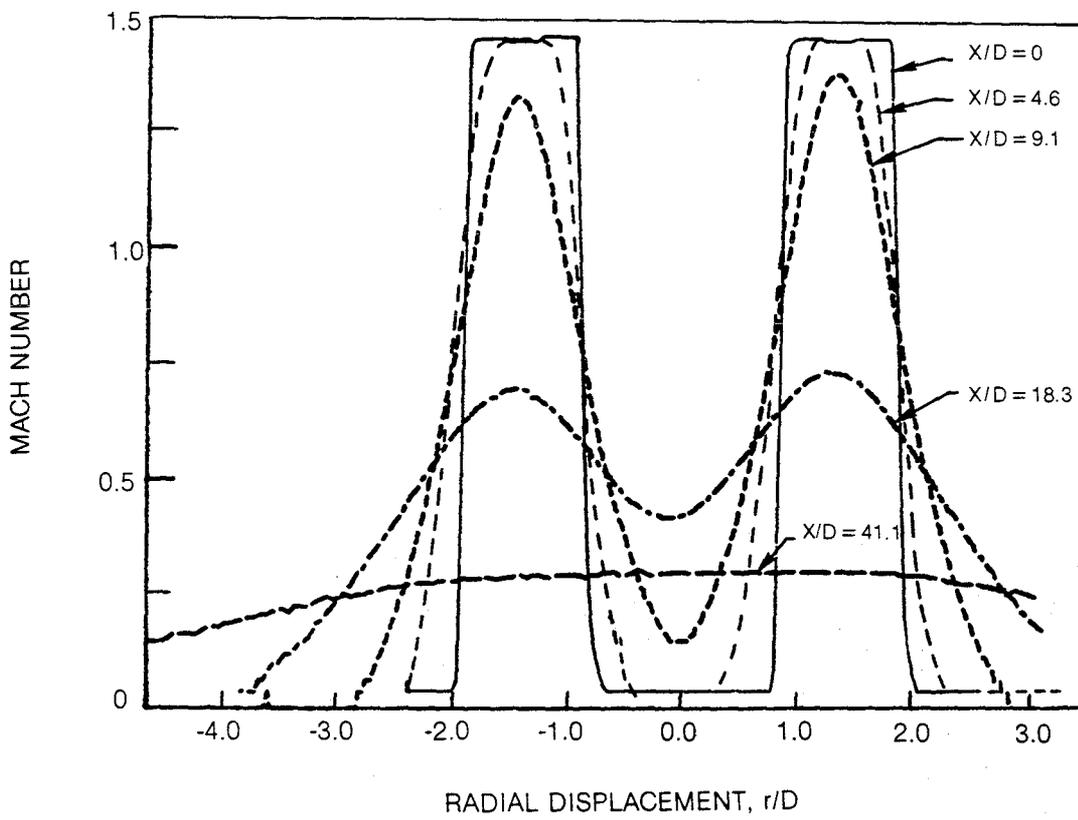
Figure 19 — Dual Jet Radial Mach Number Profile, $T_o = 811$ K, $M = 1.46$, $S/D = 2.7$

a) AXIAL REGION 0 ≤ X/D ≤ 45

b) ENLARGEMENT OF AXIAL REGION 0 ≤ X/D ≤ 9

AXIAL DISPLACEMENT, X/D
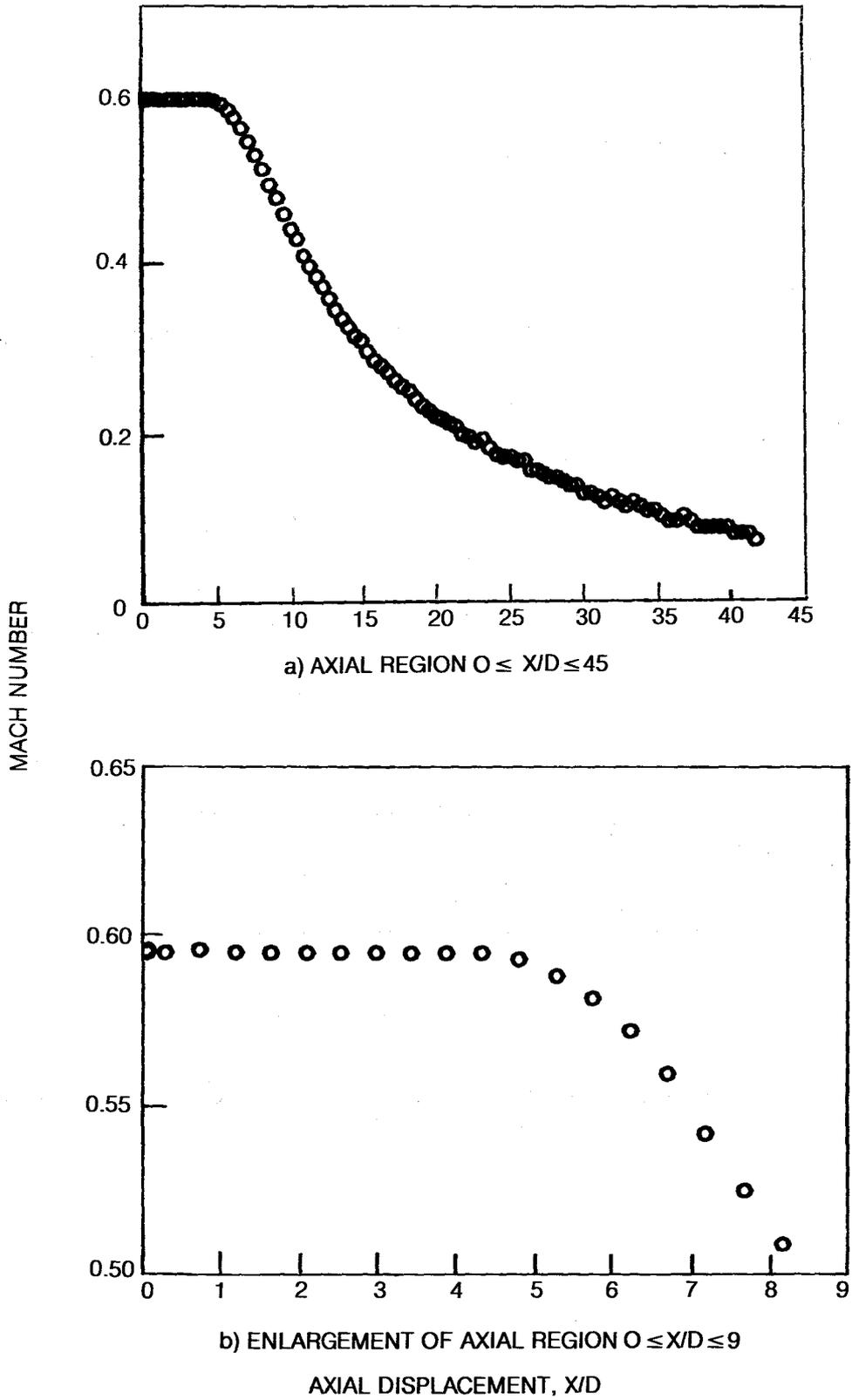
Figure 20 — Axial Centerline Mach Number Profile, $T_o = 300$ K, M = 0.6
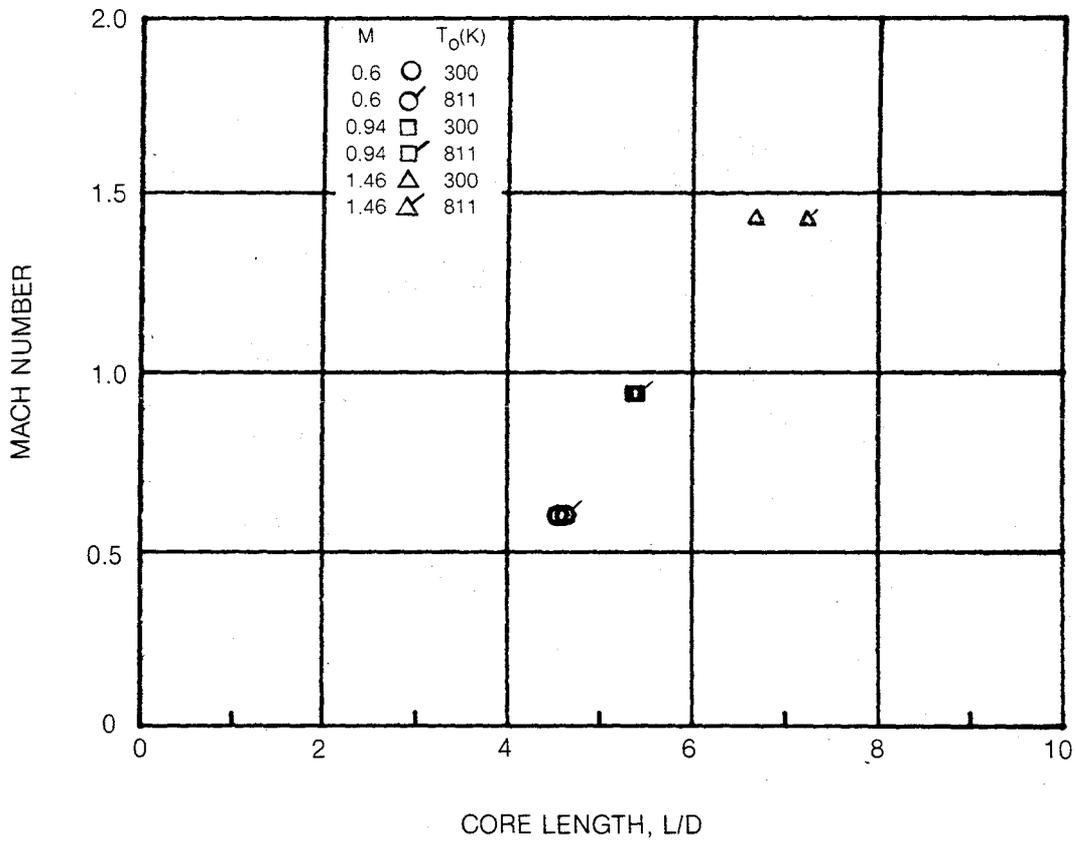
Figure 21 — Effect of Mach Number and Temperature on Potential Core Length
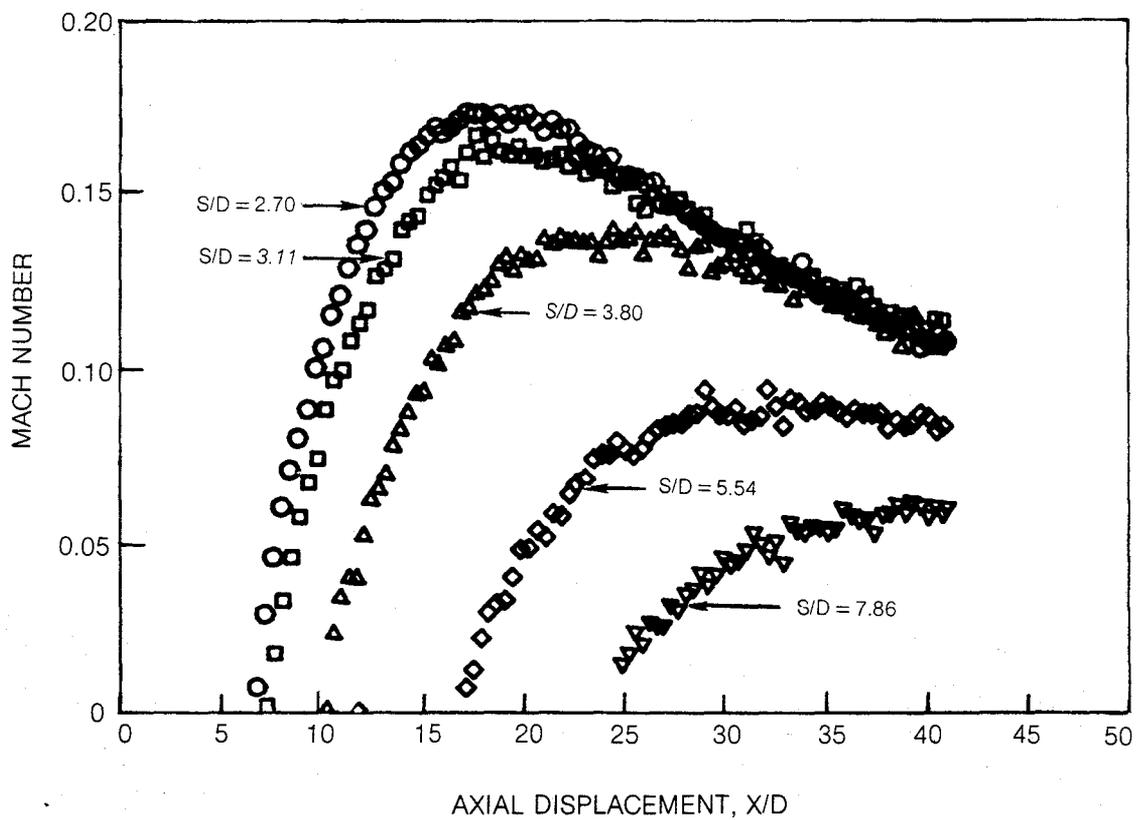
Figure 22 — Axial Mach Number Profiles on Mid-Gap Line for Various Dual Jet Spacings
$T_O = 300$ K , M = 0.6
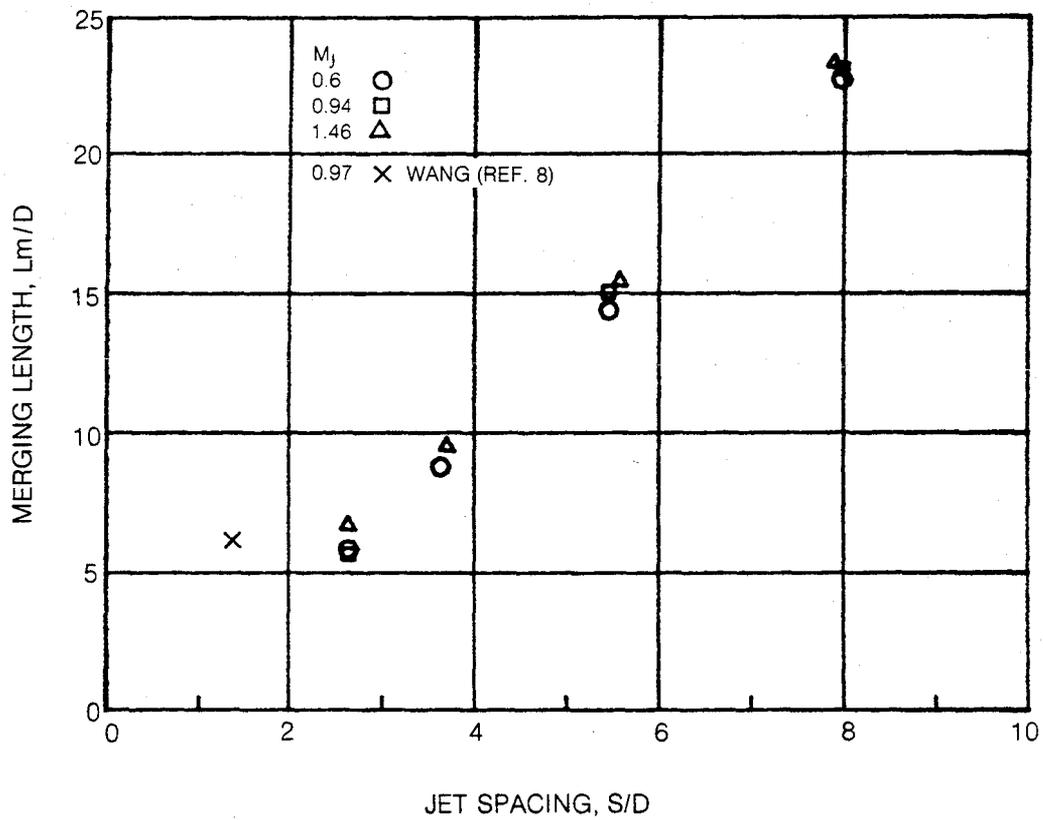
Figure 23 — Effect of Jet Spacing and Mach Number on Merging Length
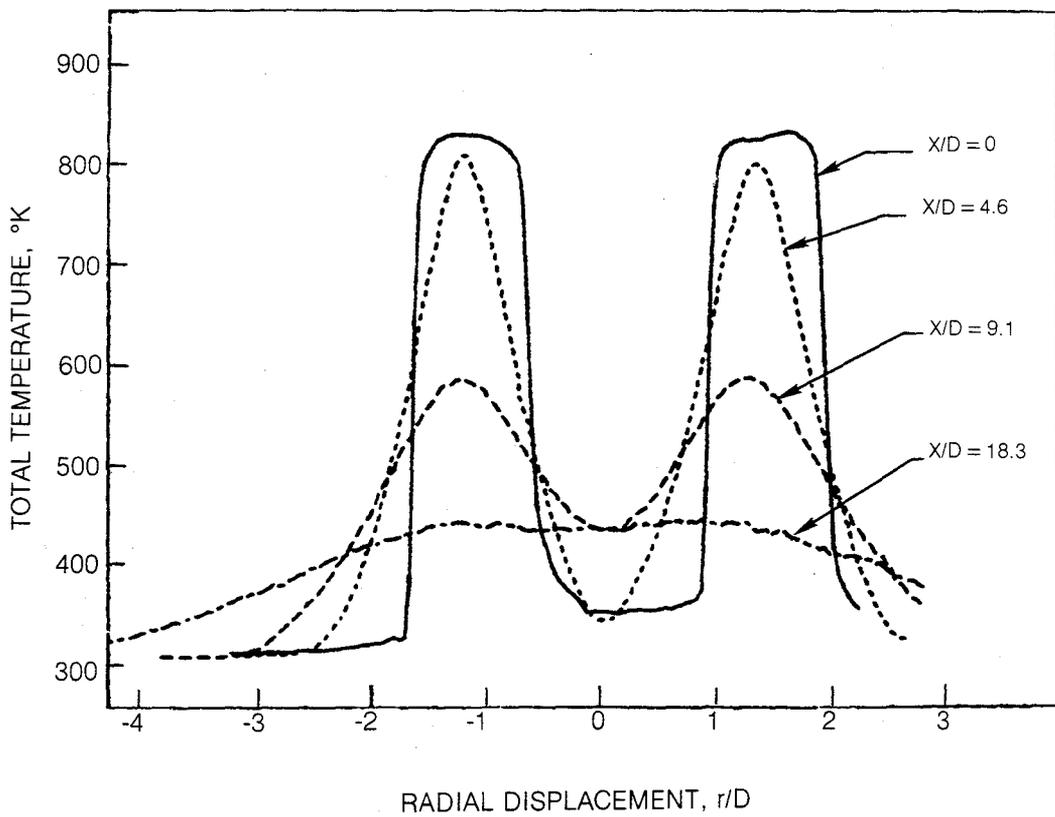
Figure 24 — Dual Jet Radial Temperature Profile, $T_O = 811$ K, M = 0.6, S/D = 2.7
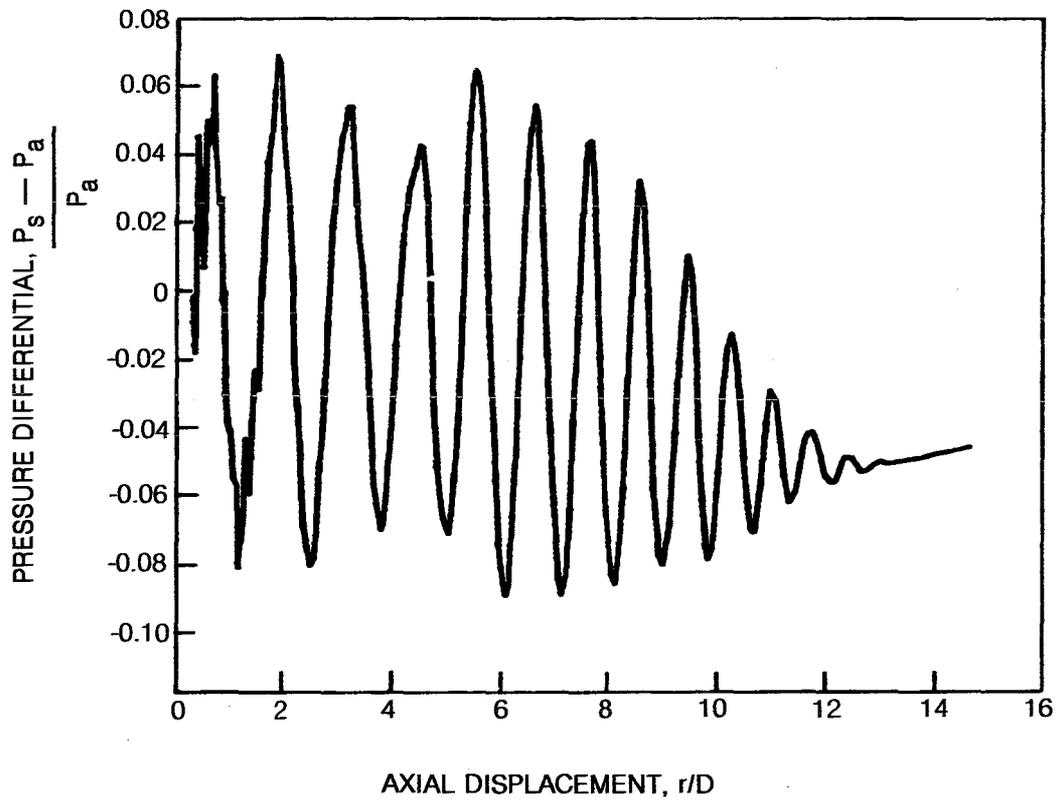
Figure 25 — Axial Static Pressure Variation on Jet Centerline, $T_0 = 300$ K, M = 1.46
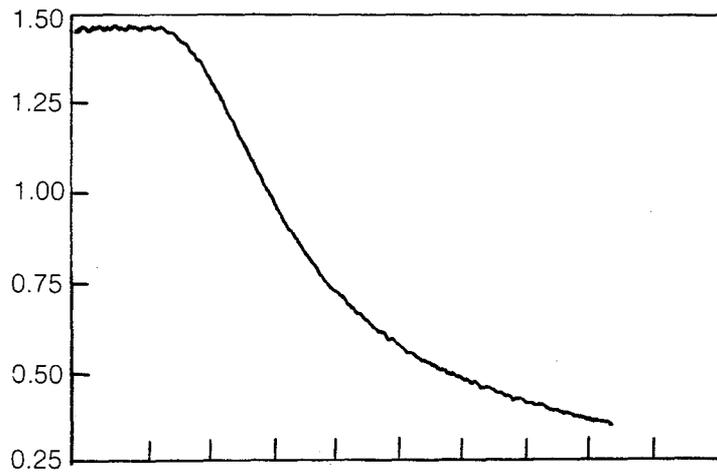
a) $0 \le X/D \le 50$
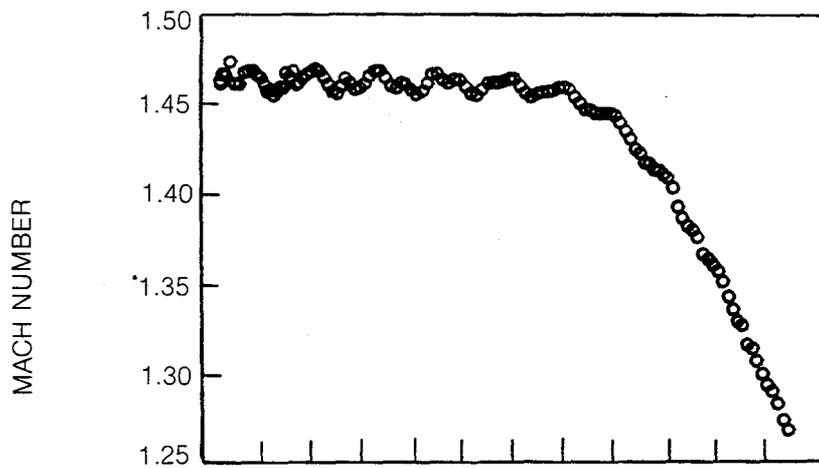
b) ENLARGEMENT OF REGION $0 \le X/D \le 12$
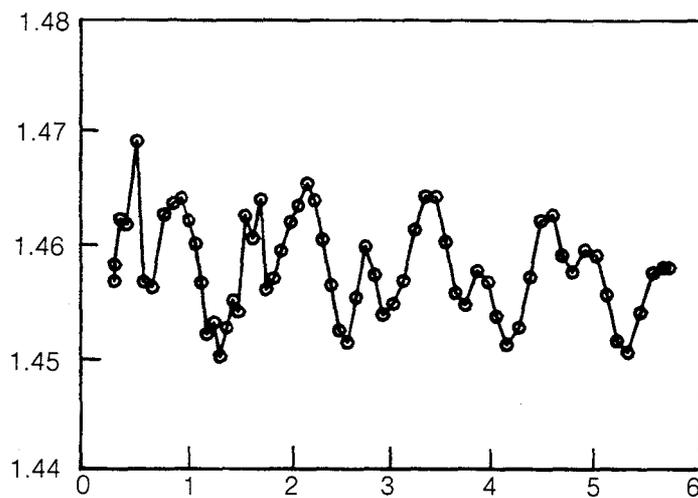
c) DETAIL OF REGION $0 \le X/D \le 6$

AXIAL DISPLACEMENT, X/D

MACH NUMBER

Figure 26 — Axial Centerline Mach Number Profile, T_O 300 K, M = 1.46
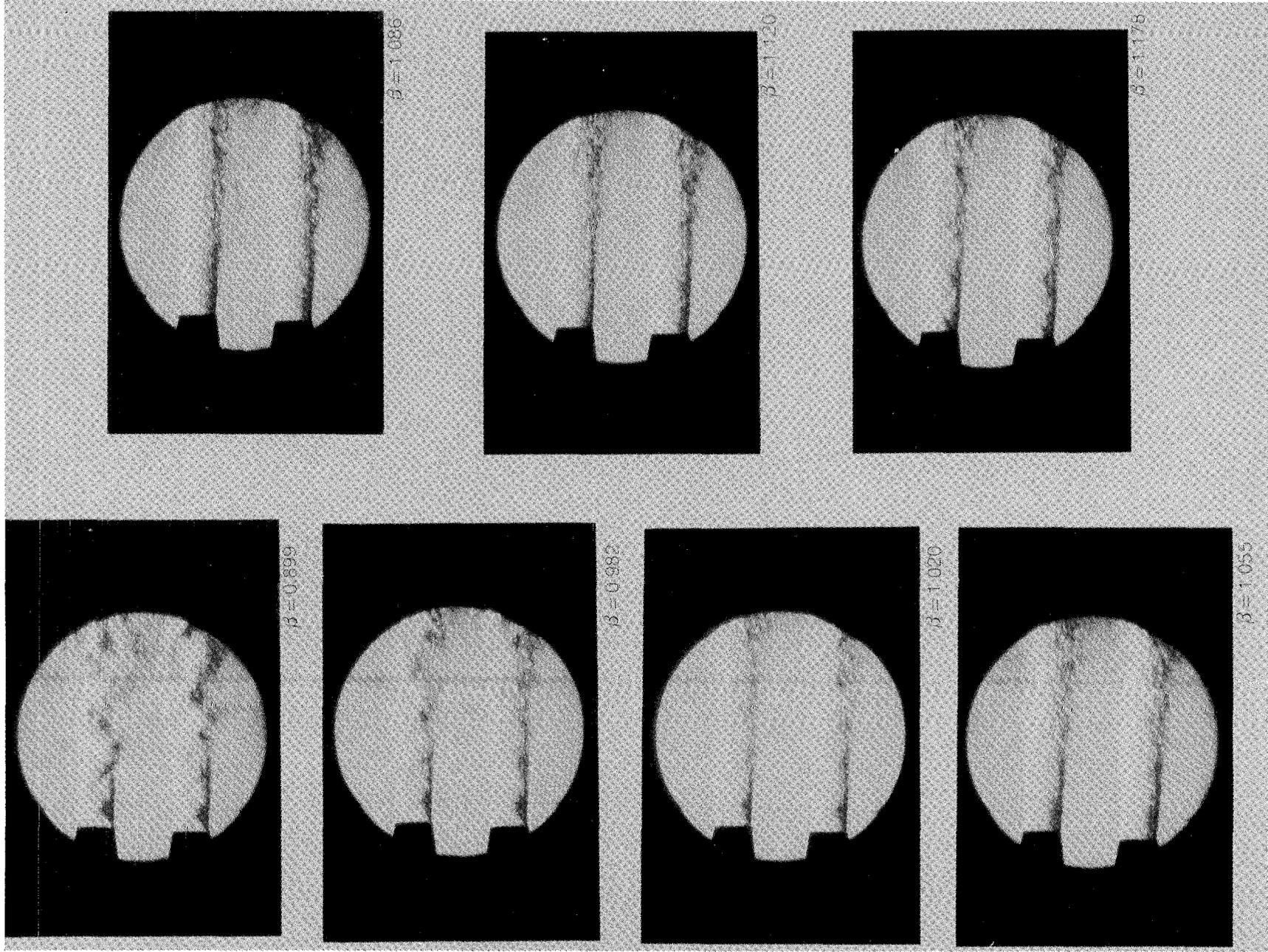
Figure 27 — Schlieren Photographs of Supersonic Nozzles at Different Expansion Ratios

a) SOURCE JET RADIATION

b) SHIELDING JET RADIATION
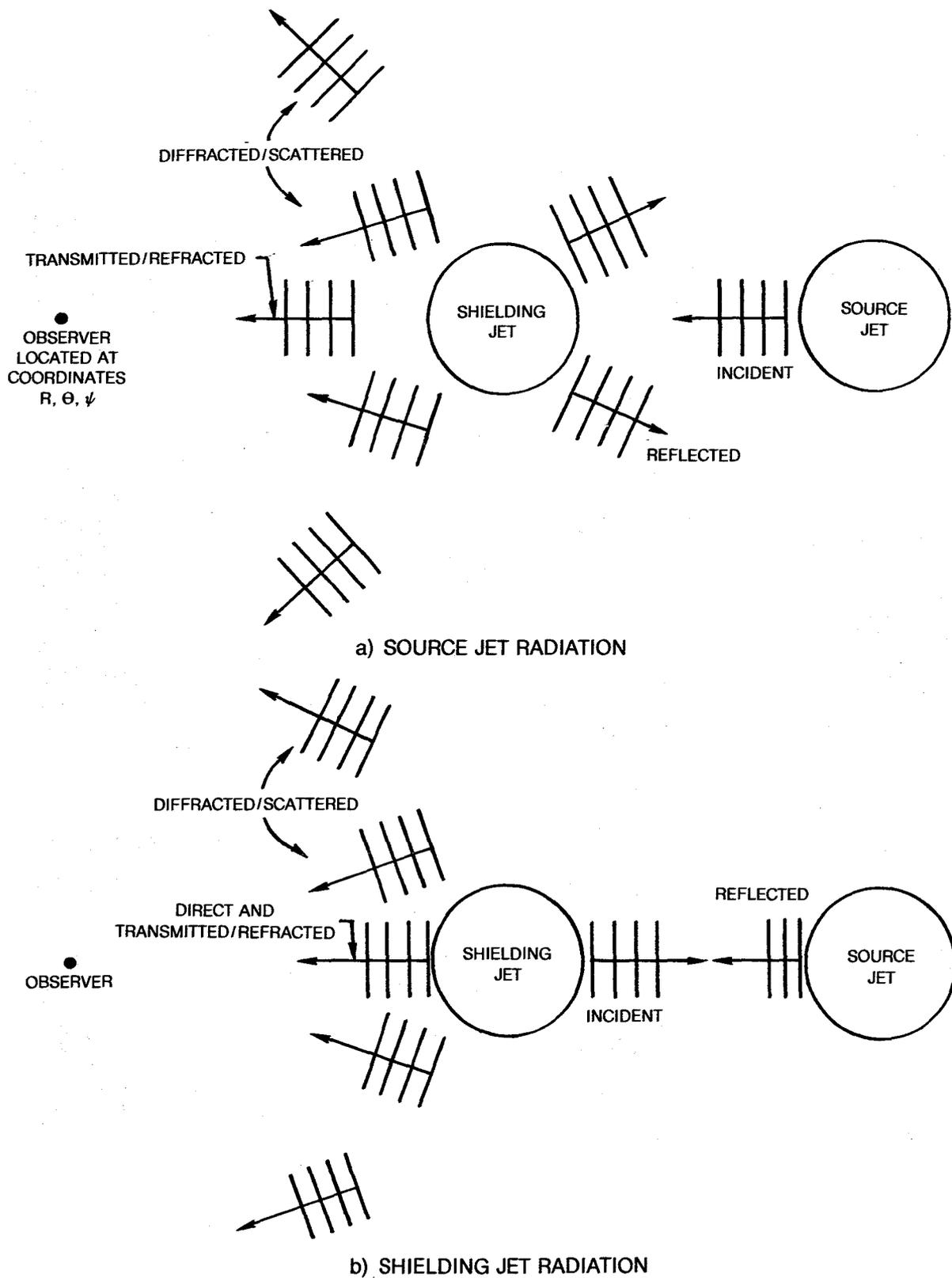
Figure 28 — Acoustic Radiation Arriving at Observer Location Due to Source and Shielding Jets
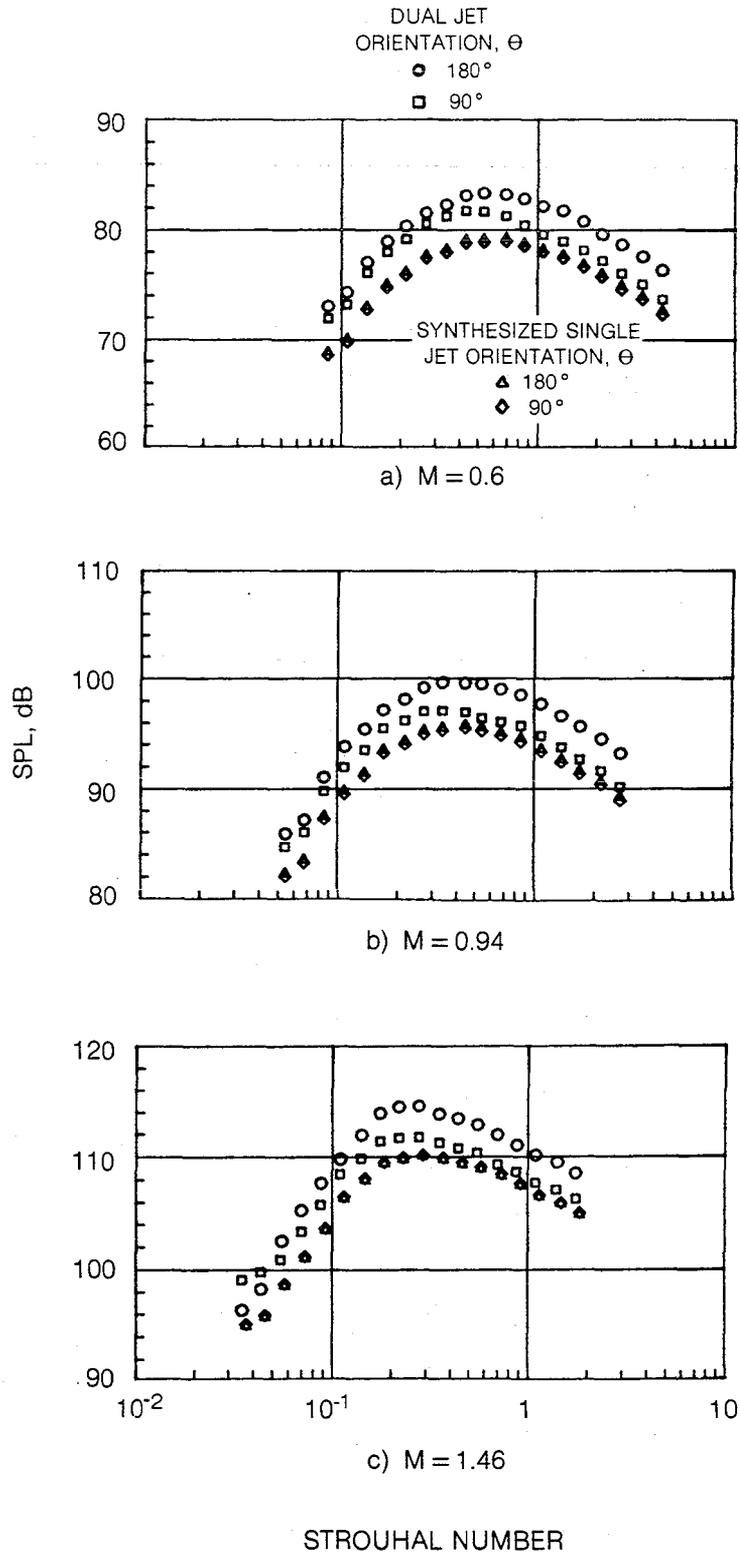
Figure 29 — Mach Number Effect on Dual Jet Spectrum, $T_O = 300$ K, $S/D = 8.1$, $\psi = 40°$

d) M = 0.6

e) M = 0.94

STROUHAL NUMBER
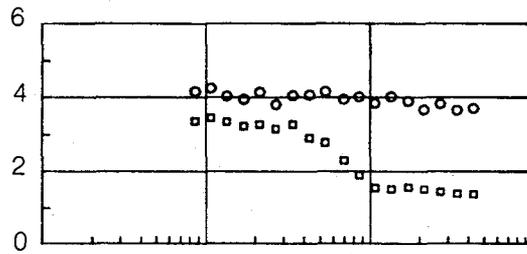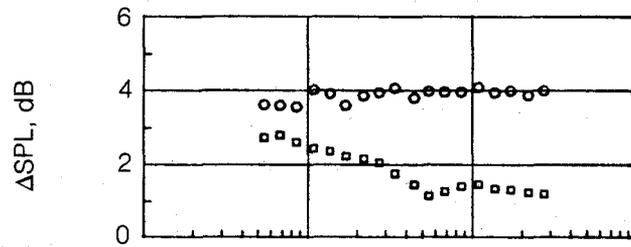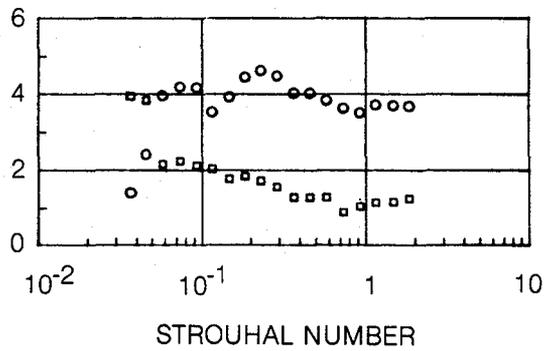
f) M = 1.46

Figure 29 — Concluded
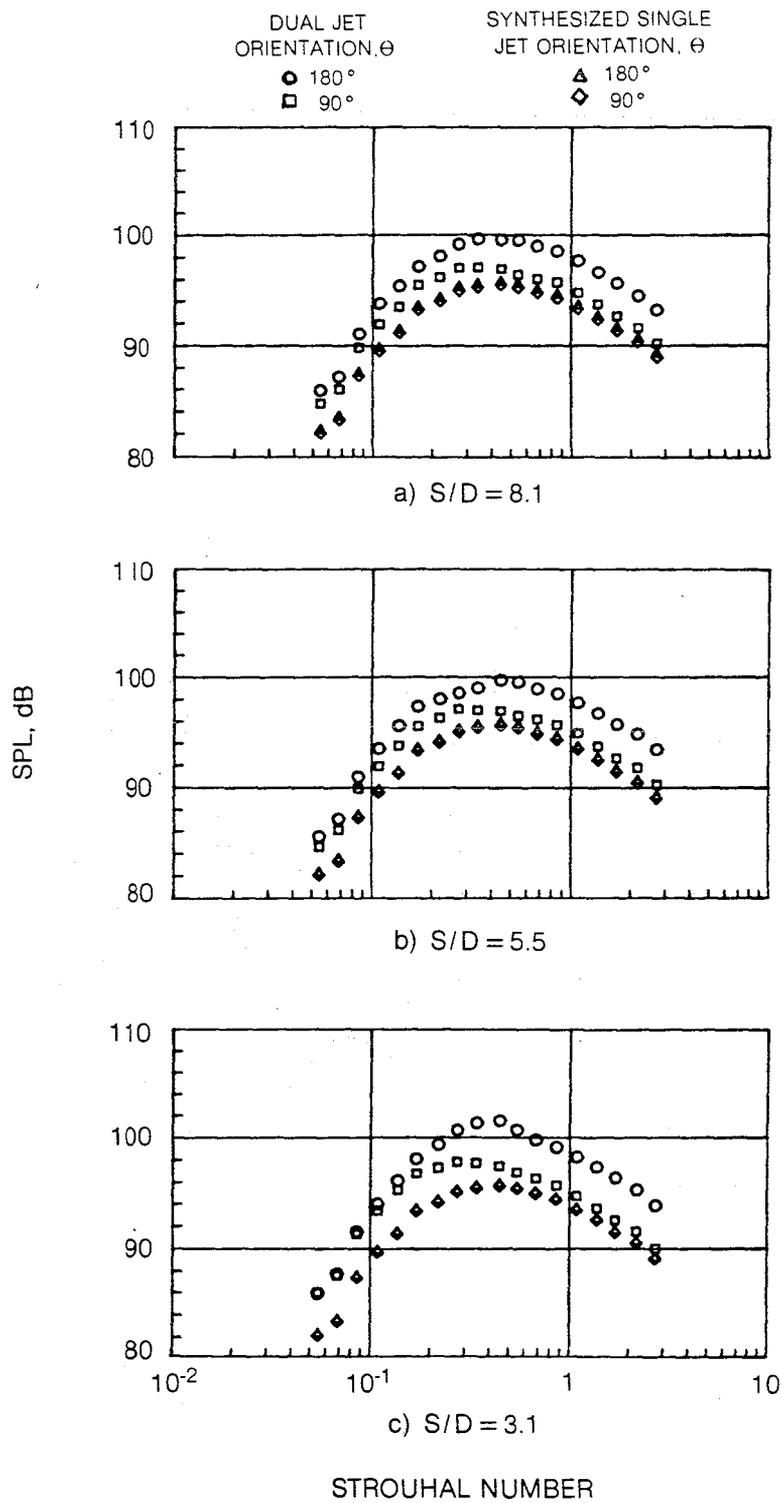
Figure 30 — Spacing Effect on Dual Jet Spectrum, $T_o = 300$ K, M = 0.94, $\psi = 40°$
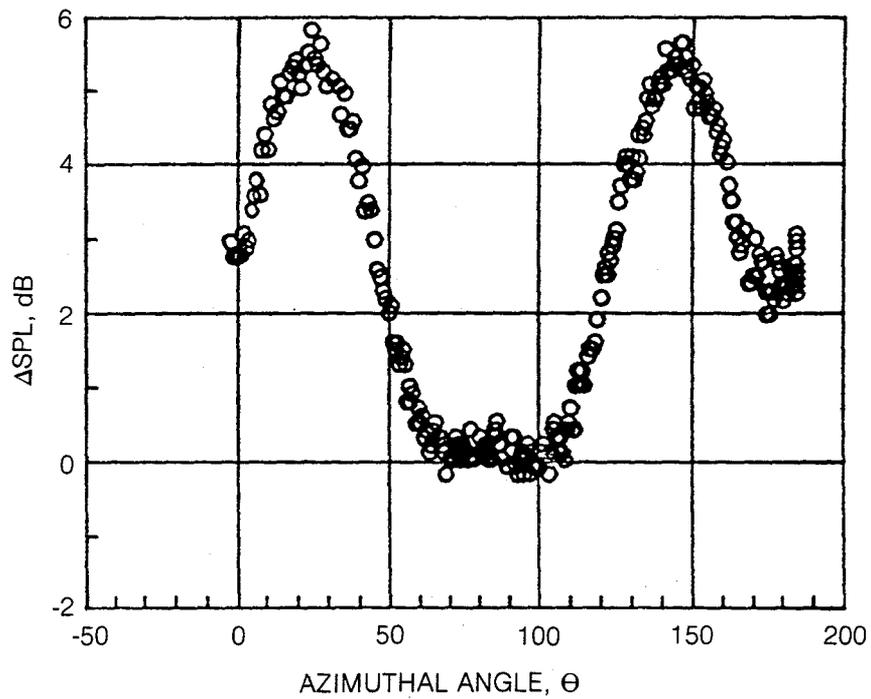
Figure 31 — Normalized Dual Jet Sound Pressure Level Dependence on Azimuthal Angle, $M = 0.6$, $T_o = 300\,°K$, $S/D = 8.1$, $f = 4$ kHz, $\psi = 20°$
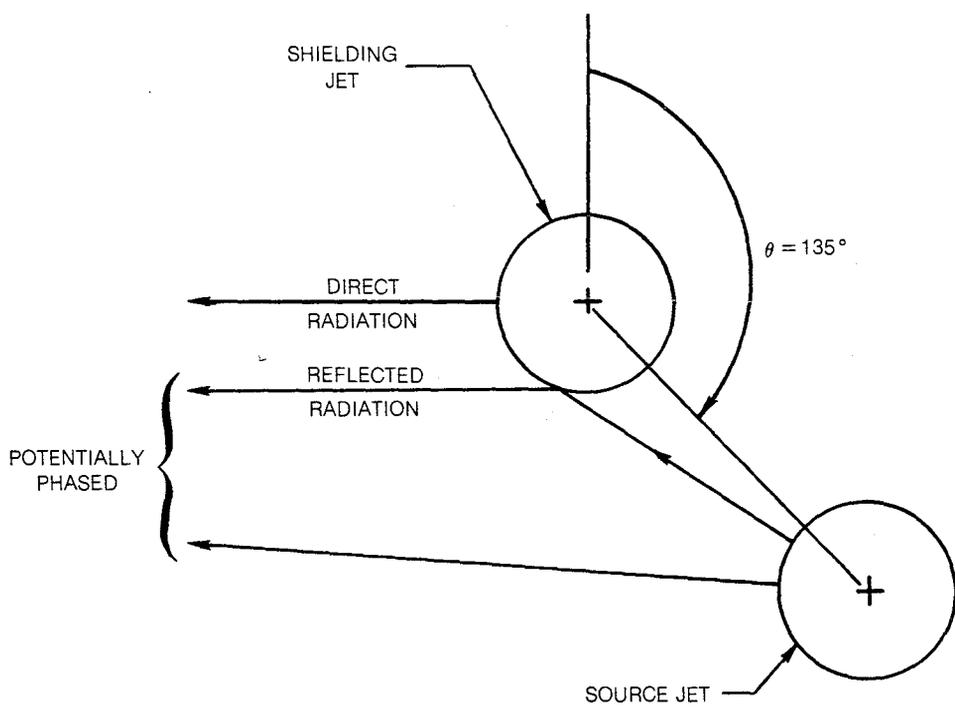
Figure 32 — Schematic Illustrating Sound Reflection by Adjacent Jet Increasing Noise at Observer Station
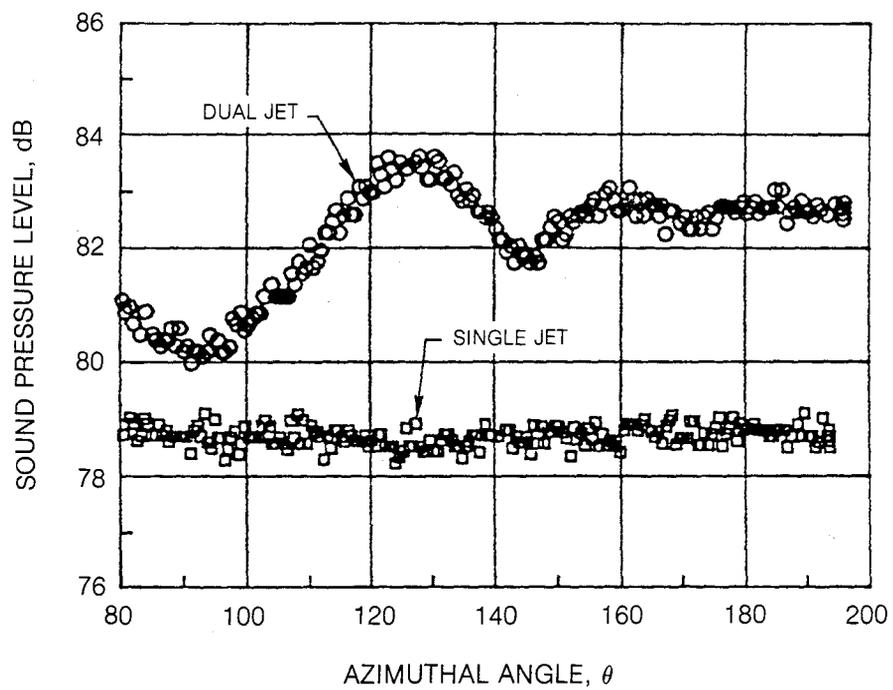
a) COMPARISON OF DUAL JET AND SINGLE JET AT f = 4 kHz

Figure 33 — Dual Jet and Single Jet Sound Pressure Level Dependence on Azimuthal Angle, M = 0.6, $T_O = 300\,°K$, S/D = 8.1, $\psi = 40°$
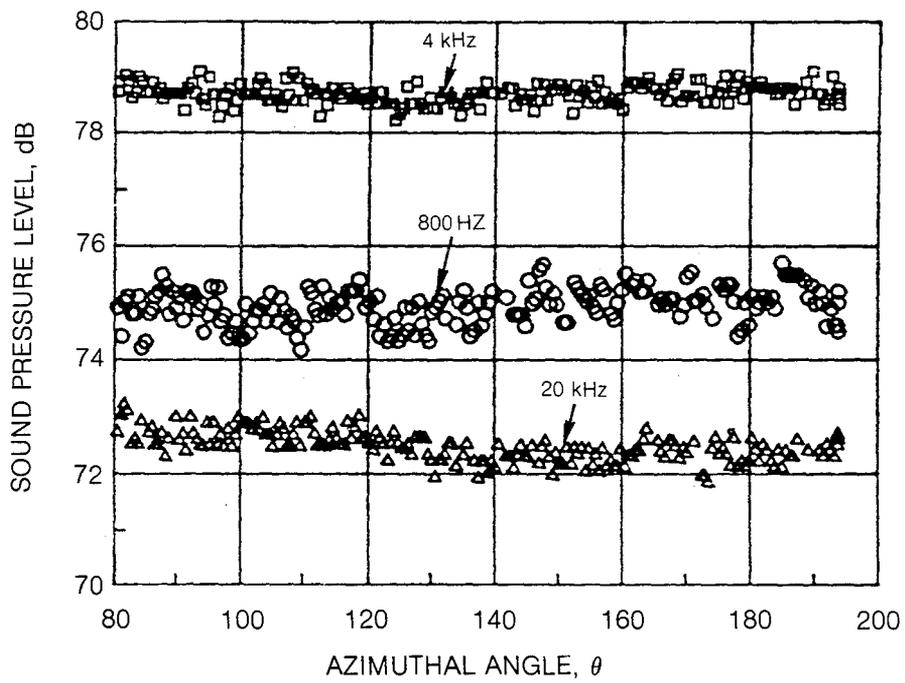
b) SINGLE JET DEPENDENCE ON FREQUENCY

Figure 33 — Concluded

SOURCE JET
MODELLED AS POINT
SOURCE

$\theta = 90°$

JET $\mathcal{C}$

ψ_1

$\mathcal{C}$

ψ_2

$\theta = 180°$

FIXED
MICROPHONE
LOCATION

ELLIPTICAL DIRECTIVITY PATTERN
USED FOR ILLUSTRATION PURPOSES ONLY
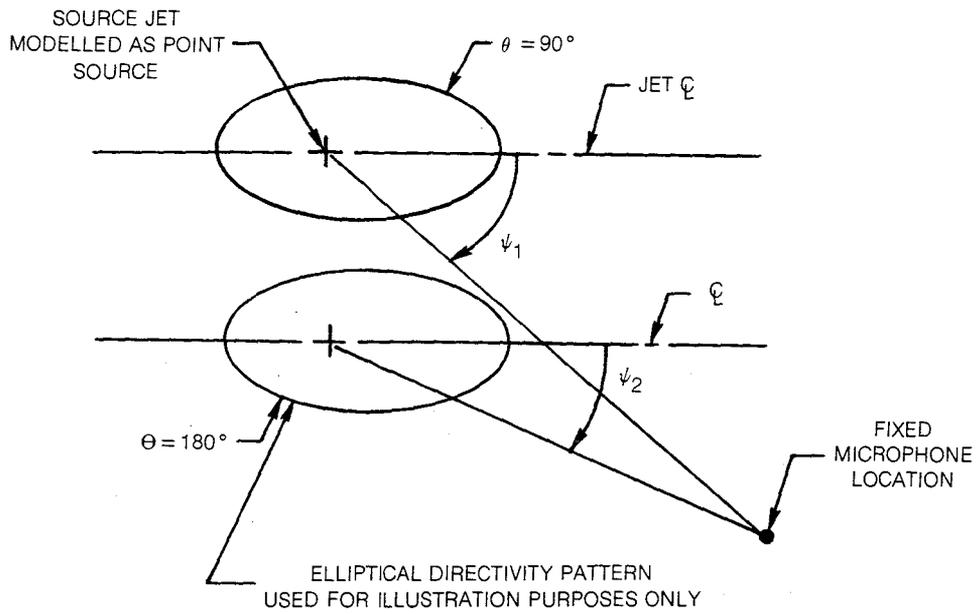
a) PLAN VIEW OF SOURCE JET SHOWING
POLAR RADIATION ANGLE CHANGES
SENSED AT FIXED MICROPHONE

SHIELDING
JET

$\theta = 90°$

$\theta = 180°$

MICROPHONE

SOURCE JET,
$\theta = 90°$
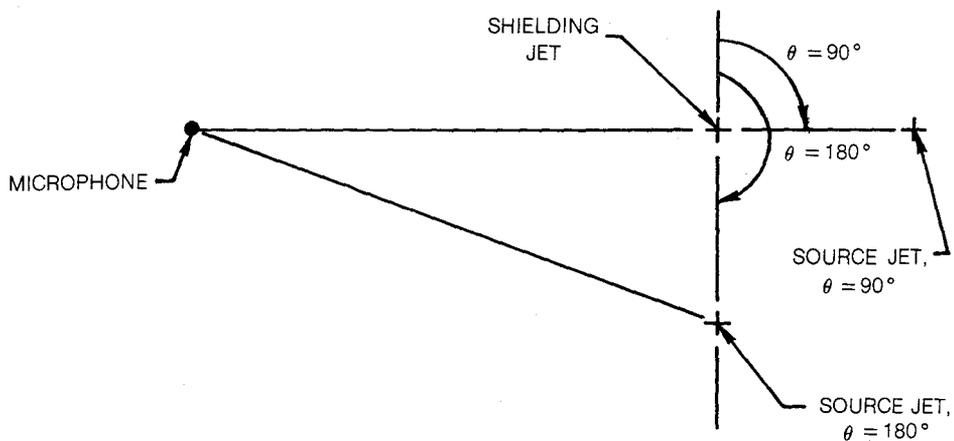
SOURCE JET,
$\theta = 180°$

b) END VIEW OF DUAL JET SYSTEM LOOKING UPSTREAM

Figure 34 — Source Jet Radiation Pattern Sensed by Fixed Microphone During Azimuthal Rotation

130
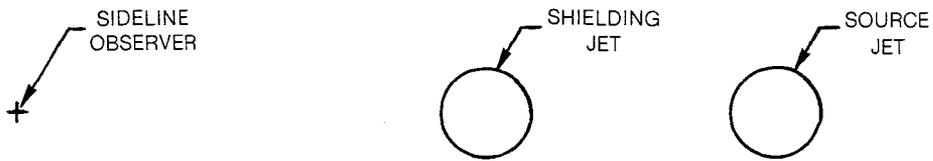
a) DUAL JET CONFIGURATION
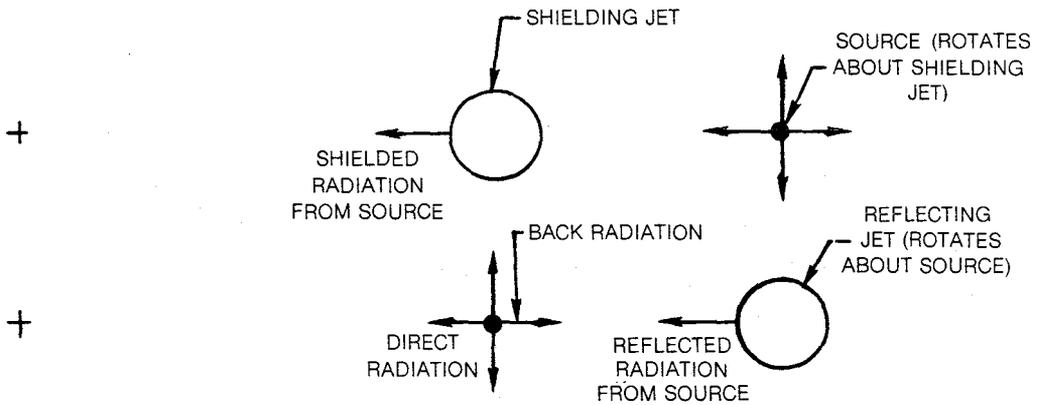
b) FULL ANALYTICAL MODEL
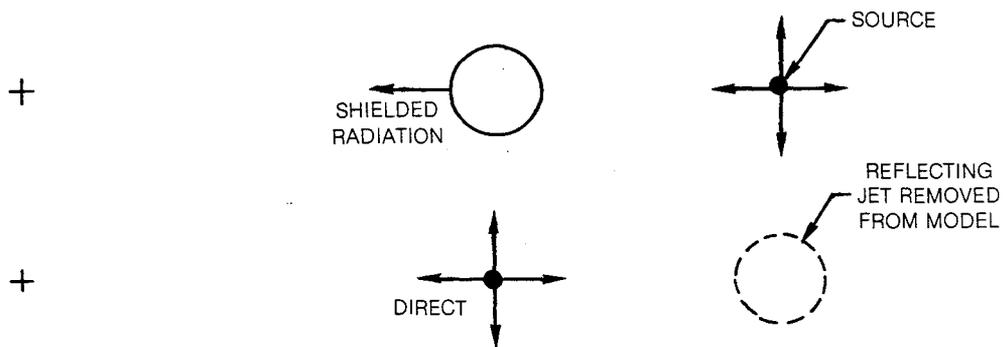
c) ANALYTICAL MODEL REPRESENTING
EXPERIMENTAL RESULTS

Figure 35 — Selection of Analytical Model Representing Dual Jet Geometry

a) DISCRETE TONE CALCULATION, f = 4 kHz
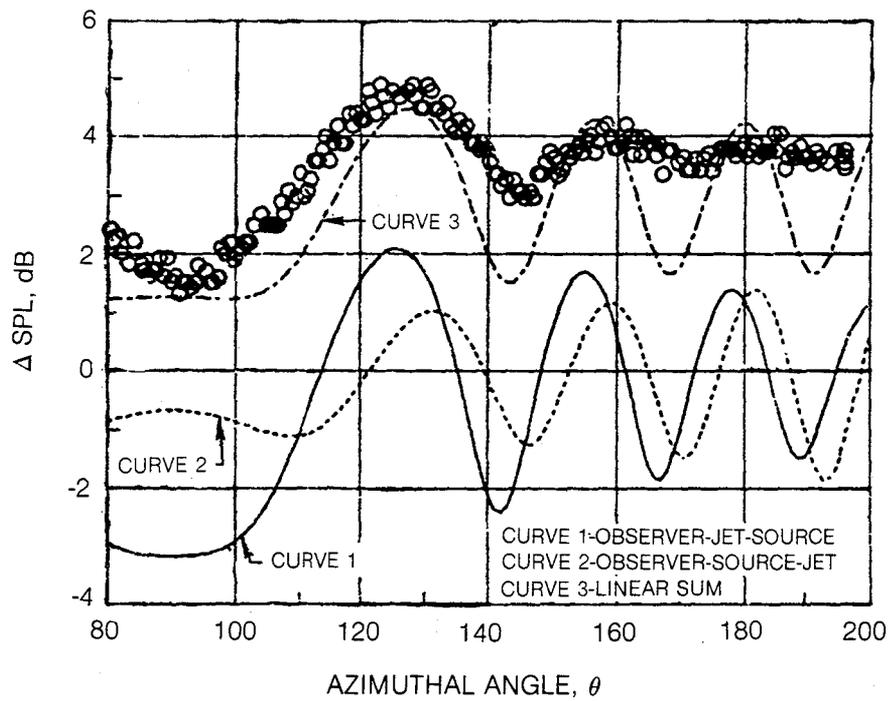
Figure 36 — Comparison of Measured and Predicted Azimuthal Directivity Pattern
$M = 0.6$, $T_O = 300°$ K, $S/D = 8.1$, $\psi = 40°$
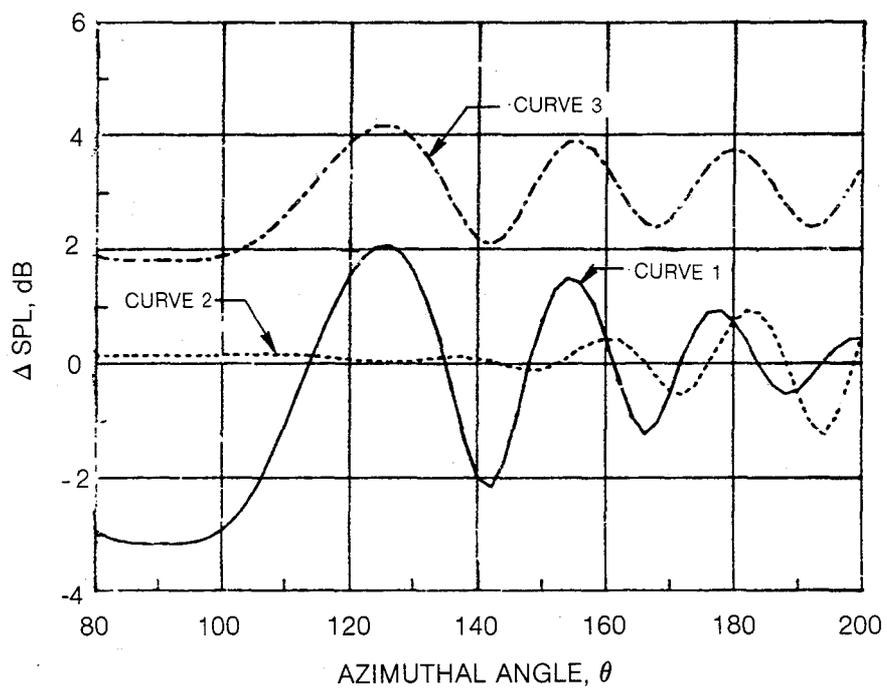
b) ⅓ OCTAVE BAND CALCULATION, f = 4 kHz

Figure 36 — Concluded
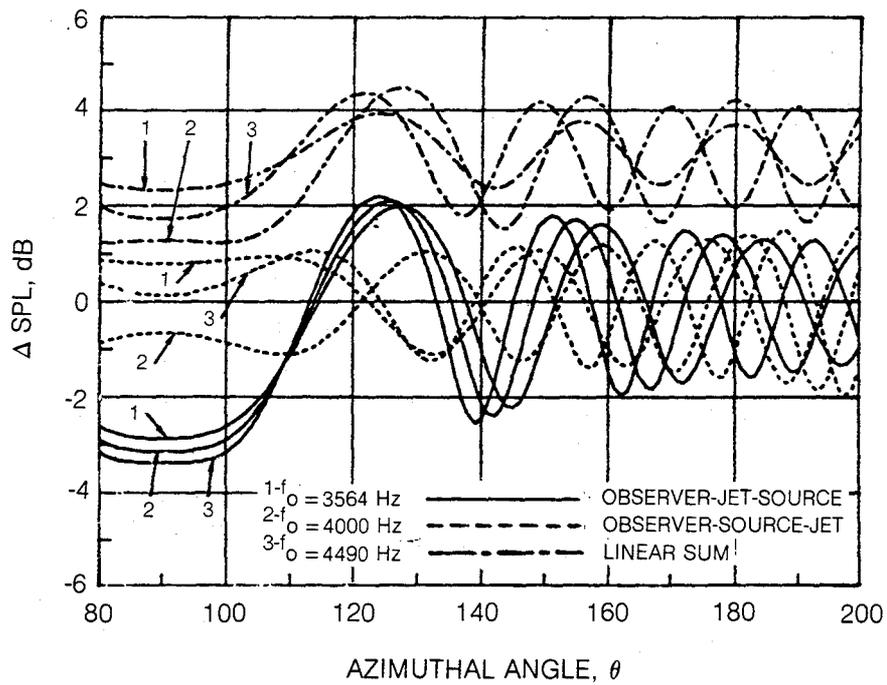
Figure 37 — Effect of Frequency on Predicted Azimuthal Directivity Pattern, $M = 0.6$, $T_o = 300°$ K, $S/D = 8.1$, $\psi = 40°$
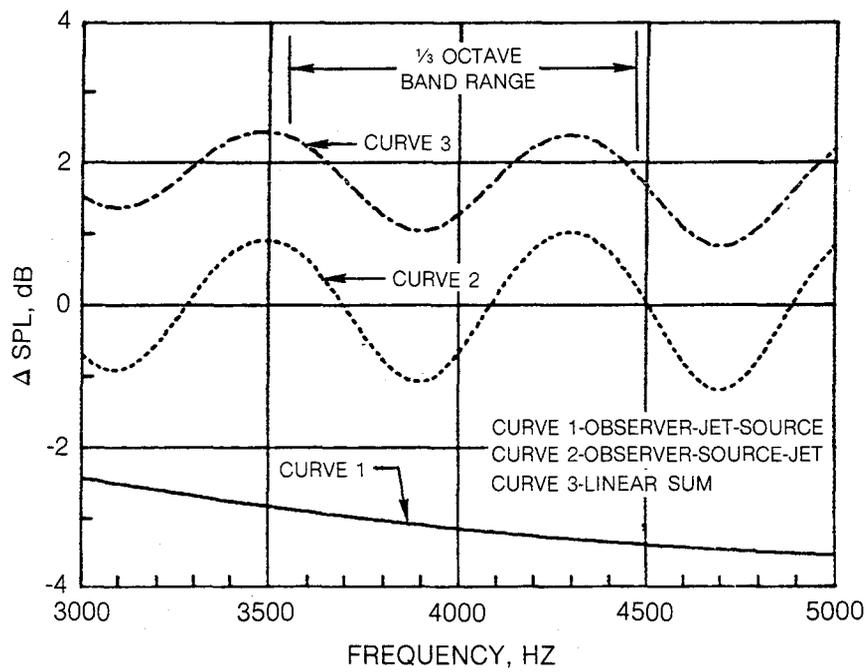
a) FREQUENCY RANGE, 3-5 kHz

Figure 38 — Frequency Dependence of Discrete Tone Prediction, M = 0.6, $T_0 = 300°$ K, S/D = 8.1, $\psi = 40°$, $\Theta = 90°$
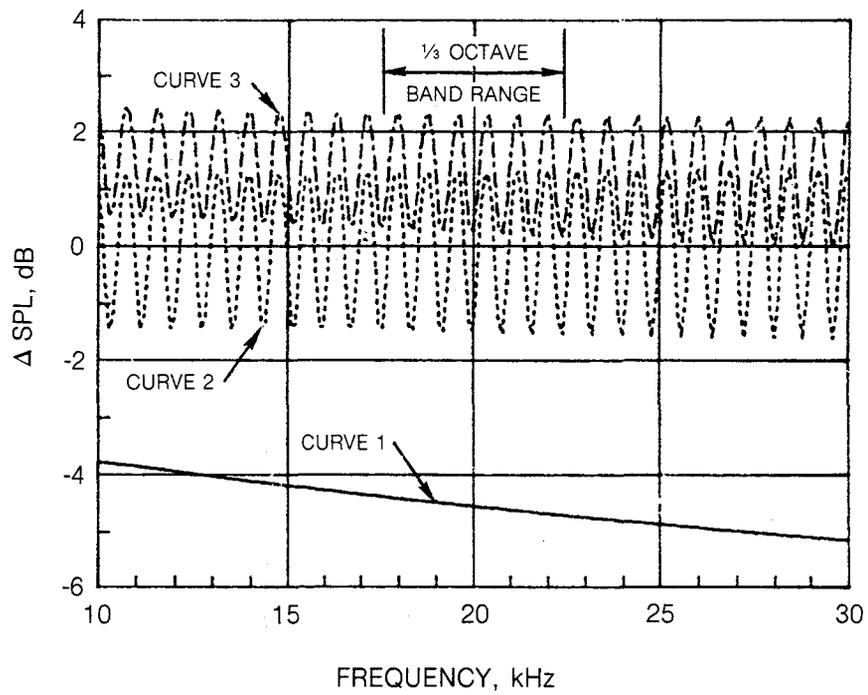
b) FREQUENCY RANGE, 10-30 kHz

Figure 38 — Continued
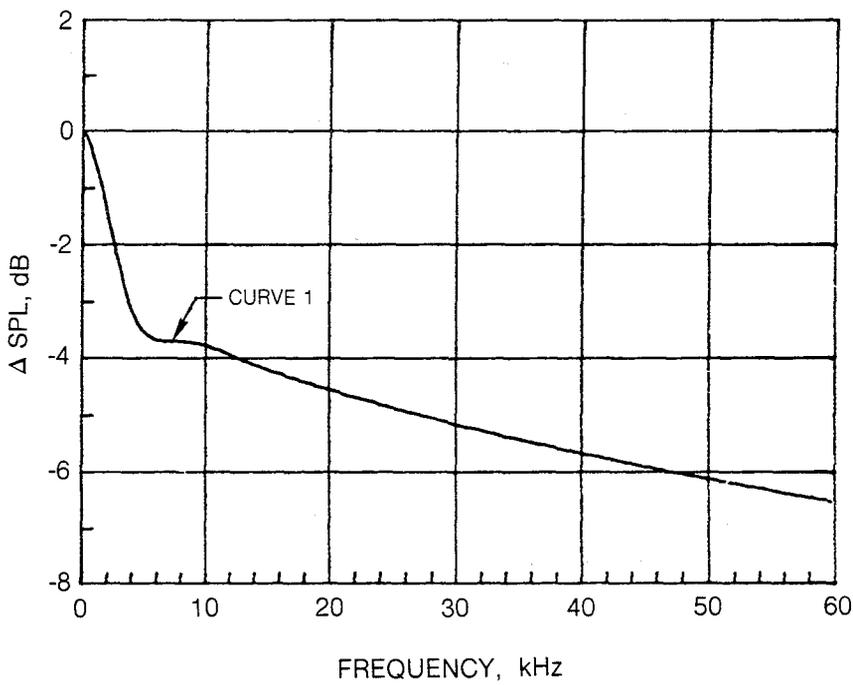
c) FREQUENCY RANGE, 0-60 kHz

Figure 38 — Concluded
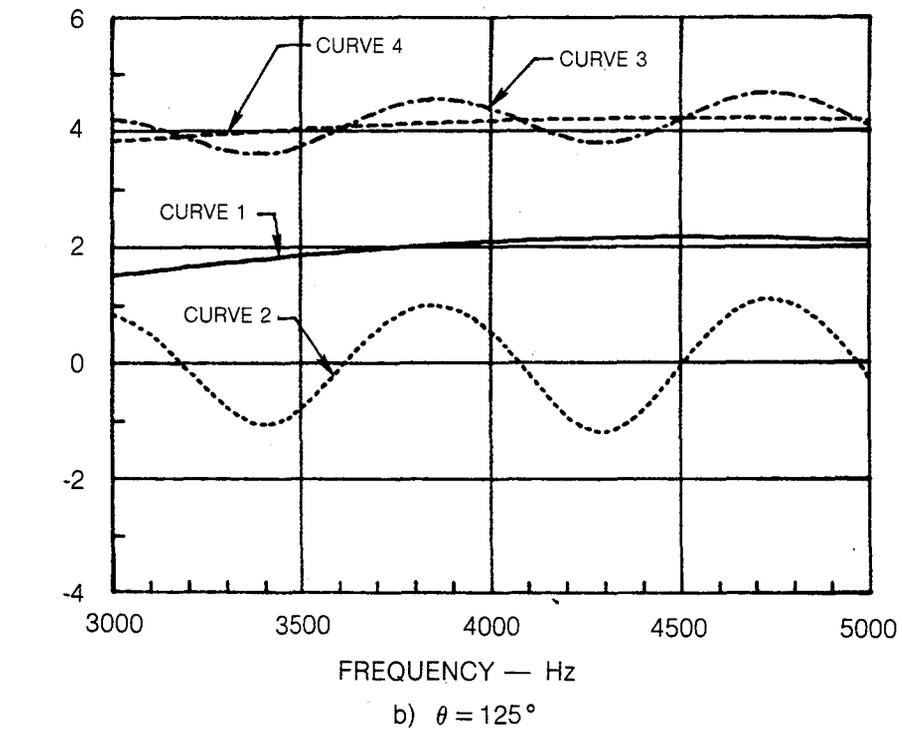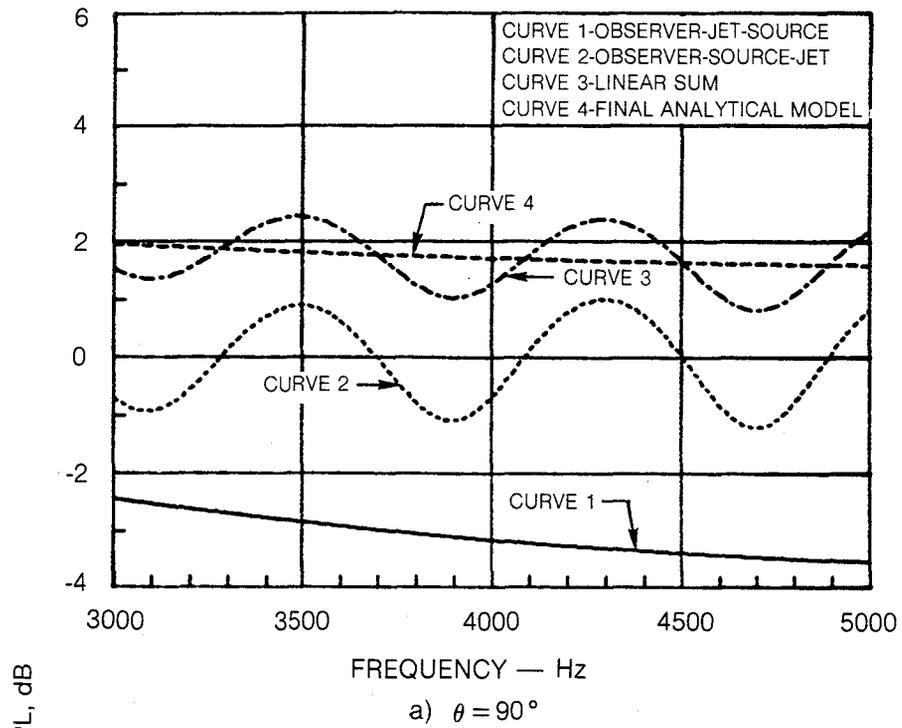
Figure 39 — Frequency Dependence of Discrete Tone Prediction at Various Azimuthal Angles, $M = 0.6$, $T_0 = 300\,°K$, $S/D = 8.1$, $\psi = 40°$

c) $\theta = 150°$

d) $\theta = 160°$
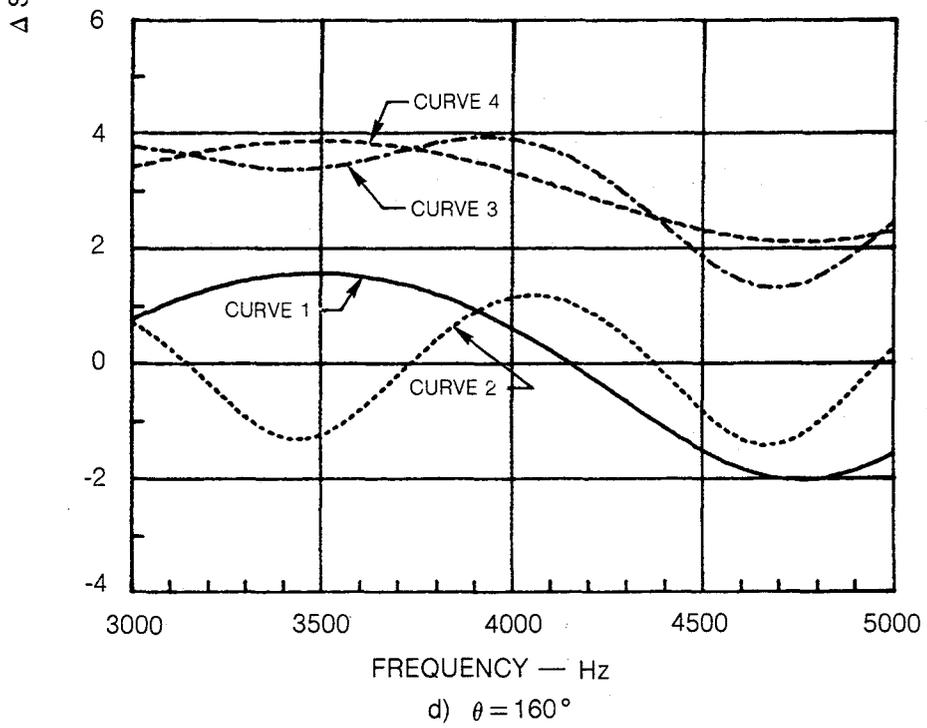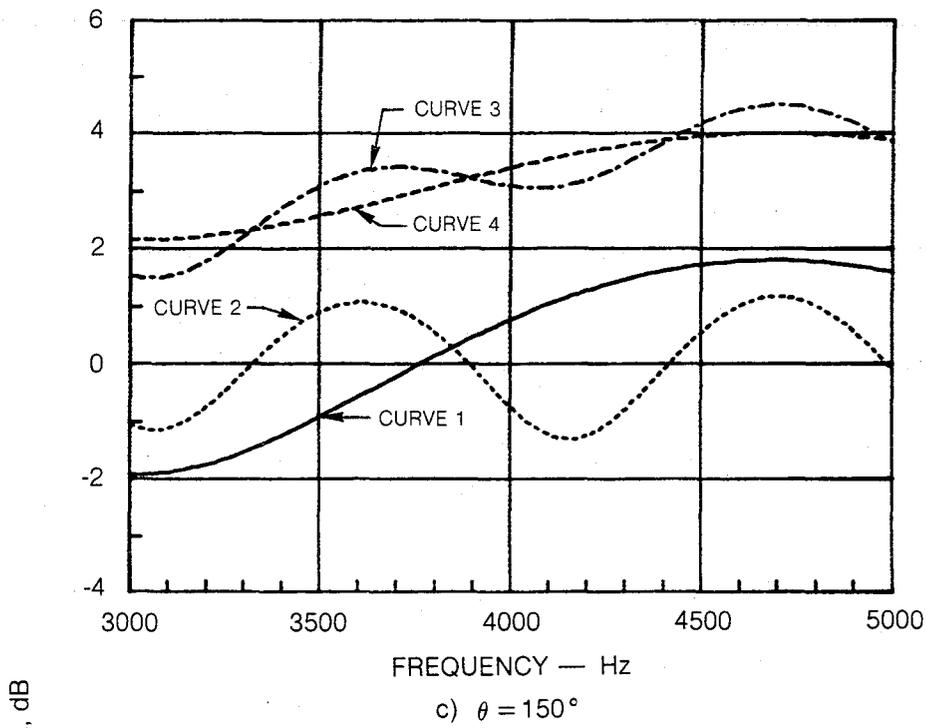
Figure 39 — Continued

139

e) $\theta = 170°$

f) $\theta = 180°$
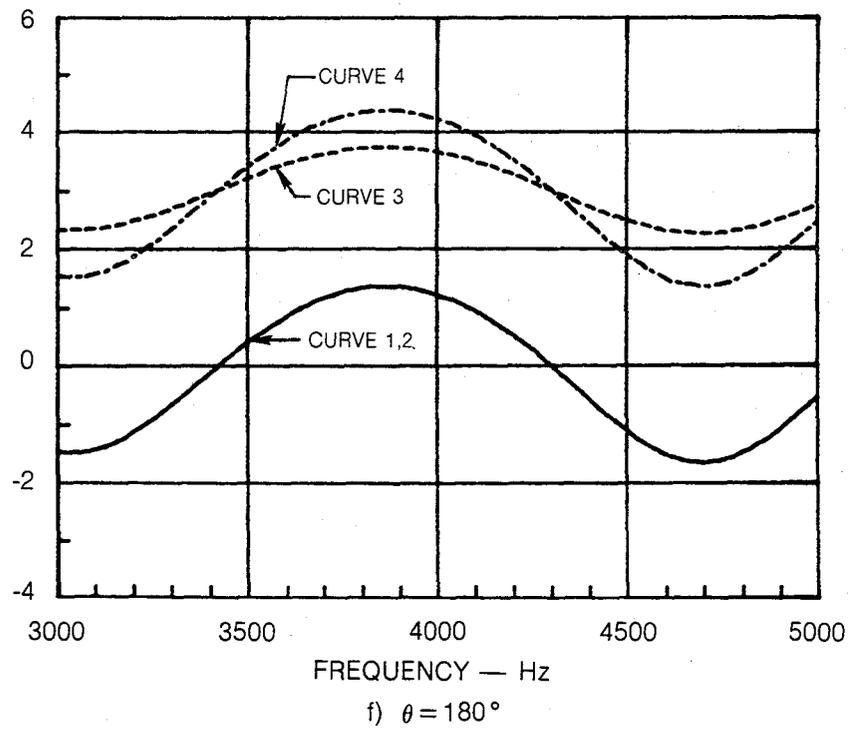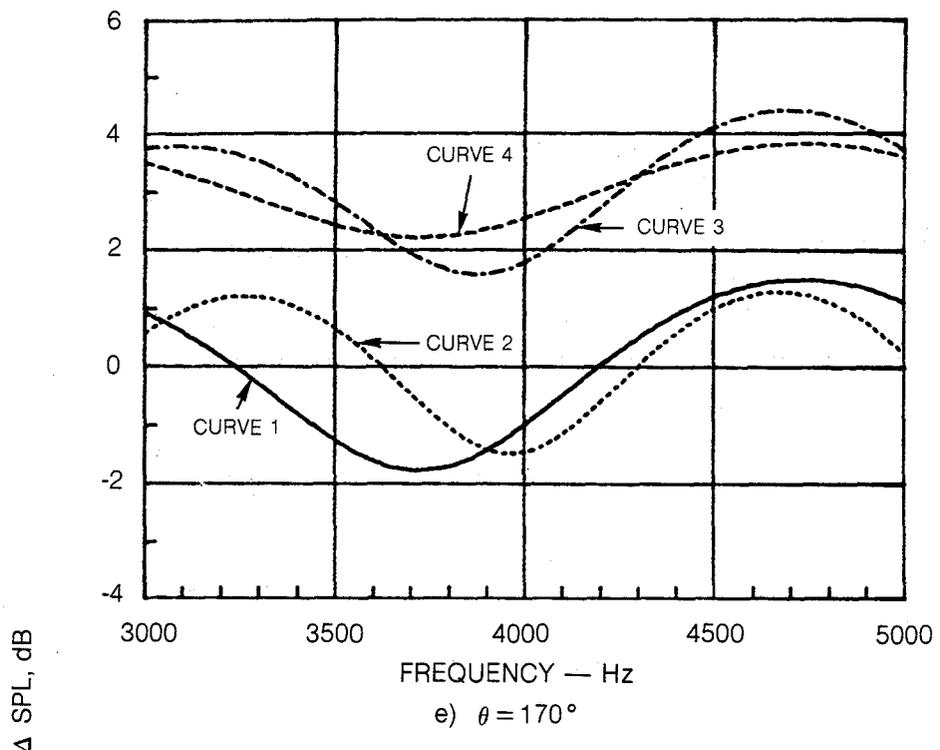
Figure 39 — Concluded
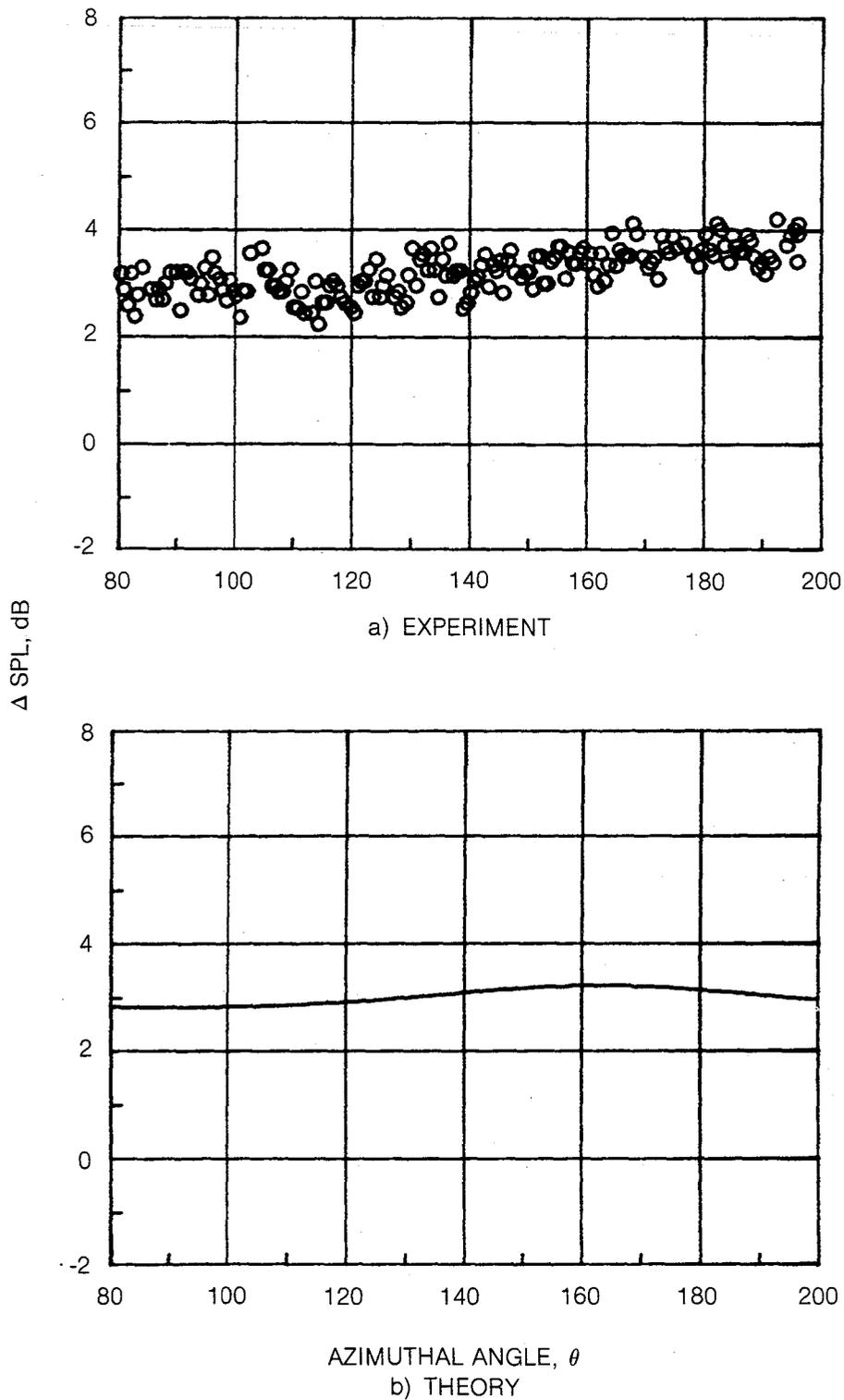
Figure 40 — Comparison of Measured and Predicted (Based on Final Theoretical Model) Azimuthal Directivity Pattern, M = 0.6, T_o = 300°K, ψ = 40°, f = 800 Hz
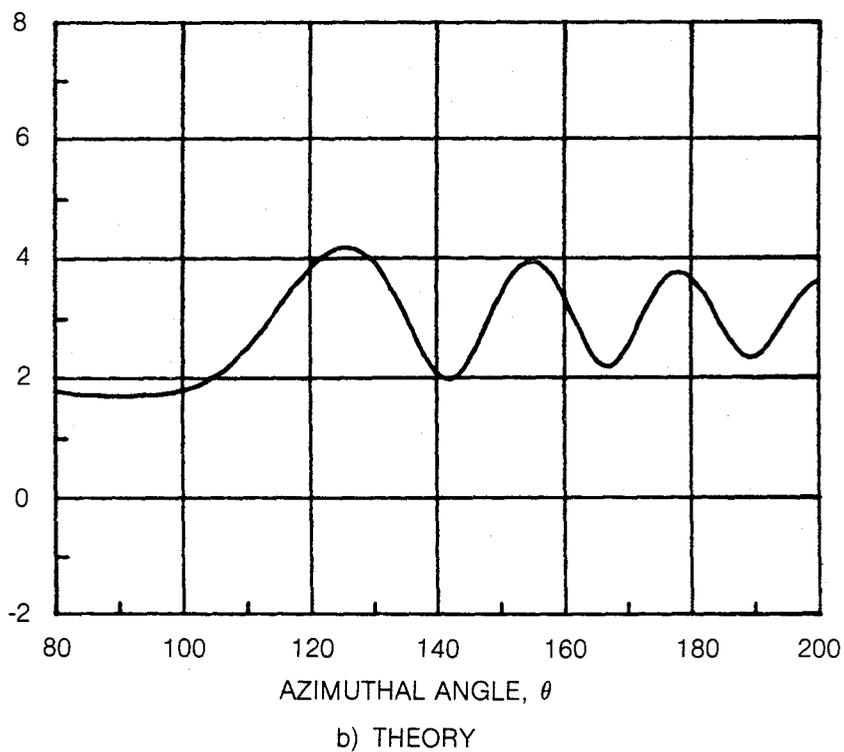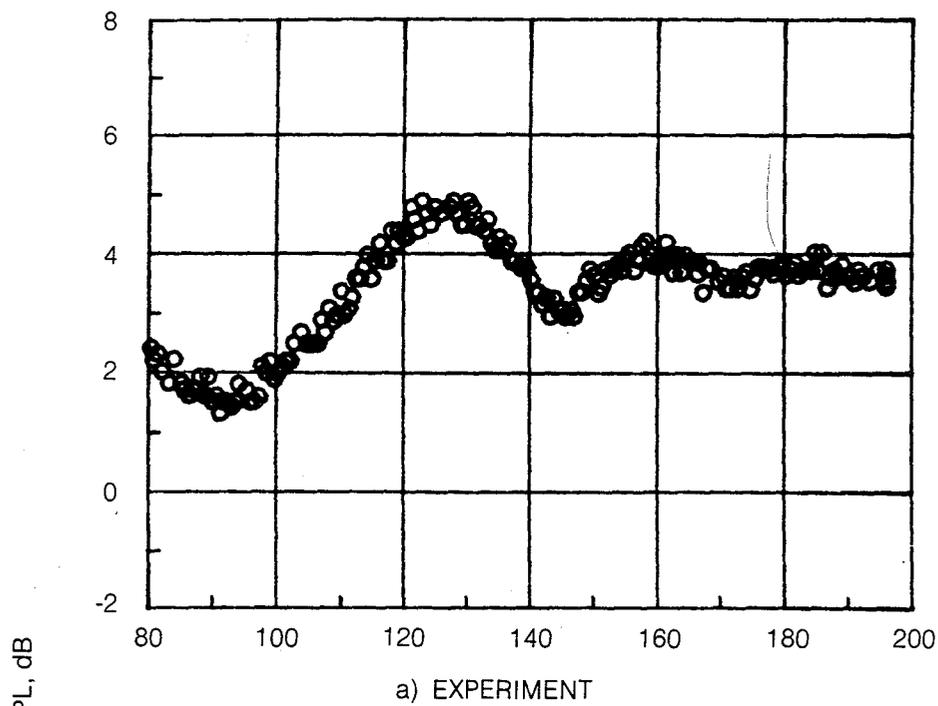
Figure 41 — Comparison of Measured and Predicted (Based on Final Theoretical Model) Azimuthal Directivity Pattern, M = 0.6, T_o = 300°K, ψ = 40° f = 4 kHz
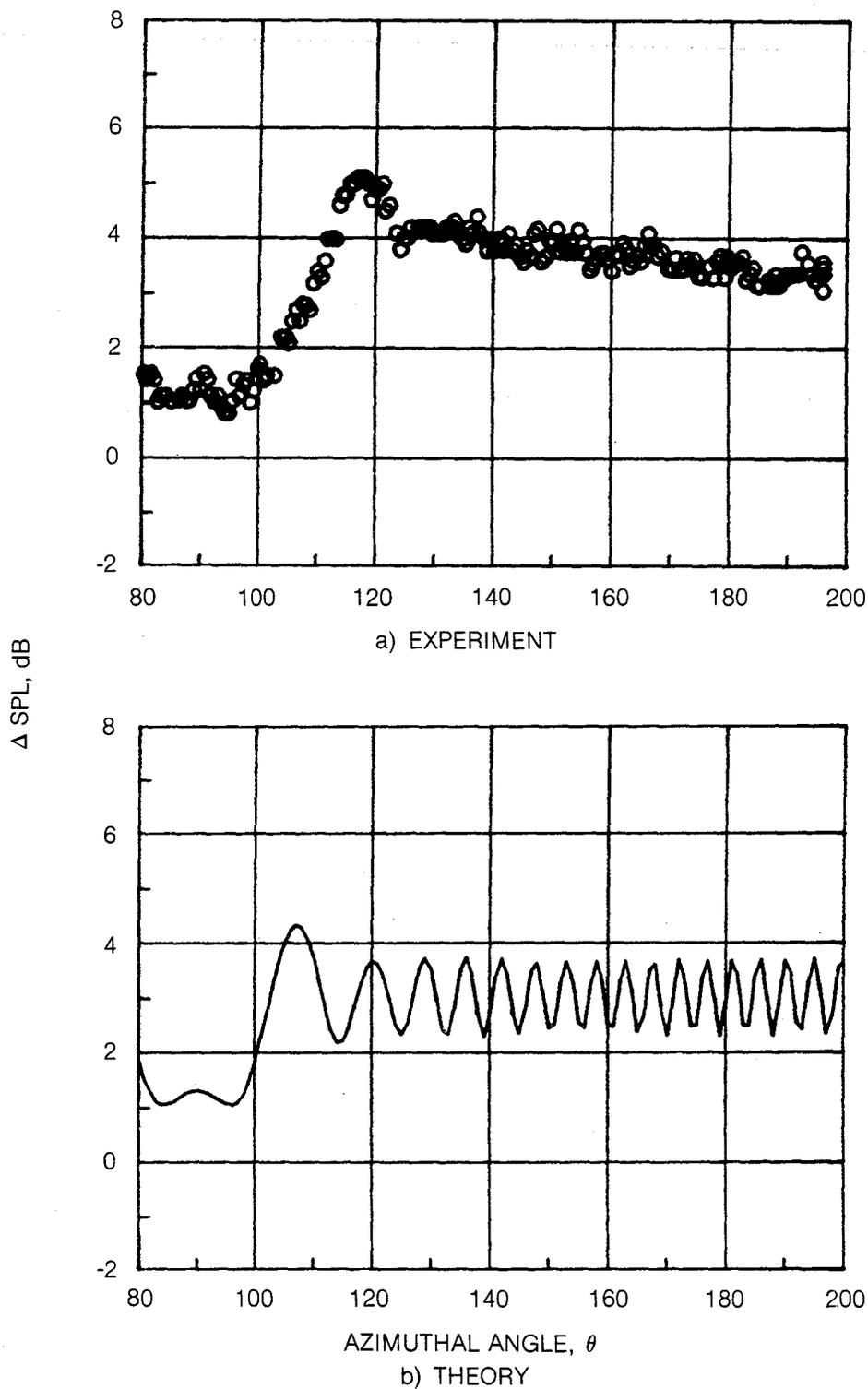
Figure 42 — Comparison of Measured and Predicted (Based on Final Theoretical Model) Azimuthal Directivity Pattern, M = 0.6, T_o = 300°K, ψ = 40°, f = 20 kHz
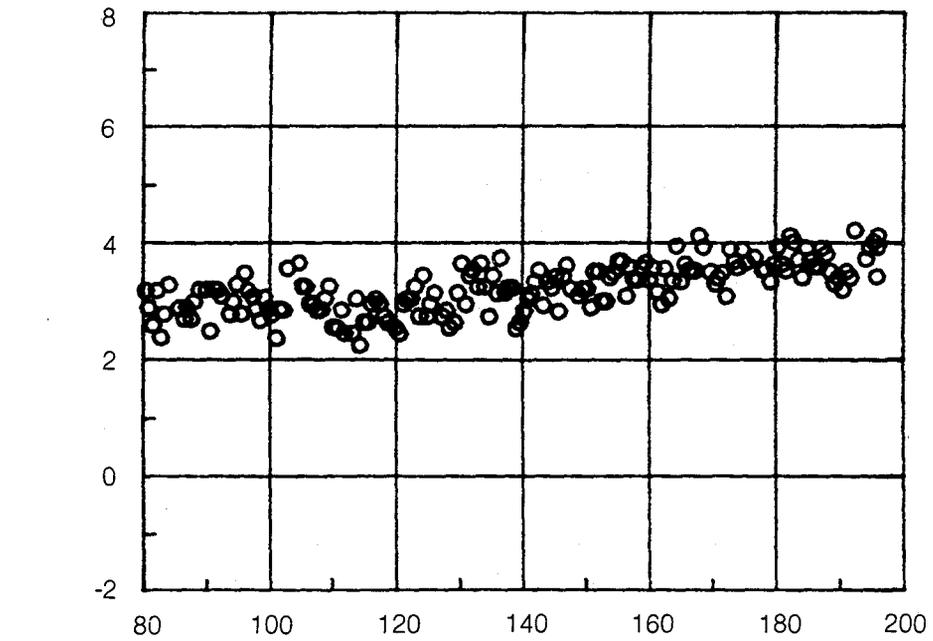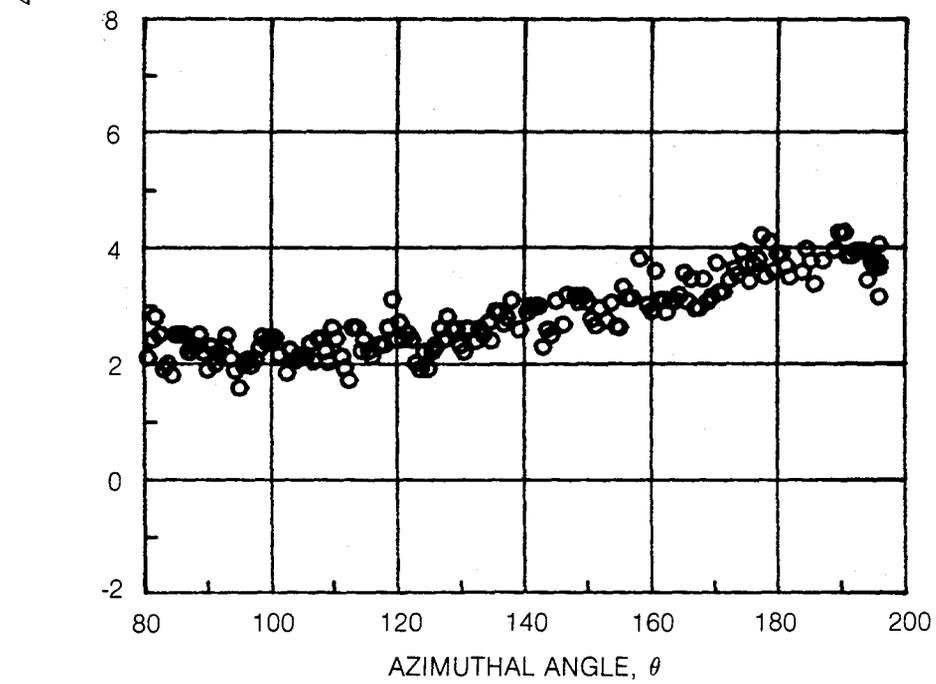
Figure 43 — Mach number Dependence of Measured and Predicted Azimuthal Directivity Pattern, $T_o = 300°$ K, S/D = 8.1, $\psi = 40°$, f = 800 Hz

c) PREDICTION, M = 0.6, 0.94, 1.46
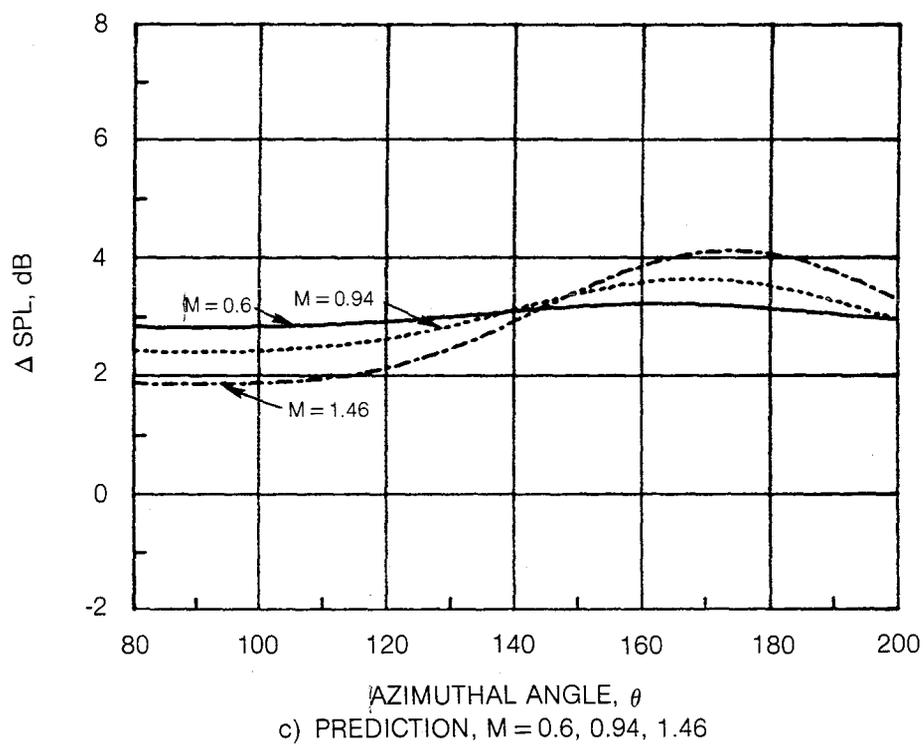
Figure 43 — Concluded
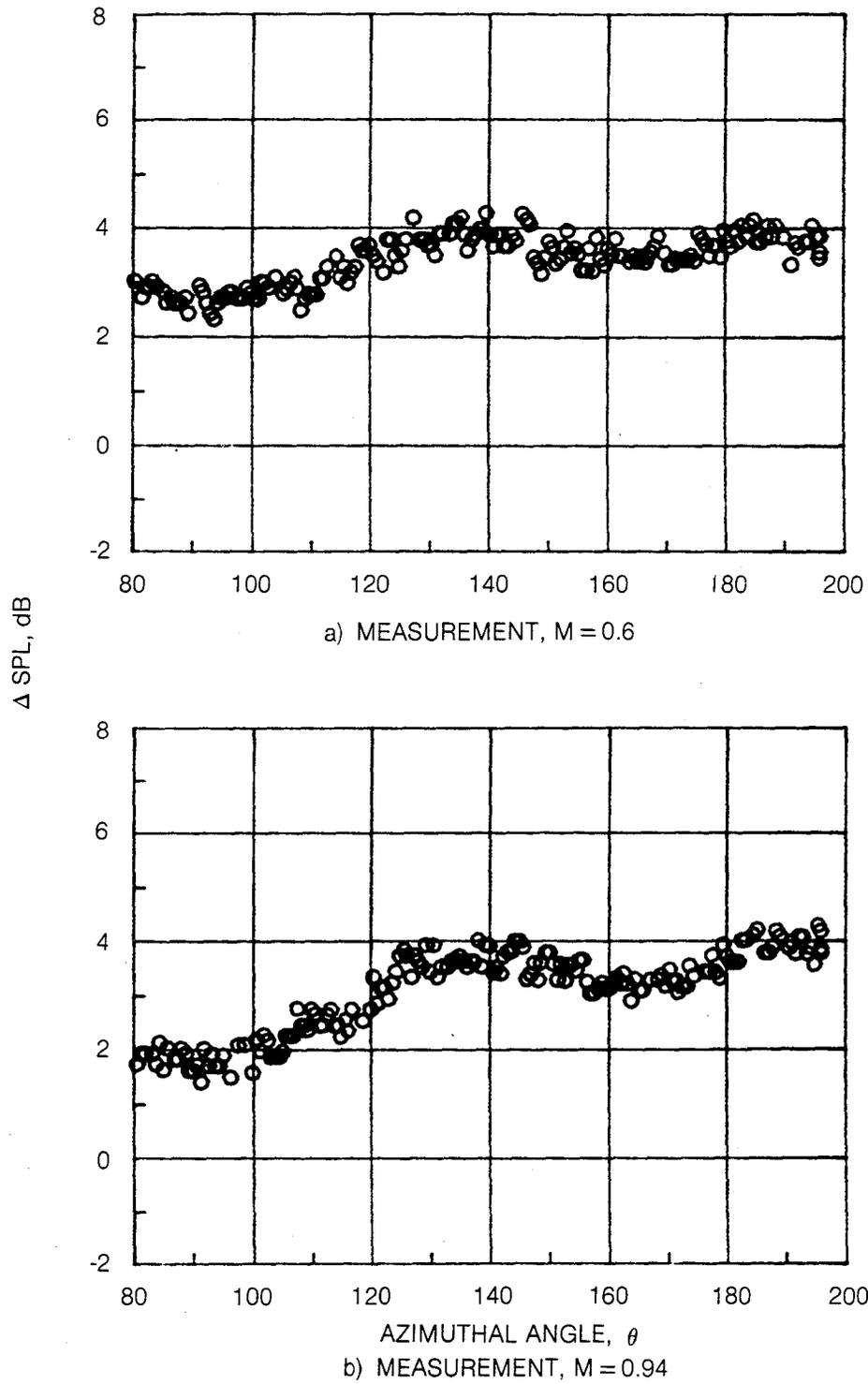
Figure 44 — Mach Number Dependence of Measured and Predicted Azimuthal Directivity Pattern, $T_0 = 300°$ K, S/D = 8.1, $\psi = 40°$, f = 2 kHz
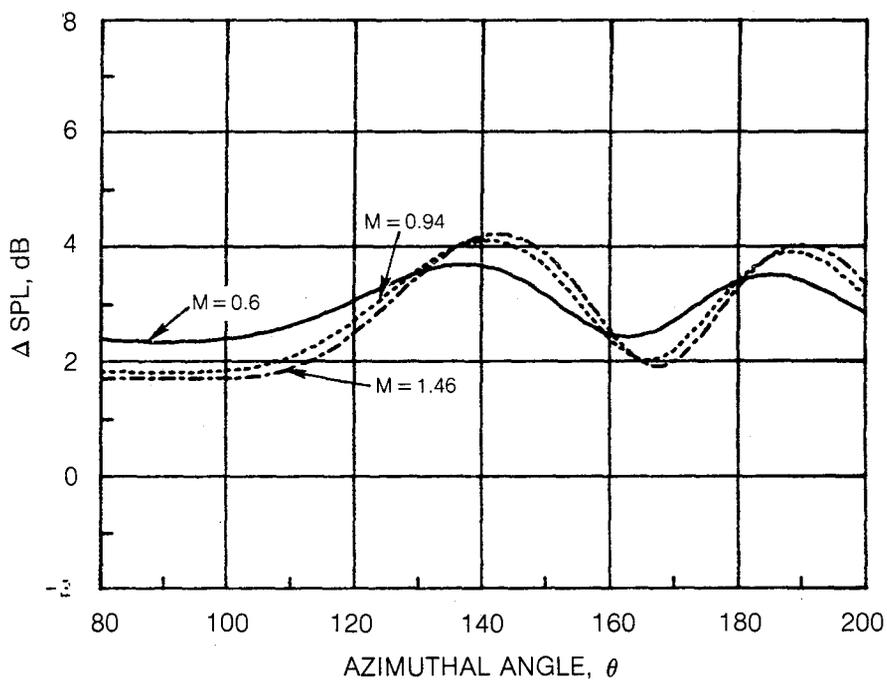
c) PREDICTION, M = 0.6, 0.94, 1.46

Figure 44 — Concluded
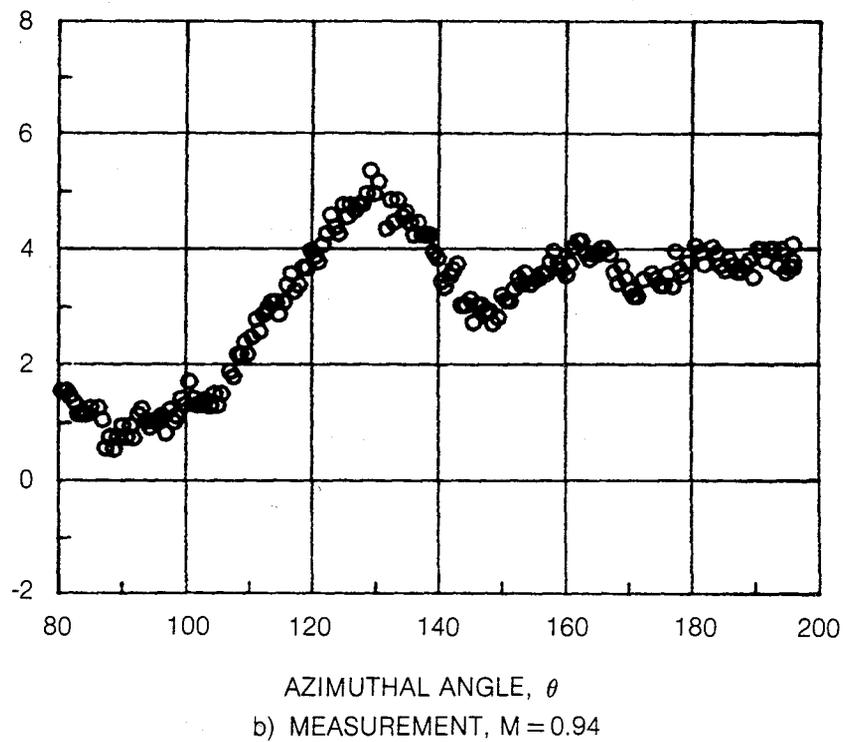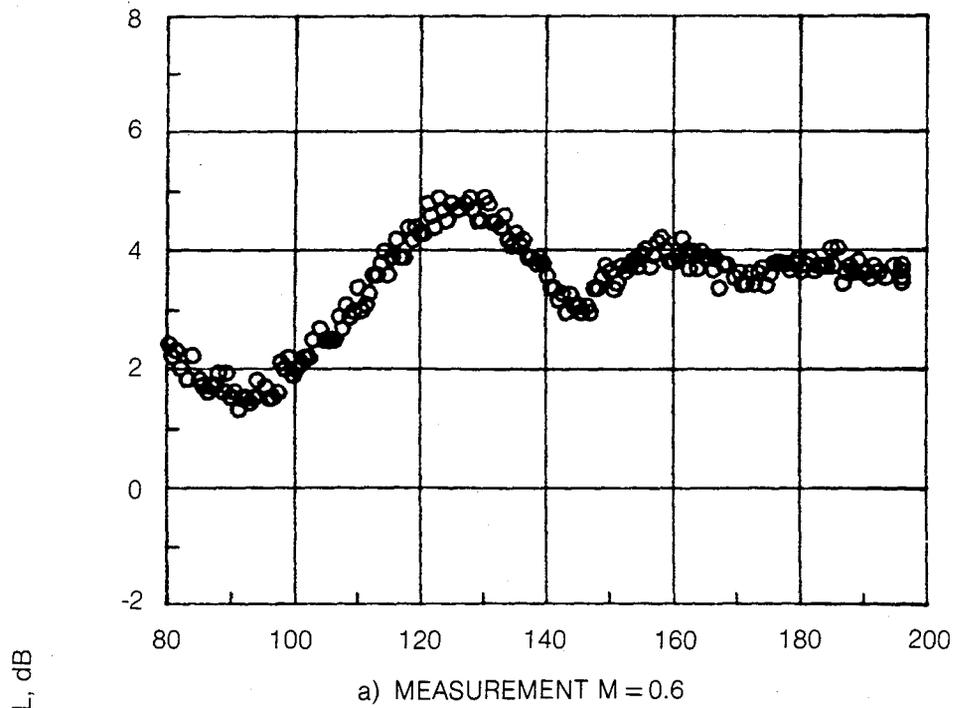
Figure 45 — Mach Number Dependence of Measured and Predicted Azimuthal Directivity Pattern, $T_o = 300°$ K, $S/D = 8.1$, $\psi = 40°$, f = 4 kHz

c) PREDICTION, M = 0.6, 0.94, 1.46

d) PREDICTION, CONSTANT STROUHAL NUMBER, ST = 0.854
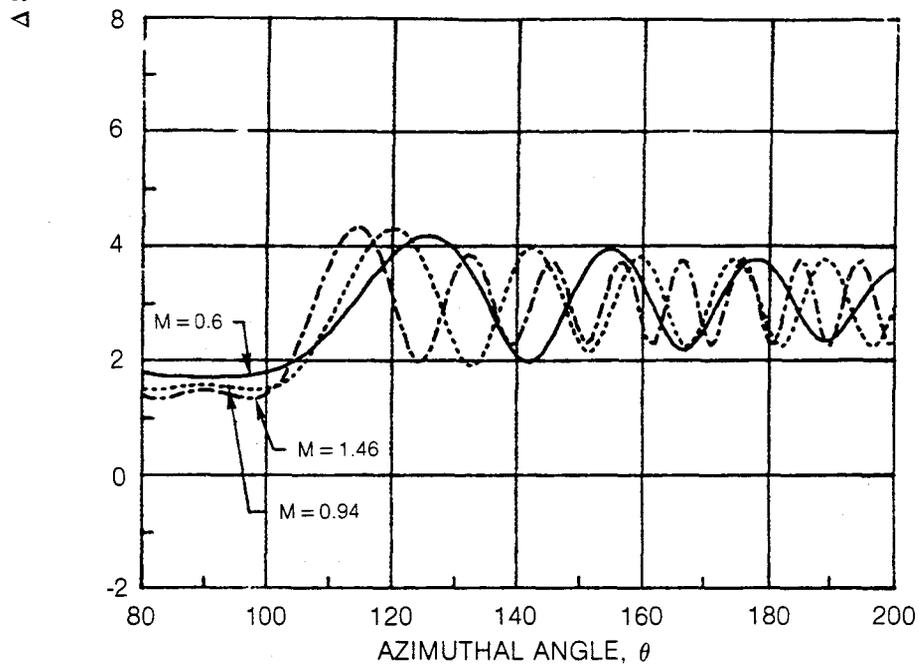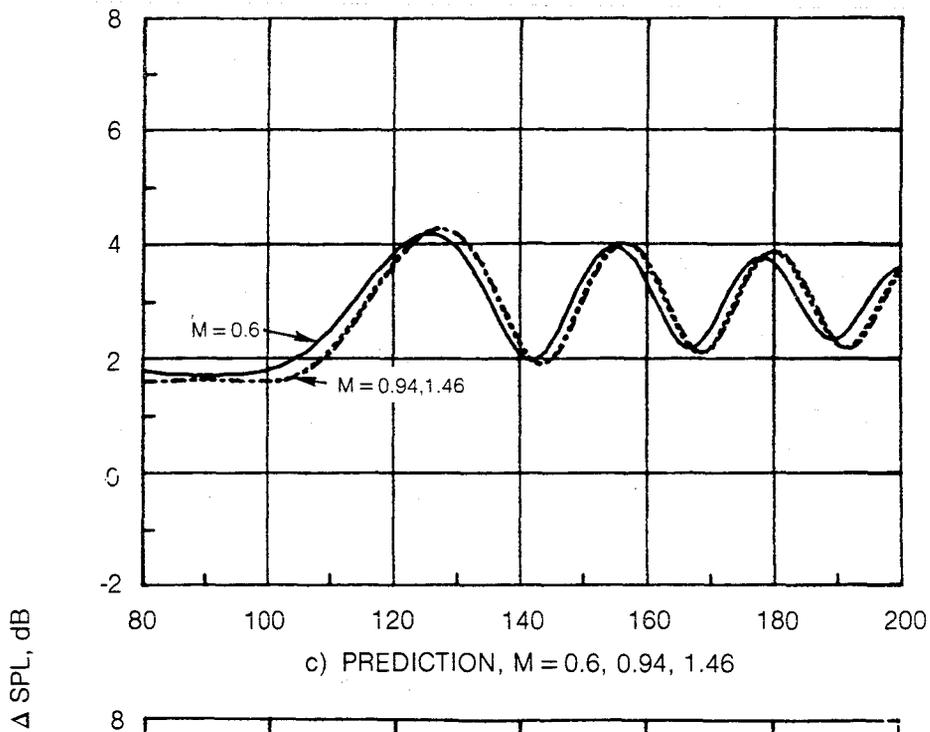
Figure 45 — Concluded
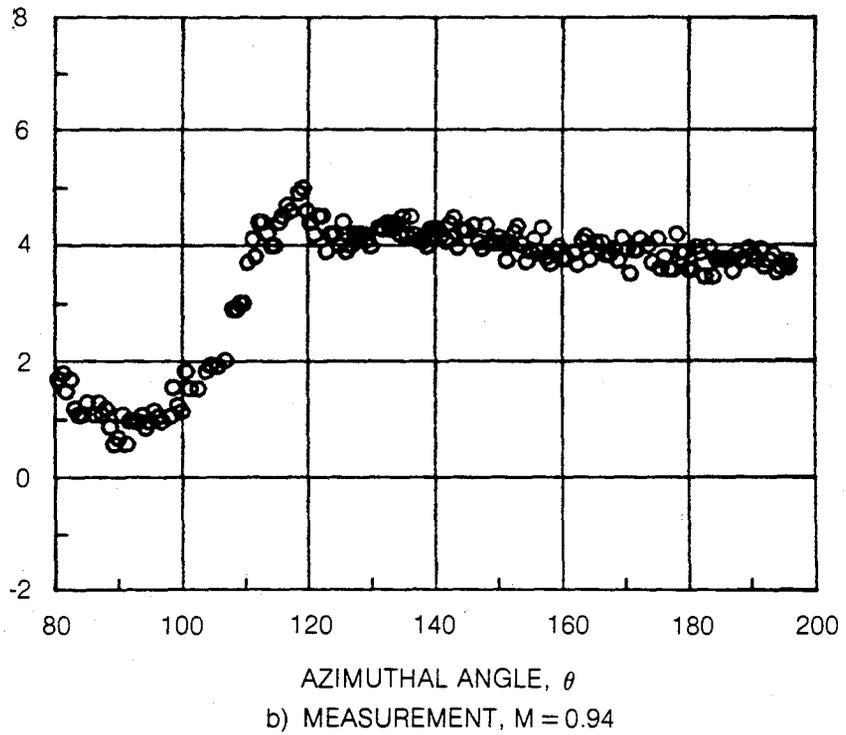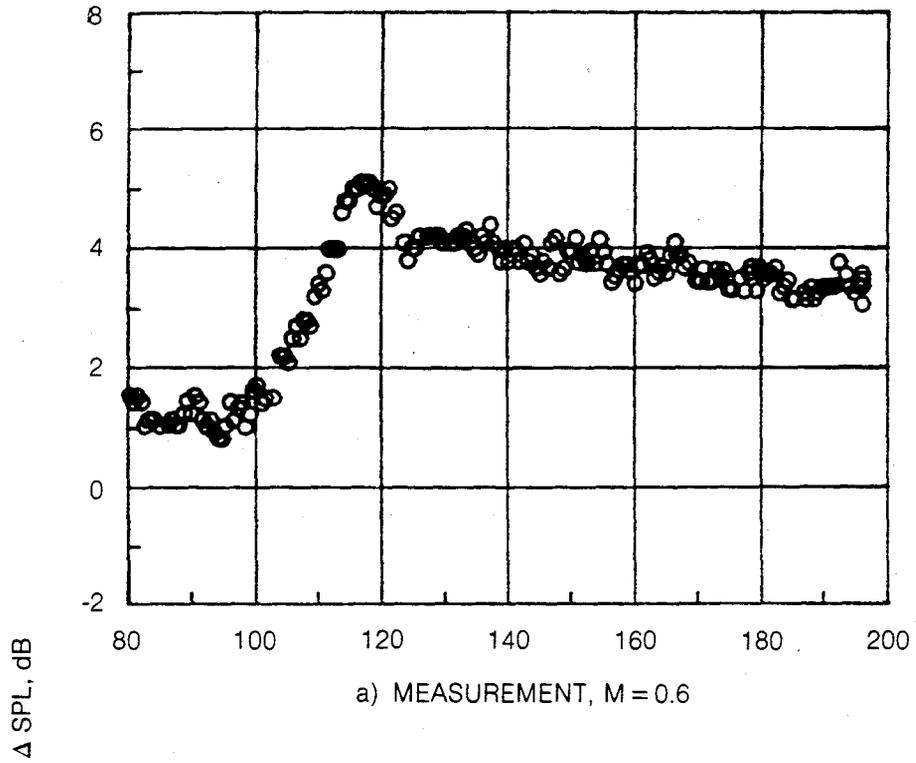
Figure 46 — Mach Number Dependence of Measured and Predicted Azimuthal Directivity Pattern, $T_o = 300°$ K, $S/D = 8.1$, $\psi = 40°$, f = 20 kHz
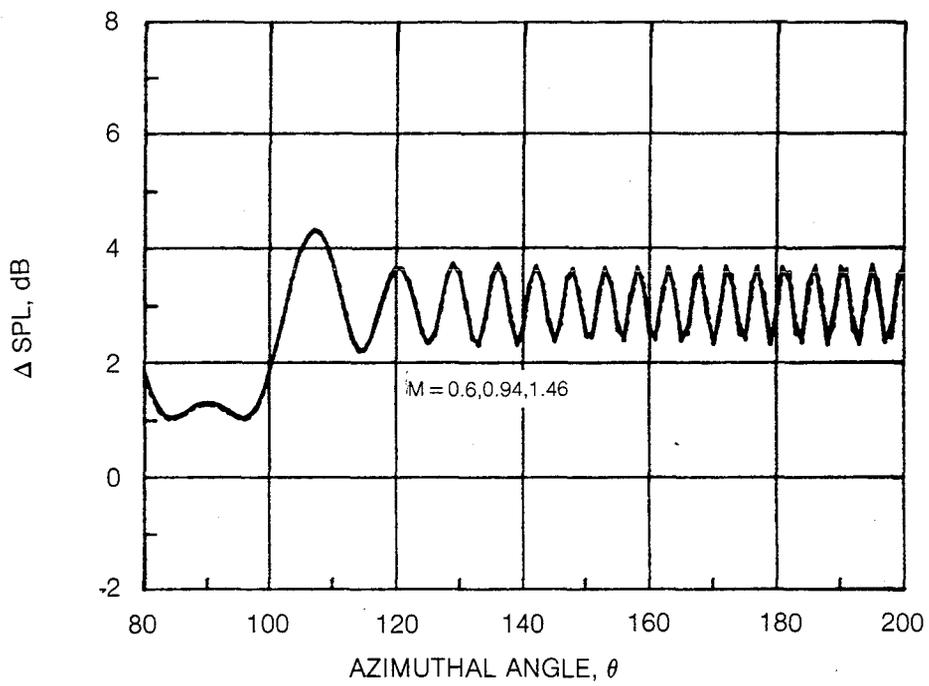
c) PREDICTION, M = 0.6, 0.94, 1.46

Figure 46 — Concluded
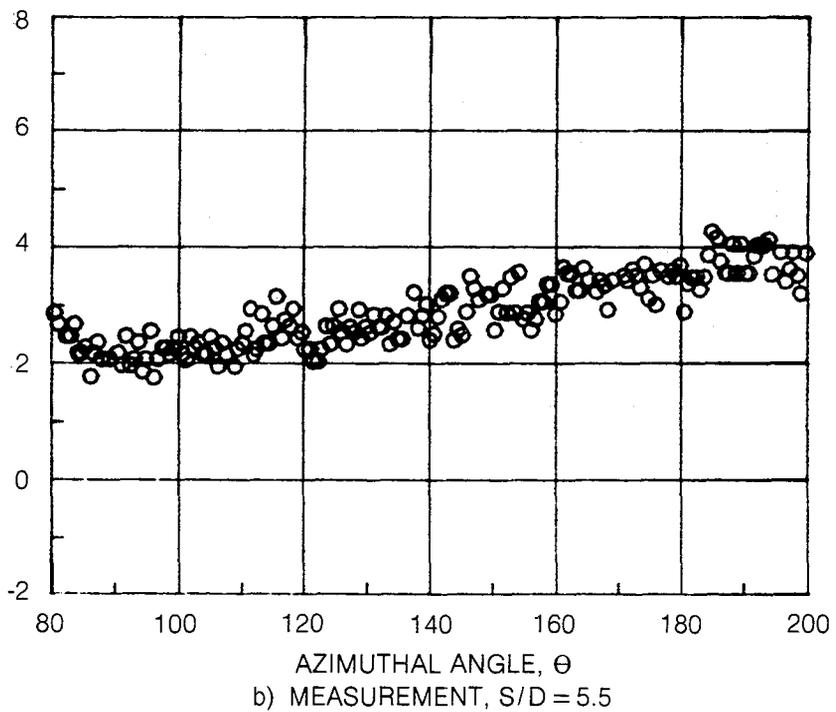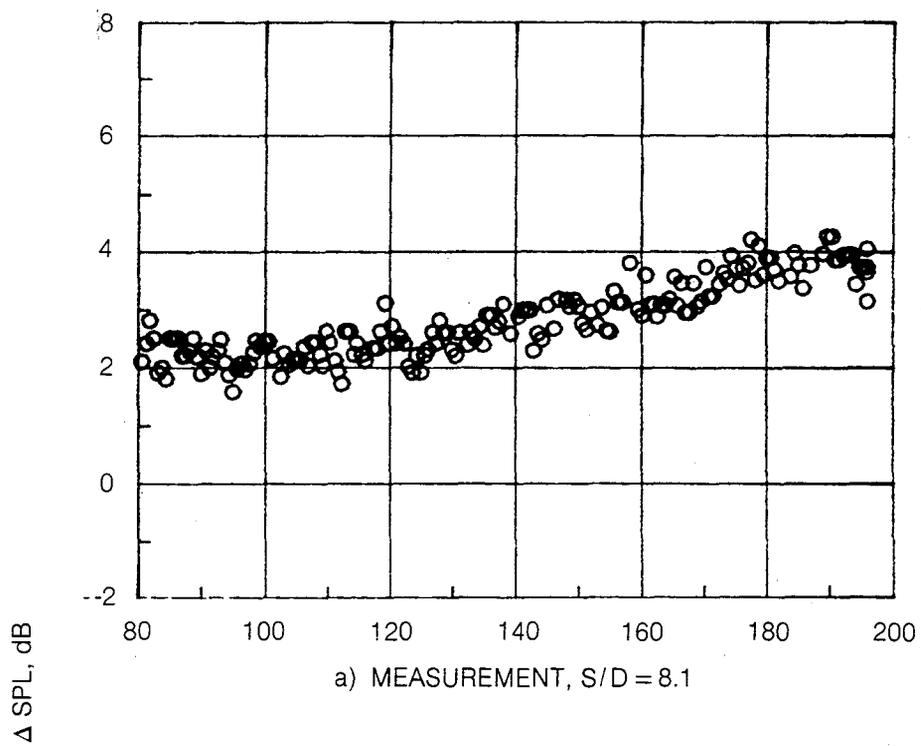
Figure 47 — Spacing Dependence of Measured and Predicted Azimuthal Directivity Pattern, M = 0.94, T_o = 300° K, ψ = 40°, f = 800 Hz

c) MEASUREMENT, S/D = 3.1

d) PREDICTION, S/D = 8.1, 5.5, 3.1
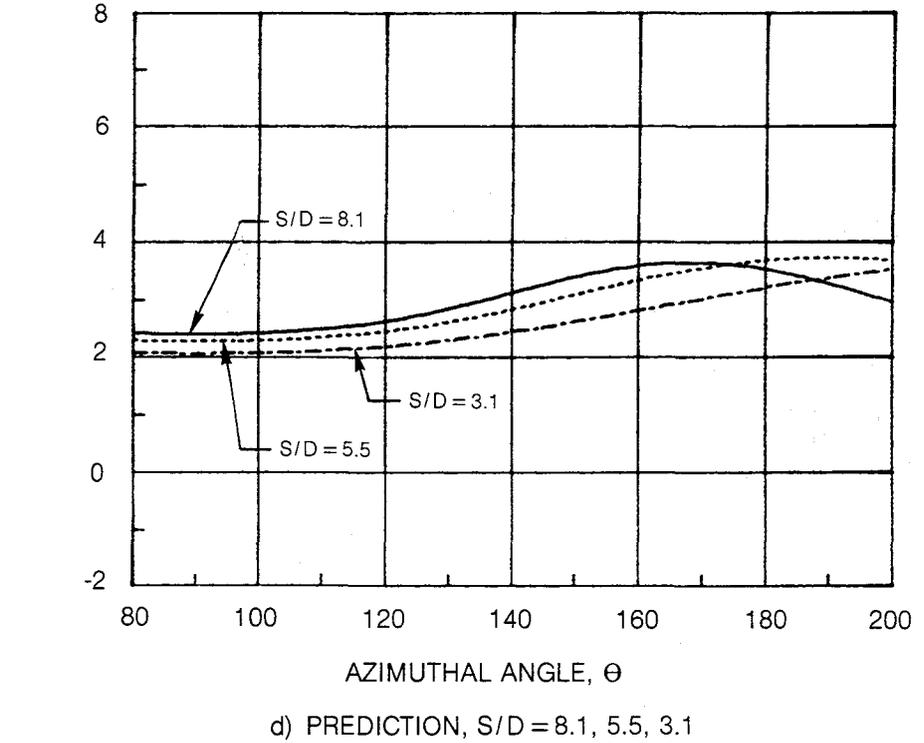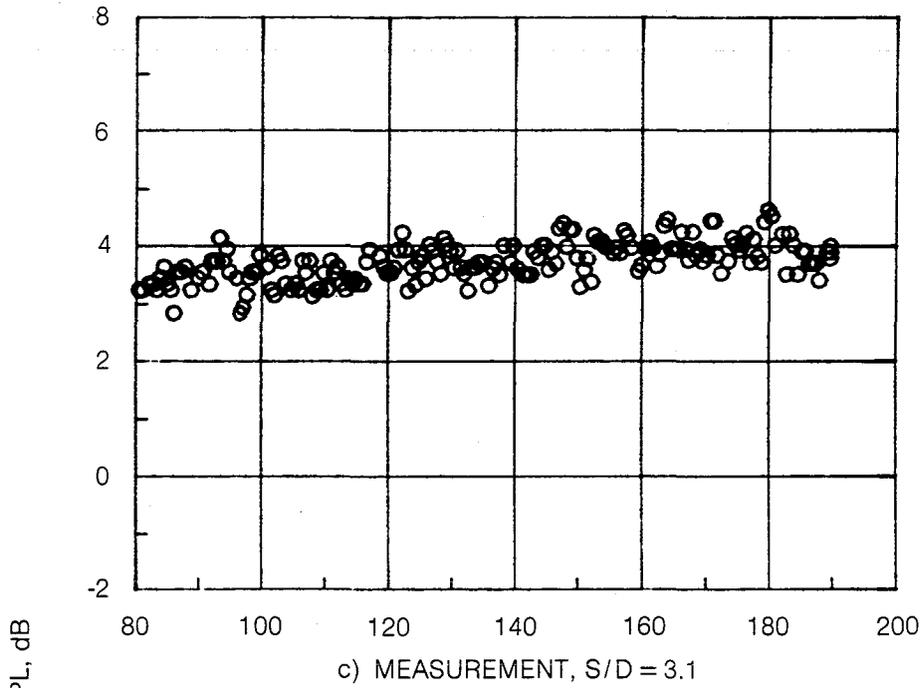
Figure 47 — Concluded

153
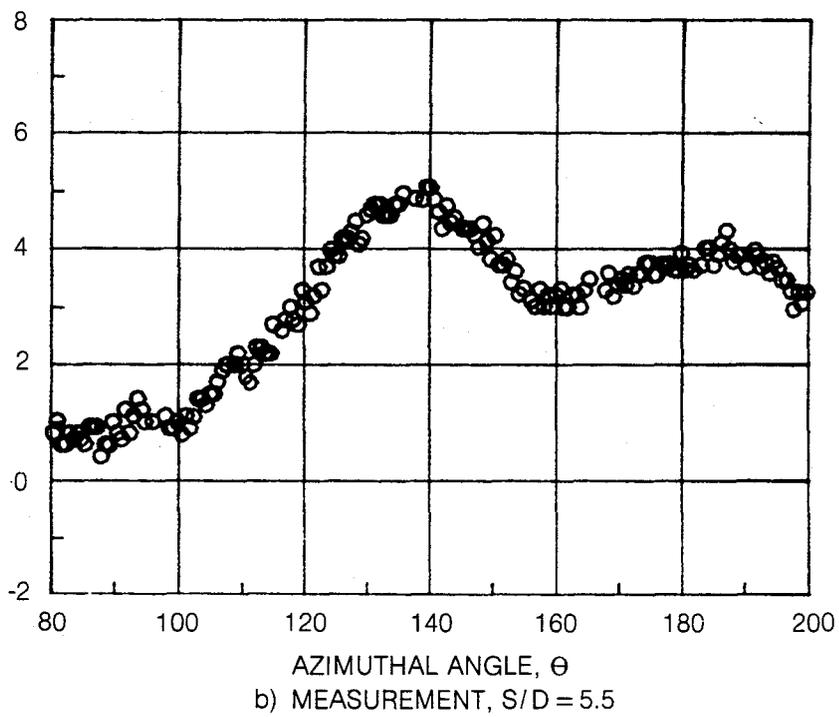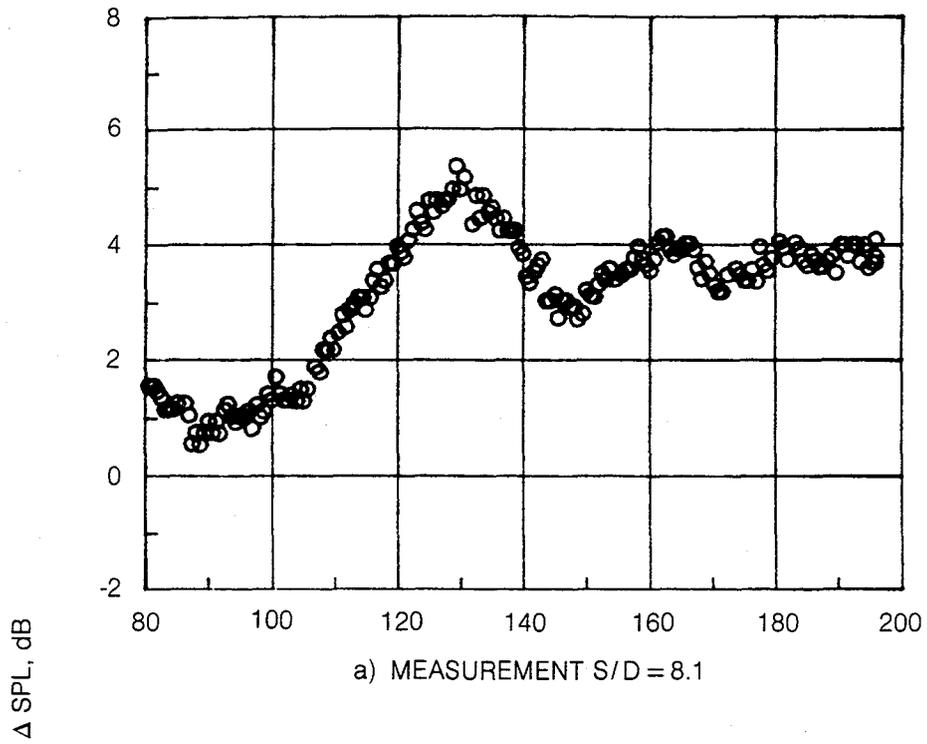
Figure 48 — Spacing Dependence of Measured and Predicted Azimuthal Directivity Pattern, M = 0.94, T_o = 300° K, ψ = 40°, f = 4 kHz
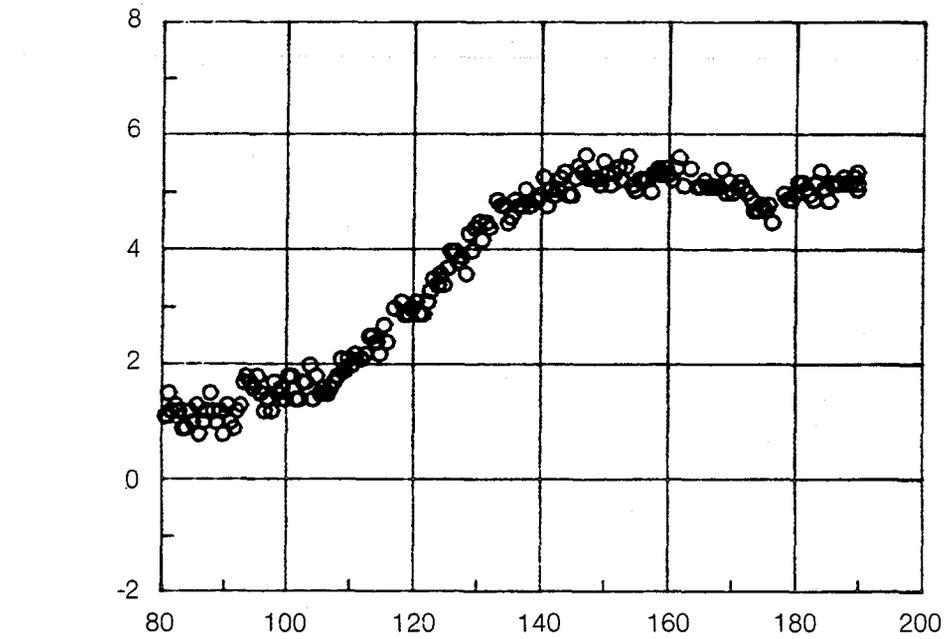
c) MEASUREMENT, S/D = 3.1
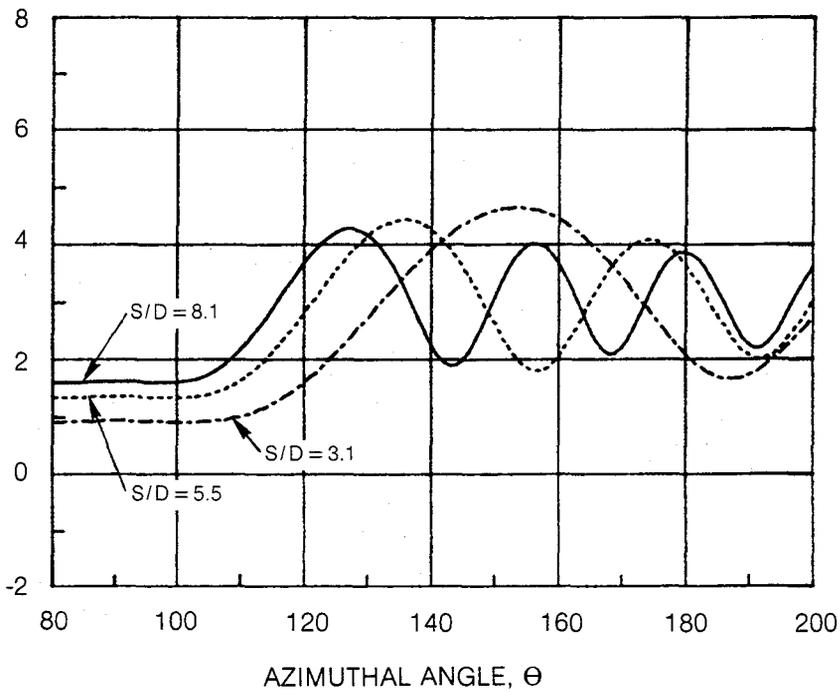
d) PREDICTION, S/D = 8.1, 5.5, 3.1

Figure 48 — Concluded

155
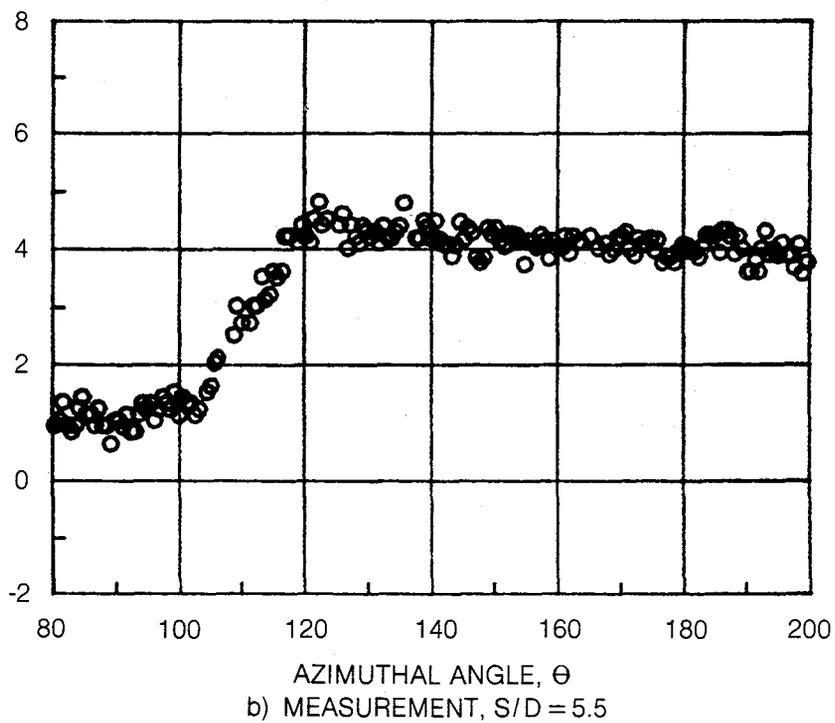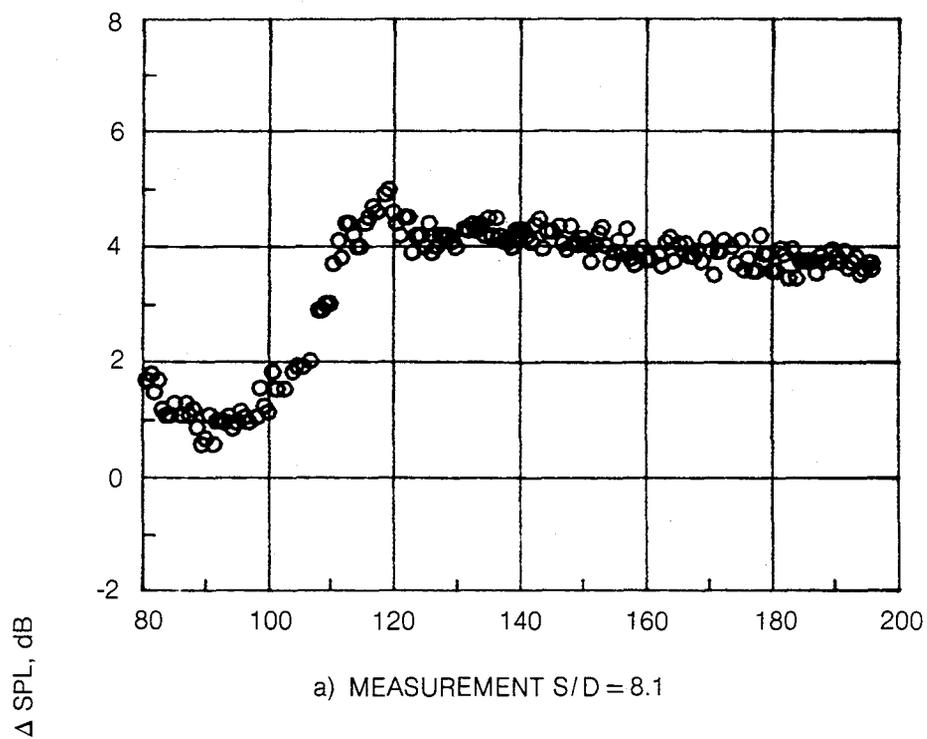
Figure 49 — Spacing Dependence of Measured and Predicted Azimuthal Directivity Pattern, M = 0.94, T_O = 300° K, ψ = 40°, f = 20 kHz

c) MEASUREMENT, S/D = 3.1

d) PREDICTION, S/D = 8.1, 5.5, 3.1

Figure 49 — Concluded

157
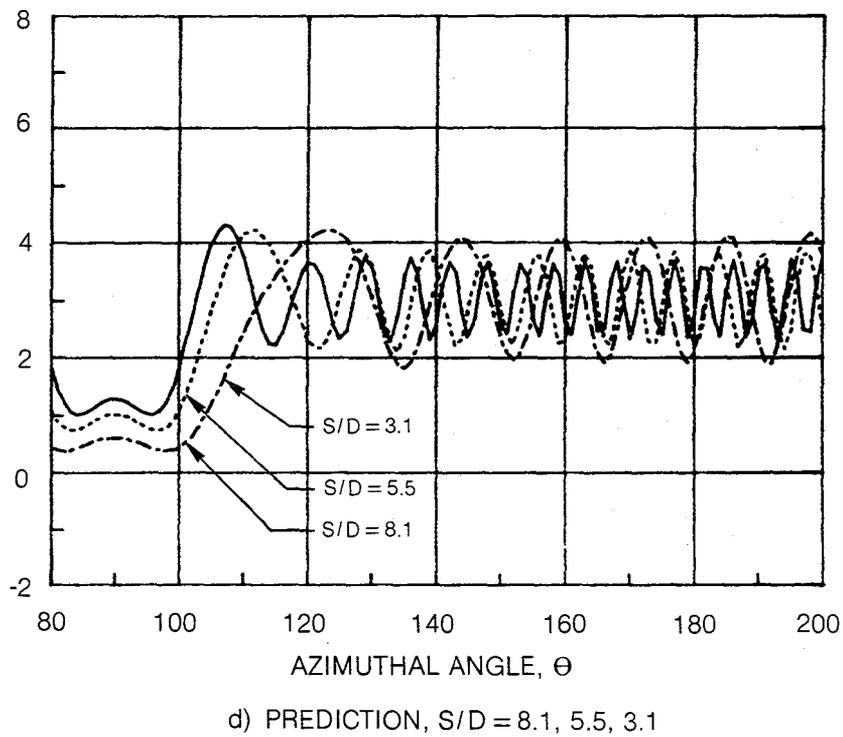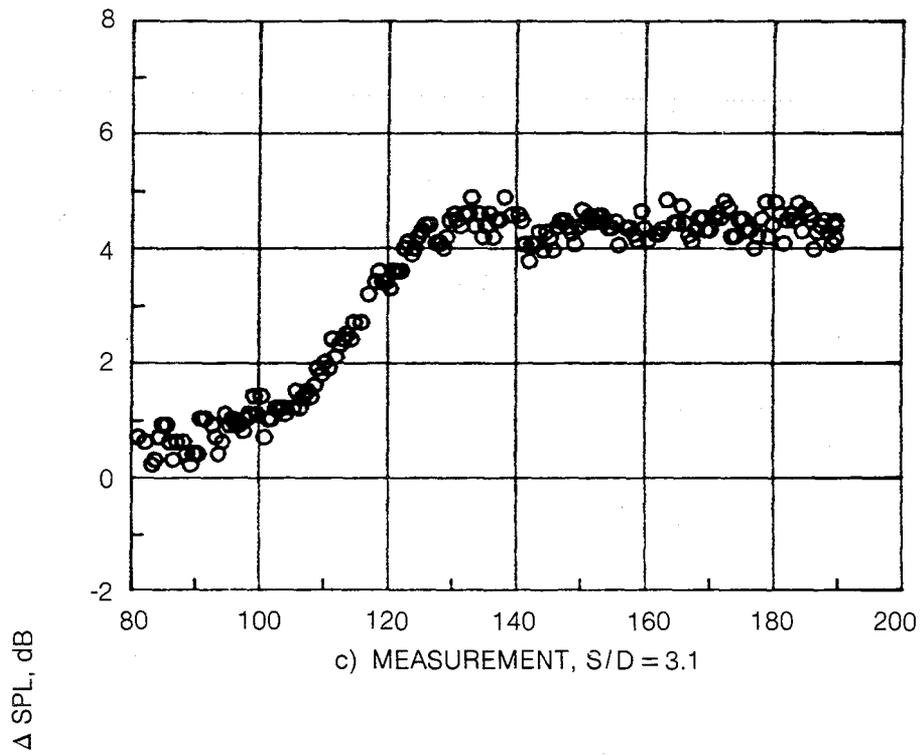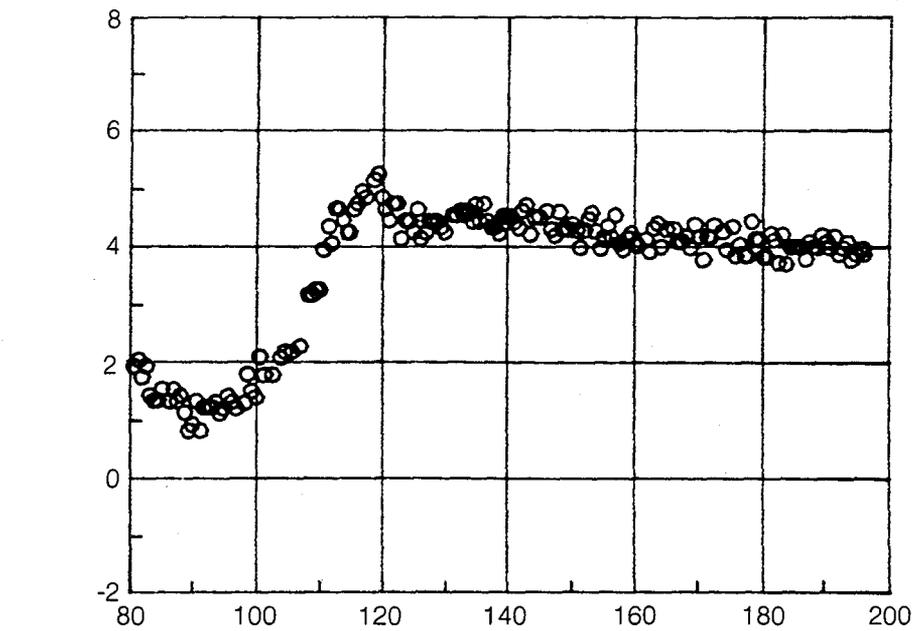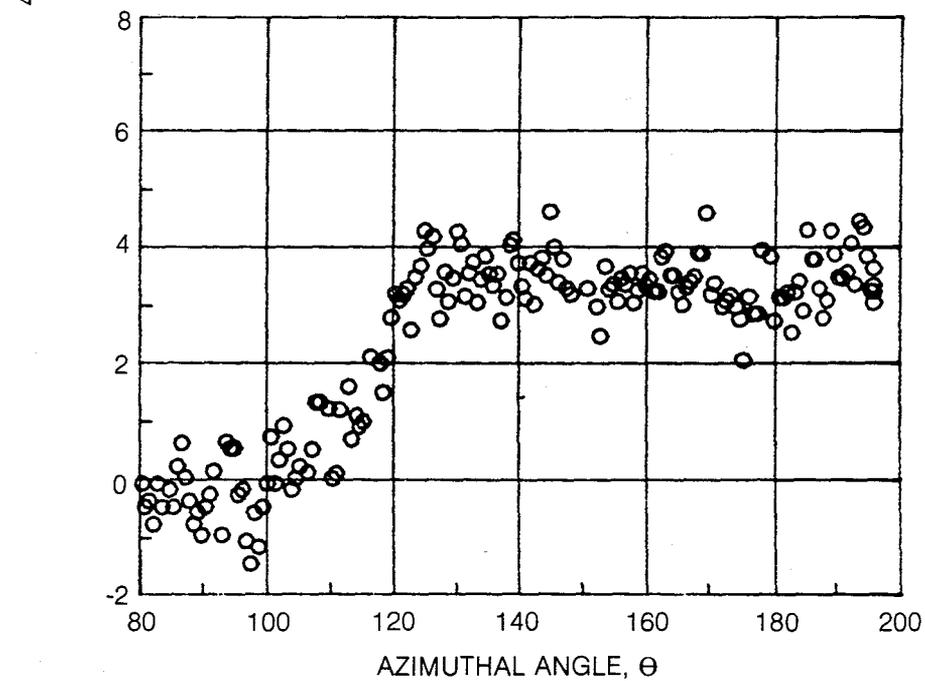
Figure 50 · Temperature Dependence of Measured and Predicted Azimuthal Directivity Pattern, M = 0.6, S/D = 8.1, ψ = 40°, f = 20 kHz
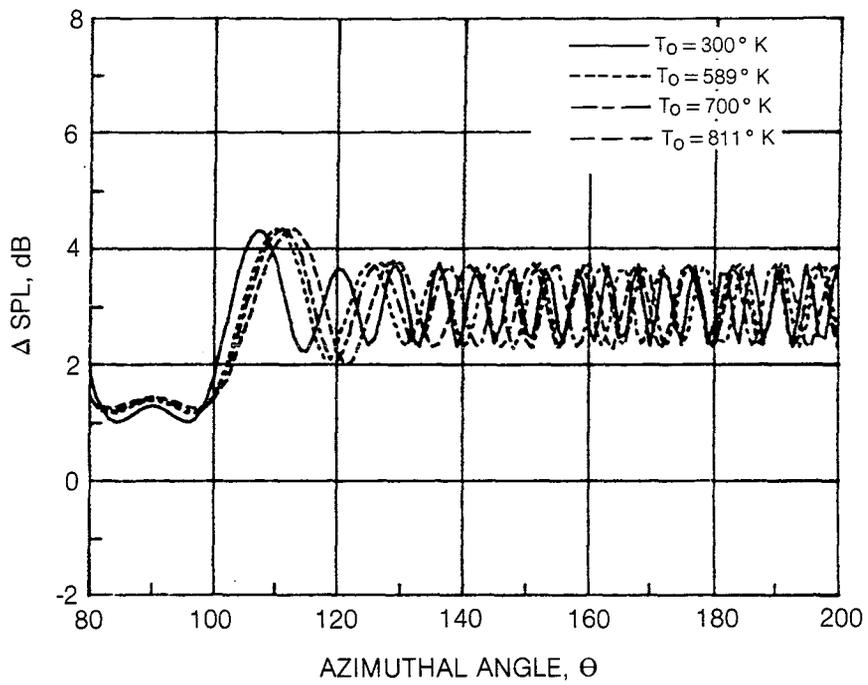
c) PREDICTION, $T_O = 300°$ K, $589°$ K, $700°$K, $811°$K

Figure 50 · Concluded
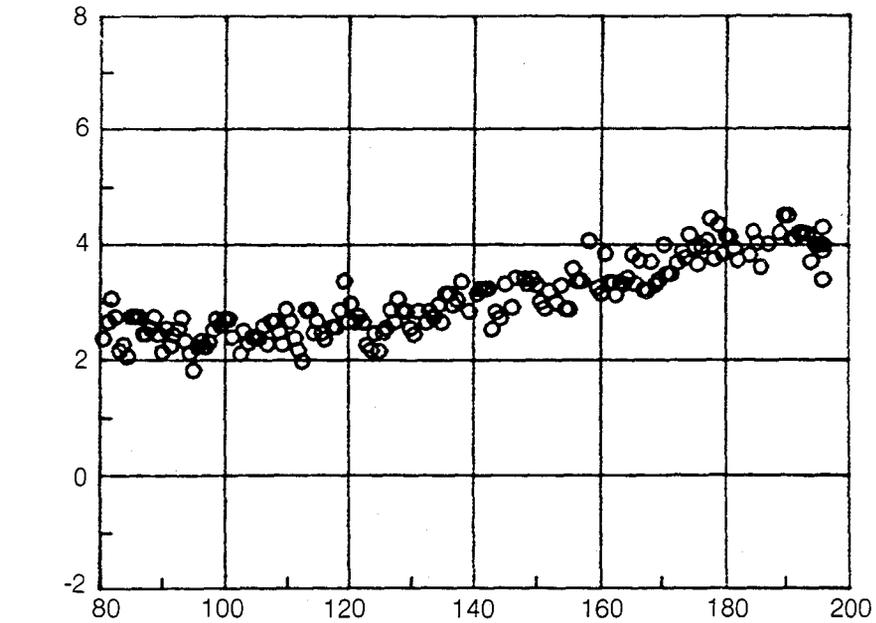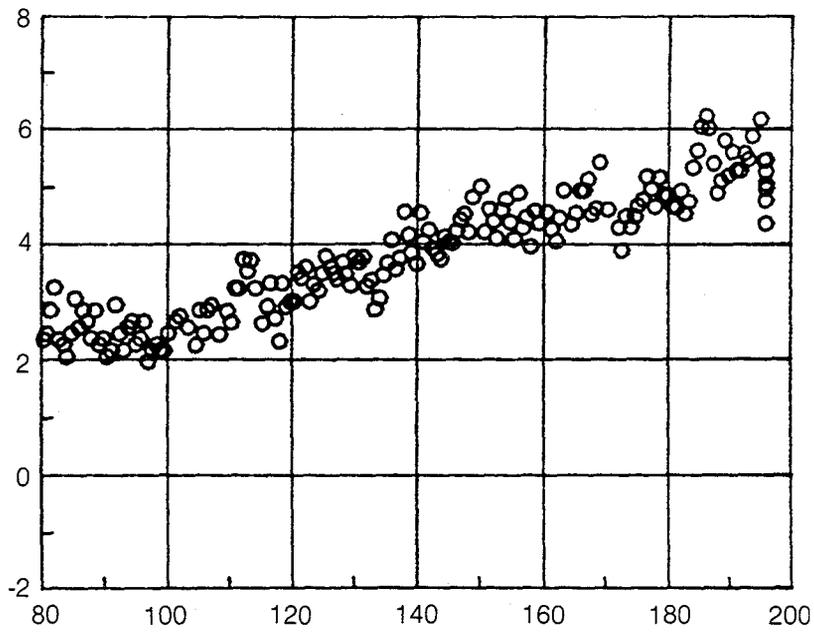
Figure 51 · Temperature Dependence of Measured and Predicted Azimuthal Directivity Pattern, M = 0.6, S/D = 8.1, ψ = 40°, f = 800 Hz

160
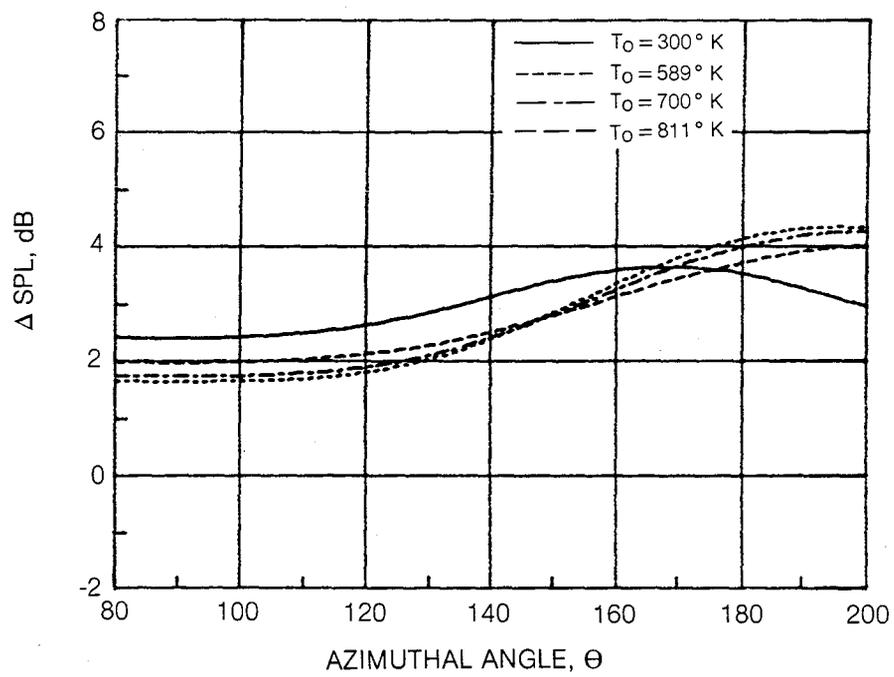
c) PREDICTION, $T_0 = 300°$ K, $589°$ K, $700°$ K, $811°$ K

Figure 51 · Concluded
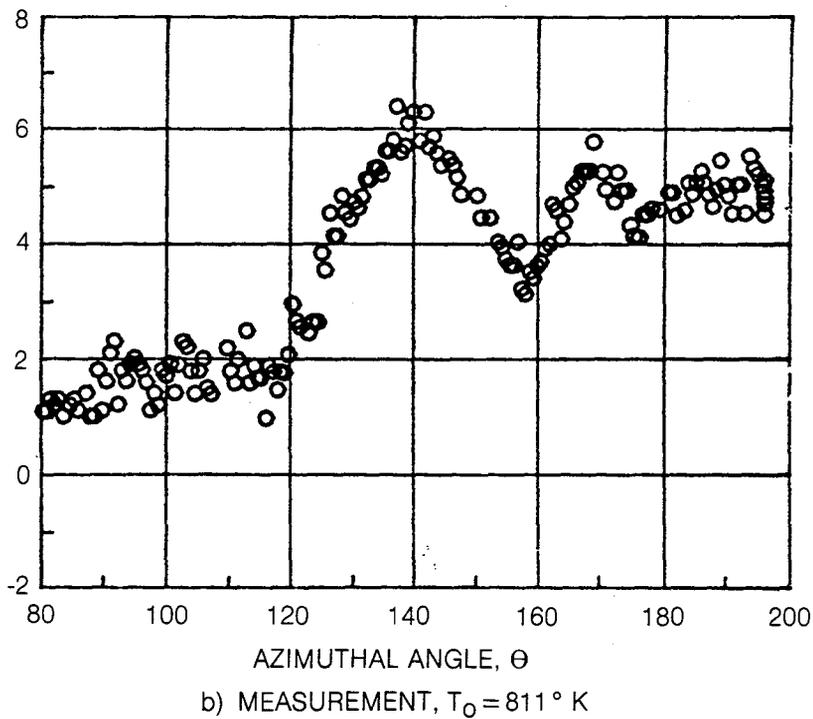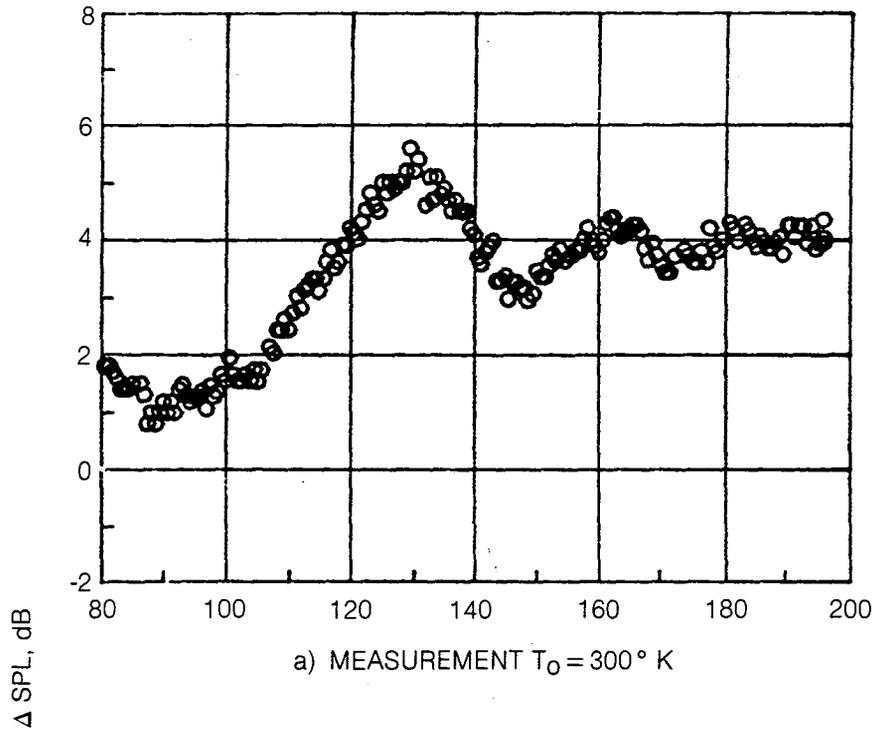
Figure 52 - Temperature Dependence of Measured and Predicted Azimuthal Directivity Pattern, M = 0.6, S/D = 8.1, ψ = 40°, f = 4 kHz
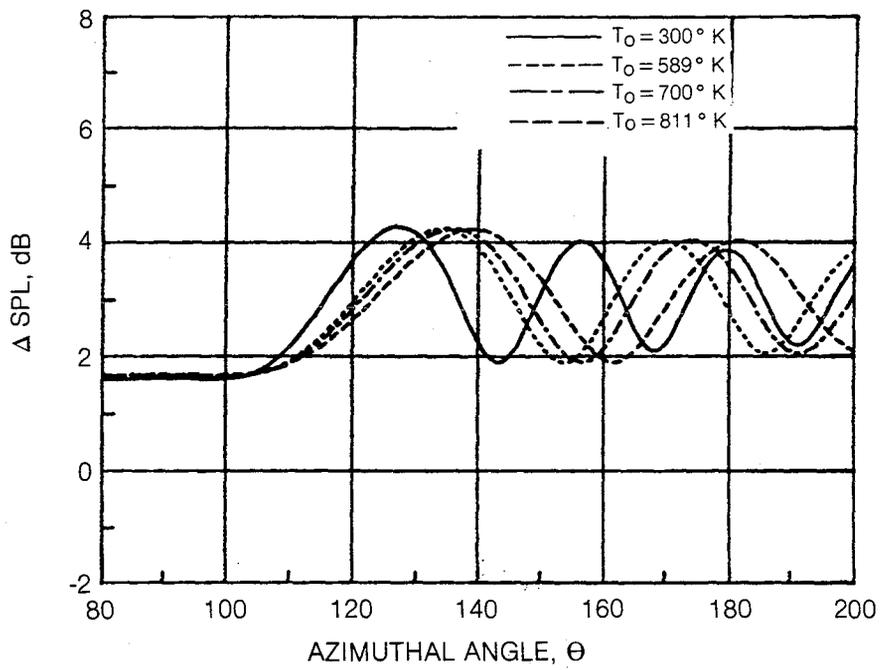
c) PREDICTION, $T_0 = 300°$ K, $589°$ K, $700°$ K, $811°$ K

Figure 52 · Concluded
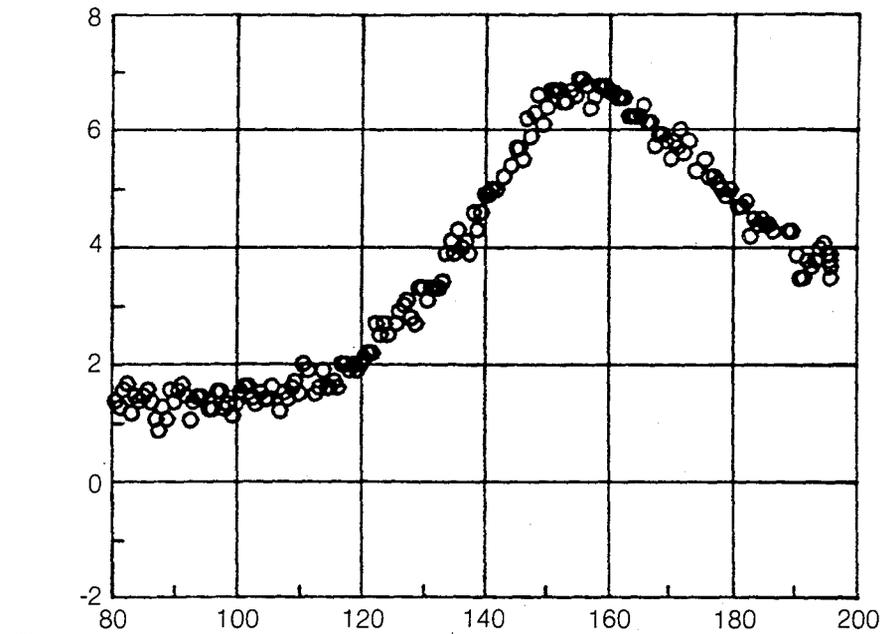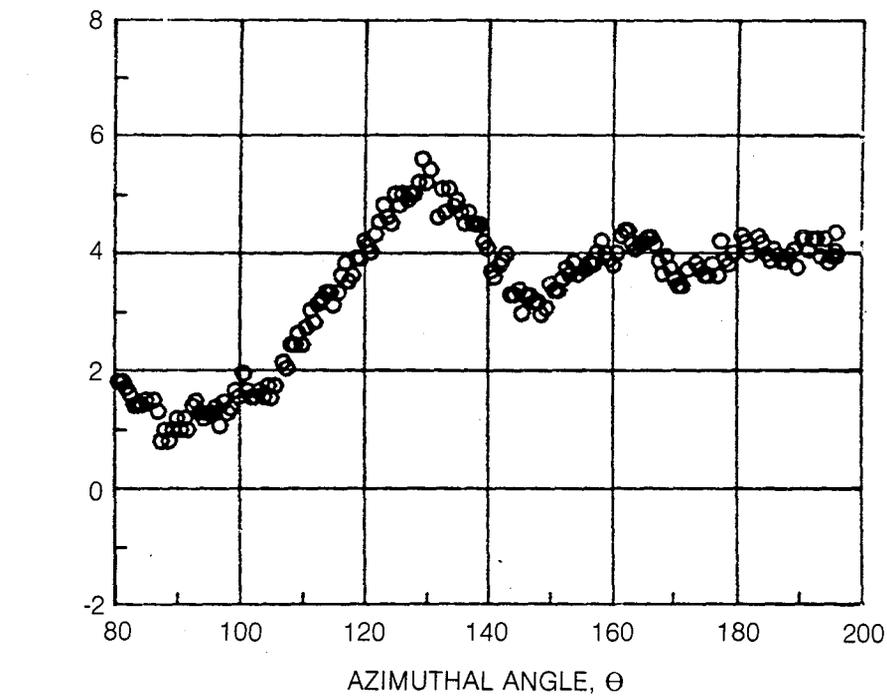
Figure 53 - Polar Angle Dependence of Measured and Predicted Azimuthal Directivity Pattern, M = 0.94, T_O = 300° K, S/D = 8.1, f = 4 kHz
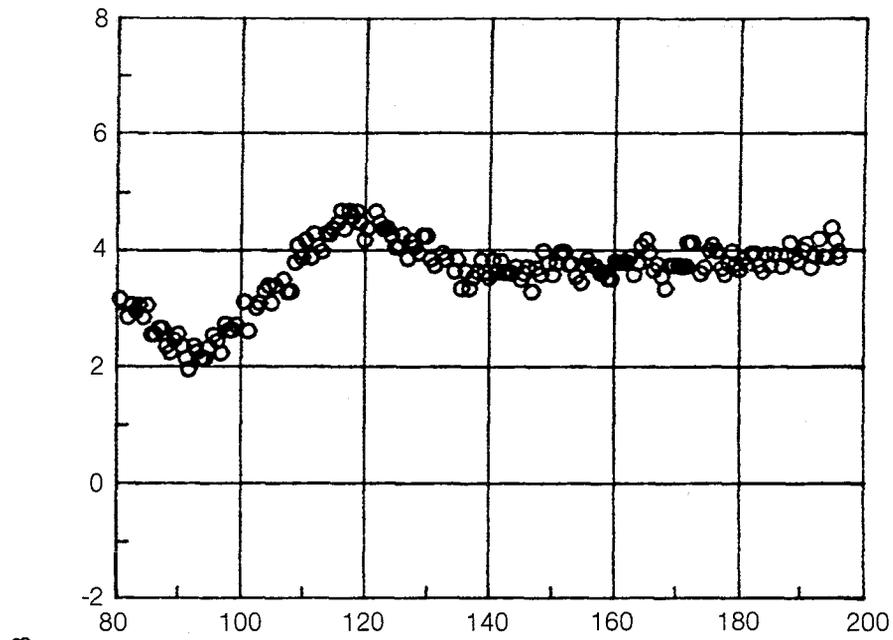
c) MEASUREMENT, $\psi = 60°$

d) MEASUREMENT, $\psi = 90°$

AZIMUTHAL ANGLE, Θ
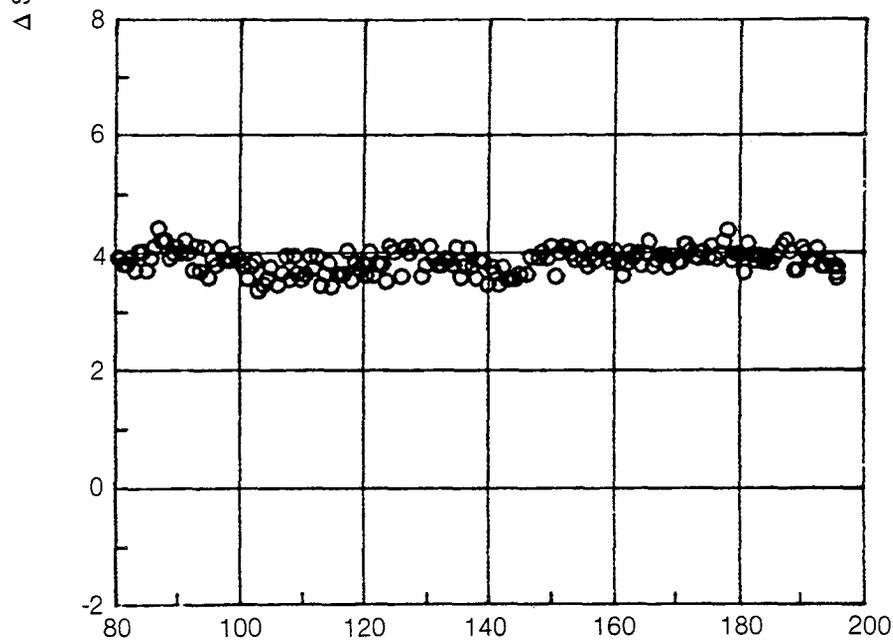
Figure 53 · Continued
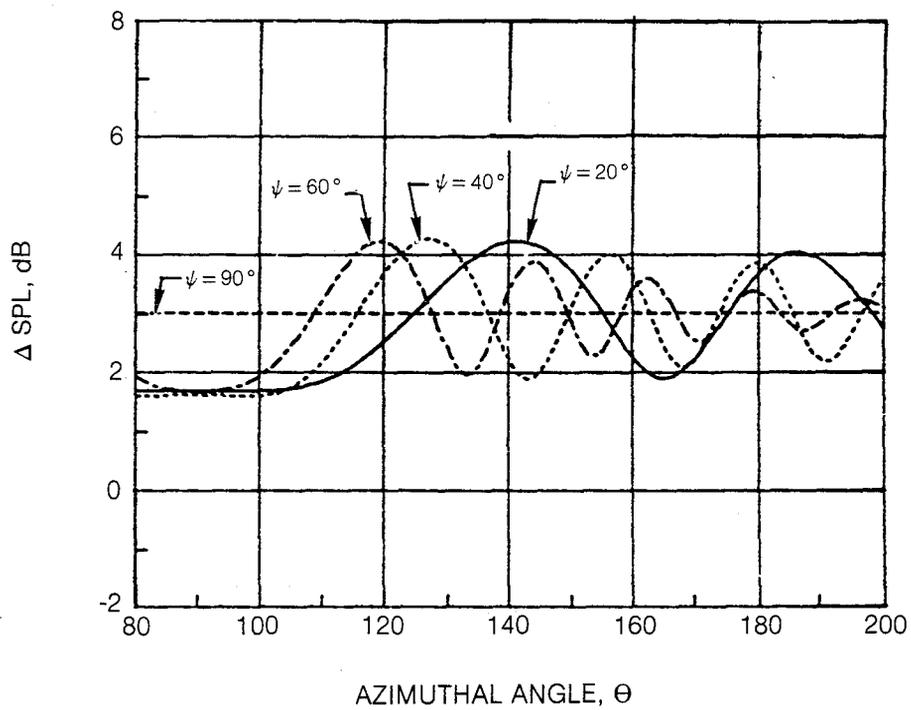
e) PREDICTION, $\psi = 20°, 40°, 60°, 90°$

Figure 53 - Concluded
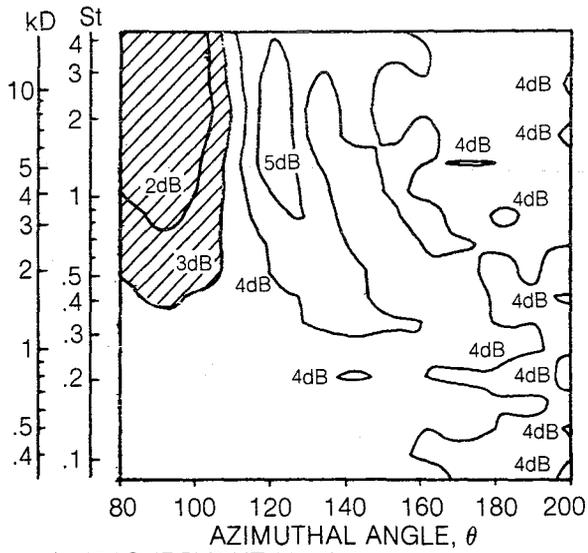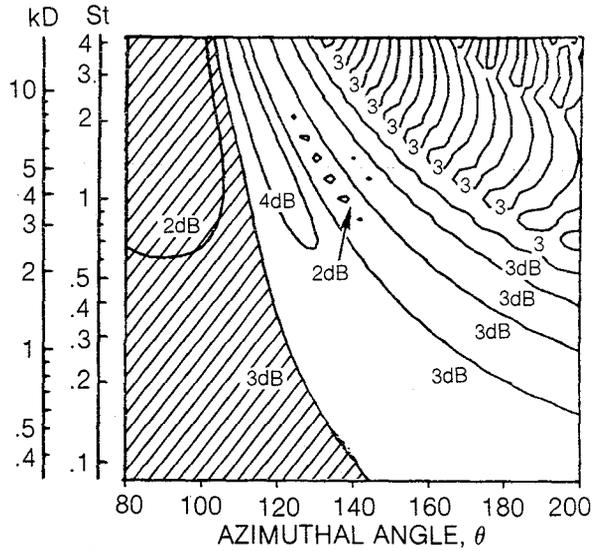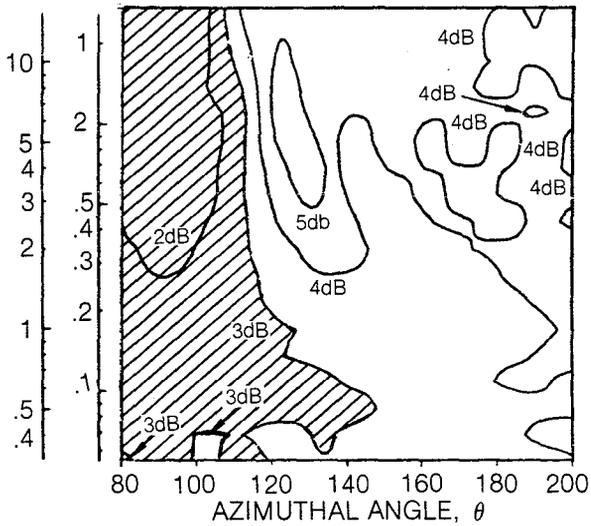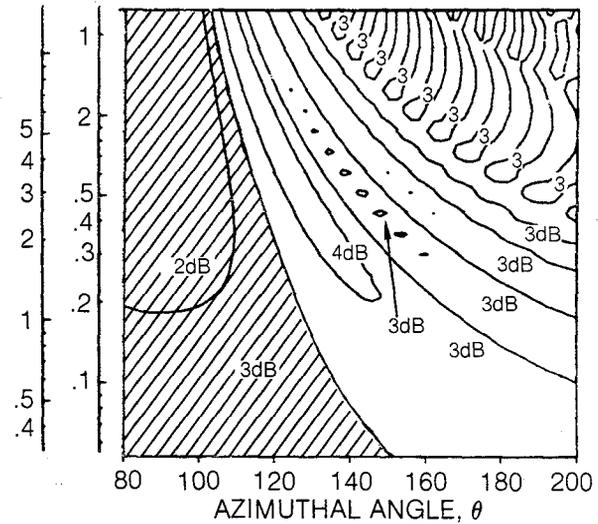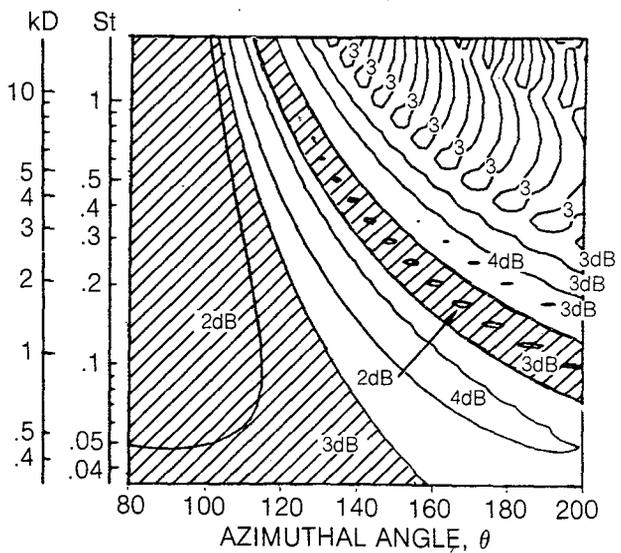
Figure 54 — Mach Number Dependence of Measured and Predicted Contour Plots,
$T_O = 300\,^\circ K$, $S/D = 8.1$, $\psi = 40^\circ$
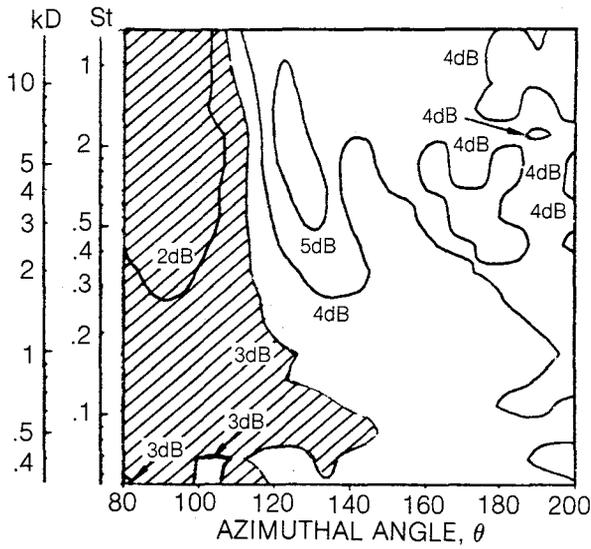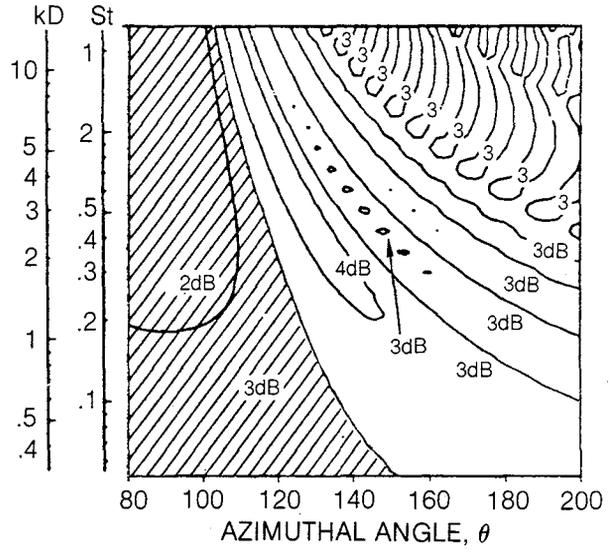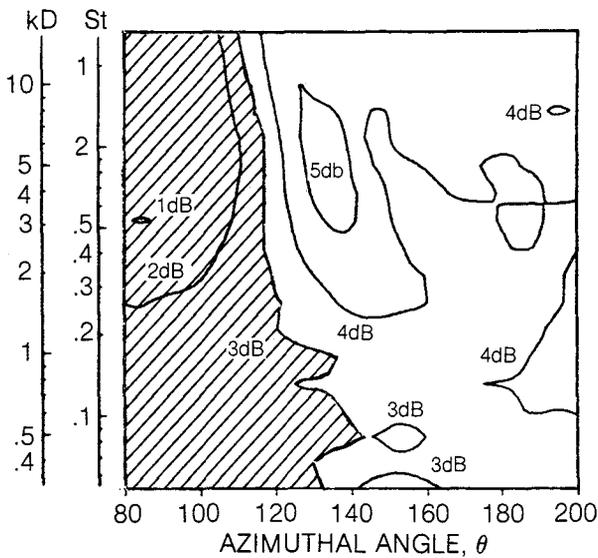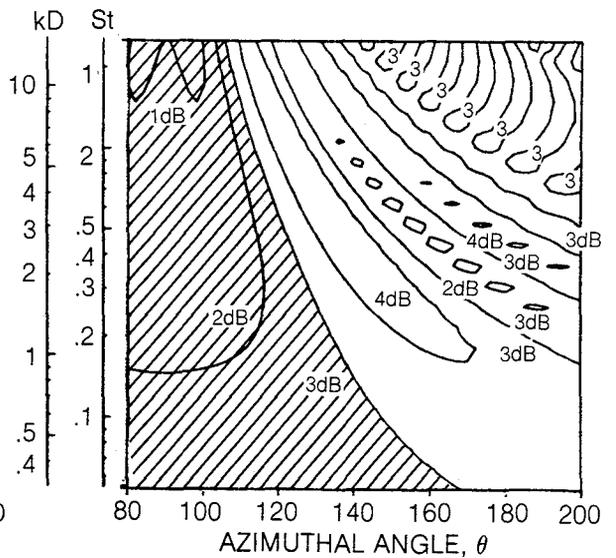
Figure 55 — Spacing Dependence of Measured and Predicted Contour Plots, M = 0.94, To = 300°K, ψ = 40°
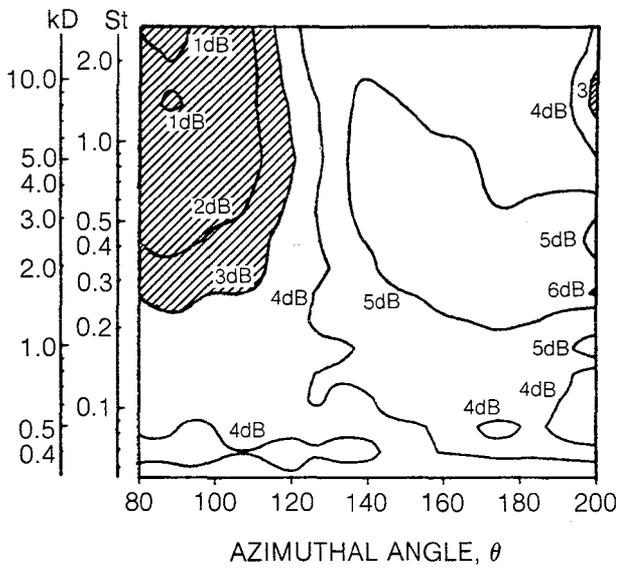
e) MEASUREMENT, S/D = 3.1
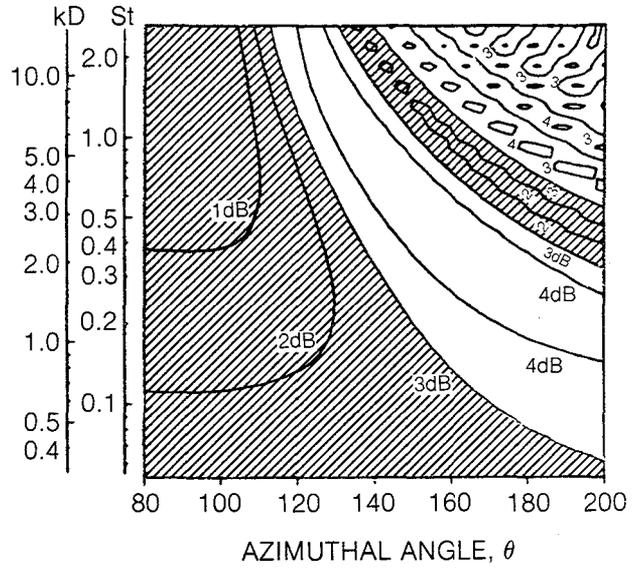
f) PREDICTION, S/D = 3.1

Figure 55 — Concluded

a) $T_O = 300\,°K$
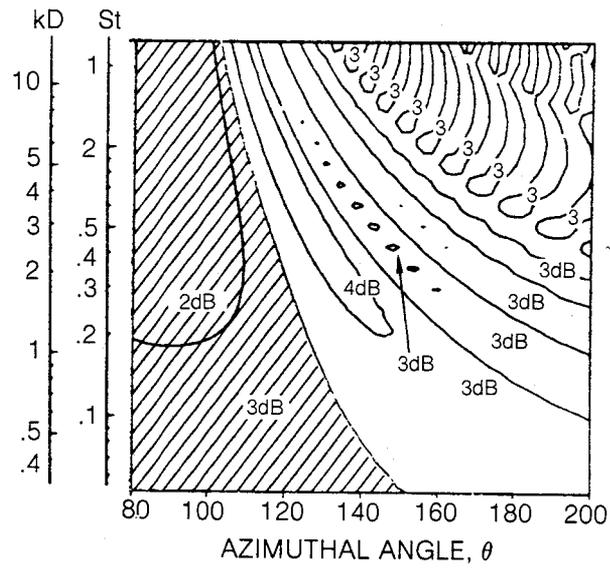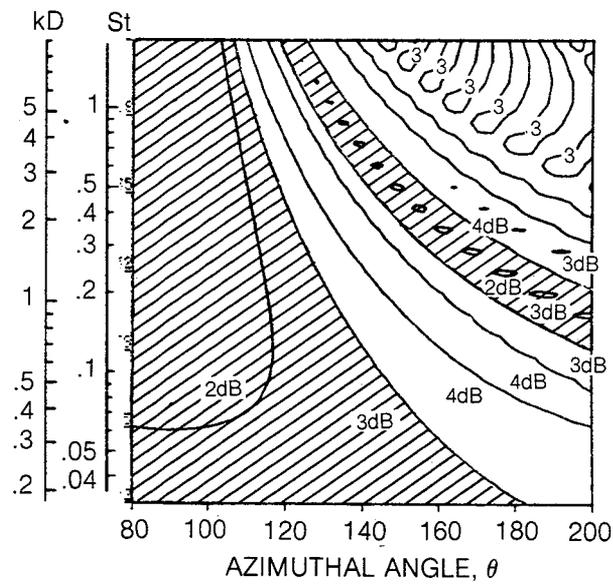
b) $T_O = 811\,°K$

Figure 56 — Temperature Dependence of Predicted Contour Plots, M = 0.94, S/D = 8.1, $\psi = 40°$
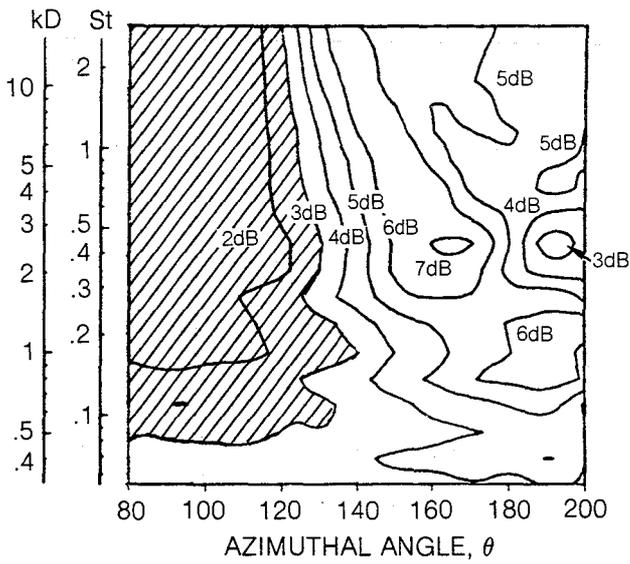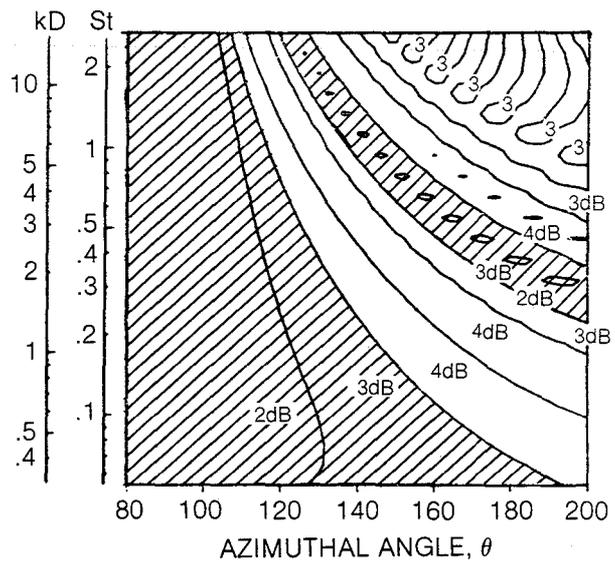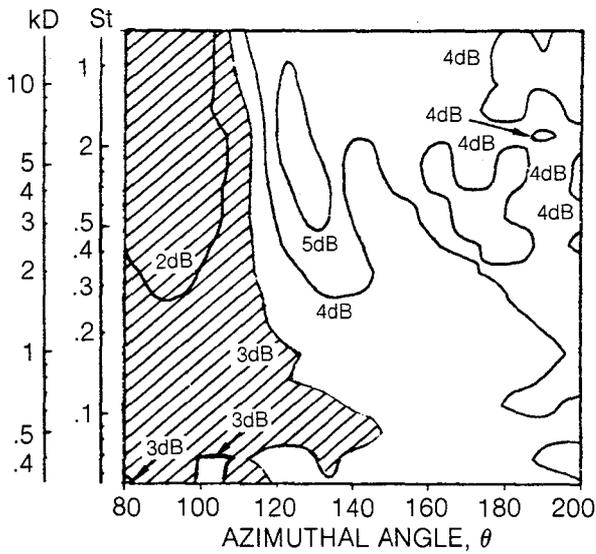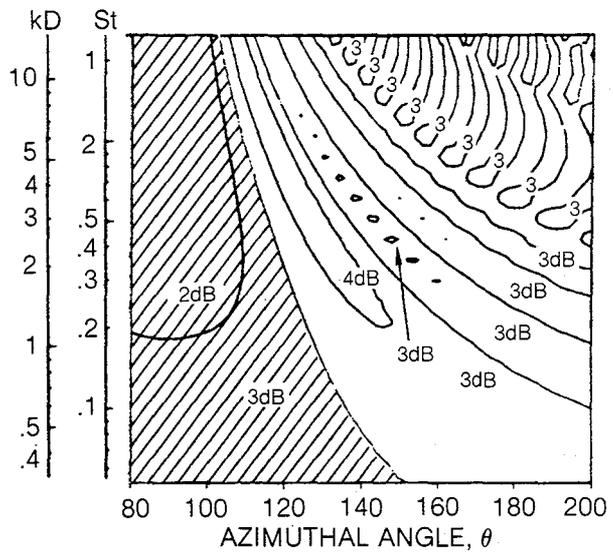
Figure 57 — Polar Angle Dependence of Measured and Predicted Contour Plots,
M = 0.94, T_O = 300°K, S/D = 8.1
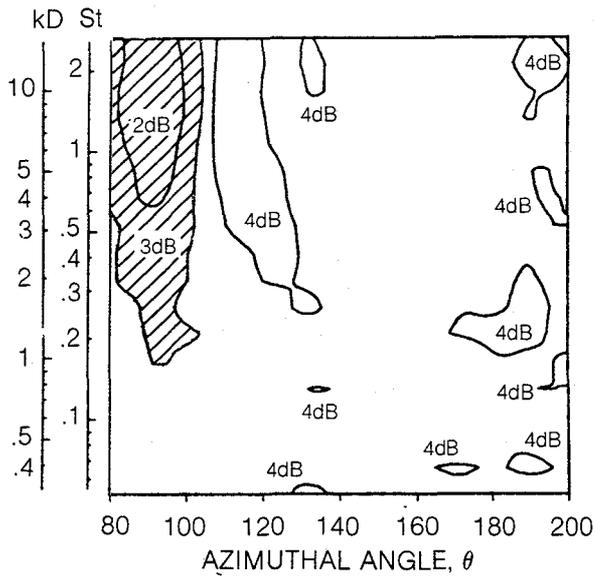
e) MEASURED, $\psi = 60°$
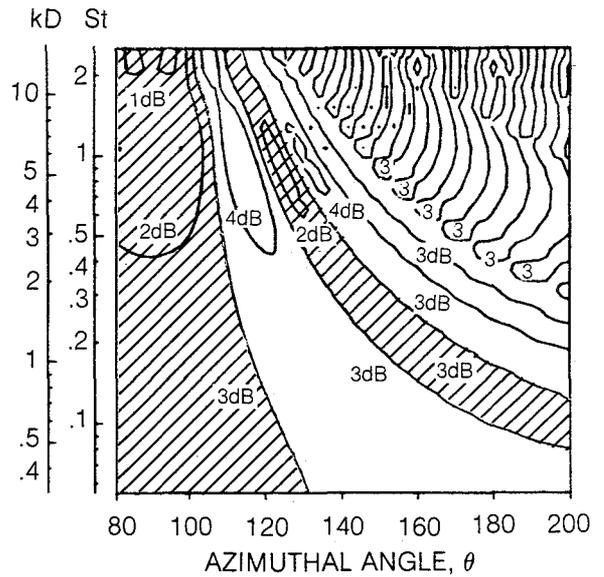
f) PREDICTED $\psi = 60°$
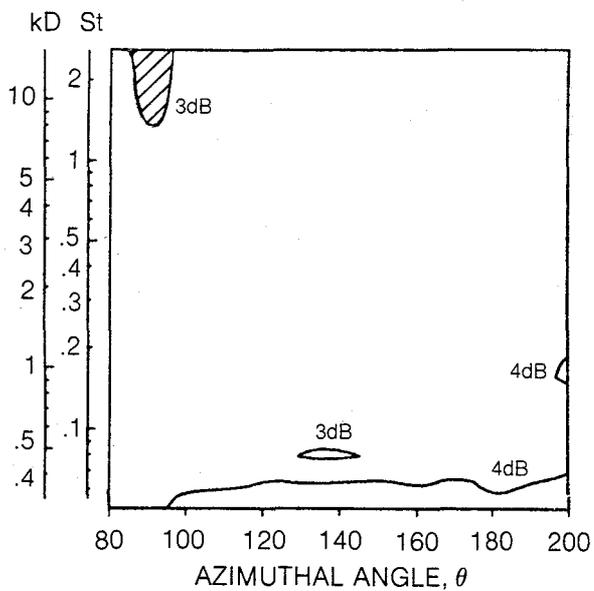
g) MEASURED, $\psi = 80°$
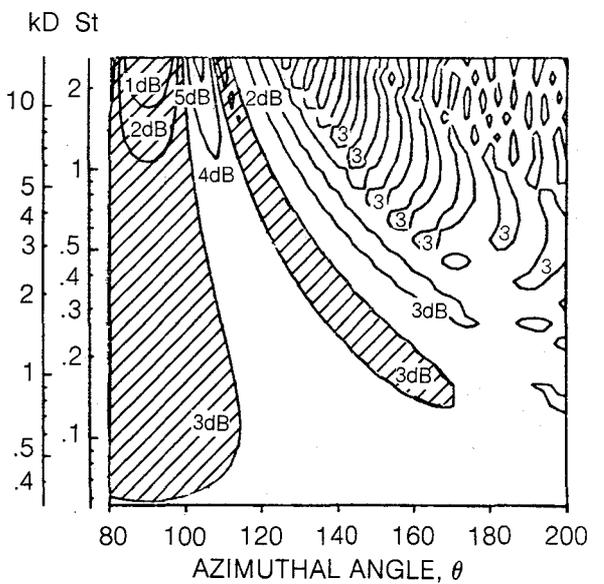
h) PREDICTED $\psi = 80°$

Figure 57 — Continued

172
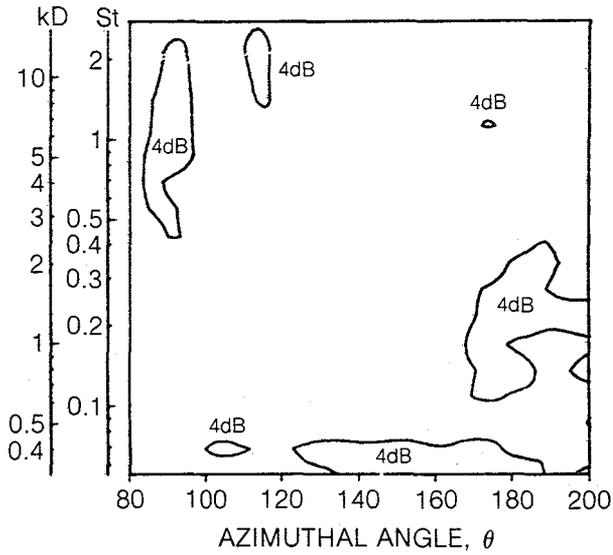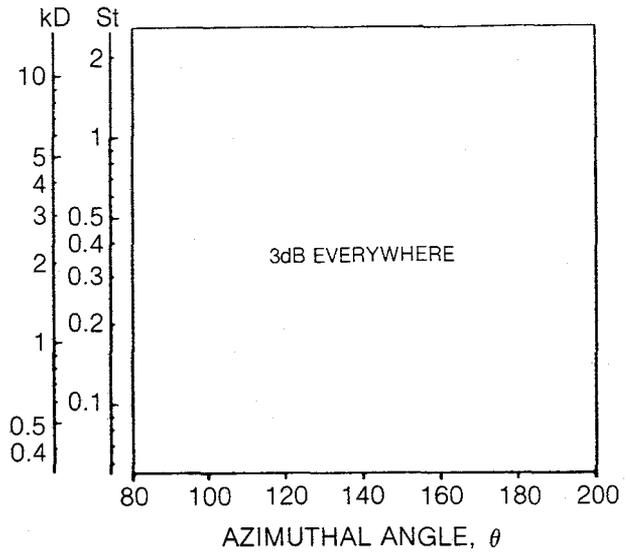
i) MEASURED, $\psi = 90°$

j) PREDICTED $\psi = 90°$
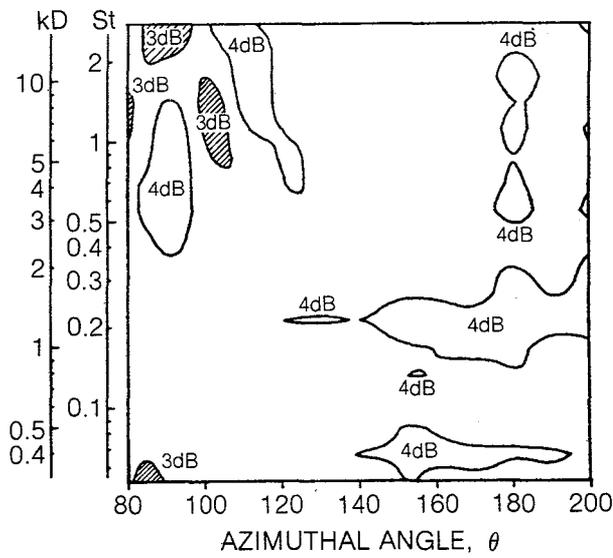
k) MEASURED, $\psi = 100°$
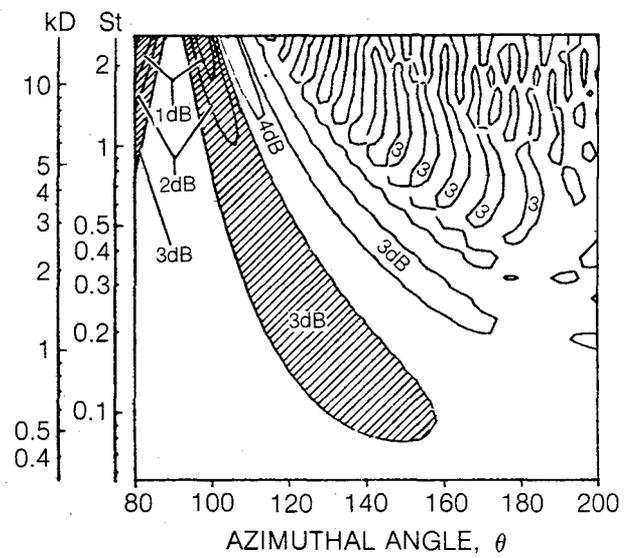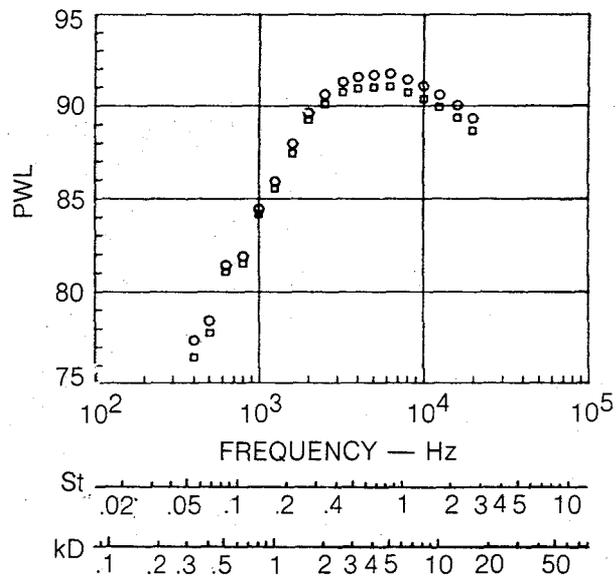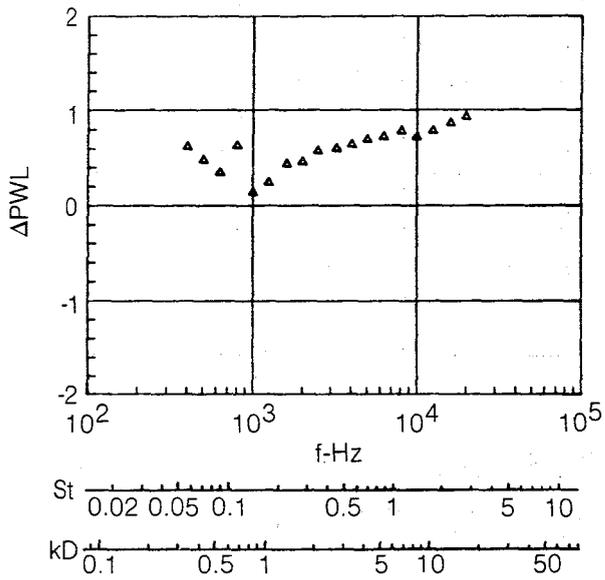
l) PREDICTED, $\psi = 100°$
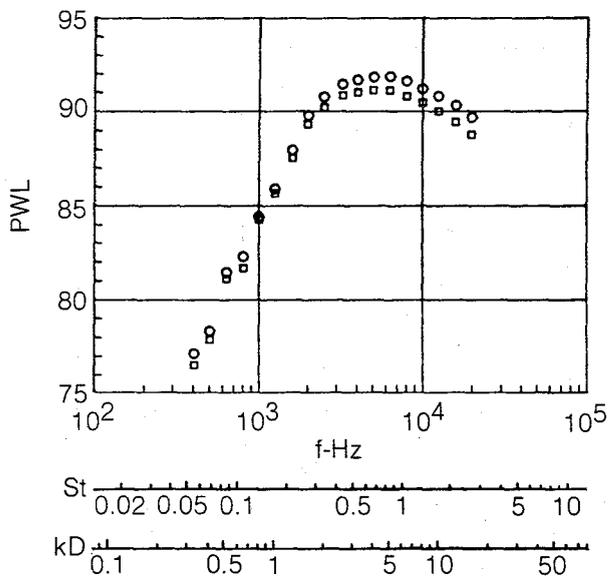
Figure 57 — Concluded
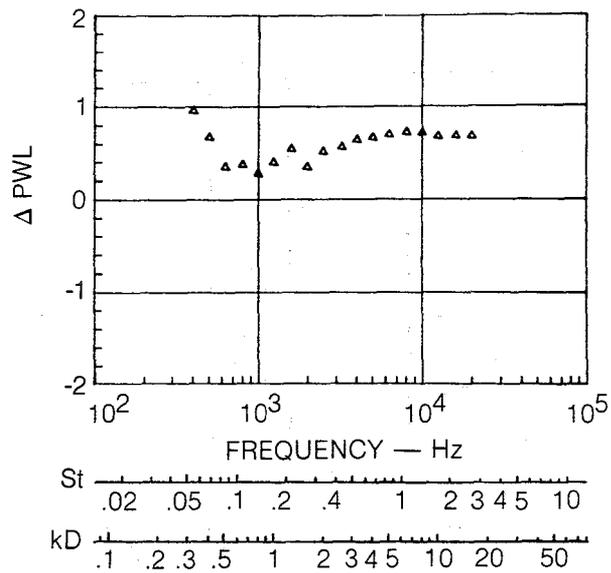
a) DIFFERENTIAL POWER, S/D = 8.1

b) POWER, S/D = 8.1

Figure 58 — Spacing Dependence of Measured Dual Jet Power Spectrum,
M = 0.94, T_o = 300°K

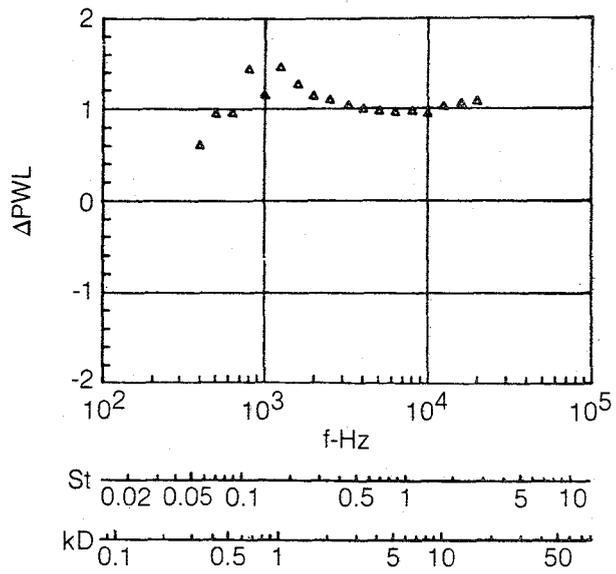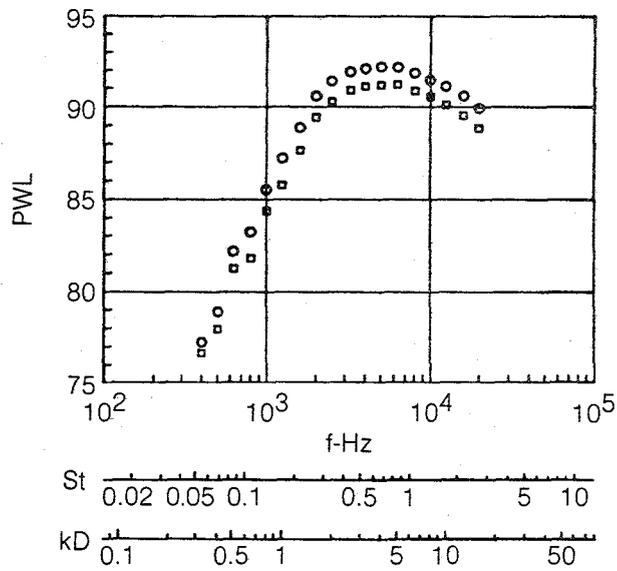c) DIFFERENTIAL POWER, S/D = 5.5

d) POWER, S/D = 5.5

Figure 58 — Continued

2

ΔPWL

1

0

-1

-2

10^2 10^3 10^4 10^5

f-Hz

St 0.02 0.05 0.1   0.5 1   5 10

kD 0.1   0.5 1   5 10   50

e) DIFFERENTIAL POWER, S/D = 3.1

95

PWL

90

85

80

75

10^2 10^3 10^4 10^5

f-Hz

St 0.02 0.05 0.1   0.5 1   5 10

kD 0.1   0.5 1   5 10   50

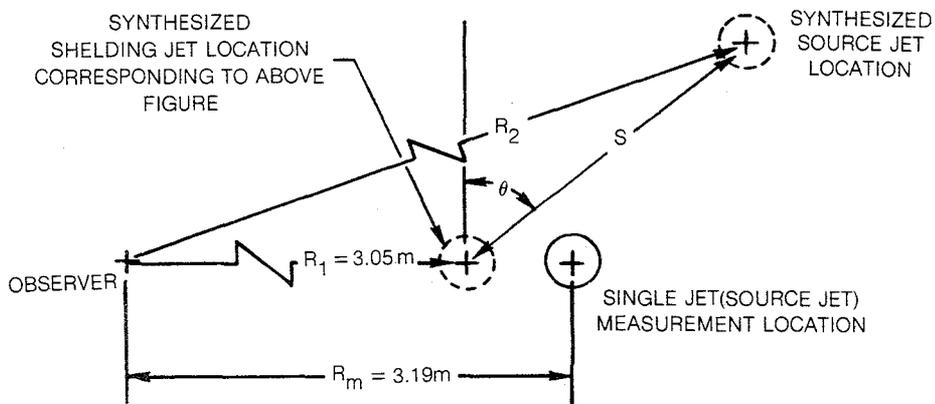f) DIFFERENTIAL POWER, S/.D = 3.1

Figure 58 — Concluded

176
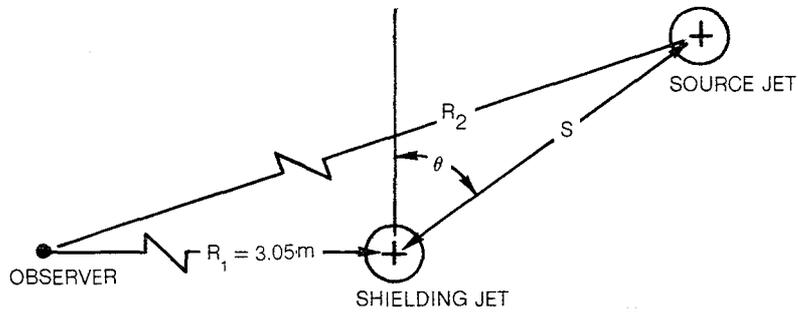
a) DUAL JET GEOMETRY VIEWED FROM DOWNSTREAM

b) TWO INDEPENDENT JETS AT SAME ORIENTATION AS DUAL JET GEOMETRY

Figure C-1 — Schematic Illustrating Synthesization of Sound Field Radiated by Two Independent Jets

177

1. Report No. NASA CR-3966	2. Government Accession No.	3. Recipient's Catalog No.
4. Title and Subtitle Jet Shielding of Jet Noise		5. Report Date April 1986
		6. Performing Organization Code
7. Author(s) John C. Simonich, Roy K. Amiet, and Robert H. Schlinker		8. Performing Organization Report No.
		10. Work Unit No.
9. Performing Organization Name and Address United Technologies Research Center East Hartford, CT 06108		11. Contract or Grant No. NAS1-16689
		13. Type of Report and Period Covered Contractor Report
12. Sponsoring Agency Name and Address National Aeronautics and Space Administration Washington, DC 20546		
		14. Sponsoring Agency Code 505-31-33-12

16. Abstract   A theoretical and experimental study was conducted to develop a validated first principles analysis for predicting the jet noise reduction achieved by shielding one jet exhaust flow with a second, closely spaced, identical jet. A generalized dual jet noise analytical model was formulated in which the acoustic radiation from a source jet propagates through the velocity and temperature discontinuity of the adjacent shielding jet. Assessment of the theory involved conducting dual jet noise and single jet noise experiments to establish the difference in directivity pattern. Analytical variables evaluated experimentally included jet Mach number (subsonic and supersonic), jet diameter, jet spacing, flow temperature, and acoustic source frequency.

Jet shielding was found to reduce noise levels in the common plane of the dual jet system with shielding extending to observer angles on either side of this plane. Outside of this region an increase of noise occurs due to the redirection of sound rays from the shielded region in addition to acoustic reflections between the adjacent flow fields. A balance exists between the noise reduction and noise increase confirming that acoustic energy is conserved. Jet shielding effectiveness increases with Helmholtz number and is most effective for frequencies above the jet noise spectrum peak. Increasing subsonic Mach number enhances shielding and shifts the onset of shielding to lower frequencies. For noninterfering dual jet flows, shielding remains constant with jet spacing. Small spacing, resulting in the aerodynamic merger of the jet flows, cause changes in the acoustic source region which increase the dual jet noise relative to two single jets. Changes of jet temperature were found to have a minimal effect. These measured dual jet shielding effects are successfully predicted by the first principles theoretical model.

17. Key Words (Suggested by Author(s)) Jet Noise Jet Shielding Subsonic Jet Noise Supersonic Jet Noise Jet Noise Reduction		18. Distribution Statement Unclassified - Unlimited Subject Category 71		
19. Security Classif. (of this report) Unclassified	20. Security Classif. (of this page) Unclassified		21. No. of Pages 177	22. Price A09

End of Document